



Eidgenössische Technische Hochschule Zürich  
Swiss Federal Institute of Technology Zurich

**Department of Electrical and  
Computer Engineering**  
Power Systems Research

University of Wisconsin-Madison  
1415 Engineering Drive  
Madison, Wisconsin 53706

**EEH –  
Power Systems Laboratory**

Head: Prof. Dr. Göran Andersson

ETH Zurich  
Physikstrasse 3 / ETL

Master Thesis

# **Grid Stabilization Control and Frequency Regulation**

## **for Inverter-connected Distributed Renewable Energy Sources**

Lucas Friedrich  
Matthias Gautschi

March 9, 2009 – September 9, 2009

Supervisor:  
Prof. C. L. DeMarco at UW-Madison

Co-Supervisors:  
Prof. B. Lesieutre at UW-Madison  
Prof. G. Andersson at ETH Zurich  
Spyros Chatzivasiliadis at ETH Zurich



## Preface

This research project is the final assignment of our Master programs at ETH Zurich. Through our tutor, Prof. G. Andersson, head of the Power Systems Laboratory in Zurich, we became aware of the unique opportunity to write our Master Thesis abroad within the scope of a research project. Prof. G. Andersson is in good contact with Prof. DeMarco and the institute here in Madison-Wisconsin, USA and so it became possible for us to travel and perform research here at the University of Wisconsin-Madison.

As students in the new Master program “Energy Science and Technology” of ETH Zurich and considering our electrical engineering background, we have particular interest in various renewable energy technologies such as wind power and their effects on power systems. To be able to set the focus of this research on wind power applications was very inspiring and we were very looking forward to a project in this area. Contributing to a more sustainable energy future was another initial motivation.

Now, 6 months later, we can say in retrospect that this half year was a unique experience and was absolutely worthwhile. The research work was very interesting and the collaboration with our supervisor, Prof. DeMarco, was always very inspiring and obliging throughout the whole project. We have had the feeling that we still learned a lot and we believe that is how it is supposed to be. Besides the research we had the opportunity to live in another country for half a year and were able to experience the American way of life. The summer here in Madison (in total contrast to the winter which we thankfully could avoid) offered a bunch of different activities. Sitting at the Memorial Union Terrace just next to the lake with some friends and enjoying the evening, is something we’ll never forget. We will definitely keep the city in good memories.

Our first thanks go to Prof. DeMarco for his commitment and patience. The way he guided us through the project, the time he sacrificed for our discussions and the many helpful inputs he gave us, formed the outcome of our project substantially.

We also want to thank our supervisor at ETH Zurich, Mr. S. Chatzivasiliadis, from whom we got always helpful inputs and motivations for the project. Big thanks also go to Prof. G. Andersson from ETH Zurich, our master program tutor, who made this project possible. And last but not least we would like to thank Prof. Lesieutre, Prof. Hiskens, the University staff and all the students we met here and who helped us in many different aspects within this project.

Madison, WI, USA, 09/09/2009

## Project Description

Subsequently, the research project description, as defined at the beginning of the project, is given.

### Overall Project Title

*Control System Design for Mimicking Inertia in Inverter Connected Alternative Energy Sources.*

### Introduction

After discussions with Professors DeMarco and Lesieutre a topic was selected that matched best to our knowledge and interests, and was in accordance with the expectations from ETH Zurich. We all agreed that it makes sense to start from a common base and therefore in a first part work together. In a second part, after having sorted out the issues we are going to face, a split-up in two individual directions is planned. The project seems to provide enough range for making progress and has great potential contributing to the integration of alternative energy sources into the electrical grid.

### Abstract

Traditionally, the vast majority of electrical generation sources connected to electric power grids have been synchronous machines. Such machines have a number of inherent dynamic characteristics that tend to contribute to the electromechanical stability of the power grid. The inertia of the synchronous machine is one of these characteristics. The use of alternative energy sources is forced all over the world and therefore the share of these energy sources in the total generation capacity is steadily increasing. In contrast to conventional generation, most of these alternative energy sources are being connected to the grid through power electronic devices (frequency converters), which do not inherently provide inertia.

In the past few years, several authors have begun to look at this issue, largely from the perspective of inertia as a form of short-term energy storage for frequency control. The work to be pursued here will seek to take a broader view. In particular, our goal will be to examine what practically achievable dynamic characteristics at the power electronic interface best enhance the grid's electromechanical stability. We anticipate that a first step will include mimicking of inertia for wind power generation (i.e., including a component of power output that varies with the derivative of electrical frequency, acceleration).

In a next step, other alternative energy sources can be taken into account. The properties that will dictate what constitutes "practically achievable" dynamic characteristics will vary with the nature of the

primary source of power. One may expect that wind turbines and small scale rotating generators in microgrids would provide fairly broad bandwidth in their ability to modulate power output based on a signal such as acceleration. Conversely, a device such as a fuel cell may only be able to vary its electrical output on a very slow time scale, and might need supplemental "fast" storage, such as supercapacitors, to achieve broad bandwidth control of power output. This tradeoff between bandwidth of the power source, versus that of possible supplemental storage, has not been widely examined in the literature, and will be a focus of the work proposed here.

### **Procedure**

As already mentioned, the first step is to develop a basic model of the generator, the control design, the grid connection and the power system itself. The model should have a flexible structure and several different approaches should be investigated. First a reproduction of some models from literature will provide a good introduction of the topic. Further on the model will be extended and adapted for special issues. Considered prospective control design tools included LQR based methods, passivity based control designs, and "direct design" to a target transfer function using the Youla Parameterization.

After the modeling is done, both students observe different aspects in their own work.

From today's perspective these could be:

- An analysis of the grid-stabilizing effect from inertia by simulating the dynamics of the wind turbine with a real data set.
- The aspect of including storage devices into the control design on a fast resp. slow scale providing additional inertia for integrating different renewable energy resources.
- Large wind power farms, mostly offshore, are more and more connected with a HVDC line to the electrical grid. Without further control implementations in the HVDC inverter system the inertia from the wind farm cannot make any contribution to the grid stability. A new control approach of these systems could lead to an additional degree of freedom in the inertia control.

**Research horizon:**                      **Start Date:**    03/09/2009                      **End Date:**        09/09/2009

### **Approved**

Christopher DeMarco, Professor, University of Wisconsin - Madison

Bernard Lesieutre, Professor, University of Wisconsin - Madison

Göran Andersson, Professor, ETH Zurich



## Abstract

Alternative energy sources constitute one of the most discussed areas around the globe at the moment. Building a more sustainable way of using world's resources to provide energy also for next generations requires a strong focus on renewable energy sources. The integration of these "new" sources to the electric power grid, however, gives rise to new challenges. Because renewable energy sources are mostly connected to the grid through power electronic inverters, an inertial response is not inherently provided. They typically do not contribute to frequency control in today's power systems, but with the implementation of an additional control path an inertia-like response can be mimicked and frequency control as well as stability enhancement is possible. The additional power for the control branches is provided by internal additional power sources as well as external energy storage devices. These power systems have different characteristics in terms of bandwidth and saturation limits and in order to account for these characteristics, modern control designs have to be developed.

The procedure of this research project is divided into two parts. In a first part, additional control on a single bus is developed and in a second part, ways are found to spread additional control onto multiple buses.

The developed concept of a single Master controller and additional distributed Slave controllers serves as promising approach, what is depicted in several simulations. The Master controller itself already shows a remarkable performance in terms of frequency deviation. The addition of distributed PD slave controllers can further improve performance and so the combined Master-Slave control design can be seen as sophisticated concept with remarkable performance in terms of stability and frequency deviation. Applying this new control design method shows an overall improvement by a factor of 5 compared to a standardized PI-control.

Through the selected design approach of the Master controller, an effective heuristic for avoiding saturation is provided, meaning that the contribution levels between control branches with different saturation levels can be set in a reasonable way. However, a complete solution of the saturation issue can not be provided. The Master controller is designed to compensate for the total frequency deviations in the grid and therefore saturation limits can still be reached, if disturbances of too large a magnitude occur. The idea of spreading the physical control action of the Master controller to several buses seems to be a reasonable path for further examinations.

## Index Terms

Frequency Control, Inertia, Inertial Response, Power Systems, Renewable Energy Sources, Stability, Wind Power





## Kurzfassung

Alternative Energieträger stellt momentan weltweit einen der am meist diskutierten Themenbereiche dar. Ein intensives Auseinandersetzen mit erneuerbaren Energieträgern ist eine wesentliche Voraussetzung um einen nachhaltigeren Weg zu finden weltweit Ressourcen, auch für nächste Generationen, bereitzustellen. Die Integration dieser „neuen“ Ressourcen ins elektrische Netz führt jedoch zu neuen Herausforderungen. Da erneuerbare Energien meist über leistungselektronische Inverter ins Netz eingespeist werden, steht hier keine „Inertial Response“ zur Verfügung. Typischerweise haben erneuerbare Energieträger keinen Einfluss auf die Frequenzregelung heutiger Energiesysteme, aber mit der Implementierung eines zusätzlichen Kontrollpfads kann eine „Inertia-like Response“ nachgeahmt werden und Frequenzregelung sowie auch eine Verbesserung der Stabilität wird ermöglicht. Die zusätzliche Leistung der Regelungswege wird von internen Leistungsquellen sowie von externen Energiespeichern zur Verfügung gestellt. Diese Energiequellen haben verschiedene Charakteristiken in Bezug auf deren Bandbreite und Sättigungslimiten, und moderne Regelungsdesigns müssen entwickelt werden um solche Charakteristiken zu berücksichtigen.

Der Ablauf dieses Forschungsprojektes ist in zwei Teile aufgeteilt. In einem ersten Teil wird die Regelung an einem einzelnen Bus behandelt bzw. entwickelt und in einem zweiten Teil werden Wege gefunden diese zusätzliche Regelung auf mehrere Busse zu verteilen.

Das entwickelte Konzept eines einzelnen Master Reglers und zusätzlichen Slave Reglern dient hier als vielversprechender Ansatz, was in vielen Simulationen gezeigt werden kann. Der Master Regler alleine zeigt schon eine bemerkenswerte Performance in Bezug auf Frequenzabweichung. Die zusätzlich verteilten PD Slave Regler können die Performance weiter verbessern, und so kann das Master-Slave Regler Design als fortgeschrittenes Konzept mit einer bemerkenswerten Performance in Bezug auf Stabilität und Frequenzabweichung gesehen werden. Die Anwendung dieses Designkonzepts bringt eine Verbesserung um das 5-fache im Vergleich zu einem Standard PI Regler.

Durch den gewählten Designansatz für den Master Regler kann eine effektive Heuristik geliefert werden um Sättigung zu vermeiden, was heisst, dass die Aufteilung zwischen den Regelungsweigen mit verschiedenen Sättigungslevels auf eine vernünftige Art und Weise eingestellt werden kann. Jedoch kann kein kompletter Lösungsansatz für diese Sättigungsproblematik geliefert werden. Der Master Regler wird designt um die komplette Frequenzabweichung im Netz zu kompensieren und daher kann bei zu grossen Störungen das Sättigungslevel nachwievor erreicht werden. Die Idee, physikalische Regelung vom Master Regler auf mehrere Busse zu verteilen, scheint ein vernünftiger Ansatz für zukünftige Untersuchungen zu sein.



# Contents

Preface .....	iii
Project Description .....	iv
Abstract .....	vii
Kurzfassung .....	ix
Contents .....	xi
Overview .....	xv
List of Figures .....	xvi
List of Tables .....	xviii
List of Symbols .....	xix
List of Acronyms .....	xxii
1 Introduction .....	1
1.1 Today's Power Systems .....	1
1.2 Initial Motivation .....	2
1.3 Project Organization .....	3
1.4 Related Work .....	4
2 Background and Motivation .....	7
2.1 Inertial Response .....	7
2.1.1 Concept of Mimicking Inertia .....	7
2.2 Generation Units .....	8
2.2.1 Classical Synchronous Generator Systems .....	8
2.2.2 Wind Turbine Generator Systems .....	9
2.3 Frequency Control in Power Systems .....	11
2.4 Concept of Balancing System through Adding Power .....	13
2.4.1 Additional Power from Internal Sources .....	14
2.4.2 Additional Power from External Sources .....	15
2.5 Bandwidth .....	15
2.6 Limits and Saturation .....	17
2.7 Motivation for Grid Stabilization Control and Frequency Regulation .....	18
3 System Modeling .....	21

3.1	IEEE 14 Bus Test System .....	21
3.1.1	Classes of Disturbance Signals .....	22
3.1.2	Per Unit Quantities.....	24
3.1.3	Standard System Configuration .....	24
3.1.4	Excitation Scenarios .....	24
3.2	Concept of Additional Power Path .....	27
3.2.1	Modeling of Single Power Control Branch .....	29
3.2.2	Modeling of Power Branches in Parallel.....	35
3.2.3	Taking Saturation into Account.....	36
3.3	Adding a Control Filter .....	41
4	Control Design on Single Bus.....	47
4.1	Youla-based Design Method .....	47
4.1.1	General Approach – SISO Youla Parameterization .....	47
4.1.2	General Approach – MIMO Youla Parameterization .....	49
4.1.3	ITAE Coefficients.....	50
4.2	Applied Approach for Additional Power Path with Single Branch.....	53
4.2.1	Design of Controller .....	53
4.2.2	Order of Controller .....	55
4.2.3	Analysis of Controller Output .....	56
4.2.4	Robustness Analysis .....	60
4.2.5	Results.....	64
4.3	Applied Approach with 2 Branches in Parallel .....	69
4.3.1	Controllers Designed Independently .....	70
4.3.2	Controllers Designed Sequentially.....	75
4.3.3	Controllers Designed on MIMO-based Method .....	84
4.4	Conclusion on Single Bus Controller Design .....	92
5	Control Design on Multiple Buses .....	93
5.1	Concept of Master Controller .....	94
5.1.1	Locating the Master Controller.....	94
5.2	Distributed PD Controllers .....	95
5.2.1	Design of PD controllers .....	95
5.2.2	PD Controller as Slave Controller .....	96

5.2.3	Behavior on Step-Change Scenario .....	98
5.2.4	Behavior on Ramp-Change Scenario .....	102
5.2.5	Battery Model as Actuator for PD Controller .....	106
5.3	Actuator Models .....	107
5.3.1	WTG Pitch-Control .....	107
5.3.2	High Power Li-Ion Battery .....	108
5.3.3	Reduction Oxidation (Redox) Flow Batteries .....	118
5.4	Control at Load Bus.....	119
5.4.1	Load Bus Modeling.....	119
5.4.2	Results.....	120
5.5	Eigenvalue Analysis.....	123
5.5.1	Eigenvalues of Basic System .....	124
5.5.2	Eigenvalues of System with Master Controller and distributed PD Controllers.....	126
5.5.3	Conclusion of Eigenvalue Analysis.....	134
6	Test Bed System.....	135
6.1	Fundamentals .....	135
6.1.1	Newton Raphson Algorithm .....	135
6.1.2	Numerical Integration using Trapezoidal Rule and Newton Raphson Algorithm .....	137
6.1.3	Computation of Jacobian Matrix .....	139
6.2	Applied State Vector and Associated Functions .....	139
6.3	Simulation Program in MATLAB .....	140
6.3.1	Code Adaptation's.....	140
6.3.2	General Structure .....	141
6.3.3	System Matrices.....	142
6.3.4	Expanded Matrices from Additional Control.....	142
7	Discussion and Results.....	145
7.1	Simulation of Master Controller .....	145
7.2	Discussion of Master Controller .....	148
7.3	Master Controller with Additional PD Controllers .....	150
7.3.1	Simulation Scenario .....	150
7.3.2	Results and Discussion .....	150
8	Conclusions and Outlook .....	155

8.1	Conclusions.....	155
8.2	Outlook.....	156
A.	Further Aspects .....	157
A.1.	Standard Control Modeling.....	157
A.1.1.	Primary Frequency Control.....	157
A.1.2.	Secondary Frequency Control .....	158
A.1.3.	Results.....	158
A.2.	Order of Controller.....	159
A.3.	Results of Modified MIMO Design Procedure.....	160
A.4.	SAFT Capacitance Battery Model.....	164
A.4.1.	State-Space Representation of Battery Model .....	164
A.4.2.	2 Batteries in Series .....	164
A.4.3.	2 Batteries in Parallel.....	165
A.4.4.	Stacked Batteries in Series and Parallel .....	165
B.	Analysis Methods and Calculations.....	166
B.1.	Eigenvalues.....	166
B.1.1.	Expanded System State Matrix .....	166
B.1.2.	Eigenvalue Analysis for Parameter Sensitivity .....	167
B.2.	State Matrix $A_0$ and System TF $G_0$ .....	168
C.	MATLAB Program – Lucas Friedrich .....	169
C.1.	General Program Description.....	169
C.2.	Detailed .m-Files.....	169
D.	MATLAB Program – Matthias Gautschi .....	176
D.1.	General Program Description.....	176
D.2.	Detailed .m-Files.....	176
	Bibliography .....	181

## Overview

As an introduction to the report, a short overview of the content is given. The overall project was divided into two parts. In a first part through Chapter 4 the focus was set on a single bus in the network. In a second part, Chapter 5, the view was extended to multiple buses and other important aspects were studied.

- **Chapter 1:**  
The first chapter gives an introduction to the topic and a review of others authors work is presented.
- **Chapter 2:**  
In Chapter 2 the background to this research is explained and the project motivation is pointed out.
- **Chapter 3:**  
Chapter 3 deals with the system modeling and the concept of the additional power path.
- **Chapter 4:**  
The control design on a single bus is developed.
- **Chapter 5:**  
Chapter 5 deals with multiple bus control, actuator models and eigenvalue analysis.
- **Chapter 6:**  
A detailed description of the test bed system is given.
- **Chapter 7:**  
Chapter 7 gives a discussion of overall simulation results.
- **Chapter 8:**  
In the last chapter conclusions are made and an outlook is given.
- **Appendix A:**  
Findings and results not shown in the chapters before are presented.
- **Appendix B:**  
More information about calculations are given.
- **Appendix C and D:**  
The two MATLAB programs are introduced.

## List of Figures

Figure 2-1: Wind turbine generation configurations .....	11
Figure 2-2: Block diagram of classical frequency control [21].....	13
Figure 2-3: Bode plot of 1st order system .....	16
Figure 2-4: Control path .....	17
Figure 3-1: IEEE 14 bus test system.....	22
Figure 3-2: Block diagram for wind turbine bus.....	27
Figure 3-3: Implemented wind power generator model at bus 2 .....	27
Figure 3-4: Basic principle of additional power path .....	28
Figure 3-5: Additional power path .....	28
Figure 3-6: Single power control branch .....	29
Figure 3-7: System of additional power path with single power branch .....	30
Figure 3-8: Parallel power branches.....	35
Figure 3-9: Parallel power branches with saturation .....	36
Figure 4-1: Standard control system structure.....	47
Figure 4-2: Closed-loop system for controller design.....	48
Figure 4-3: Equivalent open-loop system.....	48
Figure 4-4: Closed-loop MIMO system .....	49
Figure 4-5: Equivalent open-loop MIMO system.....	50
Figure 4-6: Ramp responses of ramp optimized closed-loop TF for different orders $n$ .....	52
Figure 4-7: Step responses of ramp optimized closed-loop TF for different orders $n$ .....	52
Figure 4-8: Single branch of additional power path .....	53
Figure 4-9: Transfer function of basic system .....	53
Figure 4-10: Feedback system with expanded plant $G(s)$ .....	54
Figure 4-11: Control path for lower order $G(s)$ .....	55
Figure 4-12: Step responses of optimal closed-loop TF for different $w_n$ .....	57
Figure 4-13: Ramp responses of optimal closed-loop TF for different $w_n$ .....	57
Figure 4-14: 2 parallel power branches .....	69
Figure 4-15: 2 <sup>nd</sup> control system structure for controllers designed independently .....	70
Figure 4-16: 2 <sup>nd</sup> control system structure for controllers designed sequentially .....	75
Figure 4-17: System structure for controllers designed on MIMO-based method .....	84
Figure 4-18: Open-loop equivalent system .....	85
Figure 5-1: Concept of Master and Slave controllers.....	94
Figure 5-2: Influence of Master controller location .....	95
Figure 5-3: Additional power path with PD controller .....	96
Figure 5-4: Step response resp. Bode plot of PD control open-loop .....	97
Figure 5-5: PD control - instability case.....	98
Figure 5-6: Excitation characteristic for step-change scenario.....	99
Figure 5-7: Excitation characteristic for ramp-change scenario.....	102
Figure 5-8: Second order filter actuator system.....	107



Figure 5-9: Original SAFT battery diagram .....	108
Figure 5-10: Input-output convention of actuator model .....	109
Figure 5-11: Applied SAFT battery diagram .....	109
Figure 5-12: Block diagram of SAFT battery model .....	109
Figure 5-13: Bode plot comparison of single SAFT capacitance battery model and 2nd-order filter.....	111
Figure 5-14: Batteries connected in series .....	112
Figure 5-15: Batteries connected in parallel .....	113
Figure 5-16: Batteries stacked in series and parallel.....	114
Figure 5-17: Eigenvalues of basic system .....	124
Figure 5-18: Eigenvalues of basic system (zoomed in) .....	125
Figure 5-19: Standard eigenvalue properties and the system's characteristic region in the s-plane .....	125
Figure 7-1: Overall benefit of PD controllers .....	151
Figure 7-2: PD control damps local oscillations.....	151
Figure 7-3: PD control shows improved behavior on a step change.....	152
Figure 7-4: Higher oscillations at buses with no control .....	153
Figure A-1: Implemented primary freq. control at generator bus 3 .....	157
Figure A-2: Implemented primary and secondary freq. control at generator bus 1 .....	158
Figure A-3: Diagram of 2 SAFT batteries in series.....	164
Figure A-4: Diagram of 2 SAFT batteries in parallel .....	165
Figure A-5: Diagram of battery stack.....	165

## List of Tables

Table 3-1: Classes of disturbance signals .....	23
Table 3-2: Parameters of standard system configuration .....	24
Table 3-3: Simulation Results – Reference scenarios.....	26
Table 3-4: Simulation Results – Additional power path with single power branch .....	34
Table 3-5: Simulation Results – Two parallel branches with saturation .....	40
Table 3-6: Simulation Results – Two parallel branches with PI filters .....	46
Table 4-1: Simulation Results – Controller output for varying controller parameter $w_n$ .....	59
Table 4-2: Possible variations in system characteristics.....	60
Table 4-3: Robustness analysis for a change in inertia constant.....	61
Table 4-4: Robustness analysis for line trips .....	63
Table 4-5: Simulation Results – Single power branch with control.....	67
Table 4-6: Simulation Results – Controller output for varying actuator bandwidth.....	68
Table 4-7: Simulation Results – Two parallel branches with controllers designed independently.....	74
Table 4-8: Simulation Results – Controllers designed sequentially .....	80
Table 4-9: Simulation Results – Controllers designed sequentially with saturation.....	83
Table 4-10: Simulation Results – Controllers designed on MIMO-based method.....	90
Table 4-11: Controller design methods comparison.....	92
Table 5-1: Simulation Results – PD controller with step-change scenario .....	102
Table 5-2: Simulation Results – PD controller with ramp-change scenario .....	105
Table 5-3: Operating points of battery model.....	110
Table 5-4: Parameters of SAFT capacitance battery model .....	110
Table 5-5: Maximum power of single battery cell .....	112
Table 5-6: Simulation Results – SAFT battery model .....	117
Table 5-7: Simulation Results – Load bus with PD control.....	122
Table 5-8: Simulation Results – PD parameter variations .....	133
Table 7-1: Simulation Results – Master controller (designed sequentially).....	147
Table 7-2: System Configuration .....	150
Table A-1: Comparison between controller calculations .....	159
Table A-2: Simulation Results – Controllers designed on modified MIMO-based method .....	163
Table C-1: Details on .m-files .....	175
Table D-1: Details on .m-files.....	180

## List of Symbols

$\Delta \dots$	Change in ... (general)
$\zeta$	Damping ratio
$\theta_i, \delta_i$	Electrical angle at bus $i$
$\Lambda$	Matrix of eigenvalues
$\lambda_i$	Eigenvalue
$\sigma$	Real part of complex pole ( $s = -\sigma \pm j\omega_d$ )
$\tau$	Time constant [s]
$\Phi$	Vector of eigenvectors
$\Phi_i$	Eigenvector
$\omega_0$	Reference grid frequency (i.e. 377rad/s)
$\omega_c$	Crossover frequency [rad/s]
$\omega_d$	Imaginary part of complex pole ( $s = -\sigma \pm j\omega_d$ )
$\omega_e$	Electrical frequency [rad/s]
$\omega_i$	Frequency at bus $i$ [rad/s]
$\omega_{i,meas}$	Measured frequency at bus $i$ [rad/s]
$\omega_m$	Rotational speed of generator/machine, mechanical frequency [rad/s]
$\omega_n$	Natural frequency [rad/s]
$\omega_n$	Parameter used for controller design, representing speed of reaction of closed-loop performance
$A(s)$	Actuator transfer function
$\mathbf{A}$	System state matrix
$\mathbf{A}_0$	Basic system state matrix
$\mathbf{A}_s$	State matrix of additional control
$\mathbf{B}_0$	System input matrix
$\mathbf{B}_s$	Input matrix of additional control
$C(s)$	Controller transfer function

$C_i$	Capacitance [F]
$\mathbf{C}_0$	System output matrix
$\mathbf{C}_S$	Output matrix of additional control
$D_i$	Damping constant
$d_G(s)$	Denominator of TF $G(s)$ (general)
$\deg(\dots)$	Order of ... (general)
$E$	Rotational kinetic energy [J]
$e$	Error signal
$G(s)$	Transfer function (general, not necessary G) Transfer function of plant
$\mathbf{G}, \mathbf{G}(s)$	Transfer function matrix (general, not necessary G)
$G_0(s)$	Transfer function of basic power system
$H_i$	Inertia constant [s]
$H(s)$	Desired closed-loop transfer function of controller
$\mathbf{I}$	Identity matrix
$\mathbf{I}_n$	Identity matrix of dimension $n$
$J$	Moment of inertia of a machine [kg m <sup>2</sup> ]
$\mathbf{J}(\mathbf{x})$	Jacobian matrix
$k$	Gain
$k_D$	Derivative gain
$k_I$	Integral gain
$k_P$	Proportional gain
$M(s)$	Measurement system transfer function
$M_i$	Inertia factor ( $= 2 \cdot H / \omega_0$ )
$n_G(s)$	Numerator of TF $G(s)$ (general)
$P$	Real power [MW]
$P_{add,i}$	Power of additional power path at bus $i$ [MW]
$P_e$	Electrical power [MW]
$P_l$	Power of load [MW]

$P_M$	Mechanical power set point [MW]
$P_m$	Mechanical power [MW]
$P_t$	Power of tie-lines [MW]
$p$	Number of pole pairs
$Q$	Reactive power [VAR]
$R_i$	Resistance [ $\Omega$ ]
$r$	Reference signal
$S$	Complex power [MVA]
$T$	Time period [s]
$u$	Input signal
$V_i$	Voltage magnitude [V]
$\mathbf{x}$	State vector of basic system
$\mathbf{x}_f$	State vector from 1 <sup>st</sup> order differential equations ( $\dot{\mathbf{x}}_f = \mathbf{f}(\mathbf{x}_f)$ )
$\mathbf{x}_g$	State vector from algebraic equations ( $\mathbf{0} = \mathbf{g}(\mathbf{x}_g)$ )
$\mathbf{X}^\dagger$	Pseudo-inverse of matrix $\mathbf{X}$
$\mathbf{X}^T$	Transpose of matrix $\mathbf{X}$
$y$	Output signal
$\mathbf{z}$	State vector of additional control implementations

## List of Acronyms

AGC	Automatic Generation Control
DFIG	Doubly Fed Induction Generator
DG	Distributed Generation
EV	Eigenvalue
FOC	Field Oriented Control
HVDC	High-Voltage Direct-Current
IEEE	Institute of Electrical and Electronic Engineers
LHP	Left Half Plane
LQR	Linear Quadratic Regulator
MIMO	Multiple Input Multiple Output
MPSG	Multi Pole Synchronous Generator
PCC	Point of Common Coupling
PD	Proportional and Derivative control
PHEV	Plug-in Hybrid Electric Vehicle
PI	Proportional and Integral control
PMSG	Permanent Magnet Synchronous Generator
p-p	Peak-to-Peak
PSS/E™	Power System Simulator for Engineers
pu	Per Unit quantity
PV	Photo Voltaic
RES	Renewable Energy Source
RHP	Right Half Plane
SAFT	SAFT Batteries SA
SCIG	Squirrel Cage Induction Generator
SISO	Single Input Single Output
TF	Transfer Function
V2G	Vehicle to Grid concept
WRIG	Wound Rotor Induction Generator
WTG	Wind Turbine Generator

## 1 Introduction

### 1.1 Today's Power Systems

The ever-increasing demand for electrical energy must be addressed by developing innovative and sustainable solutions in the area of electricity generation and electricity transfer. Today's power generation is still mainly based on coal, gas and nuclear, however, in order to meet global targets for reduction of carbon dioxide, renewable energy sources (RES) are going to expand rapidly. World renewable-based electricity generation - mostly hydro and wind power - is projected to more than double its share of total electricity output rising from 18% in 2006 to 23% in 2030. Renewables are predicted to overtake gas to become the second-largest source of electricity, behind coal, before 2015. [1]

In particular wind power is seen as the most promising renewable energy source. The potential for wind energy generation is vast and constant advances in technology as well as the relatively low capital costs (compared to other RES) make it additionally attractive. Governments all around the world support wind power and are making large efforts to increase their stake in electricity generation. Led by the main contributors of wind energy such as USA, Germany, Spain, China and India, wind power's global output is projected to increase eleven-fold, becoming the second-largest source of renewable electricity after hydro power by 2010. The world total installed wind capacity in 2008 has been 121 GW and is expected to be 152 GW by the end of 2009, what corresponds to a growth rate of 25%. [1], [2]

The increasing penetration of renewable energy carriers implies on the other hand major challenges in many technical issues, including power quality, reliability, and security as well as other, non-technical issues. These challenges are related to the fluctuating nature of renewable energies as well as the upcoming new generation systems, used for RES. Generators that are integrated to the electrical grid through power electronic-based converters differ significantly from the conventional generator types, particularly in terms of their impact on electromechanical stability. The inertia of synchronous machines plays a significant role in today's power systems in order to stabilize the grid frequency during a transient situation. The inertia contribution of wind turbines, for instance, is much less than that of conventional generators.

Consequently, a change in generation systems needs to be considered carefully concerning its effect to electrical frequency stability, a crucial criterion for power reliability.

This work faces these challenges and proposes possible solutions for control techniques that enable greater integration of renewable energy sources, in particular wind energy. Control structures are designed taking into account internal and external power sources. Their benefits in grid stability and performance are shown in this work. [1], [3]

## 1.2 Initial Motivation

There were several reasons for setting up this research project in the area of integrating renewables into the electrical grid.

Our educational background – we both have the Bachelor of Science in Electrical Engineering and were both continuing with the Masters of Energy Science and Technology at ETH Zurich – built the base, but then the most important factor was our interest. Our Masters program – a new introduced Masters program at ETH Zurich – gave us the opportunity to still focus on our core subjects from the Bachelor level but furthermore let us get a broader look on energy related topics. There is not only technology behind making energy accessible - it's definitely an important part - but there is a big influence coming from politics and the economy. In order to make research in the area of energy, one should keep that in mind.

As described in the previous chapter, today's situation in power systems is rapidly changing. The integration of wind energy into the electrical grid is getting a crucial challenge for today's power engineers and is consequently one of the most treated areas in research at the moment. Being part of this research and the ongoing progress, with the knowledge received from our studies, made this work particularly interesting. The work consisted of reviewing literature, programming, simulating, analyzing and discussing, and could hence exactly offer what two master students expect and can contribute best within such a research project.

Prof. DeMarco told us that with the new elected administration of President Obama, the renewable energy sector was boosted significantly throughout the USA and the integration of renewables into the electrical grid would be an interesting area of research. In collaboration with other universities under the project of the Power System Engineering Research Center (PSERC), the power systems engineering faculty, within the Department of Electrical and Computer Engineering at UW Madison itself has begun expanding its focus on this area and hence our work will help to give a new incentive here.



We want to contribute to a more sustainable and cleaner way of producing energy. It is everyone's responsibility to deal with the world's resources sustainably and reduce the carbon dioxide emissions in order to ensure an environmentally friendly future. With this work we hope we can make a contribution.

### 1.3 Project Organization

The research project was initially set up with Prof. DeMarco and Prof. Lesieutre from UW Madison with the final approval of Prof. Andersson from ETH Zurich. All sides agreed upon the topic of our research project and so we started to set up a project description (given at beginning of thesis).

The Research Project is divided into two parts. In a first part of the project, we both worked on the main goal: Developing advanced grid stabilization for inverter connected renewable energy sources. For this part, the performed tasks were the same. We decided that each student develops his own simulation tools with the intention that the use of two differently designed simulation tools allows good comparison of the performed simulations and helps to find resp. avoid failures in the simulation results and their interpretations. Further on, the findings of each of us often varied and so they offered a good basis for our regular discussions with Prof. DeMarco.

Obviously it is hard to predict the outcome of a research project from the beginning and so initial goals or procedures were redefined throughout the project phase. Initially we planned to work in a first part on the system modeling of our test bed system and in a second part each of us would focus on different individual aspects contributing to the same overall project. As a result we would have written two individual Master Theses within one research project. However, as the work continued, two clear different directions did not emerge and therefore we continued working together. Different aspects were focused in more detail by one or the other, but always in consultation with each other in order to fully understand and verify the findings. So in the end we decided with the approval from Zurich to only hand in one Master Thesis for both of us.

Our research work was always mainly influenced by all three parties: We, the two students and Prof. DeMarco within the scope of our weekly meetings. The findings were intensively discussed, evaluated and verified and the meetings always turned out to be very productive and progressing. Additionally, we regularly had email contact with our assistant at ETH Zurich, Mr. Spyros Chatzivasiliadis, in order to fulfill the expectations from our "home" institute.

*For the complete project we want to adhere, that the work presented in this report has been worked out together by both students in equal amounts.*

## **1.4 Related Work**

As introduction to the project a literature review is given and the most relevant papers are cited hereafter.

### ***Inertial Response***

Research on inertial response of power-converter connected wind turbines was found to come from mainly two groups of researchers. One group is a team among J. Morren from TU Delft in the Netherlands and the other group is among A. Mullane from UCD Dublin in Ireland.

The group of Johan Morren et al. has faced different topics in the distributed generation (DG) area. Within the problem of frequency control the inertial response is discussed in a paper [4] from 2005. Two different additional control loops have been evaluated and it has been shown that both limit the drop in frequency after a disturbance.

The second group of researchers, Alan Mullane et al., faces the problem of inertial response of power-converter connected wind turbines in several papers. In a first paper [5] from August 2005, the inertial response of induction-based wind turbines has been analyzed. The authors come up with an equivalent model for a Field-Oriented Controlled (FOC) Doubly Fed Induction Generator (DFIG) that is used to analyze the inertial response. It was found that the inertial response of a DFIG employing FOC depends on the bandwidth of the rotor current controllers. Unlike other authors reporting complete decoupling of the DFIG, they have found that complete decoupling will only occur for large current-controller bandwidths.

In a further paper [6] from November 2005, the stored kinetic energy of a tidal power system and a wind power system is determined and a comparison of their inertial responses is made. The tidal energy device was found to have lower stored kinetic energy. A modified controller for the DFIG was suggested that results in an inertial response that exceeds the response of a classical synchronous generator.

Another paper published in 2005 [7], concludes that unlike with fixed-speed wind turbines, DFIG wind turbines replacing synchronous generators reduce the frequency nadir after a loss of generation, be-

cause of negligible inertial response of DFIG wind turbine generators. In that paper a supplementary control loop is proposed, that achieves inertial responses similar to synchronous generators.

In 2006 two other papers have been published in this area. The one [8] goes more into detail of modeling the wind turbines for grid integration studies. In the other paper [9], it is shown that through the addition of a supplementary control loop an inertial response characteristic can be added to wind turbines. The implementation of such an additional control loop results in an improved inertial response of a wind turbine.

### ***Frequency Control with Renewable Energy Sources***

A more generalized view on frequency control is given in a paper [10] from J. Morren in 2005. The DG contribution to primary frequency control is discussed and the conclusion was that a mix of different DG types is needed, because primary frequency control possibilities of some DG units show complementary characteristics.

In 2006 another paper [11] has been published about emulating inertia and supporting frequency control of DG sources. Additional control paths have been described and tested in a 2 generator test system, and the conclusion was that by adding these additional loops variable speed wind turbines are able to support primary frequency control and to emulate inertia.

In the same year a paper [12] discussed fuel cells as another inverter connected source. A network with one classical generator, one wind turbine and one fuel cell was discussed and they came up with the conclusion, that fuel cells can be used in a later period of primary frequency control. In a first period the kinetic energy of wind turbines should be used to support primary frequency control.

Two further papers, [13] and [14], describe the integration of wind power into the transmission grid and arising issues as frequency control with such generation units.

### ***Modern Control Design for the Wind Power Application***

A. Wright describes modern control design methods in his doctoral thesis [15]. Modern control design methods are applied to the wind power application. New developed modern control designs were compared to classical control designs and it was concluded that actuator speed has a significant impact on the selection of control design. Modern control design benefited from fast actuators, whereas PI based control proofed more compatible with a slow actuator. This thesis offers a broad set of models for wind power generation systems.

***Energy Storage for Renewable Energy Systems***

A. Nasiri describes in two papers, [16] and [17], energy storage systems for solar PV systems and for wind turbine systems. A system configuration of a PV-cell, a storage battery and power electronic converters is proposed and evaluated for different operation principles. The storage system used is a Redox flow battery. Simulations of the system and the implementation of a low power version were successful.

The modeling of a battery energy storage system (BESS) is discussed in [18]. A centralized control strategy is presented to smooth output power fluctuations of wind power applications.

In another paper [19] a fuel cell system connected to a nonlinear load is evaluated. Interesting aspects of how to model a fuel cell and a battery are given. Time constants of the actuator systems have been determined in numerous tests.

The use of supercapacitors for the wind power application is covered in [20]. The supercapacitors are used to smooth the wind power fluctuations caused by wind speed variations. Results show a significant improvement of the wind turbine power output. The conclusion is that supercapacitors could be very valuable for future wind power applications.

## 2 Background and Motivation

In Chapter 1 an introduction into today's power systems is given and the general goals of this project are described. In this chapter, background and motivation are pointed out more extensively. Aspects like inertial response, frequency control, bandwidths in power systems and limitations are explained in more detail and it is described how they contribute to the motivation of this project.

### 2.1 Inertial Response

Disturbances in an interconnected power system lead to frequency deviations in the grid. The period immediately following a disturbance, the frequency deviation is primarily characterized by the amount of inertia in the system. This initial reaction of the power system to a disturbance is called inertial response of the system. It can be described as a stabilizing effect in response to a change from the equilibrium condition in the power system. Such an inertial response has long been treated as given in power systems due to the prevalence of synchronous generators. But with the increasing penetration of renewable energy resources, often connected to the grid through power electronic devices, the overall inertial response of the system is decreasing.

To what extent renewable energy sources provide an inertial response is discussed in papers [4]-[9], already mentioned in Chapter 1. The conclusion from these papers is that RES which are not completely direct connected to the grid have little inertial response and full inverter connected sources do not have any inertial response. This conclusion endorses the statement of the general decrease in systems inertial response from additionally installed RES.

To preserve the positive effect of inertia on power systems stability, ways have to be found to allow for an inertial response also from inverter connected RES. Mimicking inertia is the concept coming along with this aim. Mainly the two research teams mentioned before have focused on the concept of mimicking inertia.

#### 2.1.1 Concept of Mimicking Inertia

Mimicking inertia refers to the idea that with additional control an inertial response can be mimicked for inverter connected and therefore in fact from the grid decoupled systems. This mimicking of inertial response for renewable energy sources allows preserving the positive stabilizing effect in power systems also with an increasing share of renewable energy sources.

The initial gradient of the frequency deviation resulting from a disturbance is characterized by the system's inertia. Hence inertia is linked to the derivative of system frequency and in order to mimic an inertial response, the additional control has to be based on the derivative of the system frequency.

Inspired from papers described before, the first idea of this research project was to extend and further develop the mimicking inertia approach. In literature, simulations concerning mimicking inertia are based on simple bus networks for the most part. Therefore one of the first steps of this project was to reproduce and confirm results, presented in literature, in a larger and more accurate grid system.

In a first step, the concepts from literature of additional control and mimicking inertia were reviewed and implemented in our test bed system. The used concepts are described in more detail in the modeling part of Chapter 3.

## 2.2 Generation Units

In the following sections, generation systems are reviewed that are used in this work.

### 2.2.1 Classical Synchronous Generator Systems

Classical power plants are equipped with synchronous generators. Today, these conventional power plants accomplish the frequency control described later on. What is unique with synchronous generators, is their inherent inertial response. Immediately after a drop in grid frequency the generator system will release kinetic energy from its rotating mass. The rotational kinetic energy stored in the rotating mass can be written in terms of moment of inertia at the machine  $J$  and rotational speed  $\omega_m$ .

$$E = \frac{1}{2} J \omega_m^2 \quad (2.1)$$

The so called inertia constant  $H$  describes then the characteristic of the inertial response.

$$H = \frac{J \cdot \omega_m^2}{2 \cdot S} \quad (2.2)$$

The constant has dimension time and describes how long it would take to bring the machine from synchronous speed to standstill, if rated power were applied as braking torque and the mechanical power inflow to the turbine was cut off. Typical values for inertia constants of large power plants are in the range of 1 - 10sec [21]-[23]. As the name indicates, synchronous generators operate in synchronism and

therefore their rotational speed is strongly coupled to the grid frequency. This strong coupling leads to the described inertial response of the turbine-generator system.

$$\omega_m = \frac{\omega_e}{p/2} \quad (2.3)$$

Using electrical angles the so-called swing equation describes the dynamic characteristics of the synchronous generator. The swing equation represents the model of a synchronous generator used for grid studies.

$$\frac{2H}{\omega_0} \frac{d^2\theta}{dt^2} = \frac{2H}{\omega_0} \frac{d\omega}{dt} = M\dot{\omega} = P_m - P_e \quad (2.4)$$

### 2.2.2 Wind Turbine Generator Systems

As an example for the fast growing share of renewable energy sources, wind power is definitely one of the most widely deployed technologies. The focus of this research project will therefore be laid on wind turbine generator (WTG) systems.

Today a range of technologies for wind power generation systems exist. The technologies can be divided into two groups: fixed speed and variable speed wind turbine generator systems. The most common system configurations are described here. [3]

- **Fixed Speed (Type A)**

Fixed speed wind turbines were typically installed 3 - 10 years ago. As the name indicates, they are rotating at a fixed speed.

- **Squirrel Cage Induction Machine (SCIG)**

This fixed speed design uses a Squirrel Cage Induction Machine directly connected to the mechanical system of the wind turbine to convert mechanical energy into electrical energy. In this configuration there is a strong coupling between the generator stator and the power system. Due to that strong coupling and the low nominal slip of 1-2%, any system frequency deviation will result in a change in rotational speed. This change in rotational speed is the inertial response of the wind turbine system.

- **Variable Speed (Type C and D)**

Variable speed wind turbines are used most commonly today. By regulating their rotational speed, power production can be optimized according to the actual wind speed.

- **Doubly Fed Induction Generator (DFIG)**

Both stator and rotor of the machine are connected to the grid. The stator is directly coupled with the grid and the rotor is connected through an AC-DC-AC back-to-back converter to the grid in order to control the rotational speed of the machine. In this configuration inertial response will only be observed, if the converter control is fairly slow. With controllers used in modern wind turbines, with response times in the range of milliseconds, negligible inertial response will be obtained.

- **Multi-Pole Synchronous Generator (MPSG)**

In this configuration, an AC-DC-AC back-to-back converter is directly connected to the stator of the synchronous machine. This allows variable speed operation, but because the stator is isolated from the grid, no inertial response is inherently obtained from the generator system.

Generator system configurations of type B, not mentioned above, refer to limited variable speed configurations not widely used anymore. In our work, we focus on the variable speed wind turbine configurations. As in these configurations the wind turbine system is fully or at least partly decoupled from the grid through a power electronic device, these systems have no or very small inertial contribution to the grid.



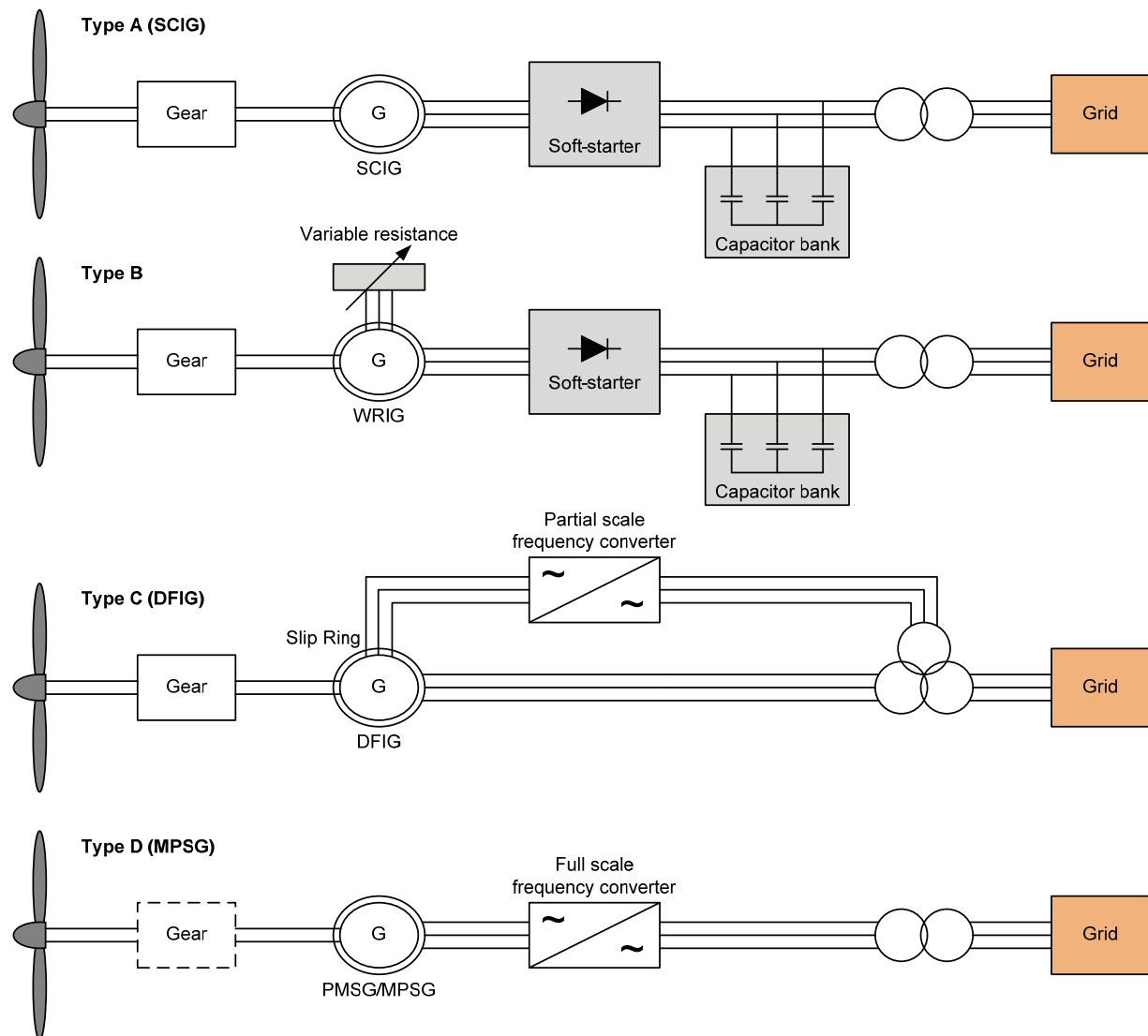


Figure 2-1: Wind turbine generation configurations

## 2.3 Frequency Control in Power Systems

The frequency in power systems represents the balance between generated power and demanded power. In normal operation small load variations occur spontaneously. In addition, more severe power imbalances might occur from power plant outages or line tripping and result in larger frequency deviations. In order to avoid these large deviations and secure a stable electrical grid, a frequency control mechanism must be implemented in power systems.

Besides these classical disturbances affecting frequency stability, in more and more deregulated power systems, conditions imposed by market-mechanisms affect the system additionally. In [24] the influence of market dynamics on the stability of interconnected power systems is analyzed and it is concluded that these dynamics significantly affect the design of control in power systems. With these findings in addition, proper frequency control becomes again very important in today's power systems.

In the following sections classical frequency control mechanisms are reviewed shortly. As described in Section 2.1, in a first, immediate phase following a disturbance, the frequency deviation is dependent on the total inertia  $H$  of the system and the damping, described with the damping constant  $D$  [21]. The inertial contribution is inherently provided by classical generators in power systems and no control is activated within this phase. In a next phase after a disturbance as soon as the frequency exceeds a pre-defined threshold value, a control mechanism is activated, denoted as primary frequency control.

### ***Primary Frequency Control***

Conventional power plants usually have installed primary frequency or droop controllers. These controllers regulate the amount of power flowing to the prime movers. Between droop control activation and the physical contribution a certain filtering occurs. This filtering in physical reaction arises from the turbine system. For instance, considering a steam turbine with reheating the time constant of the turbine system is in the range of several seconds. [21], [25]

### ***Secondary Frequency Control***

In order to bring the system frequency back to the equilibrium value (i.e. 60Hz in the US) an integral controller needs to be implemented in the system additionally. The integrating characteristic brings the frequency back to its nominal value. Historically, integral controllers were installed only on a single "master" generator to avoid interferences with other generators. Today, a single area-wide integral control correction may be shared via automatic generation control (AGC).

An overview of the described frequency control mechanisms is given in the block diagram below. [21]

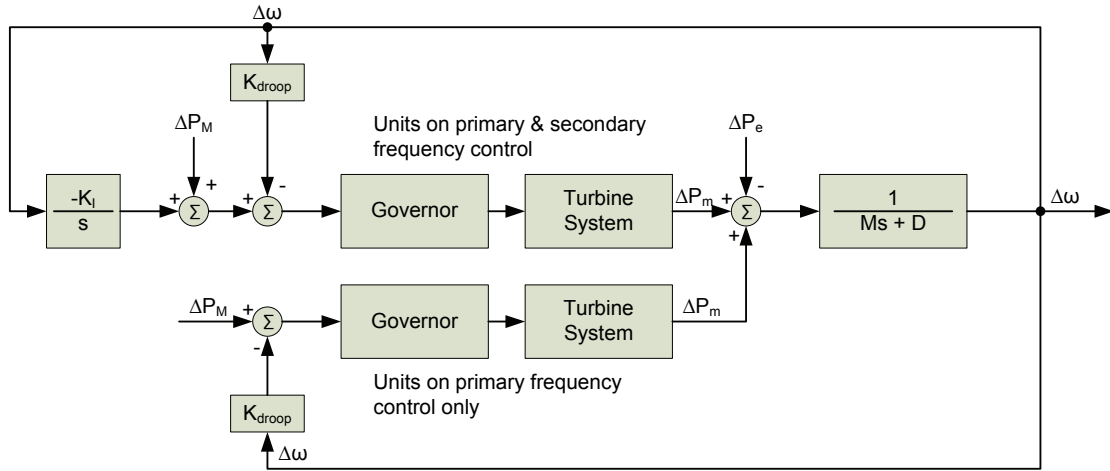


Figure 2-2: Block diagram of classical frequency control [21]

The described frequency control installed on classical synchronous generators represents the actual situation in today's power systems. Control is performed by varying power at the turbine system itself. That is reasonable for power plants with synchronous machines, but how to deal with a wind power plant that is neither flexible in controlling power nor offers inertia due to the inverter structure? Additional storage devices could deliver the missing power for frequency control and act as "virtual inertia". The following sections take a closer look at these issues of non classical frequency control with inverter connected energy sources.

## 2.4 Concept of Balancing System through Adding Power

As seen before, the purpose of frequency control is to regulate the frequency very close to a constant level (i.e. 60 Hz in North America) and that is associated with keeping the generated and consumed active power in balance. Outside of new upcoming concepts that consider load management, frequency control is mainly performed by constantly aligning generated power at selected units. Depending on whether the system frequency is above or beneath the steady-state value (i.e. 60Hz) either positive or negative power has to be fed into the system in order to bring the frequency back to its steady-state value. Assuming for example a loss of a load anywhere in the system, the frequency will consequently increase and a negative power increment will be required, meaning that the generated power needs to be reduced.

Renewable energy sources, as for example wind power, typically do not contribute to frequency control today. But as shown in literature [10]-[14] there are concepts that make a contribution to frequency control from inverter connected energy sources possible.

Making wind energy more constant and reliable is one of the major goals in research currently. The approach introduced in this work should help finding suitable solutions.

The approach of this work is to enable and to control the access of additional power to renewable energy generation buses, like wind power buses, in order to contribute to frequency control. The additional power can either come from internal sources or external sources and the feed-in point to the system can vary.

#### **2.4.1 Additional Power from Internal Sources**

Classical generators have a control system that allows adjusting the power set-point of the prime-mover, the input to the turbine. On selected units, this concept is used to regulate the electrical power output of the generator in order to participate in frequency control. This is the classical example of an internal source widely used in today's power systems.

Since inverter-connected renewable energy sources do not contribute to frequency control so far due to their fluctuating characteristics (e.g. wind power) or their small amount of power (e.g. solar power), renewable energy generation systems are normally operated at their maximum power output.

WTG systems are kept at an operating point that allows the extraction of maximum power. Usually they reach rated power at a wind speed of between 12-16 m/s, depending on the type of wind turbine. At wind speeds higher than the rated wind speed, the power production is limited and so not all available primary energy can be generated. The cut-out wind speed, defining where the wind turbine stops its production, is in the range of 20-25 m/s [3]. The described regulation of output power for wind turbines is achieved with pitch- or stall-control. The pitch of the blades is adjusted to keep the rotational speed of the blades in a certain range in order to maximize the power production. This mechanism is comparable to the adjusting of the prime-mover set-points in classical generators and so it might be applicable for frequency control as well. The practical implementation, on the other hand, is not as trivial. The lack of reliability of wind power makes an adequate frequency control with pitch-control rather inapplicable. However, considering an aggregation of many wind turbines and applying a more global approach for pitch-control might increase reliability and could make pitch-control an adequate instrument for frequency control. Further aspects of pitch-control are considered in more detail later on. For now, pitch-control - the control of the wind turbine blades – is viewed as one component that can be used for frequency control making use of the inherent power source.

Two other concepts, making use of internal sources that are recently found in literature need to be mentioned as well: Taking additional resp. supportive power from DC-link capacitances of converter structures of the WTG System itself seems to be one promising approach to reduce output power fluctuations [26]. The other similar approach [27] uses the rotor inertia as an energy storage component to mitigate output power fluctuations.

#### 2.4.2 Additional Power from External Sources

Another approach of feeding the system with additional power in order to keep it in balance is taking it from external sources. Plenty of research studies can be found in literature [16]-[20] that deal with external storage devices for additional power support. Fast and flexible storage devices such as fuel cells, supercapacitors, flywheels and batteries can be implemented and may bring a significant benefit to the operation of today's power systems.

If one considers for instance an offshore-wind-park as a generator bus, additional external power sources that are fed-in at the Point of Common Coupling (PCC) can help improving the energy reliability and security of the wind park. One advantage is that the auxiliary power can be installed flexibly at a central place and need not to be added to the WTG system itself.

The transition from gasoline powered vehicles to battery powered electric vehicles is becoming real in the near future and is creating many opportunities as well as challenges for today's power systems. Car batteries are therefore another possible upcoming external source. The Plug-in Hybrid Electric Vehicle (PHEV) combined with the concept of Vehicle-to-Grid (V2G) is a very active research topic and first test systems have already been installed in Europe [28]. If one thinks of a car park with about 100 plugged-in cars whose batteries are all connected together, the car park would represent a considerable additional electrical storage possibility for the electrical grid. Adequate control designs would then enable supporting grid frequency control and appropriate load management.

### 2.5 Bandwidth

An important property of a control system is its bandwidth. The bandwidth characterizes how fast a system is able to react on imbalances and is defined by the crossover frequency  $\omega_c$ . In the case of a simple first order system, bandwidth can also be represented with a time constant  $\tau$  that may be more intuitive if one considers the speed of reaction.

$$\omega_c = \frac{1}{\tau} \quad (2.5)$$

Pitch-control for example is a system with a low bandwidth. This is based on the fact that the position of a large blade needs time to be adjusted. Blades of a wind turbine have a large inertia (associated with its size and mass) and so they cannot be adjusted as quickly as desired. A time constant  $\tau$ , of 2 - 3sec seems to be appropriate for modeling the pitch-control actuator. This is equivalent to a crossover frequency of  $\omega_c = 0.3 - 0.5$  rad/s.

The crossover-frequency describes the transition point where the magnitude gains. In terms of a first-order filter model, defined as

$$A(s) = \frac{1}{\frac{s}{\omega_c} + 1} = \frac{1}{\tau \cdot s + 1} \quad (2.6)$$

the low frequencies, below  $\omega_c$  are passed with near unity gain, but the high frequencies above  $\omega_c$  are attenuated. A typical Bode plot for a first-order filter is depicted in Figure 2-3 ( $\tau = 2s$ ,  $\omega_c = 0.5$ rad/s).

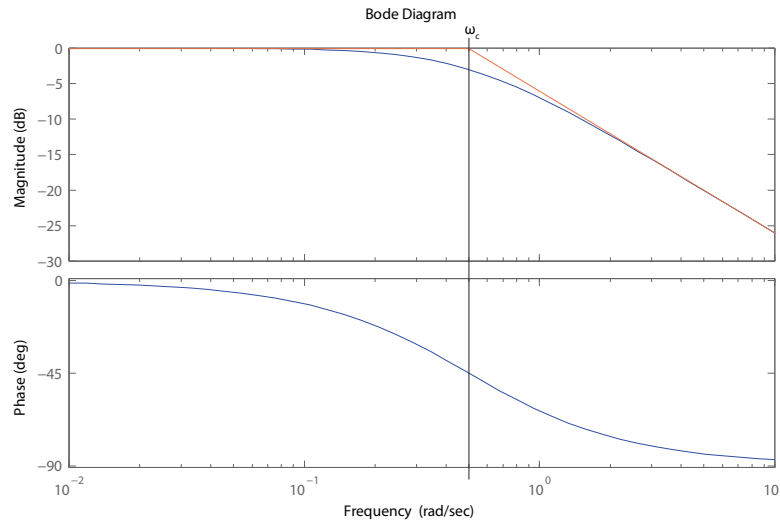


Figure 2-3: Bode plot of 1st order system

In contrast to the pitch-control system, a battery provides an example of a system with a very high bandwidth. As shown later in this work, batteries have very fast reaction times and therefore very high bandwidths.

From an idealized control design perspective, control systems with actuators of high bandwidth yield advantages and are preferable. However, physical limitations and cost play often an important role in control design; e.g. for a battery, the amount of energy is obviously quite limited. These kinds of limitations are treated in more detail in the next section.

An additional control path consists of a controller followed by an actuator system in series that represents the physical characteristics of the system providing the additional power.

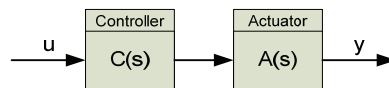


Figure 2-4: Control path

The controller and the actuator are both characterized by a certain bandwidth. The bandwidth of the controller is an important parameter that can be manually adjusted by the designer. The bandwidth of the actuator, on the other hand, is given from the physical properties of the device.

The overall control loop bandwidth is dominated by the lower bandwidth that can either come from the controller or the actuator. Typically, the controller bandwidth allows very fast reaction and so the limiting factor is the actuator with its bandwidth and its physical limitations, such as power output or energy storage (described in the next section). The adjustment of the controller bandwidth is flexible and needs to be aligned with the actuator. It is a crucial parameter in terms of performance and stability of the overall system.

## 2.6 Limits and Saturation

Actuator systems are described by their physical capabilities and it is important to deal with associated limitations properly. Besides their limitations of bandwidth described in the previous section, two other limitations have to be considered very carefully: The individual physical power limit as well as the energy storage of the actuator system.

Storage devices from external sources and internal sources have such limits. The power range of a pitch-control system for instance can be considered as quite limited depending on the operating point of the wind turbine, the wind speed and the numbers of wind turbines contributing to pitch-control. In any case, a WTG system that is used for frequency control needs to reduce its rated output power and needs to provide a certain power range for frequency control. This results in a lower harvest of available wind by the WTG system.

Energy limits do not really seem to be an issue for WTG systems because wind is an unlimited source. On the other hand, wind power can also drop out completely if no wind is blowing or the turbine has to be shut down due to heavy wind. These two scenarios result in a complete loss of the actuating system and consequently the control system.

Batteries have very limited power outputs and energy storage capabilities in relation to the power magnitudes of the electrical power grid. On the other side, batteries have a very fast reaction and so they can be used for supportive control action within a small time period but can not compensate large power changes over extended time periods, as in case of an outage.

An interesting point is that in general a certain correlation between bandwidth and limitation can be observed. A rule of thumb seems to be that actuator systems with a high bandwidth usually have tighter power and energy limits and actuators with a lower bandwidth have broader limits. We mentioned before that from a control point of view fast actuator systems are preferable. However, they are hardly associated with a generous power output and so a combination of systems with high and low bandwidth may offer a suitable approach for an appropriate control design. The general design philosophy is that the fast system with high bandwidth contributes to frequency control in the first moment after a disturbance and the slower system with a relatively low bandwidth compensates for slower time scale, larger magnitude changes of power.

## **2.7 Motivation for Grid Stabilization Control and Frequency Regulation**

Making sustainable energy power generation such as wind power generation more reliable and applicable for today's power system is one of the main motivations of our work here.

The enormous development in wind generation and the tremendous rise of wind power as one of the leading renewable energy sources for satisfying the still-increasing demand for electrical energy leads to the motivation of finding new, sustainable and stable ways of integrating wind power into the electrical grid. The big challenge of controlling the fluctuating power characteristic of wind needs to be further addressed and research effort needs to keep on track for reaching this goal. The potential is vast and the technology for it already exists.

Our approach with this work deals in particular with a control design that includes additional power from internal and external sources. Our goal is to use power sources with different bandwidths (i.e. very



fast, fast and/or slow reacting characteristics) that can be implemented into one control concept and can so offer certain flexibility in control action.

As introduced in the sections before, developing a concept of implementing additional power sources with different bandwidths as well as with individual limitations into one control design that supports frequency control with inverter connected renewable energy sources such as wind power, is the objective of this work. In particular the saturation characteristics need to be addressed and a way of how to deal with these limits in a control design have to be found.



### 3 System Modeling

A first goal of this project is to mimic an inertial response for improving stability of integrating inverter connected RES into the electrical grid. As mentioned before the focus is hereby set on WTG systems. If a wind generator system with a DFIG is considered, the inertial response is very limited or negligible, as mentioned in Chapter 2.

Before starting with the system modeling, a suitable test bed system has to be determined in order to develop reference scenarios and conduct adequate simulations.

#### 3.1 IEEE 14 Bus Test System

Simulations and results presented in this work are based on the data and topology of the IEEE 14 bus test system. The IEEE 14 bus test system represents a 14 bus power system with 5 generator buses and 9 load or transfer buses. Certainly one could think of using more complex or simpler networks, but for initial simulations this size of model provides a good trade-off between a representative system and a manageable simulation effort. Therefore the use of the 14-bus test system, representing a small electricity grid, seems to be a reasonable choice.

In Figure 3-1 a single line diagram of the test system is given. The buses 1, 2, 3, 6 and 8 represent the generator buses. The other buses represent load buses. In this work bus 2 and 8 are assumed to represent those buses with wind power generation systems.

For simulations of the IEEE 14 bus test system, MATLAB is used as software tool. The functionality of our MATLAB program is then explained in detail in Chapter 6.

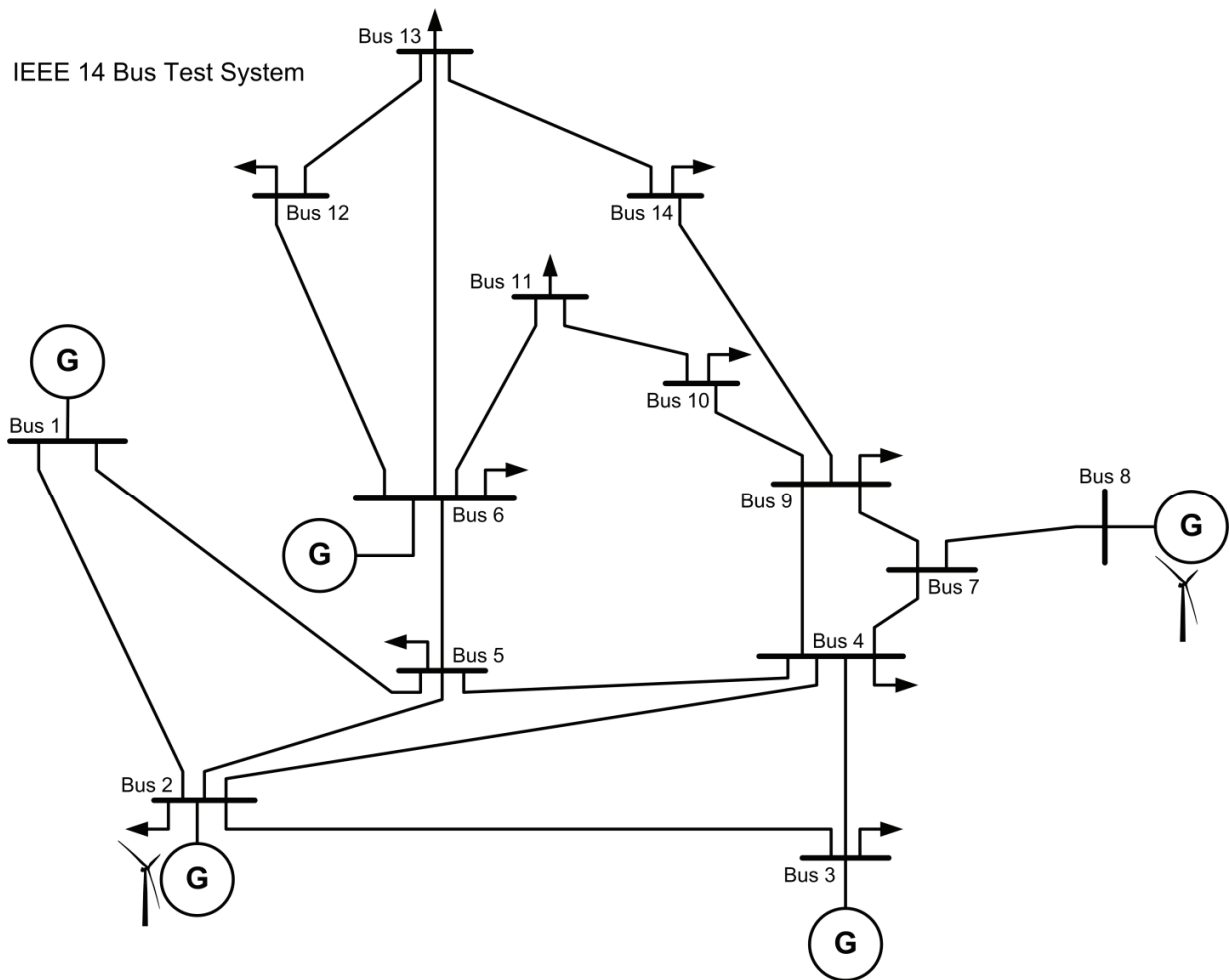


Figure 3-1: IEEE 14 bus test system

### 3.1.1 Classes of Disturbance Signals

A power system is a large interconnected system with many sources of disturbances. Our focus here will be on disturbances representing variation in injected (or demanded) power; such variations may display a wide range of time waveforms characteristics in a realistic power system. For analytic tractability using the control system design methods to be described here, standard classes of disturbance signals are employed. While much more limited than the full range of possible behavior, these provide useful benchmarks to help judge the quality of a controller's frequency regulation, and stability of system response. These test signals are illustrated in Table 3-1.

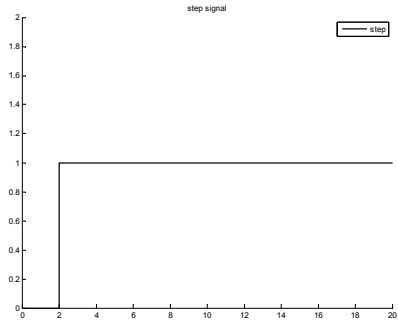
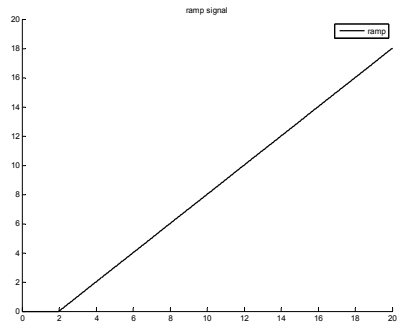
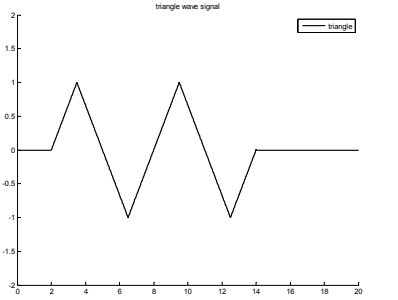
Signal type	Plot of signal	Transfer function
Step signal		$TF(s) = \frac{1}{s}$
Ramp signal		$TF(s) = \frac{1}{s^2}$
Triangle-wave signal		

Table 3-1: Classes of disturbance signals

The step and triangle-wave signals are primarily used for our simulations as well as combinations of these two signals. A step-signal refers to a sudden disturbance in a power system such as a line trip or an immediate disconnection of a load or a generator. A ramp input represents a continuous change and can be further arranged to a triangle-wave with increasing and decreasing ramps.

In normal operation, load disturbances or wind power output variations resembling ramp-signals or triangle-wave signals were judged more likely to occur. These signals represent for example an increase in wind-speed and therefore a steadily increase in power production.

### 3.1.2 Per Unit Quantities

The simulation program uses the per unit (pu) quantities. The used common base is 100MVA and all power quantities refer to this common base.

### 3.1.3 Standard System Configuration

Intermediate results presented in the following chapters are all based on the same system configuration. The underlying system for that configuration is the described 14 bus test system. Classical primary and secondary frequency control on synchronous generators is not considered. Generators 2 and 8, the WTG systems, each have a power generation of 0.2pu. In the per unit base employed, this would represent an active power of 20 MW generated at each bus. Today's WTG systems are typically rated at 1 to 5 MW of power. A WTG bus in this simulation case therefore represents a group of 4 to 20 generators.

Parameter	Value	Description	Parameter	Value	Description
$H_1$	8.0s	Inertia Constants	$S_{net,1}$	0.4951+j0	Net complex power generation at generator buses
$H_2$	0.1s		$S_{net,2}$	0.2+j0	
$H_3$	8.0s		$S_{net,3}$	0.4+j0	
$H_6$	8.0s		$S_{net,6}$	0.5+j0	
$H_8$	0.1s		$S_{net,8}$	0.2+j0	
$D_i$	0.02	Damping Constant			

Table 3-2: Parameters of standard system configuration

### 3.1.4 Excitation Scenarios

Based on disturbance signals described in Section 3.1.1 different excitations are used for simulations. For the first part, chapters 3 and 4, two standard simulation scenarios of different disturbances are used.

- **Excitation scenario 1:** The disturbance is a step change of 0.2pu active power at the load bus 4.
- **Excitation scenario 2:** A triangle-wave disturbance of the WTG generated power at bus 2 is applied. The peak-to-peak power change is 0.2pu.

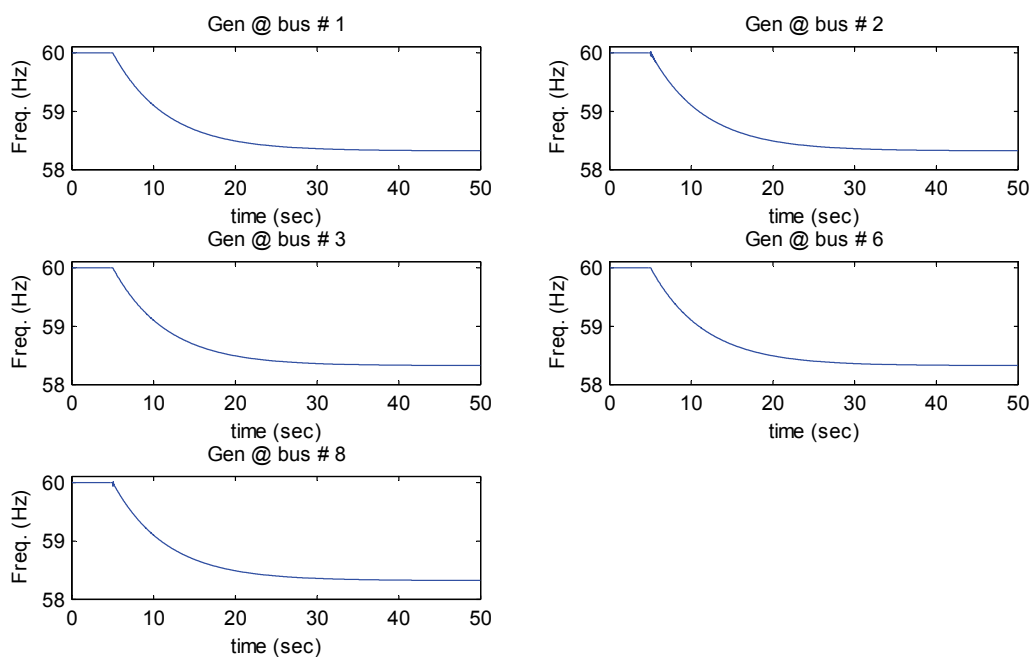
All the conducted simulations (if not mentioned differently) are based on the standard system configuration (3.1.3) and use these excitation scenarios. Results of these two simulation cases will be presented as intermediate results, against which performance with additional control paths will be described in the

succeeding chapters. The basic reaction of the power system to the two applied disturbances is shown in the following reference case.

### Simulation Results – Reference scenarios

#### Simulation 1

- Based on standard system configuration (Chapter 3.1.3)
- No primary and secondary freq. control
- Excitation scenario 1: 0.2pu step disturbance at load bus 4

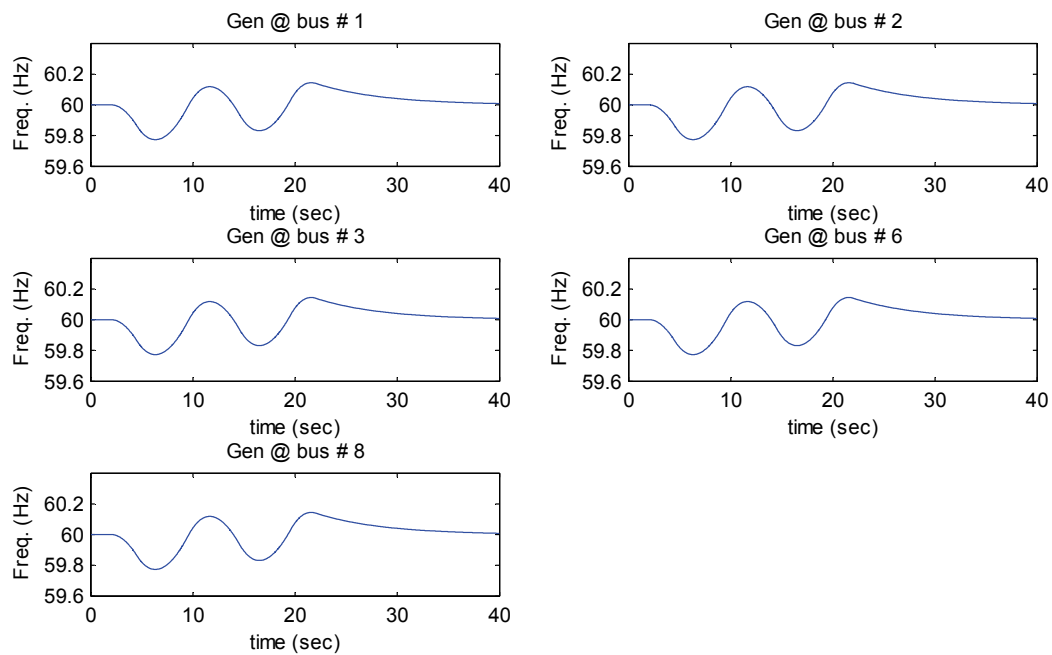


#### Results

- At  $t=5s$ , the frequency drops due to the additional load of 0.2pu at bus 4.
- The frequency decreases to a value of 58.2Hz, that represents the new steady-state value.

**Simulation 2**

- Based on standard system configuration (Chapter 3.1.3)
- No primary and secondary freq. control
- Excitation scenario 2: 0.2pu p-p triangle-wave disturbance at generator bus 2

**Results**

- At  $t = 2$  s, the triangle-wave disturbance is applied.
- The maximum frequency deviation is 0.2 Hz.

Table 3-3: Simulation Results – Reference scenarios



### 3.2 Concept of Additional Power Path

In order to mimic inertia and to enable frequency control, a power path is added to the system. A wind turbine bus is considered for applying this concept, illustrated in Figure 3-2.

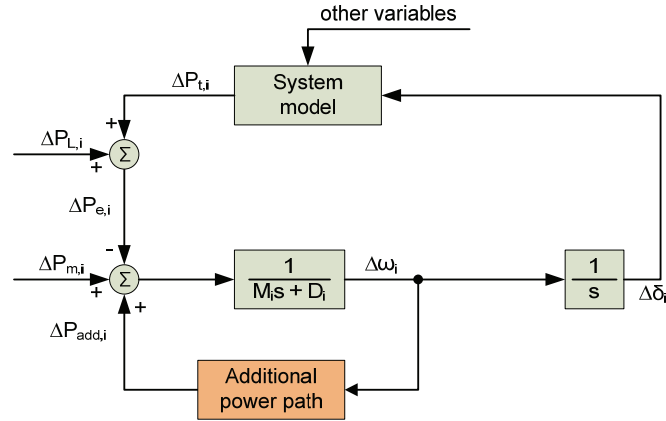


Figure 3-2: Block diagram for wind turbine bus

As first step the wind turbine generator model is introduced.

#### Wind Turbine Generator Model

As can be seen in the block diagram of Figure 3-2, the WTG is modeled with the swing equation as classical synchronous generators are. In Chapter 2 it is explained that a DFIG WTG system has a very small inertial response. By selecting a very small inertia constant  $H$  in comparison to that one of synchronous generators, it is anticipated to imitate the DFIG WTG characteristics reasonable enough for the purpose of this project. In essence, the low inertia and small damping behaves like a perturbation of the strict power balance equation at the bus.

Generators at buses 2 and 8 are considered as wind turbine buses. The implemented model at these buses is shown as block diagram in Figure 3-3.

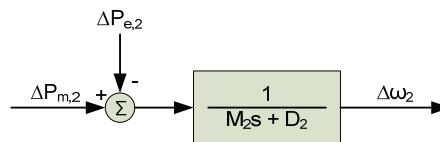


Figure 3-3: Implemented wind power generator model at bus 2

### Additional Power Path

With the knowledge of the WTG systems model, the additional power path at a wind generator bus (Figure 3-2) can be defined. From the frequency deviation signal at the wind generator bus,  $\Delta\omega_i$ , an additional power contribution,  $\Delta P_{add,i}$ , is derived and is fed back into the system.

For first studies of the functionality, a simple control path is examined. The basic principle of this additional control path is described in Figure 3-4. Based on the frequency  $\Delta\omega_i$  at the generator bus, additional power  $\Delta P_{add,i}$  is provided from the generator itself (internal source) or from external power sources. (Chapter 2.4)

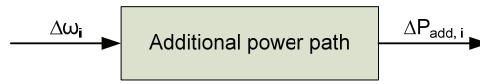


Figure 3-4: Basic principle of additional power path

The goal of the added control is to have inertia-like characteristics. Inertia-like behavior is associated with the time rate of change of frequency. Therefore the control should not react on the measured frequency, but on the derivative of that signal.

By adding a differentiator we get the input signal for the additional control.

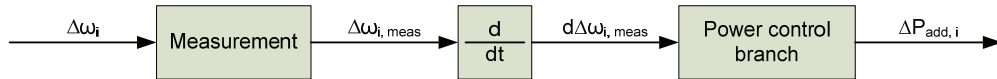


Figure 3-5: Additional power path

The measurement characteristic is modeled as a first order filter, with a fast time constant.

$$M(s) = \frac{1}{s \cdot \tau_M + 1} \quad (3.1)$$

In the next section, we take a closer look at the “power control branch” block from Figure 3-5, introducing a single added power branch within the power path.

### 3.2.1 Modeling of Single Power Control Branch

For a first examination, one single additional power system is considered. A block diagram of the branch is shown in Figure 3-6.

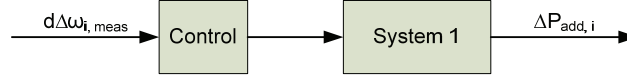


Figure 3-6: Single power control branch

The block “System 1” represents the actuator system of the control path. Additional power is assumed to be provided at the point of common coupling (PCC) of the generator and the grid, and can have many sources. In the case of a wind turbine we can think of pitch-control as internal source as well as flywheels or fuel cells as external sources (see 2.4).

Such actuator systems could have very different characteristics. Some of these have a very fast reaction; others may have longer time constants and therefore react slower on an input change. In order to take the different characteristics into account, but without knowing the exact characteristics of these systems, the work here models the systems with an overdamped 2<sup>nd</sup> order filter.

$$A(s) = \frac{1}{(s \cdot \tau_1 + 1) \cdot (s \cdot \tau_2 + 1)} \quad (3.2)$$

The time constants  $\tau_1, \tau_2$  are then representing the systems characteristics. Slower and faster system characteristics can be modeled by choosing appropriate time constants. With increasing time constants, the response to a disturbance then becomes slower.

The “control” block in the block diagram of Figure 3-6 is selected to be unity for now and will be faced in the next chapter.

$$C(s) = -1 \quad (3.3)$$

*The minus sign of the unity controller comes from the fact that measured frequency and fed back power should typical be of opposite sign, consistent with negative feedback.*

In order to keep the overview, the aggregate additional control path with one single power branch is shown again in the block diagram below. Note that the control block operates on the time derivative of the measured frequency error. This is intended to be an inertia-mimicking control action.

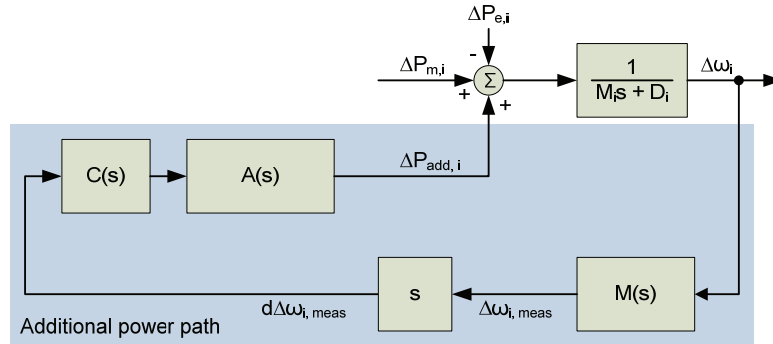


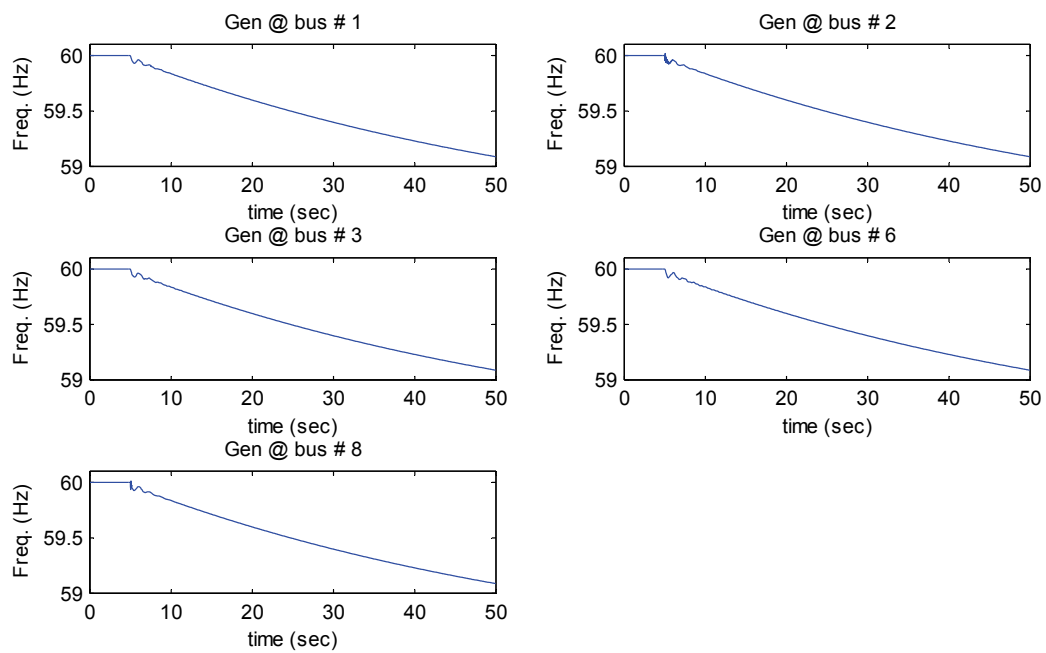
Figure 3-7: System of additional power path with single power branch

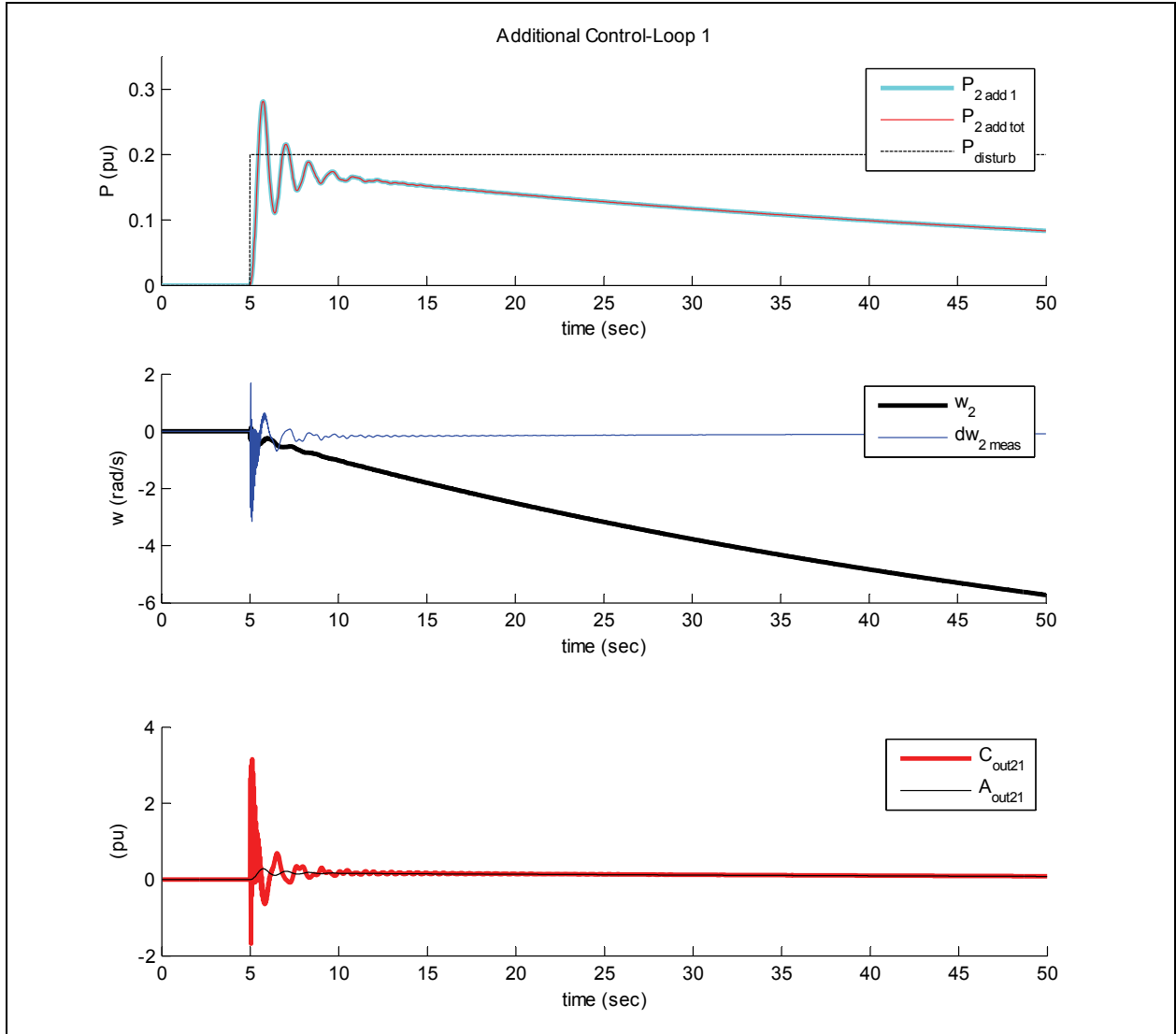
A simulation of this additional power path is shown in the following table.

### Simulation Results – Additional power path with single power branch

#### Simulation 1

- Based on standard system configuration (Chapter 3.1.3)
- Additional power path at bus 2
  - Measurement:  $\tau = 0.1\text{s}$
  - Power branch 1
    - Actuator 1:  $\tau_1 = \tau_2 = 0.5\text{s}$
- Excitation scenario 1: 0.2pu step disturbance at load bus 4





Because all intermediate results in Chapters 3 and 4 are presented with the plots above, a short explanation of the notation is given here.

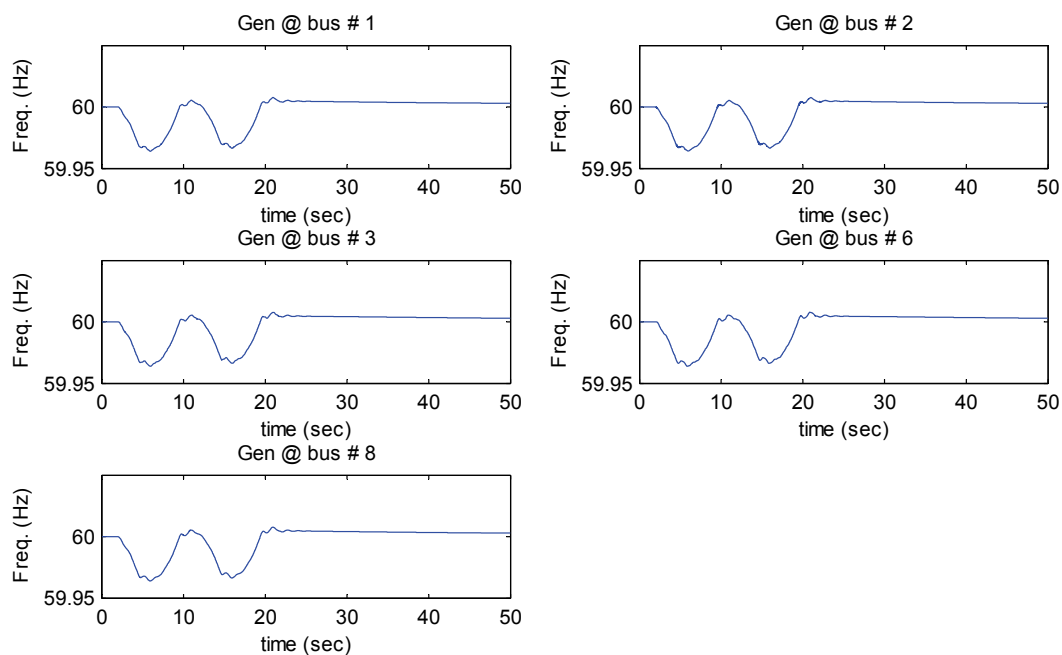
- The 1<sup>st</sup> plot shows the local frequencies at the generator buses in Hz (reference is 60Hz).
- The second plot, also referred as power-contributions plot shows the total additional power fed back to the network ( $P_{2\text{ add tot}}$ ) and the individual contributions of the branches ( $P_{2\text{ add 1}}$ ,  $P_{2\text{ add 2}}$ ).  $P_{disturb}$  shows the applied excitation for the simulation case.
- The 3<sup>rd</sup> plot shows the measured frequency at the selected bus ( $w_2$ ) of the additional control and its derivative ( $dw_2\text{ meas}$ ).
- In the last plots, the individual power branches are shown with controller and actuator. The two signals shown for the first branch are the controller output signal ( $C_{out21}$ ) and the actuator output ( $A_{out21}$ ), that is also the fed back power of that branch. In case of a second branch, the signals are then  $C_{out22}$  and  $A_{out22}$  accordingly.

### Results

- The frequency is decreasing slower in comparison to the reference case due to the added control path with its power branch
- The simulation will reach a steady-state value of 58Hz like in the reference case, but much later. (approx. 200 sec)
- Because no control dynamics are implemented (i.e. the control block is just a static gain), the actuator output simply follows the measured control input signal  $\Delta\dot{\omega}_{2,meas}$  with a certain filtering. ( $A_{out21} \approx C_{out21} = -d\omega_{2meas}$ )

### Simulation 2

- Based on standard system configuration (Chapter 3.1.3)
- Same additional configuration as in simulation 1
- Excitation scenario 2: 0.2pu p-p triangle-wave disturbance at generator bus 2



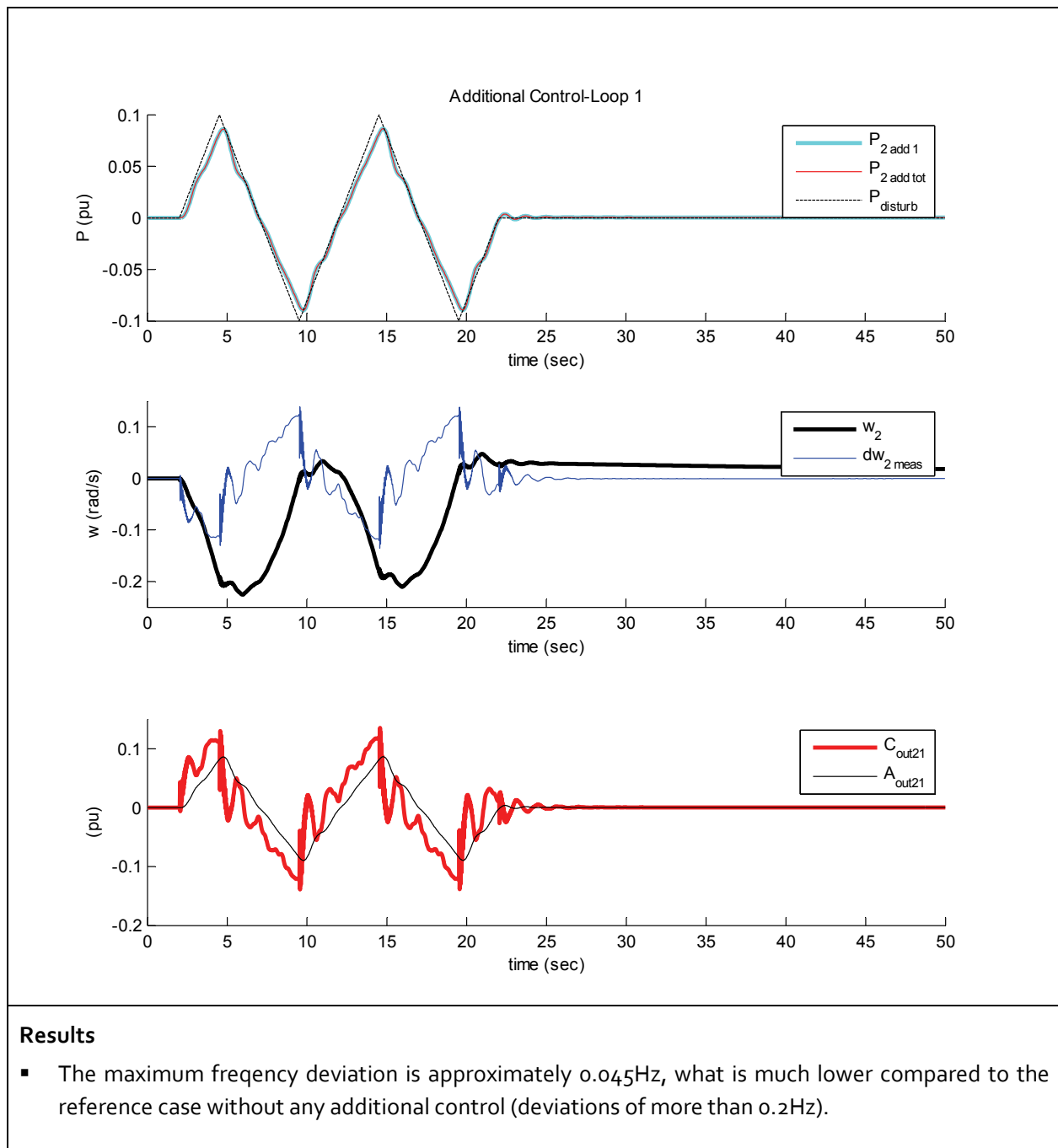


Table 3-4: Simulation Results – Additional power path with single power branch

Simulations presented in Table 3-4 show that with only one additional power branch and unity control an inertia-like response can be mimicked. The triangle-wave simulation shows already a significant improvement in terms of frequency deviation, compared to the reference case.



### 3.2.2 Modeling of Power Branches in Parallel

In future installations, it is likely that added power for control will be supplied from more than one power contributing system. Systems can be operated in parallel configuration. In this work, we selected up to three parallel system branches adding up to the total added power.

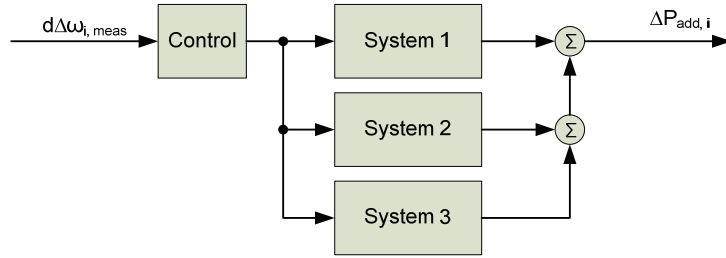


Figure 3-8: Parallel power branches

As already mentioned, for first studies of the additional control the actual control is set to unity. Therefore the controller output signal just follows the derivative of the measured frequency. The controller output signal is then filtered by the actuators and hence represents the additional power.

The three parallel branches are represented by different actuator systems, with specific time constants resp. bandwidths. Providing different bandwidths and different power and/or energy limits enables certain flexibility in control design.

Simulations of this scenario did not show improvement in performance, if the fastest actuator system was present in both the parallel and the single branch simulation. Because the fastest system in the path is responsible for the immediate reaction of the overall control, it is obvious that both simulations show comparable results. In the parallel configuration, the slower actuator systems contribute to the total added power with a slower time constant compared to the faster actuator. But after the initial individual contribution, the power is distributed among the parallel systems according to a dispatch factor of the actuator filters. This means that a factor  $k$  is multiplied with the actuator filter resulting in the modified TF:

$$A(s) = \frac{k}{(s \cdot \tau_1 + 1) \cdot (s \cdot \tau_2 + 1)} \quad (3.4)$$

If a slow actuator system is chosen in the single branch configuration and faster actuators in the parallel configuration, then the performance in the parallel configuration was better, what agrees with the fact that the faster actuator is mainly responsible for the improvement of performance.

The interesting fact of the parallel configuration is the redundancy of systems. By using first the faster system to give an immediate reaction and in a second resp. third step using the slower systems to keep the power at a satisfactory level for a certain time, characteristics like limits and bandwidths of actuator systems can be taken into account. These observations lead to further insights regarding limits of actuator systems that will be discussed in the next section.

### 3.2.3 Taking Saturation into Account

So far power limits of the power contributing systems have not been considered. But it is obvious that the amount of extracted power resp. energy from a storage device is limited. In order to mimic an inertial response, the attention is primarily focused on the first couple seconds after a network disturbance because the control acts on a signal that is the time derivative of frequency error. Therefore in that stage, power limits seem to be more important than energy limits.

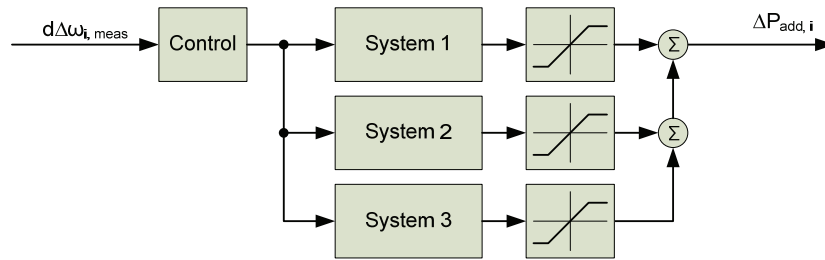


Figure 3-9: Parallel power branches with saturation

Considering the actuator systems, modeled as 2<sup>nd</sup> order filters, a saturation function has to be added in order to take saturation into account. The resulting block diagram is shown in Figure 3-9 above.

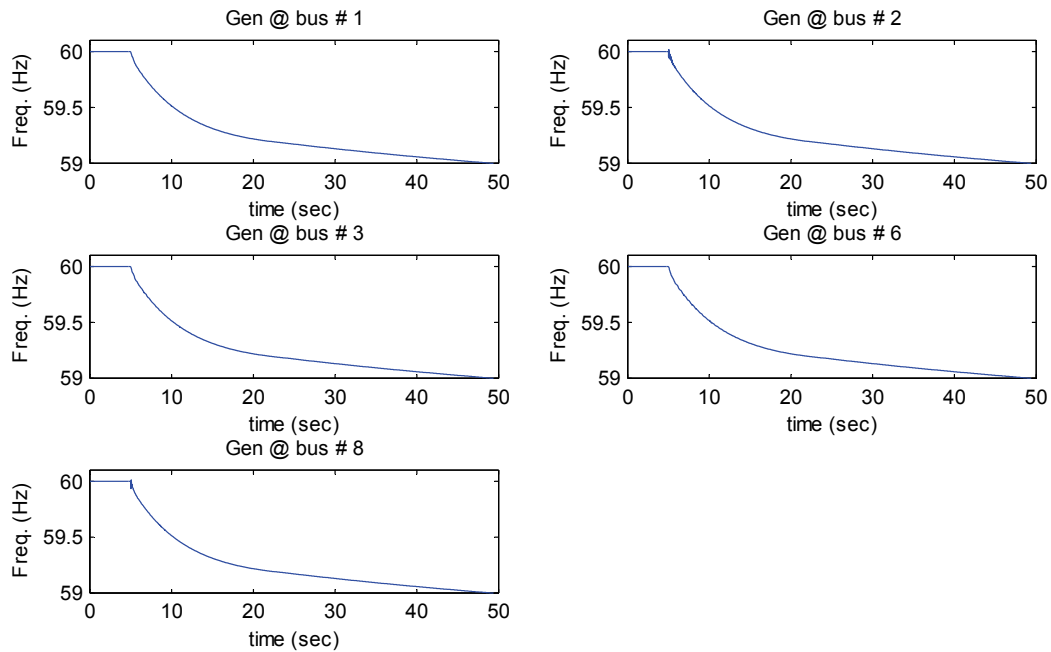
It should be noted here, that saturation functions are nonlinearities that cannot be represented with transfer functions. Therefore it is not trivial to implement saturation in a system model and such nonlinearity blocks have to be handled carefully.

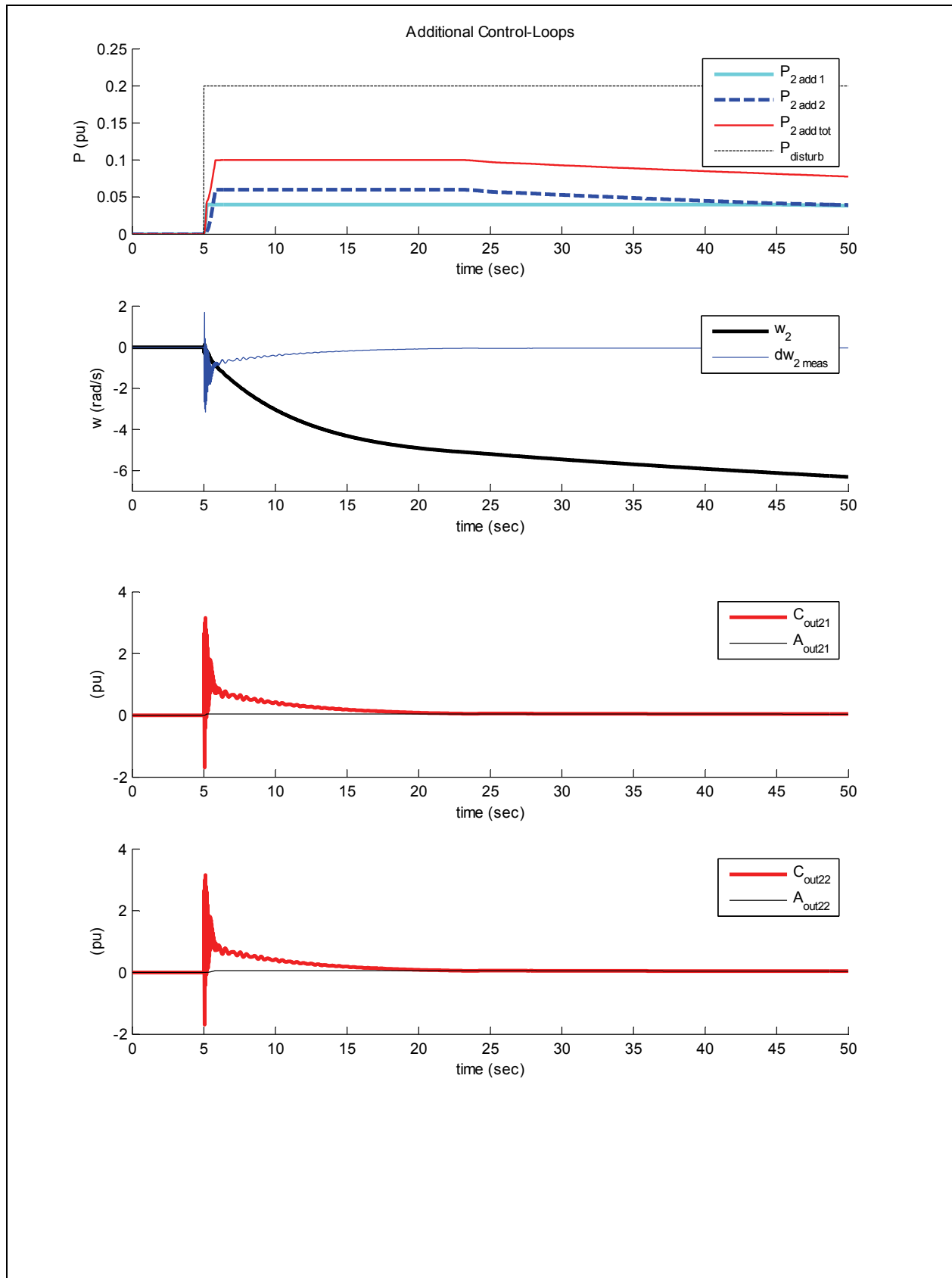
In the following table, simulations with saturation are shown. The same system from before is used with now activated saturation levels.

### Simulation Results – Two parallel branches with saturation

#### Simulation 1

- Based on standard system configuration (Chapter 3.1.3)
- Additional power path at bus 2
  - Measurement:  $\tau = 0.1\text{s}$
  - Power branch 1
    - Actuator 1:  $\tau_1 = \tau_2 = 0.5\text{s}$
    - Power Limits 1:  $\pm 0.04\text{ pu}$
  - Power branch 2
    - Actuator 2:  $\tau_1 = \tau_2 = 2\text{s}$
    - Power Limits 2:  $\pm 0.06\text{ pu}$
- Excitation scenario 1: 0.2pu step disturbance at load bus 4



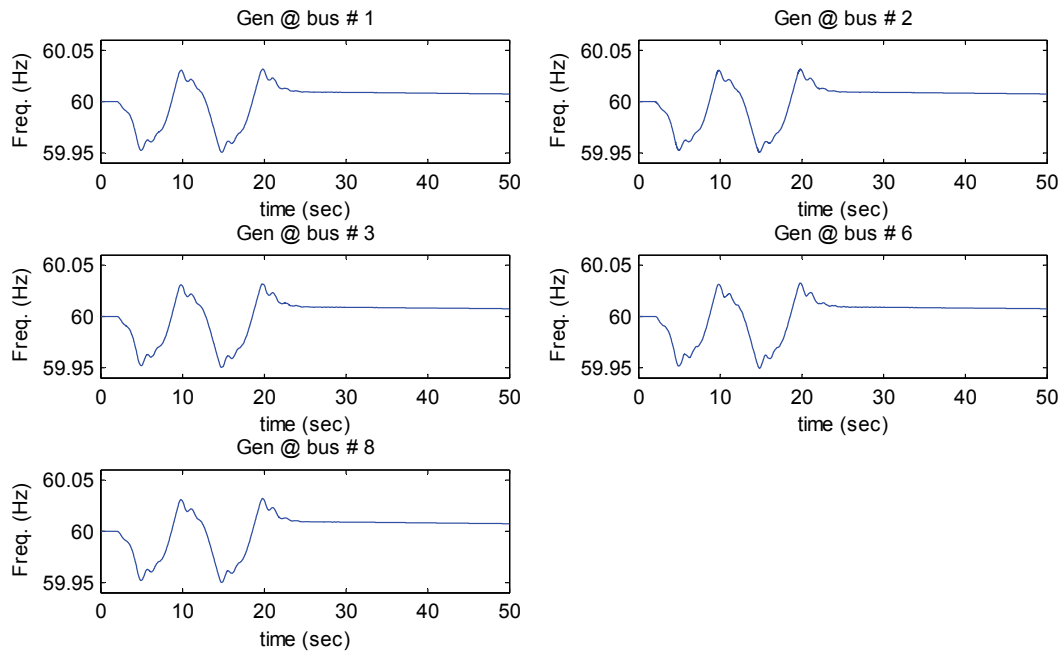


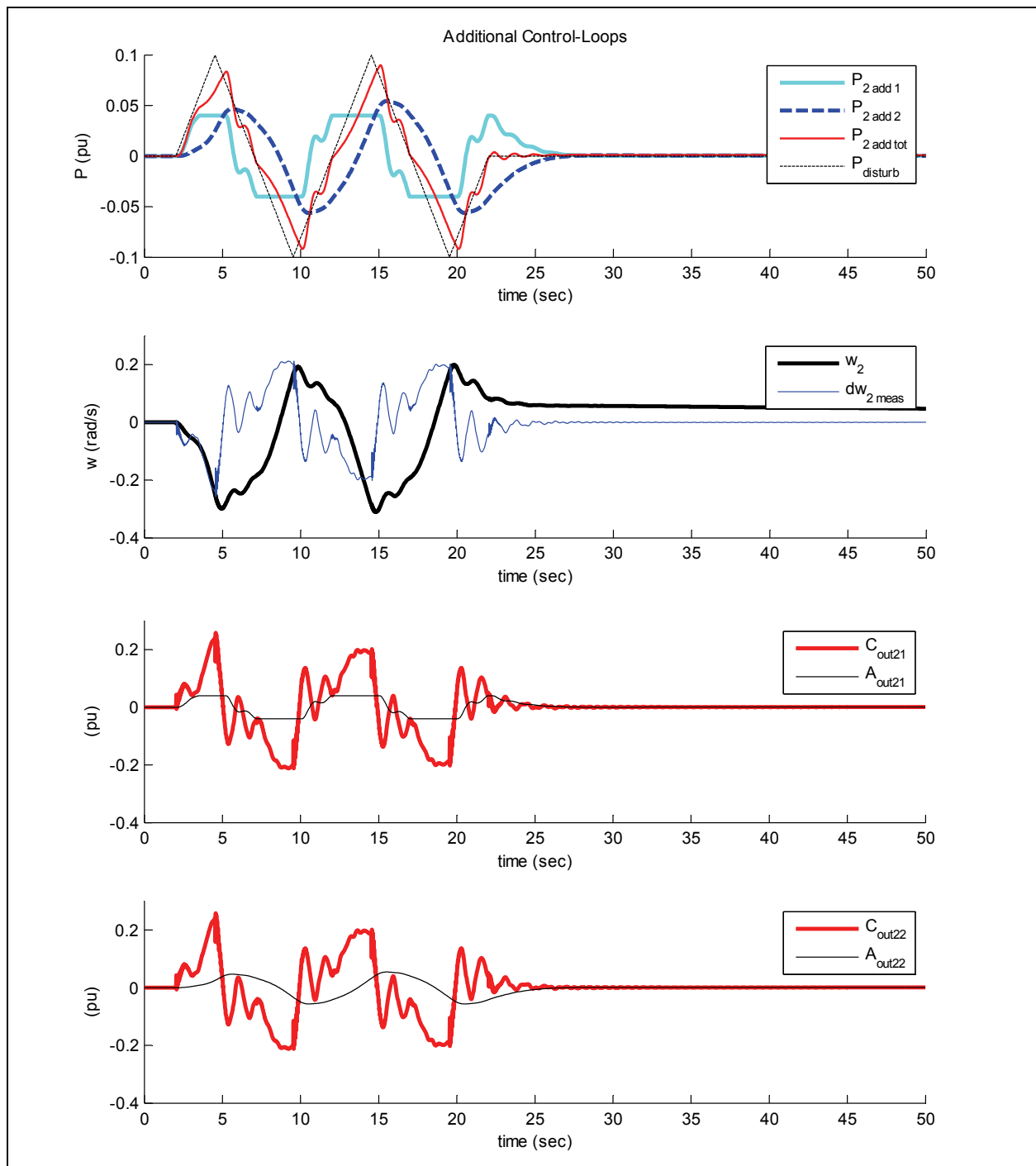
### Results

- Because no control dynamics are implemented, the actuator outputs simply follow the measured control input signal  $\Delta\dot{\omega}_{2,meas}$  with a certain filtering. ( $A_{out21} \approx A_{out22} = -d\omega_{2meas}$ )
- Once reached the saturation level, the actuator output is limited and remains in saturation till the controller output signal falls again below the saturation level.
- The different reaction times of the actuator systems, arising from their different bandwidths, can be seen from the power contribution plot. ( $P_{2add1}$  shows a faster reaction than  $P_{2add2}$ )
- Actuator systems stay at their saturation level for a too long time.

### Simulation 2

- Based on standard system configuration (Chapter 3.1.3)
- Same additional configuration as in simulation 1
- Excitation scenario 2: 0.2pu p-p triangle-wave disturbance at generator bus 2





### Results

- The maximum frequency deviation is 0.05Hz, what is a little more than in the case without saturation.
- The sharing of control effort between the two systems can be seen clearly in the power plot. Once the actuator with the broader bandwidth ( $P_{2 \text{ add } 1}$ ) reaches its saturation level, the slower system ( $P_{2 \text{ add } 2}$ ) starts compensating for the remaining power.

Table 3-5: Simulation Results – Two parallel branches with saturation

In general, what can be seen in simulations is that once a saturation level is reached, the control branch remains in saturation for a long time. In a control perspective, remaining in saturation means that the controller loses its ability to react on further disturbance signals. The conclusion of this finding is that in order to avoid losing controllability caused by saturation, the unity gain of the control loop has to be replaced by a more sophisticated controller.

*A significant body of work can be found in literature in the area of control design techniques taking saturation into account. Among these contributions, many are attributed to Saberi and his co-workers, and are all collected in the research monograph [29]-[31].*

### 3.3 Adding a Control Filter

Until now, the additional control path has been considered with only a unity control block. It represents therefore a simple proportional feedback loop, where the additional power follows an input signal  $r$ . In our case, the signal  $r$  is the derivative of the measured frequency deviation at the considered generator bus  $\Delta\dot{\omega}_{i,meas}$ . A next step is now to add control dynamics, which regulate the added power and in addition try to keep the power output in a range where saturation is not reached. Disregarding saturation for the moment, one could think of a simple PI controller.

For comparison of results obtained in the next chapter, a parallel branch control with a PI controller has been simulated and the results are shown in the next table. The unity controller, used so far, is simply replaced by a PI control filter.

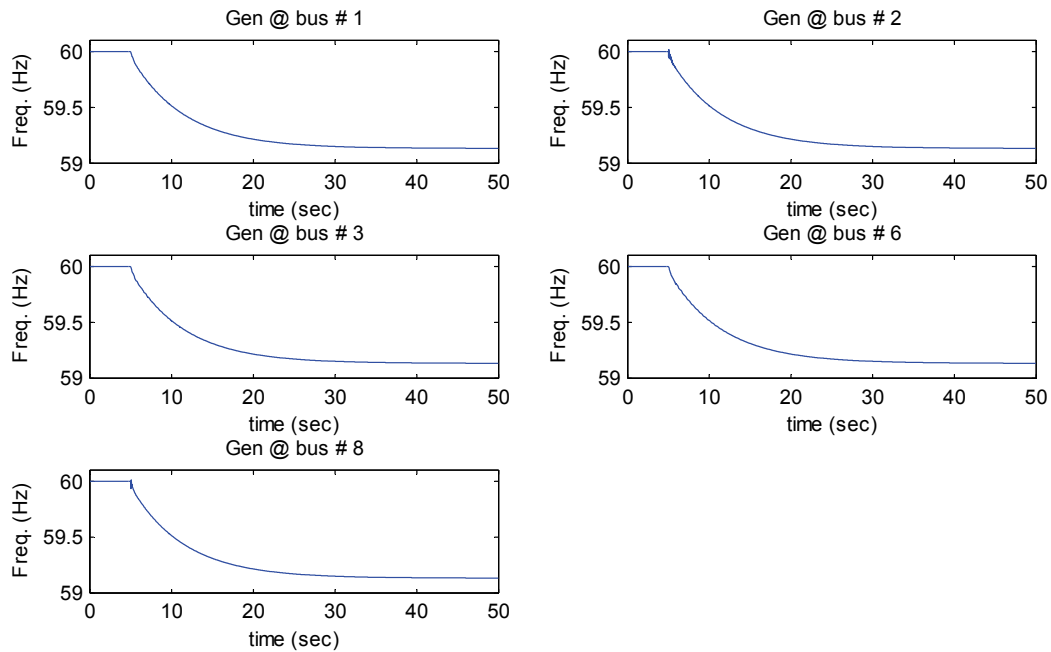
$$C(s) = k_p + \frac{k_I}{s} \quad (3.5)$$

However, as we will see, the performance of such a control can be significantly improved if higher order controllers based on more sophisticated design techniques are used instead.

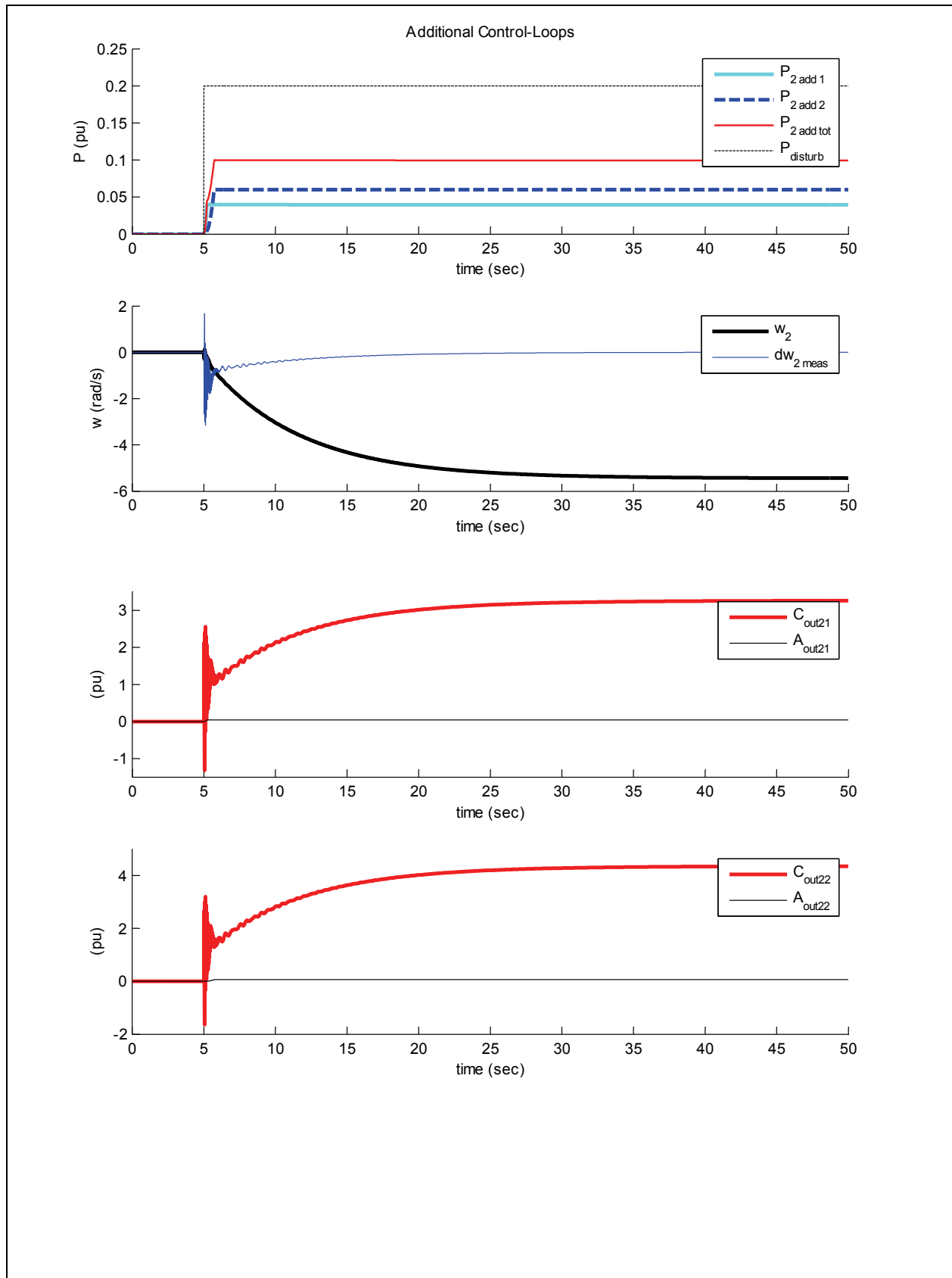
### Simulation Results – Two parallel branches with PI filters

#### Simulation 1

- Based on standard system configuration (Chapter 3.1.3)
- Additional power path at bus 2
  - Measurement:  $\tau = 0.1\text{s}$
  - Power branch 1
    - Actuator 1:  $\tau_1 = \tau_2 = 0.5\text{s}$
    - Power Limits 1:  $\pm 0.04\text{ pu}$
  - Power branch 2
    - Actuator 2:  $\tau_1 = \tau_2 = 2\text{s}$
    - Power Limits 2:  $\pm 0.06\text{ pu}$
- Excitation scenario 1: 0.2pu step disturbance at load bus 4





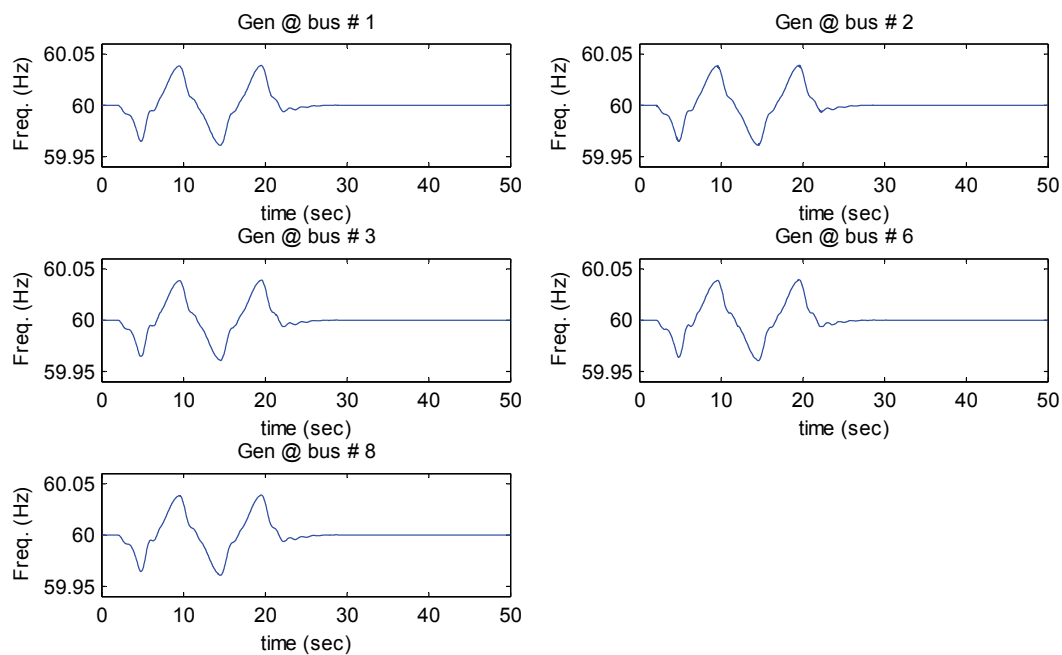


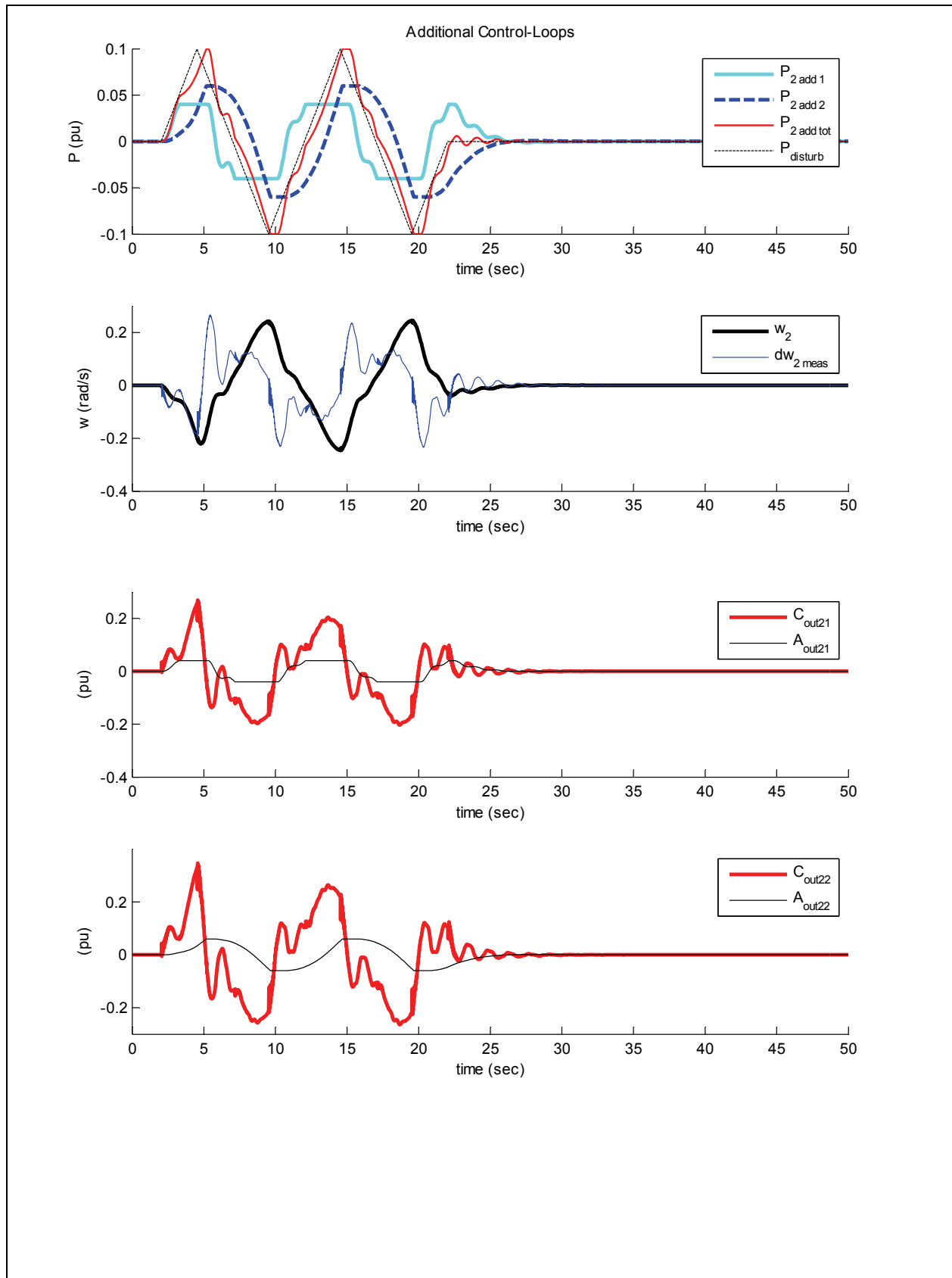
**Results**

- The frequency deviations look very similar to the case without a control filter, but a certain steady-state value is reached at 59.15Hz.
- Unlike in the case without a control filter, the output power remains at the maximum saturation level of in total 0.1pu and does not drop due to the integrating behavior of the control filter.

**Simulation 2**

- Based on standard system configuration (Chapter 3.1.3)
- Same additional configuration as in simulation 1
- Excitation scenario 2: 0.2pu p-p triangle-wave disturbance at generator bus 2





**Results**

- The results with a PI controller are similar to the same simulation case with unity control. Comparing the frequency plots to the other case, no significant improvement can be seen.
- The sharing of control action between the two cases is comparable to the unity control case.
- The delay of actuator systems can be seen in the lower graphs at  $t=2s$ . For system 1, with the fast time constants, the actuator output follows the controller output nearly exactly, whereas for the slower system 2 the actuator output has a certain delay.

**Table 3-6: Simulation Results – Two parallel branches with PI filters**

Simulations show that the use of a PI controller results in a sort of smoother power-tracing of the triangle-wave disturbance. With saturation limits considered, as used in the simulation above, the PI controller shows a modest advantage compared to the unity control. But the improvement is only marginally and the use of a PI controller cannot solve the underlying problem of saturation. Different simulations show, that actuators still remain too long at their saturation level.

Using PI control is a standard in industry. Wherever control is required, adding a PI filter is a regular choice. Also for WTG systems, PI control was or still is widely used. Nevertheless, today more complex control designs are considered. Alan D. Wright describes, for instance, such modern control design concepts for WTG systems in his doctor thesis [15]. For the upcoming development of more advanced control designs here, the PI design will serve as a reference case.

## 4 Control Design on Single Bus

In this chapter, the control design at a single bus is developed. The main goal of this project is to find a control design that improves overall performance and stability including a suitable solution of the saturation issue.

The standard control system structure is shown in Figure 4-1 [32]. Neglecting the sensor gain  $H$ , this feedback system reduces to the simple block diagram shown on the right side.

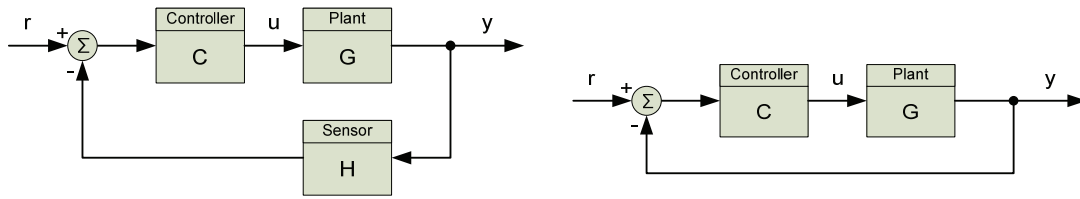


Figure 4-1: Standard control system structure

There are many known methods for controller design. This project computes the controller design that achieves the desired closed-loop through a method known as Youla Parameterization or Q-Parameterization that seeks a pre-specified, “desirable” closed-loop transfer function. [33]

### 4.1 Youla-based Design Method

#### 4.1.1 General Approach – SISO Youla Parameterization

Suppose the plant  $G$ , the system to be controlled, is known and has the transfer function:

$$G(s) = \frac{n_G(s)}{d_G(s)} \quad (4.1)$$

#### Assumptions

- i) Strictly proper transfer function  $G(s)$   
 $\deg(n_G(s)) < \deg(d_G(s))$
- ii) All poles of  $G(s)$  are in LHP  
 $\text{Re}\{\text{poles}(G(s))\} < 0$
- iii) All zeros of  $G(s)$  are in LHP  
 $\text{Re}\{\text{zeros}(G(s))\} < 0$

Hence,  $G(s)$  has to be strictly proper, stable and minimum-phase.

### Design Goal

With the design method presented here, we want to find a sophisticated controller  $C(s)$  for the feedback system drawn below, in a way that the closed-loop transfer function of the system  $T(s)$  has “desirable” performance. The controller to be computed should be stable and “strictly proper” itself.

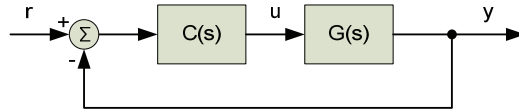


Figure 4-2: Closed-loop system for controller design

### Design Procedure

1. A closed-loop transfer function  $H(s)$  from theory is chosen, that provides optimal closed-loop performance for the feedback system.

$$H(s) \approx T_{cl}(s) = \frac{C(s) \cdot G(s)}{1 + C(s) \cdot G(s)} \quad (4.2)$$

2. The controller and feedback system is then replaced by a new-introduced transfer function  $Q(s)$ . The system reduces to a simple open-loop system as depicted below.

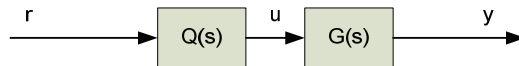


Figure 4-3: Equivalent open-loop system

$$T_{eq}(s) = Q(s) \cdot G(s) \quad (4.3)$$

The transfer function  $T_{eq}(s)$  can then be replaced by the desired optimal closed-loop transfer function  $H(s)$  selected in step 1 and  $Q(s)$  can be calculated straightforward.

$$Q(s) = G(s)^{-1} \cdot T_{eq}(s) = G(s)^{-1} \cdot H(s) = \left[ \frac{d_G(s)}{n_G(s)} \right] \cdot H(s) \quad (4.4)$$

$G(s)$  must not have any zeros in the RHP otherwise its inversion is unstable and consequently  $Q(s)$  as well.

3. To get the transfer function of the controller  $C(s)$ , equations (4.2) and (4.3) are set equal and solved for  $C(s)$ .

$$T_{cl}(s) = T_{eq}(s) \rightarrow \frac{C(s) \cdot G(s)}{1 + C(s) \cdot G(s)} = Q(s) \cdot G(s) \quad (4.5)$$

$$C(s) = \frac{Q(s)}{1 - Q(s) \cdot G(s)} \quad (4.6)$$

The controller TF,  $C(s)$ , can be rewritten in terms of numerator and denominator of  $G(s)$  and  $Q(s)$ .

$$C(s) = \frac{n_Q/d_Q}{1 - (n_Q/d_Q) \cdot (n_G/d_G)} = \frac{n_Q \cdot d_G}{d_Q \cdot d_G - n_Q \cdot n_G} \quad (4.7)$$

In practice, an approximation of  $G(s)$  has to be computed sometimes in order to fulfill the requirement of stability. The associated issues are discussed in detail in Chapter 4.3.

#### 4.1.2 General Approach – MIMO Youla Parameterization

Considering multiple inputs and multiple outputs (MIMO) systems means that cross couplings between the systems may be included. The general procedure as described for a single input single output (SISO) system has to be slightly modified in order to match with the MIMO case. Single transfer functions are replaced by matrices of transfer functions and the calculations change to matrix calculations. The system structure looks like before, the only difference is that the blocks are no longer single TFs, but matrices of transfer functions.

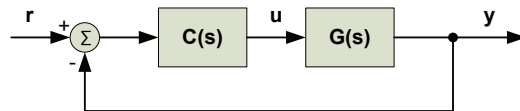


Figure 4-4: Closed-loop MIMO system

#### Design Goal

We want to find two or more controllers, represented by a matrix  $\mathbf{C}$  for the feedback system shown above. The closed-loop transfer functions of the system  $\mathbf{T}$  should have “desirable” performance.

### Design Procedure

1. A set of desired optimal closed-loop transfer functions  $\mathbf{H}$  is chosen from theory that provides an optimal closed-loop performance for the feedback system.

$$\mathbf{H} = \mathbf{T}_{cl} = (\mathbf{I} + \mathbf{T}_{ol})^{-1} \cdot \mathbf{T}_{ol} = (\mathbf{I} + \mathbf{C} \cdot \mathbf{G})^{-1} \cdot \mathbf{C} \cdot \mathbf{G} \quad (4.8)$$

2. The controller and feedback system is then replaced by a new-introduced transfer function  $\mathbf{Q}(s)$ . The system reduces to a simple open-loop system as depicted below.

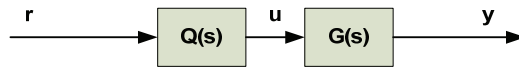


Figure 4-5: Equivalent open-loop MIMO system

$$\mathbf{T}_{eq} = \mathbf{Q} \cdot \mathbf{G} \quad (4.9)$$

The transfer function matrix  $\mathbf{T}_{eq}$  can then be replaced by the optimal closed-loop transfer function set  $\mathbf{H}$  selected in step 1 and  $\mathbf{Q}$  can be calculated from equation (4.9).

$$\mathbf{Q} = \mathbf{G}^{-1} \cdot \mathbf{T}_{eq} = \mathbf{G}^{-1} \cdot \mathbf{H} \quad (4.10)$$

3. The controller matrix  $\mathbf{C}$  is then computed as follows:

$$\mathbf{C} = (\mathbf{I} - \mathbf{Q} \cdot \mathbf{G})^{-1} \cdot \mathbf{Q} \quad (4.11)$$

#### 4.1.3 ITAE Coefficients

In literature the ITAE coefficients have been proposed to evaluate the quantity of performance of transfer functions. [34]

$$ITAE = \int_0^T t \cdot |e(t)| \cdot dt \quad (4.12)$$

From the ITAE index in equation (4.12) the ITAE coefficients for closed-loop transfer functions can be calculated.

They represent optimal coefficients for each order of transfer functions of a closed-loop system optimized to certain input excitations. Two types of optimal closed-loop transfer functions are found. The first type of transfer functions is optimized to a step response and the second type is optimized to a ramp response. The transfer functions for the two cases are in the form as below.



$$H_{Step}(s) = \frac{b_0}{s^n + b_{n-1} \cdot s + \dots + b_1 \cdot s + b_0} \quad (4.13)$$

$$H_{Ramp}(s) = \frac{b_1 \cdot s + b_0}{s^n + b_{n-1} \cdot s + \dots + b_1 \cdot s + b_0} \quad (4.14)$$

An important consideration is now if the controller should show optimal performance to a step change or a ramp change. Given our interest in control design for varying outputs of alternative energy sources (e.g. wind power) under normal operation, the judgment made here is that step change disturbances are less of a concern. Wind power variations can be better represented by a ramp or triangle-wave response than an immediate step change of power. Because the design should show best performance in normal system operation, the class of target closed-loop transfer functions optimized with respect to ramp responses is selected.

*A step change could occur in the system (e.g. an immediate power loss), but that cannot be called "normal operation" anymore. It is though one of the goals to provide an inertial response to such a system disturbance. Therefore in general a tradeoff between good response to ramp changes and good responses to step changes has to be made.*

Plots of step- and ramp-responses of an optimal ramp transfer function (4.14) for given orders, allow a comparison of the different characteristics. The system transfer function  $G(s)$  can be of high order and therefore the closed-loop performance should also be of high order. An initial guess is taking the 5<sup>th</sup> order transfer function. From the ramp- and step-responses of figures 4-6 and 4-7, a selection of the 4<sup>th</sup> order ramp TF was judged to show the best reference closed-loop performance. The step-response of a 5<sup>th</sup> order function showed worse performance compared to the 4<sup>th</sup> order function (overshoot is significantly higher). The 3<sup>rd</sup> order function showed very similar performance to the 4<sup>th</sup> order function for ramp- and step-response and so the choice was made for the higher 4<sup>th</sup> order ramp transfer function that will serve as the desired closed-loop transfer function  $H(s)$ .

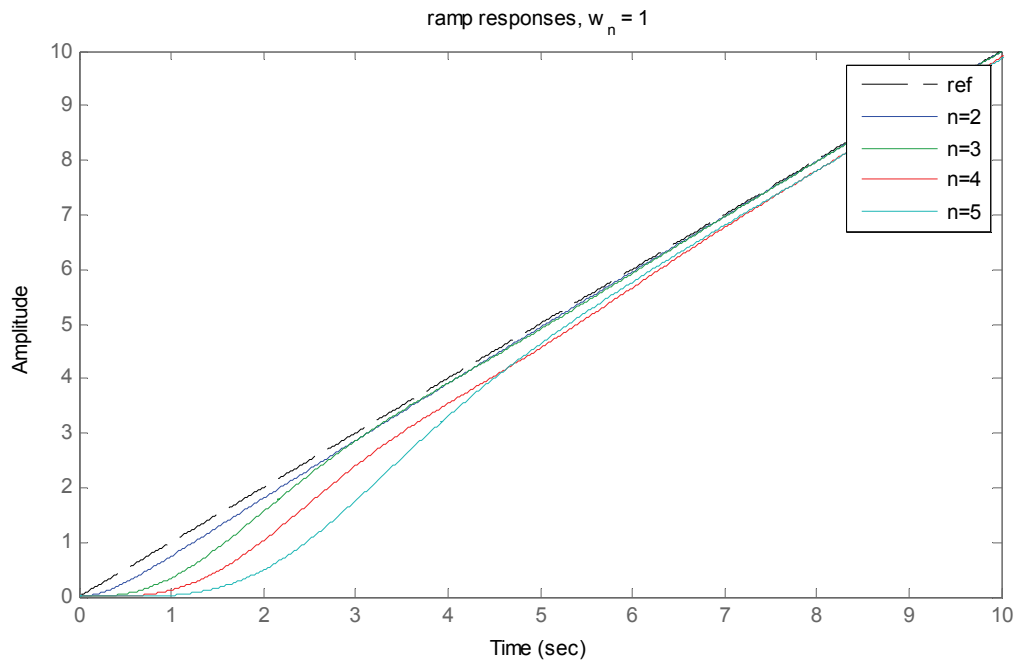


Figure 4-6: Ramp responses of ramp optimized closed-loop TF for different orders  $n$

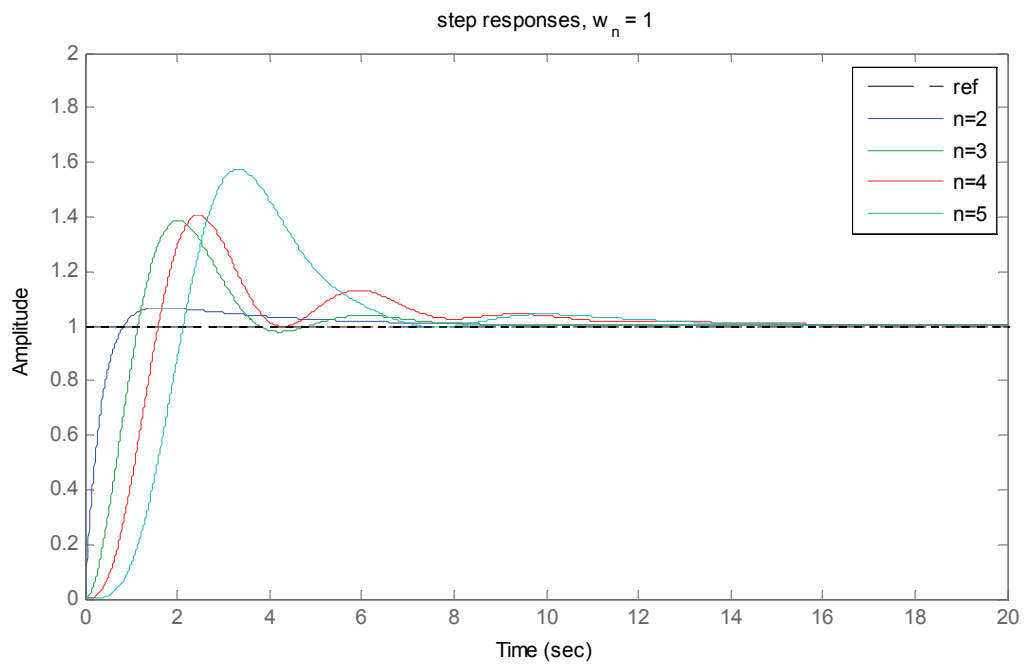


Figure 4-7: Step responses of ramp optimized closed-loop TF for different orders  $n$

## 4.2 Applied Approach for Additional Power Path with Single Branch

Considering the single additional power branch concept from before, the optimal control design procedure is now applied with one branch consisting of a single controller and actuator.

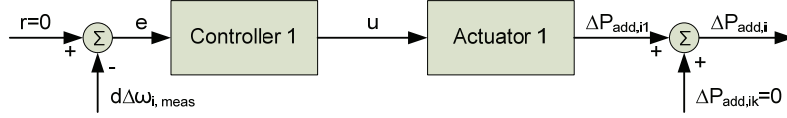


Figure 4-8: Single branch of additional power path

### 4.2.1 Design of Controller

In the following, the design procedure of a single controller is described.

#### Design Goal

The goal is to develop a controller that regulates the additional power that is fed into the point of common coupling at the selected wind turbine.

#### System Description

The system has to be transformed into the general control feedback system structure, shown in Figure 4-2. In a first step, we consider only a single control branch at one wind turbine generator bus in the network.

The linearized system equations from the basic system form a state Matrix  $A_0$ . This matrix contains the frequency dependences of all the generators in the system. Selecting appropriate input and output matrices  $B_0$  and  $C_0$  for the considered controller location, allows the calculation of the transfer function  $G_0(s)$  of the specific bus. Details of the calculation of  $G_0(s)$  are given in the Appendix.

$$G_0(s) = C_0^T \cdot (s \cdot I - A_0)^{-1} \cdot B_0 \quad (4.15)$$

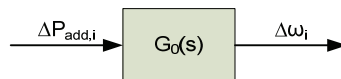


Figure 4-9: Transfer function of basic system

The output of  $G_0(s)$  is the grid frequency deviation at bus  $i$  and the input is the added power fed by the additional control path to its bus  $i$ .

The block diagram of the feedback control system is shown in Figure 4-10. Multiplying  $G_0(s)$  with the transfer functions at its input and output results in the expanded transfer function  $G(s)$  forming the “new” system that has to be controlled.

$$G(s) = A_1(s) \cdot G_0(s) \cdot M(s) \cdot s \quad (4.16)$$

In equation (4.16)  $A_1(s)$  represents the transfer function of the actuator system of the 1<sup>st</sup> control branch,  $M(s)$  represents the measurement filter and  $s$  the differentiator.

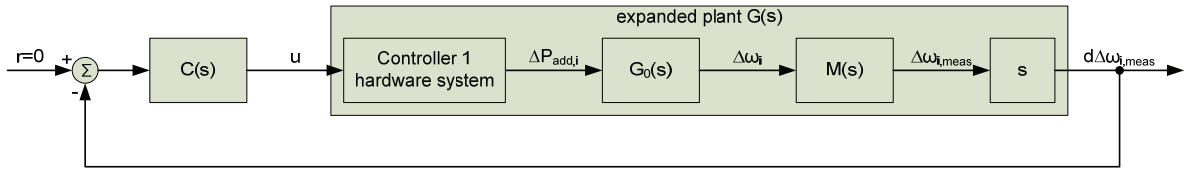


Figure 4-10: Feedback system with expanded plant  $G(s)$

The system is now in the standard feedback control loop form and the controller  $C(s)$  can be designed in a next step.

The reference value is set to zero (i.e.  $r = 0$ ). This means that the input of the controller is just the negative measured signal or zero, if the derivative of the frequency is zero.

### Procedure

1. An optimal closed-loop transfer function  $H(s)$  has to be chosen. Such a transfer function can be built with the ITAE coefficients from Chapter 4.1.3.

Using the coefficients from literature [34], [35], the selected 4<sup>th</sup> order transfer function optimized on a ramp is then of the form:

$$H_{R4}(s) = \frac{5.14 \cdot \omega_n^3 \cdot s + \omega_n^4}{s^4 + 2.41 \cdot \omega_n \cdot s^3 + 4.93 \cdot \omega_n^2 \cdot s^2 + 5.14 \cdot \omega_n^3 \cdot s + \omega_n^4} \quad (4.17)$$

It can be seen, that the transfer function is dependent only on a single parameter  $\omega_n$ . This fact will be used in a later step for the overall control design.

2. Find  $Q(s)$

$Q(s)$  can be calculated from the system  $G(s)$  and the defined optimal closed-loop transfer function  $H(s)$  using equation (4.4). In larger systems or in systems with multiple control loops,  $G(s)$  can have very high order. To avoid a controller of too high order, we try to reduce already

the order of the system transfer function  $G(s)$  to a lower order with nearly identical frequency response characteristics. Through this reduction, the approximation to  $G(s)$  may display unwanted zeros in the RHP, meaning, that  $G(s)$  becomes “non-minimum phase” and its inverse is unstable. By deleting zeros in the RHP and/or moving them to the LHP (plus sometimes adjusting the proportional gain), the requirements for  $G(s)$  in the design process can be satisfied again, whilst still adequately approximating the characteristics of the unreduced system.

### 3. Solving for $C(s)$

By solving equation (4.6) we get a controller  $C(s)$  that realizes the desired target closed-loop transfer function. This controller can be of very high order. For realistic implementations, the controller should have an order as low as possible but at least below 20. We again try to reduce the order of the controller, while keeping the characteristic very similar and the controller itself stable.

#### 4.2.2 Order of Controller

Our calculations have shown that for the expanded plant  $G(s)$  it is nontrivial to find a controller with reasonable order. If the controller actuator is not included to the expanded plant  $G(s)$ , then a controller of lower order can be found more easily.

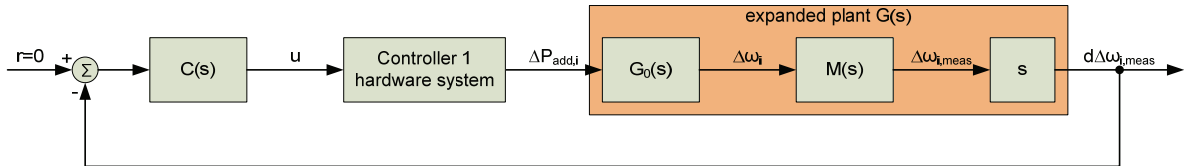


Figure 4-11: Control path for lower order  $G(s)$

The transfer function  $G(s)$  of the expanded plant is then simply the basic system transfer function  $G_0(s)$  multiplied by the measurement filter TF and the derivative.

$$G(s) = G_0(s) \cdot M(s) \cdot s \quad (4.18)$$

And the equivalent open-loop transfer function  $Q(s)$  contains the actuator 1. If we take the inverse of  $G(s)$ , we have a plant of lower order and therefore also a  $Q(s)$  of lower order. Solving for the controller again results in theory in the same equations as with the methodology used before. (see appendix)

Despite this modification, we still had the issue of a too high order controller. MATLAB offers a broad set of tools to reduce the order of systems. One of the most important commands for this is *minreal* that allows pole/zero cancellations (we kept in mind that no RHP pole/zero cancellations occurred!) in an adjustable region of numerical uncertainty. MATLAB is based on numerical computations and so pole and zero values can shift resulting in the fact that they are sometimes not cancelled. Therefore the additional possibility to adjust the region of numerical uncertainty helped a lot in reducing the system's order.

Further on, using the Hankel<sup>1</sup> singular values [36], system modes can be identified that only have very small influence to the overall system performance. A reduction of these modes resulted in a lower order system with nearly the same characteristics as the original system.

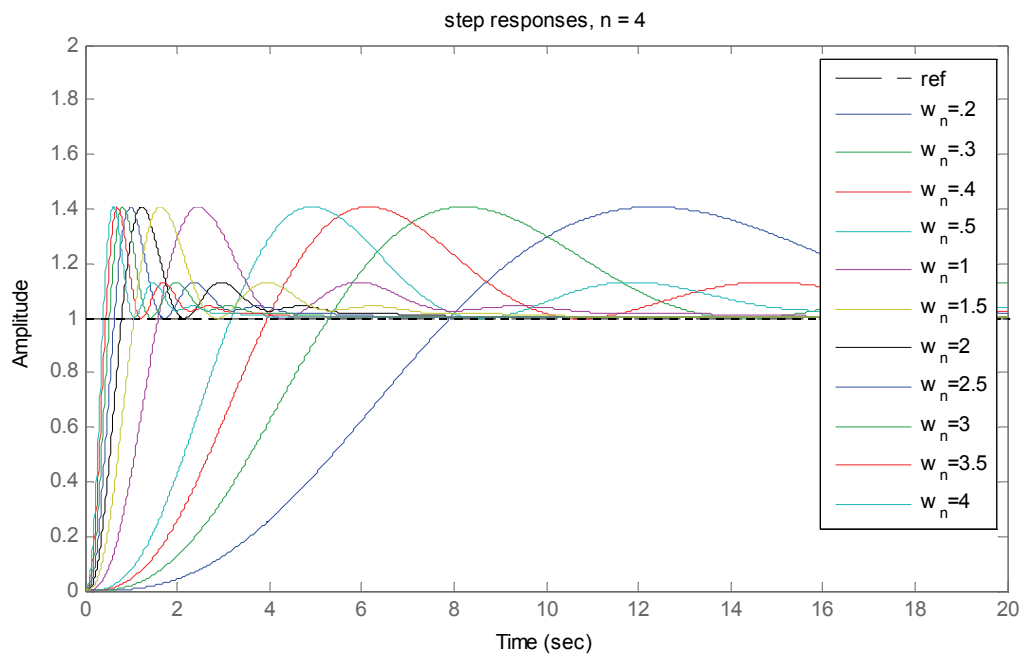
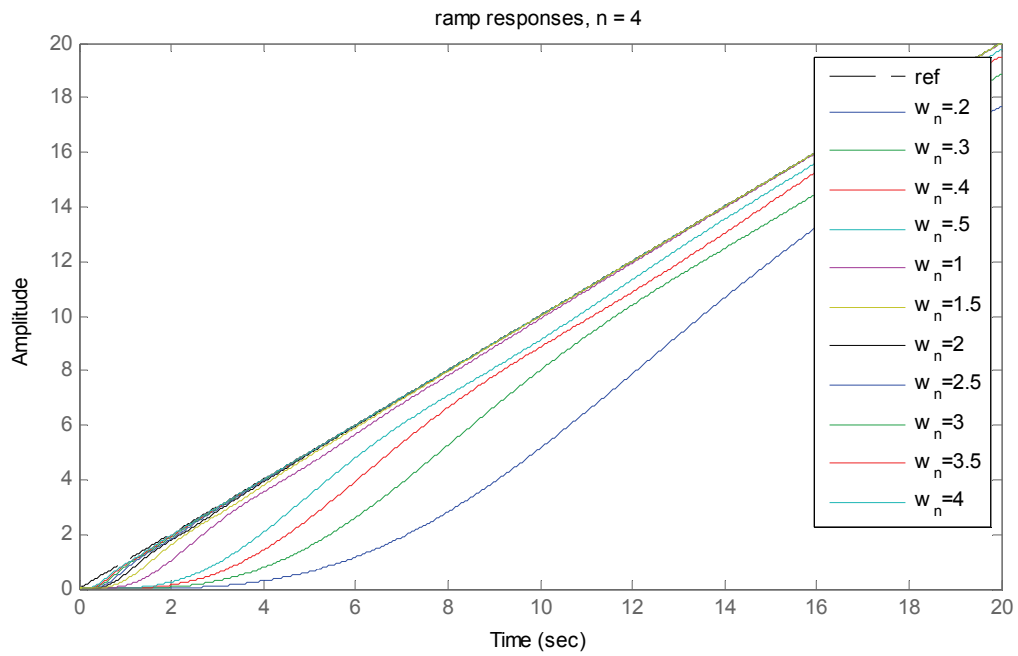
In the end a comparison of the Bode plots of the original system and the system with the reduced blocks could provide a proof of validity if the plots showed nearly the same characteristics.

#### 4.2.3 Analysis of Controller Output

Following the control design procedure as described above, a controller for a specific  $\omega_n$  is designed. The parameter  $\omega_n$  is the only parameter and is therefore of special interest. With the parameter  $\omega_n$  the speed of reaction of the controller can be set. A bigger  $\omega_n$  results in a faster control action, whereas a smaller  $\omega_n$  results in a slower control action. This behavior is by some means intuitive; if the optimal closed-loop transfer function  $H(s)$  is considered, and with the knowledge that the controller is designed to show such an optimal closed-loop performance, one might see that with the only controller parameter  $\omega_n$ , the output signal can be limited.

---

<sup>1</sup> Hankel singular values define the "energy" of each state in the system. Keeping larger energy states of a system preserves most of its characteristics in terms of stability, frequency, and time responses.

Figure 4-12: Step responses of optimal closed-loop TF for different  $w_n$ Figure 4-13: Ramp responses of optimal closed-loop TF for different  $w_n$

From the two figures above, the step- and ramp-responses of the optimal closed-loop TF  $H(s)$ , it can be seen that a smaller parameter  $\omega_n$  results in a loss of speed of performance, or in other words, in a slower reaction.

One goal for the controller design is to take saturation into account and hence a solution has to be found on how to limit the controller output signal. As already seen, by tuning controller parameter  $\omega_n$  the reaction of the controller can be slowed down. The key intuition in the design approach here is that, slowing down a controller should also result in lower amplitude of the controller output. This fact is then used for the objective to keep signals in the control loop within saturation limits.

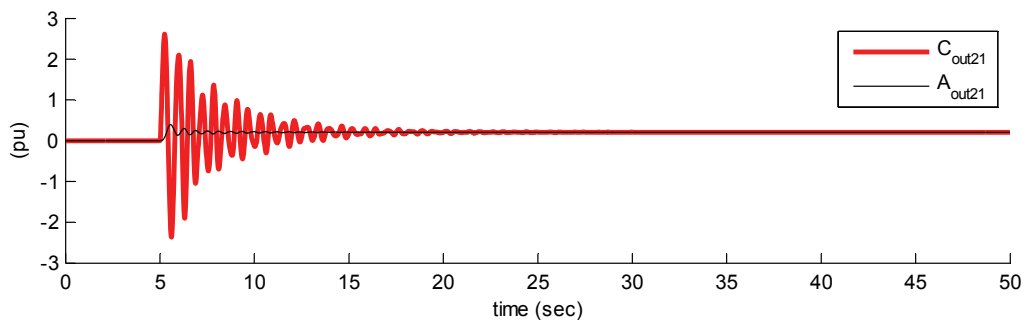
In order to observe if the controller output signal can be limited by the single parameter  $\omega_n$ , the system is slightly rearranged by moving the actuator TF and plant TF to the feedback loop. The output signal  $y$  is then equal to the controller output signal and the closed-loop TF can be written as:

$$TF_{cl} = \frac{C(s)}{1 + C(s) \cdot A(s) \cdot G(s)} \quad (4.19)$$

Simulations show, that indeed the amplitude of the controller output signal can be limited through a smaller parameter value  $\omega_n$ . The controller parameter  $\omega_n$  also defines the performance of the controlled system. With a higher  $\omega_n$ , actuator characteristics are compensated more, resulting in better performance and faster reaction of the actuator system.

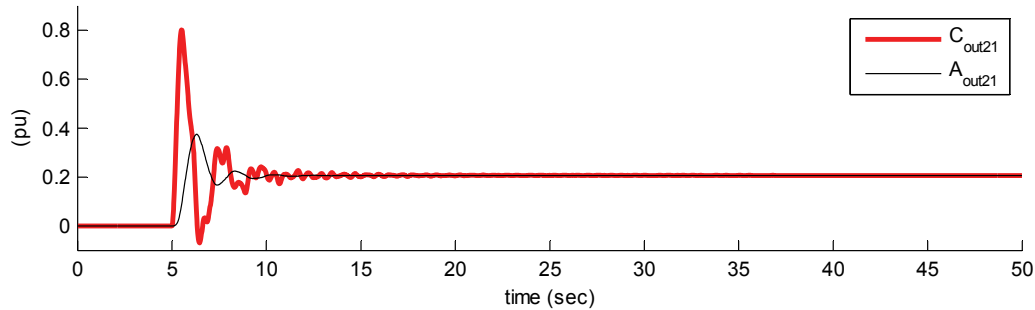
#### Simulations Results – Controller output for varying controller parameter $\omega_n$

Controller parameter  $\omega_n = 5$

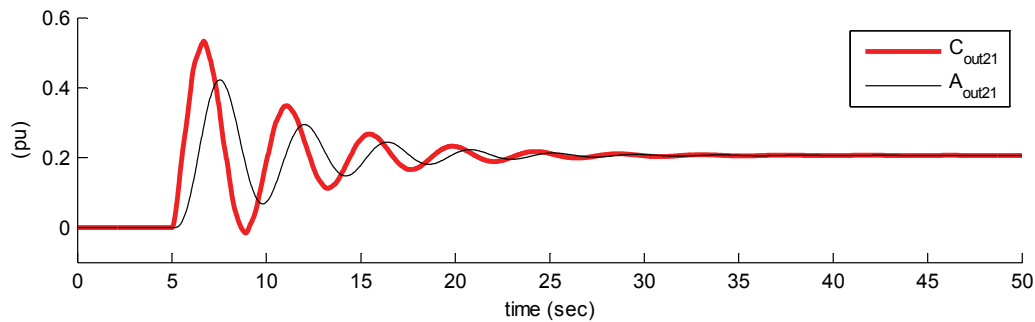




Controller parameter  $\omega_n = 2$



Controller parameter  $\omega_n = 1$



### Results

- The 3 plots show the controller output signal and the actuator output for a varying controller parameter  $\omega_n$ . Having a look at the y-axis scale, it can be seen that the amplitude of the controller output signal is limited with a decreasing  $\omega_n$  of the controller.
- The controller output signal is not only limited in its amplitude but also in its frequency, meaning that the controller acts slower with a decreasing parameter  $\omega_n$ .
- In all plots, the actuator output is tending to a value of 0.2pu in steady-state, irrespectively of the controller output magnitude.
- The characteristic of the actuator system, a certain filtering, can be seen very well in the plots. A faster controller, as the one with  $\omega_n = 5$ , compensates very well for the actuator characteristic, resulting in a very fast and accurate actuator output.

Table 4-1: Simulation Results – Controller output for varying controller parameter  $\omega_n$

#### 4.2.4 Robustness Analysis

In control design it is very important that developed controllers have a robust design. In a robustness analysis the controller behavior with respect to changes in the system can be evaluated. With such an analysis, weak system conditions can be found, which need to be determined for a robust control design. In our case, we first calculate a Youla-based controller for a specific initial system  $G$ . The calculated controller is then evaluated in respect to a disturbed system  $G_{dist}$ . That means that the system  $G$  changes, while the controller remains unchanged. There is a broad set of possible disturbances to the grid and the system  $G$ .

<b>Change in:</b>	Net active power at bus $i$
	Inertia Constants at generator $i$
	Damping constant at generator $i$
	Line admittance from bus $i$ to bus $j$ (or shut down of line)

Table 4-2: Possible variations in system characteristics

Remembering the standard control system structure, one can come up with two important transfer functions that will be evaluated for robustness. The TF  $G_{dist}(s)$  stands for the disturbed system TF  $G(s)$ .

$$\begin{aligned}
 TF_{ol}(s) &= C(s) \cdot G_{dist}(s) \\
 TF_{cl}(s) &= \frac{TF_{ol}(s)}{1 + TF_{ol}(s)} = \frac{C(s) \cdot G_{dist}(s)}{1 + C(s) \cdot G_{dist}(s)}
 \end{aligned} \tag{4.20}$$

The open-loop TF is of particular interest. Properties such as stability and pole-zero movements can be well observed from that transfer function.

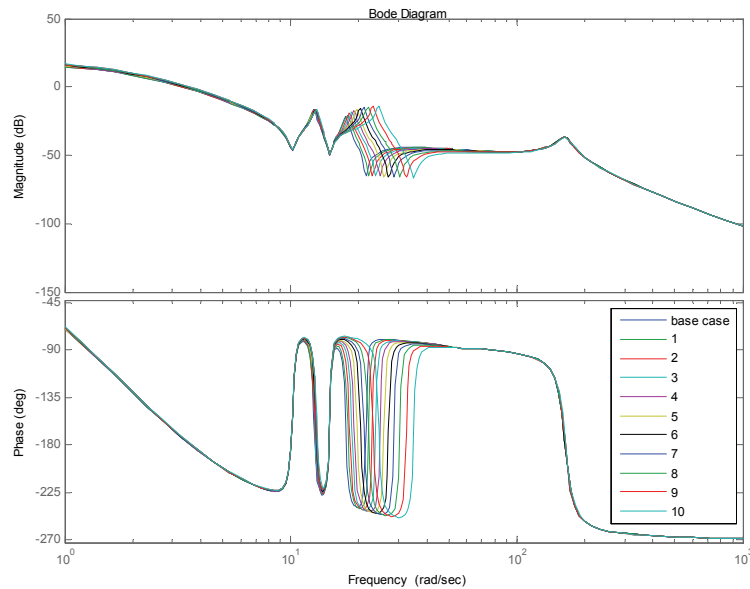
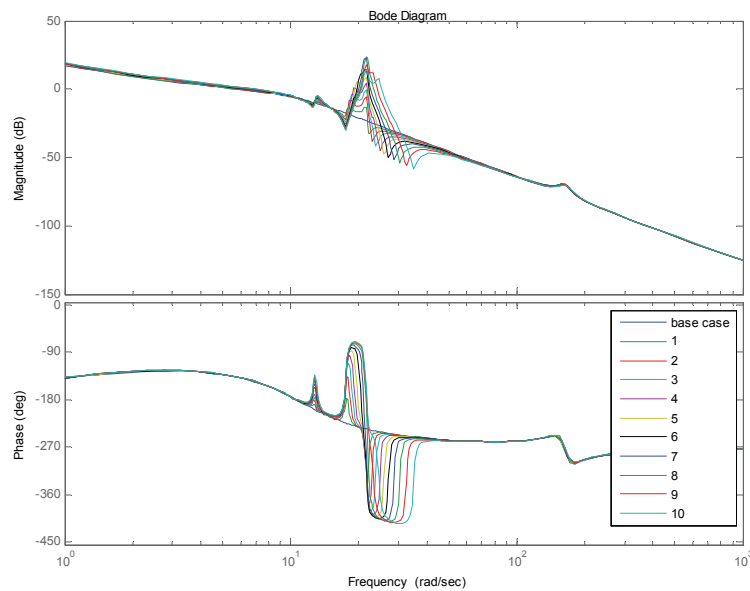
Simulations have been made for the disturbances listed before. Some disturbances have shown more influence, others less. Disturbances in net active power at buses have a rather little influence. Also the damping at generators has little influence. Changes in inertia constants  $H_i$  at bus  $i$  did show a significant influence, suggesting that control should be designed with good quality data on generator inertia.

**Example: Change in inertia  $M_1$** 

Applied change:  $H_1 = H_1 - 0.5$  for 10 steps. ( $M = \frac{2 \cdot H}{2 \cdot \pi \cdot 60}$ )

System transfer function

$$G_{dist}(s)$$

Open-loop transfer function  $TF_{ol}(s)$ **Results**

- These figures show the relative strong influence of disturbances on  $G(s)$ .

Table 4-3: Robustness analysis for a change in inertia constant

If different transmission lines are shut down, a strong influence on transfer functions including  $G(s)$  can be seen. Some lines are found to be more critical for stability. Lines 1, 2, 3, 6 and 10 are found to be critical. Line 10, the connection from bus 2 to bus 5 is the most critical. Shut-down of this line together with a high parameter  $\omega_n$  resulted in instability. Shut-down of line 10 was found to be a worst-case scenario for the considered test-system.

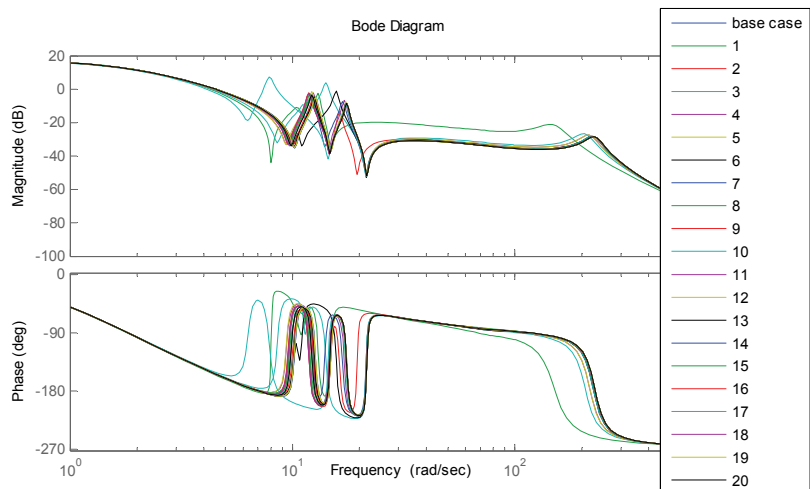
*Considering this specific worst-case scenario, in practice, additional control systems would be switched on in order to conduct certain emergency operations. It is not objective of this work to consider this emergency control design in detail.*

#### Example: Shut down of lines 1 to 20

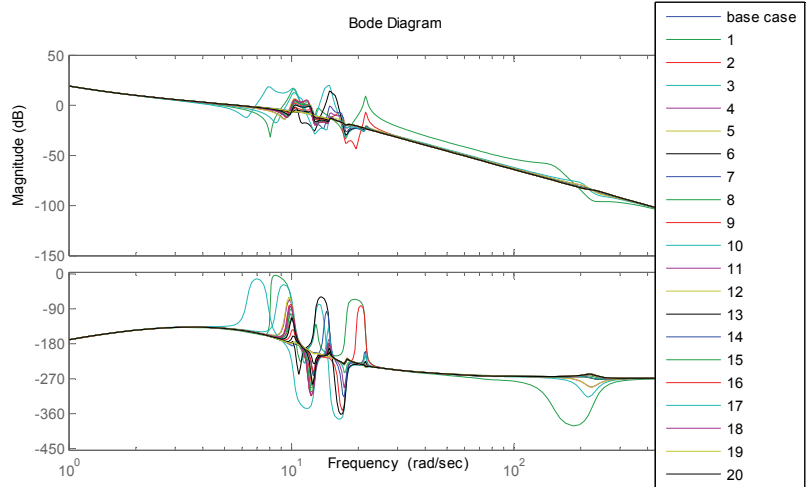
Applied change: switched off lines one line after another.

System transfer function

$$G_{dist}(s)$$



Open-loop transfer function  $TF_{ol}(s)$



### Results

- The disturbances result in different characteristics of the open-loop transfer functions.
- The stability of the closed-loop system is no longer guaranteed if some lines are shut down.

Table 4-4: Robustness analysis for line trips

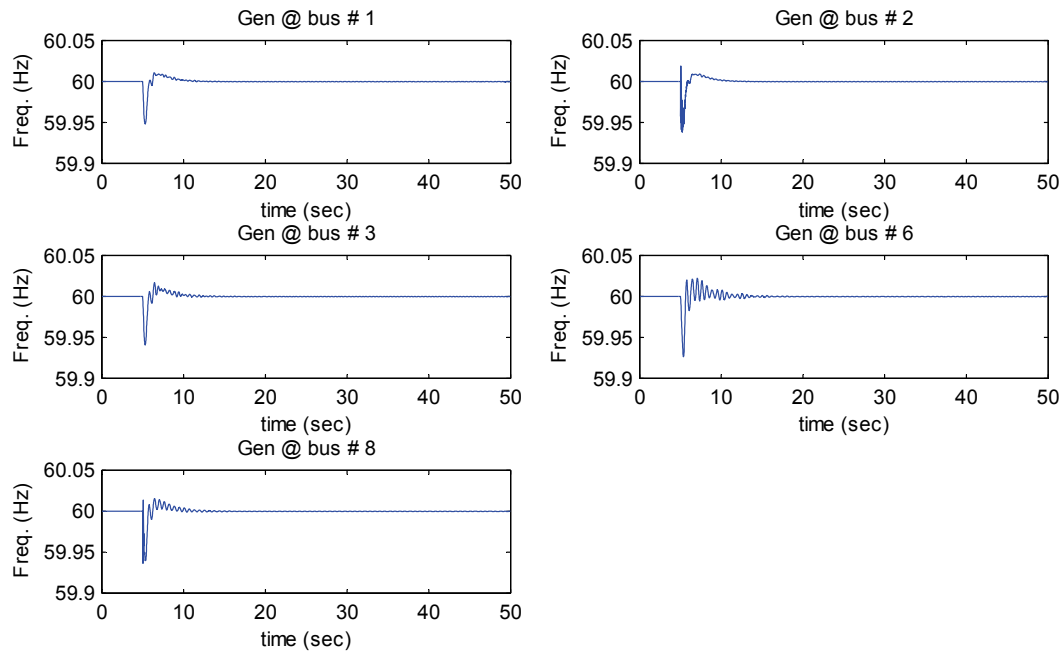
#### 4.2.5 Results

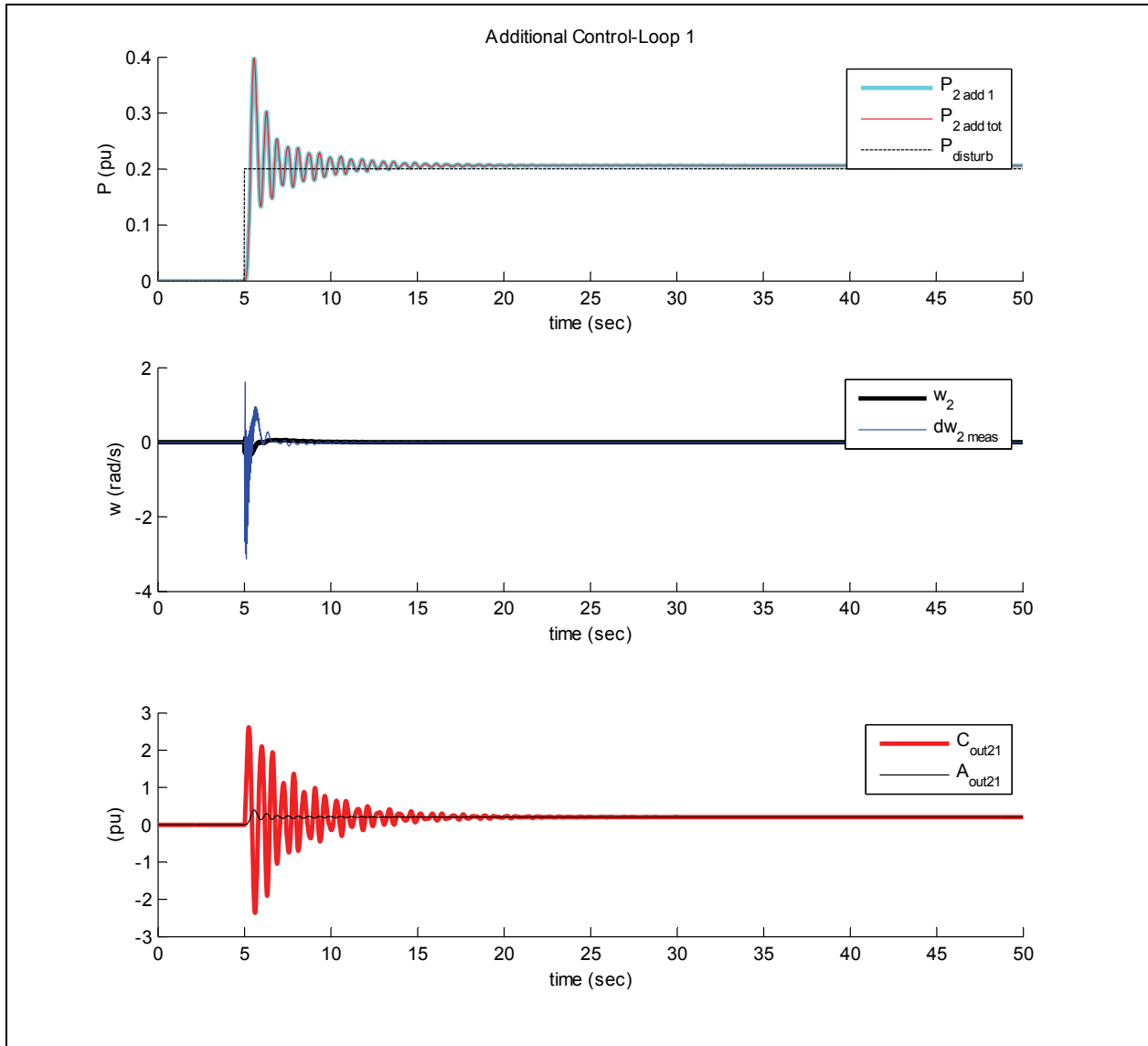
Simulation results of the single control branch with a first Youla-based control design are presented here. With this controller, the performance is significantly improved. Compared to previous results these simulations show an improvement up to a factor of 5.

#### Simulation Results – Single power branch with control

##### Simulation 1

- Based on standard system configuration (Chapter 3.1.3)
- Additional power path at bus 2
  - Measurement:  $\tau = 0.1\text{s}$
  - Power branch 1
    - Actuator 1:  $\tau_1 = \tau_2 = 0.5\text{s}$
    - Controller 1:  $\omega_n = 5$
- Excitation scenario 1: 0.2pu step disturbance at load bus 4



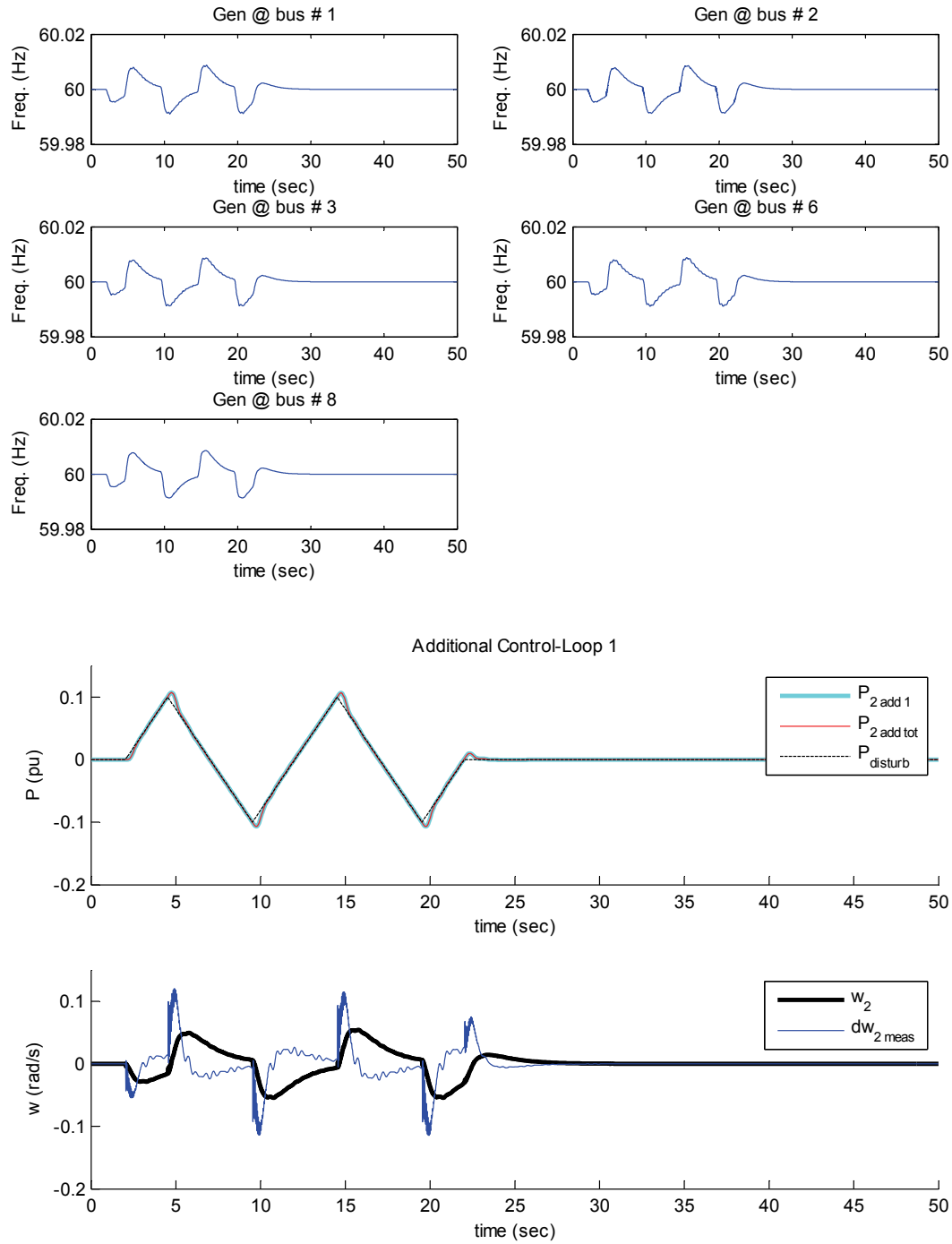


### Results

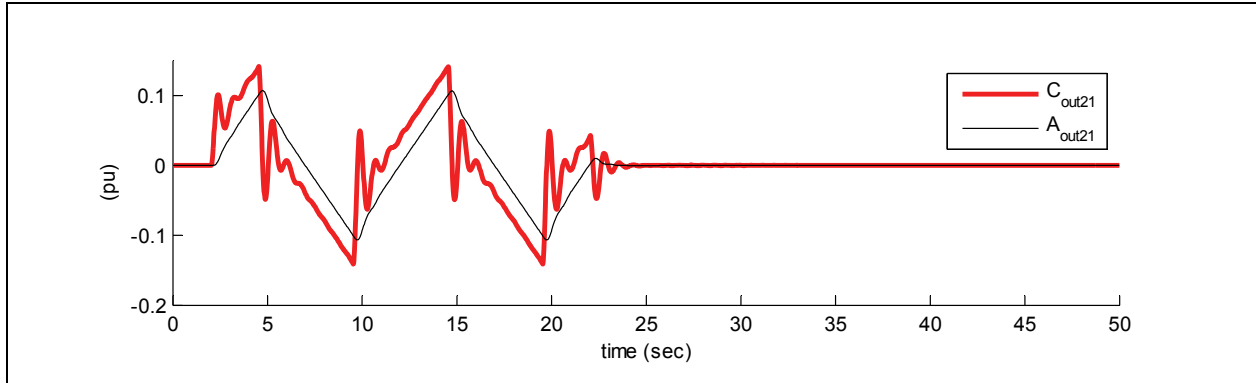
- The implemented controller results in a very fast reaction of the actuator system providing additional power ( $A_{\text{out21}}$ )
- Without implemented saturation limits, the controller compensates for all the power and brings the frequency deviation back to a zero value.

**Simulation 2**

- Based on standard system configuration (Chapter 3.1.3)
- Same additional configuration as in simulation 1
- Excitation scenario 2: 0.2pu p-p triangle-wave disturbance at generator bus 2







### Results

- The frequency plots show a very good performance in terms of frequency deviation. The maximum frequency deviation is 0.01Hz.
- Without implemented saturation limits, the controller compensates for all power.
- Comparing the controller output signal with the actuator output power, it can be seen clearly that the controller tries to compensate the characteristics of the actuator system. The controller output signal  $C_{out21}$  leads the actual actuator output in order to make the power output as accurate to the power disturbance in the system.

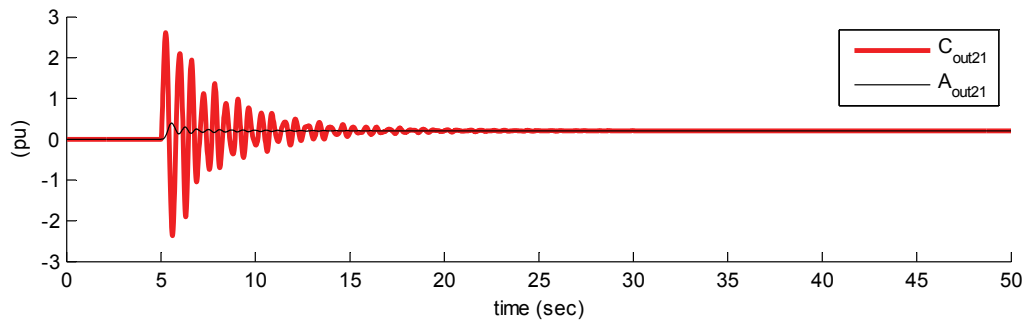
Table 4-5: Simulation Results – Single power branch with control

### Findings

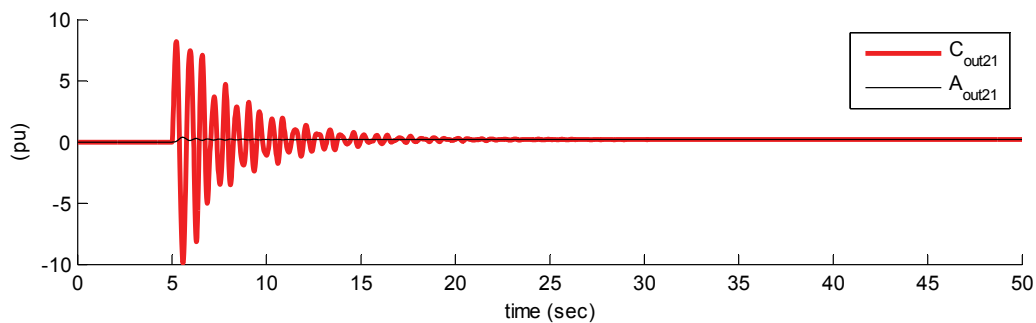
- Simulations show, that the reaction time of the actuator system is compensated by the controller. The reaction of the overall control can only be varied by the design parameter  $\omega_n$  of the controller itself. If for example a slow actuator system is chosen, the controller then compensates for this slower actuator system by increasing the controller output signal so that the slope of the closed-loop response looks the same as it would look like with a faster actuator. This is because the controller is optimized to an optimal closed-loop performance that is the same for both cases. A simulation for this can be seen in Table 4-6.
- Saturation limits have to be considered, because complete compensation by very large magnitude control action is not a realistic behavior. In these cases only a realistic inertial response should be provided.
- The realistic limits on the control path's power contribution can be enforced by suitable choice of the control parameter  $\omega_n$ .

### Simulation Results – Controller output for varying actuator bandwidth

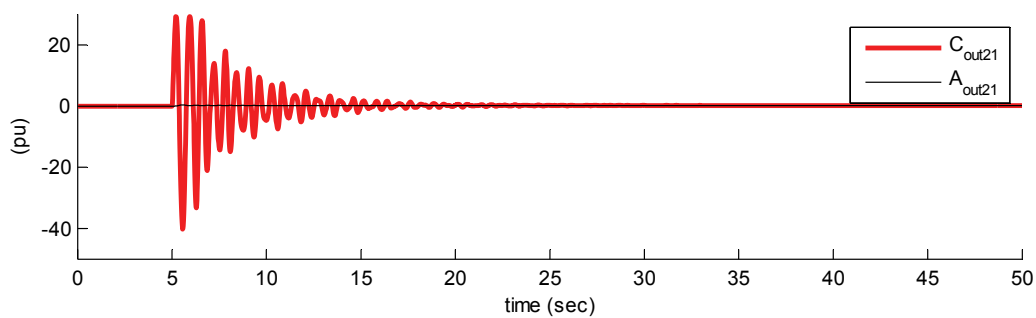
Actuator 1:  $\tau_1 = \tau_2 = 0.5\text{ s}$



Actuator 1:  $\tau_1 = \tau_2 = 1\text{ s}$



Actuator 1:  $\tau_1 = \tau_2 = 2\text{ s}$



### Results

- The 3 plots show the controller output signal and the actuator output for actuator systems with different time constants. As can be seen from the y-axis scales of the 3 plots, the controller increases its output signal amplitude to compensate for a slower actuator system.
- The additional power contributions, the actuator output signals, look exactly the same. The controller totally compensates for slower actuator systems.

Table 4-6: Simulation Results – Controller output for varying actuator bandwidth

### 4.3 Applied Approach with 2 Branches in Parallel

Until now, only one controlled additional power branch at a wind turbine bus was considered. In the studies without control, up to 3 parallel branches with different actuator characteristics were considered. The next step is now to develop the control design for control branches operating in parallel. Two parallel additional power branches with two controllers and two different actuators, that have different time constants and saturation characteristics, are considered.

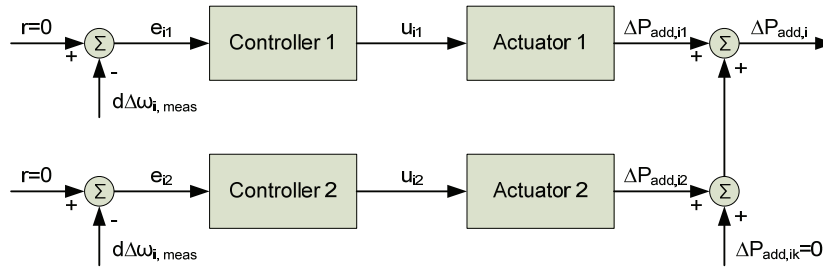


Figure 4-14: 2 parallel power branches

This work treats three different approaches for the control design of 2 controllers. The simplest way is to use the same design algorithm for both controllers independent from each other, referring as independently-designed controllers. As a further refinement the design of controller 2 should take controller 1 into account. This approach is referred as sequentially-designed controllers. And a third approach should take both controllers as coupled into account; this refers to a MIMO-based control design.

The different control designs are compared to each other and we will test the “natural” hypothesis that the performance of control will increase from the parallel, to the sequential and finally to the MIMO approach.

### 4.3.1 Controllers Designed Independently

For the calculation of the 2<sup>nd</sup> controller, the same algorithm as for controller 1 is used. This means that controller 1 has no influence for the calculation of controller 2. The system TF  $G(s)$  for both controller calculations is the same as used before for the one controller case.

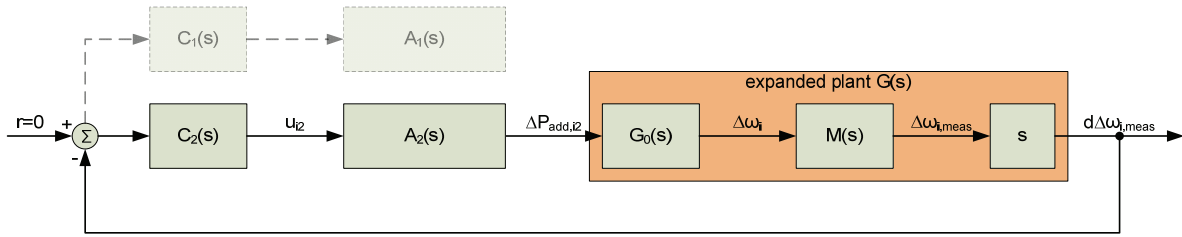


Figure 4-15: 2<sup>nd</sup> control system structure for controllers designed independently

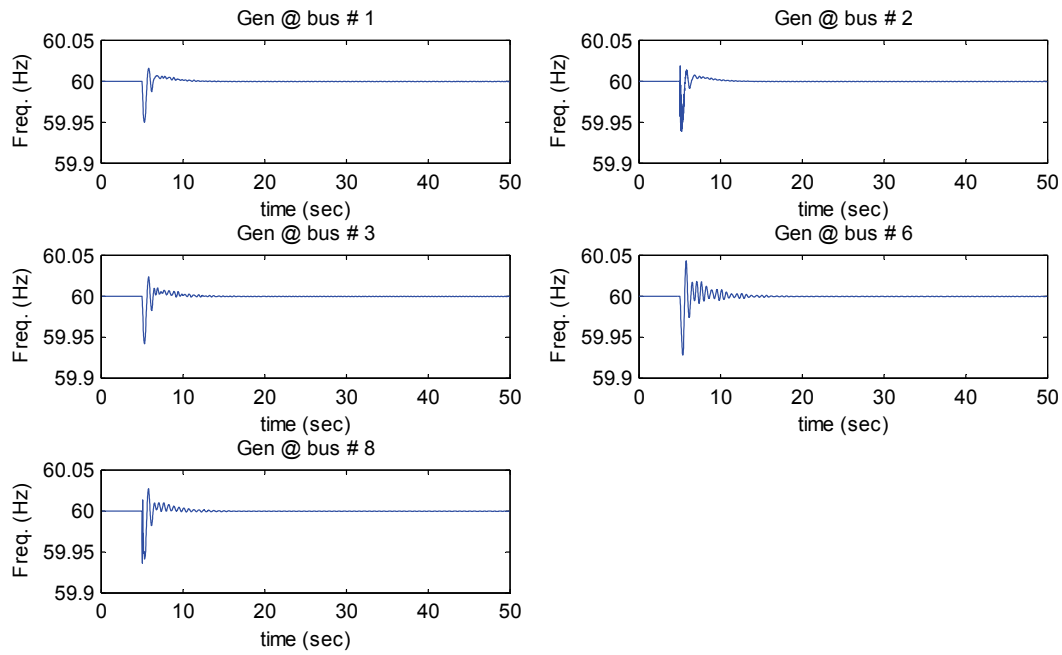
The two control paths have different actuator systems with different characteristics. Obviously in the case of parallel controller design it is not important which controller is calculated first, because both calculations are performed independently and parallel, based on the same plant TF  $G(s)$ . The only difference exists in the actuator systems  $A_1(s)$  and  $A_2(s)$ .

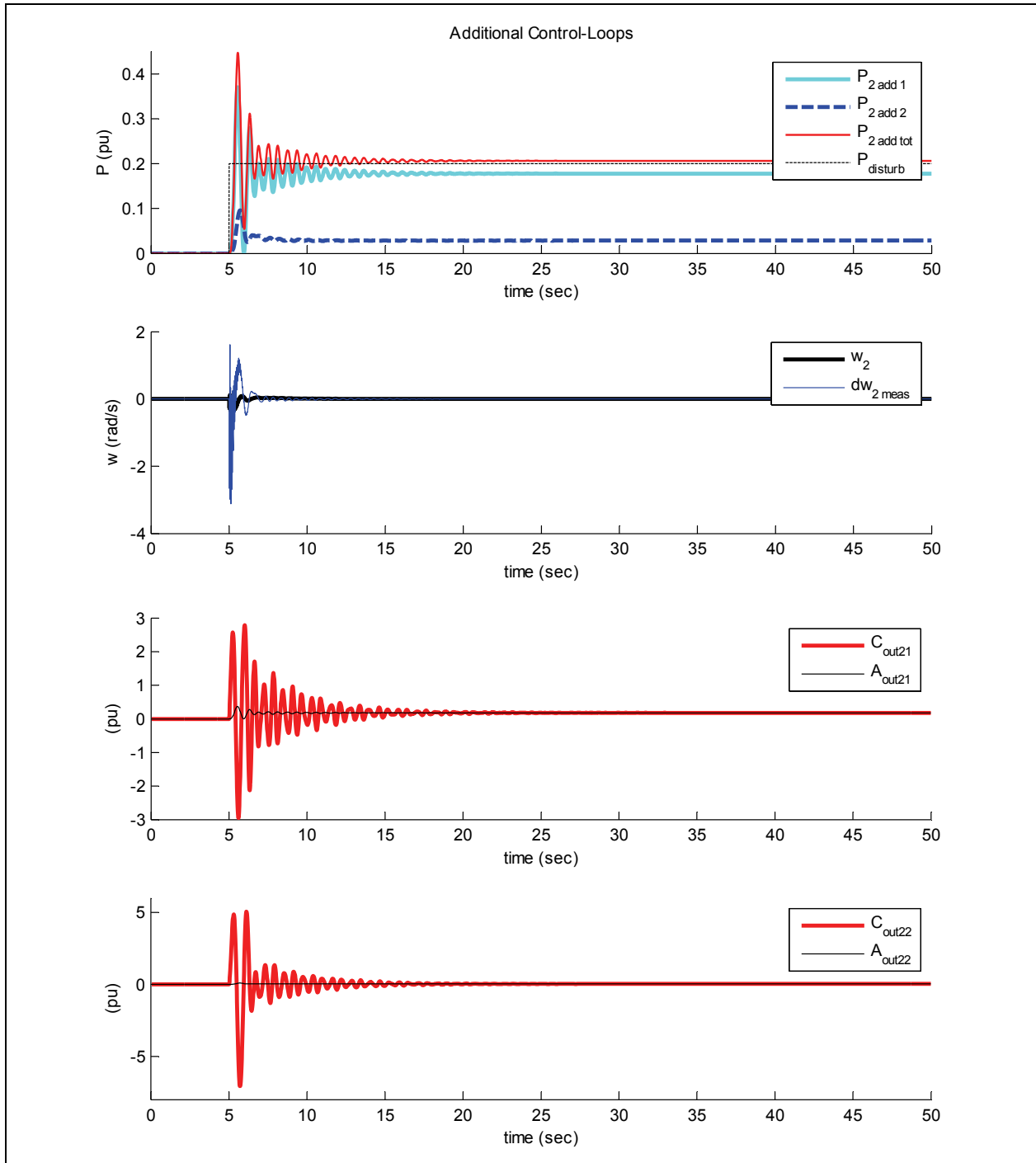
First results of this implementation are presented below. Simulations show that with the control parameter  $\omega_n$ , the individual contribution of the two control loops can be adjusted. As seen in simulations before, the actuator systems have almost no influence on the overall performance but rather change the characteristics of the internal signals of the control loops. The nature of the Youla Parameterization design method is such that controllers compensate for the actuator characteristics by adjusting their output signals.

### Simulation Results – Two parallel branches with controllers designed independently

#### Simulation 1

- Based on standard system configuration (Chapter 3.1.3)
- Additional power path at bus 2
  - Measurement:  $\tau = 0.1\text{s}$
  - Power branch 1:
    - Actuator 1:  $\tau_1 = \tau_2 = 0.5\text{s}$
    - Controller 1:  $\omega_{n1} = 5$
  - Power branch 2:
    - Actuator 2:  $\tau_1 = \tau_2 = 2\text{s}$
    - Controller 2:  $\omega_{n2} = 2$
- Excitation scenario 1: 0.2pu step disturbance at load bus 4



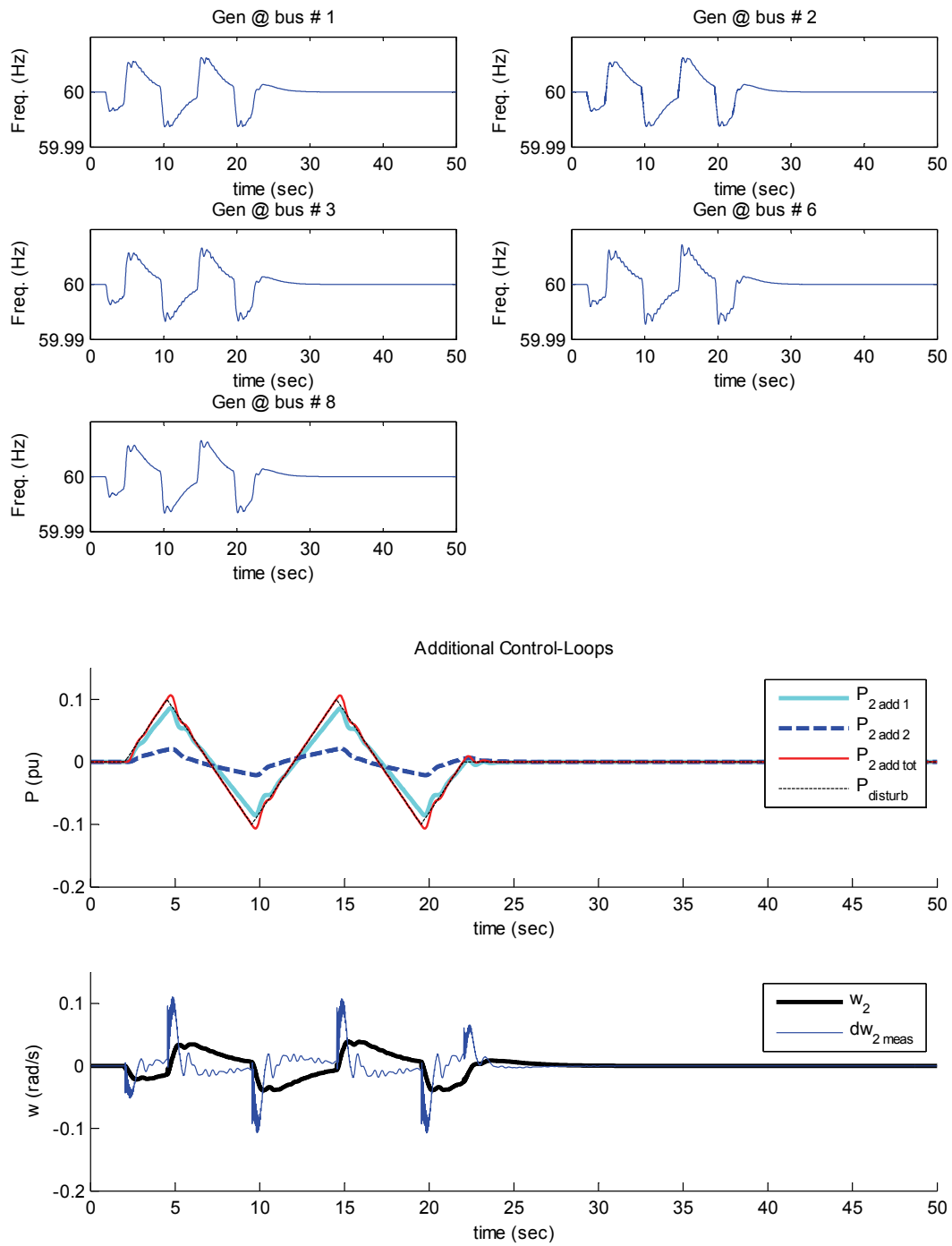


### Results

- Considering the frequency plots, no significant improvement through the 2<sup>nd</sup> controller can be seen compared to the single controller case.
- The sharing of control action can be seen in the power contribution plot. The additional control branch 1 compensates for nearly 100% of the disturbance, whereas the added second branch compensates only for a little amount. Considering saturation aspects the partition between the control paths should be exactly the opposite.

**Simulation 2**

- Based on standard system configuration (Chapter 3.1.3)
- Same additional configuration as in simulation 1
- Excitation scenario 2: 0.2pu p-p triangle-wave disturbance at generator bus 2



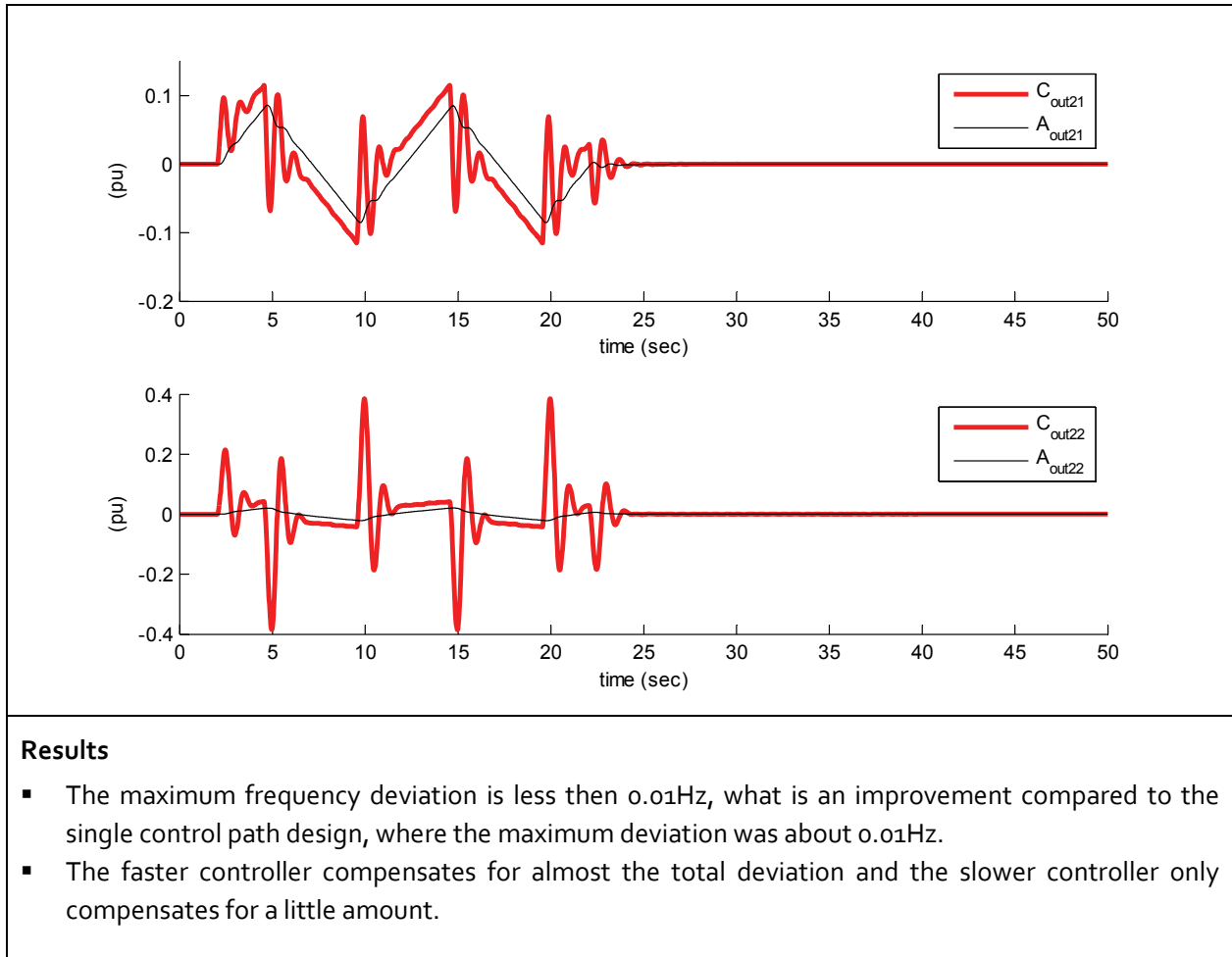


Table 4-7: Simulation Results – Two parallel branches with controllers designed independently

### Findings

- The sharing of control action is difficult with this method. The controller with the larger  $\omega_n$  has a faster reaction, but also compensates for most of the deviation. Considering saturation, this is not the desirable behavior, because our assumption is that typically the higher bandwidth control path will have a lower saturation limit.
- As before, the actuator filters are fully compensated by the controllers in the Youla Parameterization method.



### 4.3.2 Controllers Designed Sequentially

In the sequential design approach, the second controller is calculated based on the first controller. As a first step, the plant TF  $G(s)$  is expanded with the first control branch as illustrated in Figure 4-16 below.

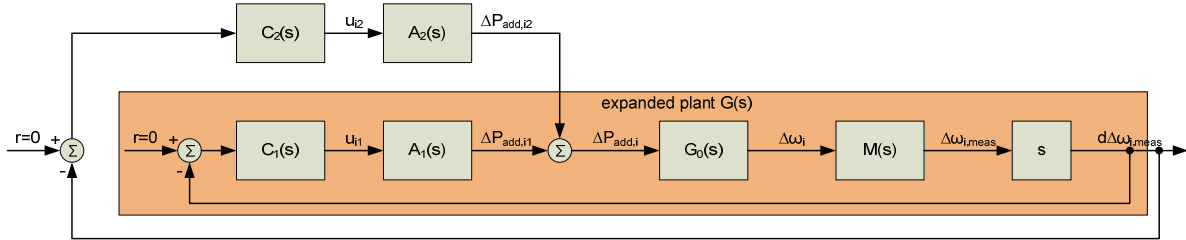


Figure 4-16: 2<sup>nd</sup> control system structure for controllers designed sequentially

The expanded  $G(s)$  is then defined as

$$G(s) = \frac{G_0(s) \cdot M(s) \cdot s}{1 + G_0(s) \cdot M(s) \cdot s \cdot (C_1(s) \cdot A_1(s))} \quad (4.21)$$

This expanded  $G(s)$  serves now as the new system plant and is used for the calculation of the 2<sup>nd</sup> controller applying the same algorithm as for the first controller. We call this design method “sequential design methodology”, because controller 2 takes into account the influence of controller 1 and the design method refers to a sequential procedure.

Now, using the sequential computation, it makes a difference which controller is calculated first. The question arises, in what order the controllers should be designed: The slow control branch first and then the fast one, or conversely? Both approaches have been simulated and evaluated.

The first hypothesis was that it would be best to begin with the slower controller and design the faster afterwards. Since control speed can be influenced mainly by the selection of  $\omega_n$ , as we have seen before, the parameter  $\omega_{n1}$  is chosen to be smaller than the parameter for the second controller  $\omega_{n2}$ . In addition the actuator system of the first controller is chosen slower than the actuator system of the 2<sup>nd</sup> controller.

$$\begin{cases} \omega_{n1} < \omega_{n2} \\ \tau_{11}, \tau_{12} > \tau_{21}, \tau_{22} \end{cases} \quad (4.22)$$

Simulations have shown that controller 2 with the faster control reaction as well as the faster actuator almost takes all control effort. By varying  $\omega_{n2}$  of the second controller, the allocation of control effort

cannot be varied significantly. Controller 2 (calculated on basis of controller 1) always takes nearly all control effort. These simulation results didn't show the originally hypothesized behavior and so in a second approach the faster controller was calculated first.

The calculation order has changed now. Controller parameters  $\omega_n$  and actuator time constants are set the other way round to represent a fast system on control branch 1 and a slower system on branch 2.

$$\begin{cases} \omega_{n1} > \omega_{n2} \\ \tau_{11}, \tau_{12} < \tau_{21}, \tau_{22} \end{cases} \quad (4.23)$$

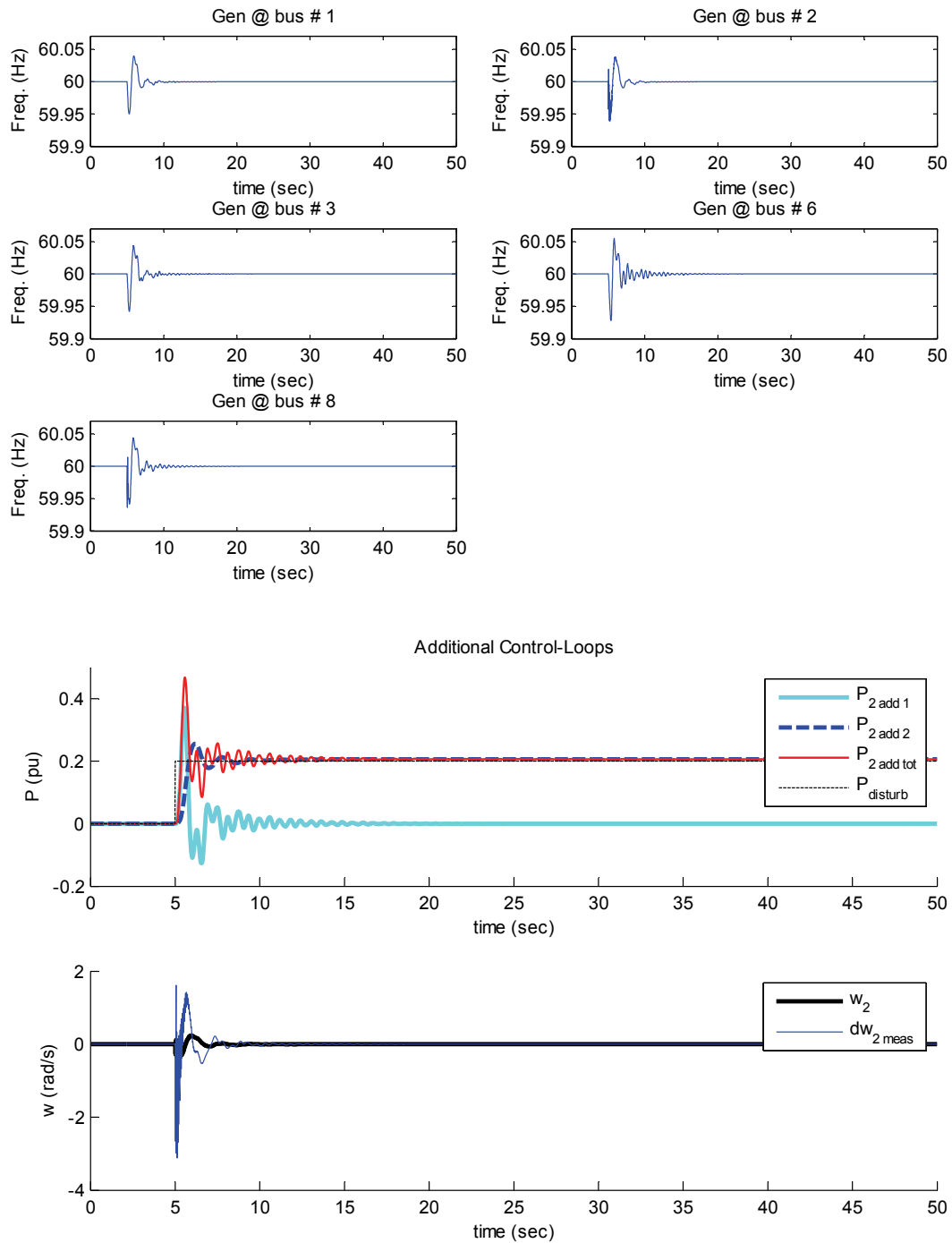
Simulations in this configuration show surprisingly good results. By tuning parameter  $\omega_{n2}$  of the slower 2<sup>nd</sup> controller, the contribution of controller 2 can be adjusted. Setting the control contribution of controller 2, means that the contribution of controller 1 is set as well. This means, that in average one can set the power output of the faster controller to a certain level. The faster controller compensates for a limited amount in the first moment and the rest is compensated by the slower controller with limited bandwidth. The results show pretty much the desired behavior and the performance is very satisfying.

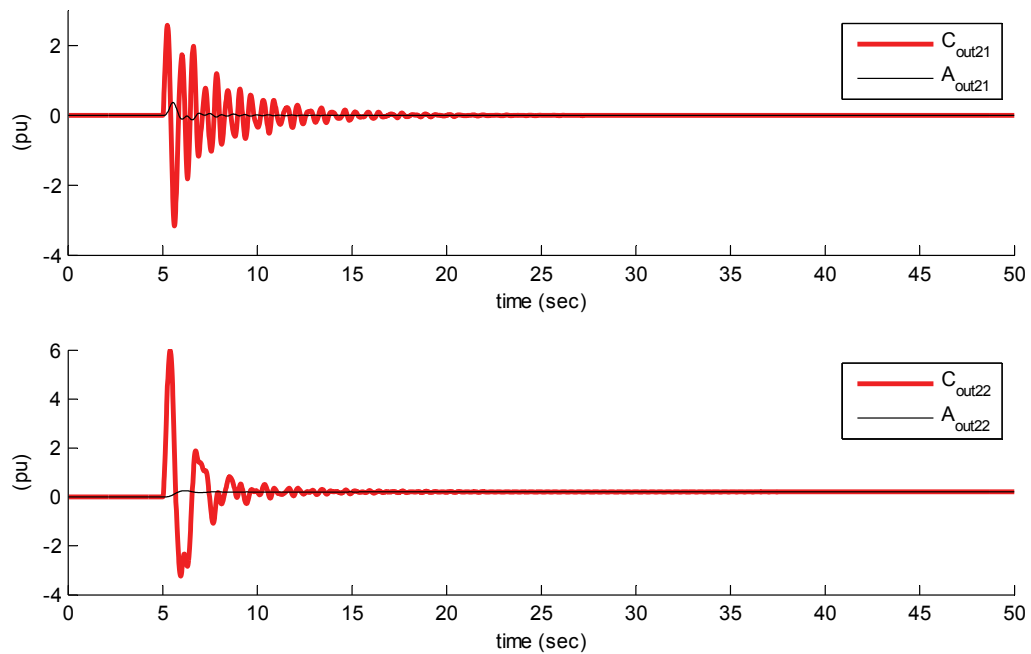
The selected design method for the following simulations is the latter one: The slow controller is designed on the basis of the fast one.

#### Simulation Results – Controllers designed sequentially

##### Simulation 1

- Based on standard system configuration (Chapter 3.1.3)
- Additional power path at bus 2
  - Measurement:  $\tau = 0.1\text{s}$
  - Power branch 1:
    - Actuator 1:  $\tau_1 = \tau_2 = 0.5\text{s}$
    - Controller 1:  $\omega_{n1} = 5$
  - Power branch 2:
    - Actuator 2:  $\tau_1 = \tau_2 = 2\text{s}$
    - Controller 2:  $\omega_{n2} = 2$
- Excitation scenario 1: 0.2pu step disturbance at load bus 4



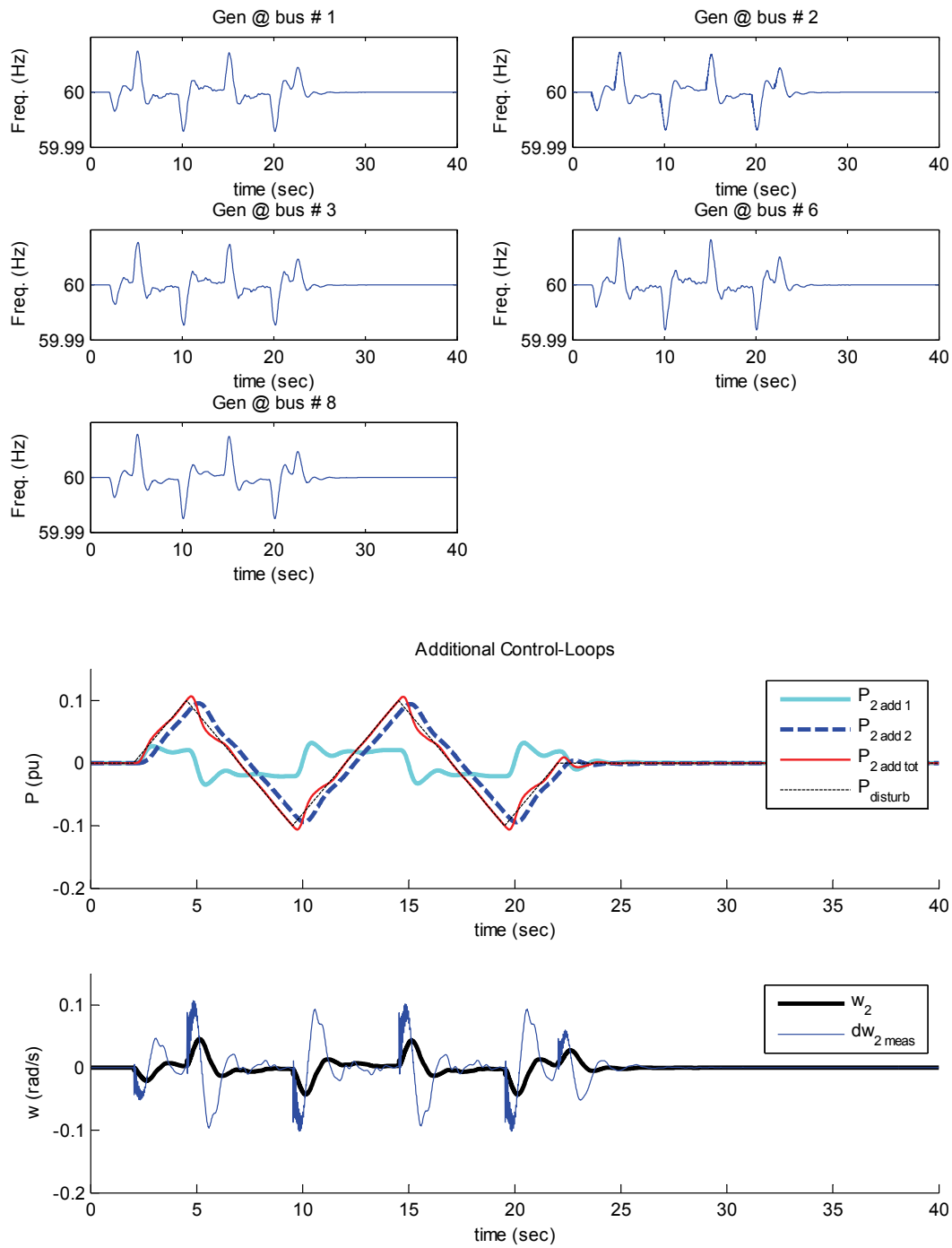


### Results

- In terms of maximum frequency deviation, no significant improvement compared to the individual design method can be seen, but one should keep in mind, that the controllers are designed in terms of a ramp input.
- The sharing of control-action looks promising, meaning that the faster controller acts only in a first moment, then the slower control branch takes over.

**Simulation 2**

- Based on standard system configuration (Chapter 3.1.3)
- Same additional configuration as in simulation 1
- Excitation scenario 2: 0.2pu p-p triangle-wave disturbance at generator bus 2



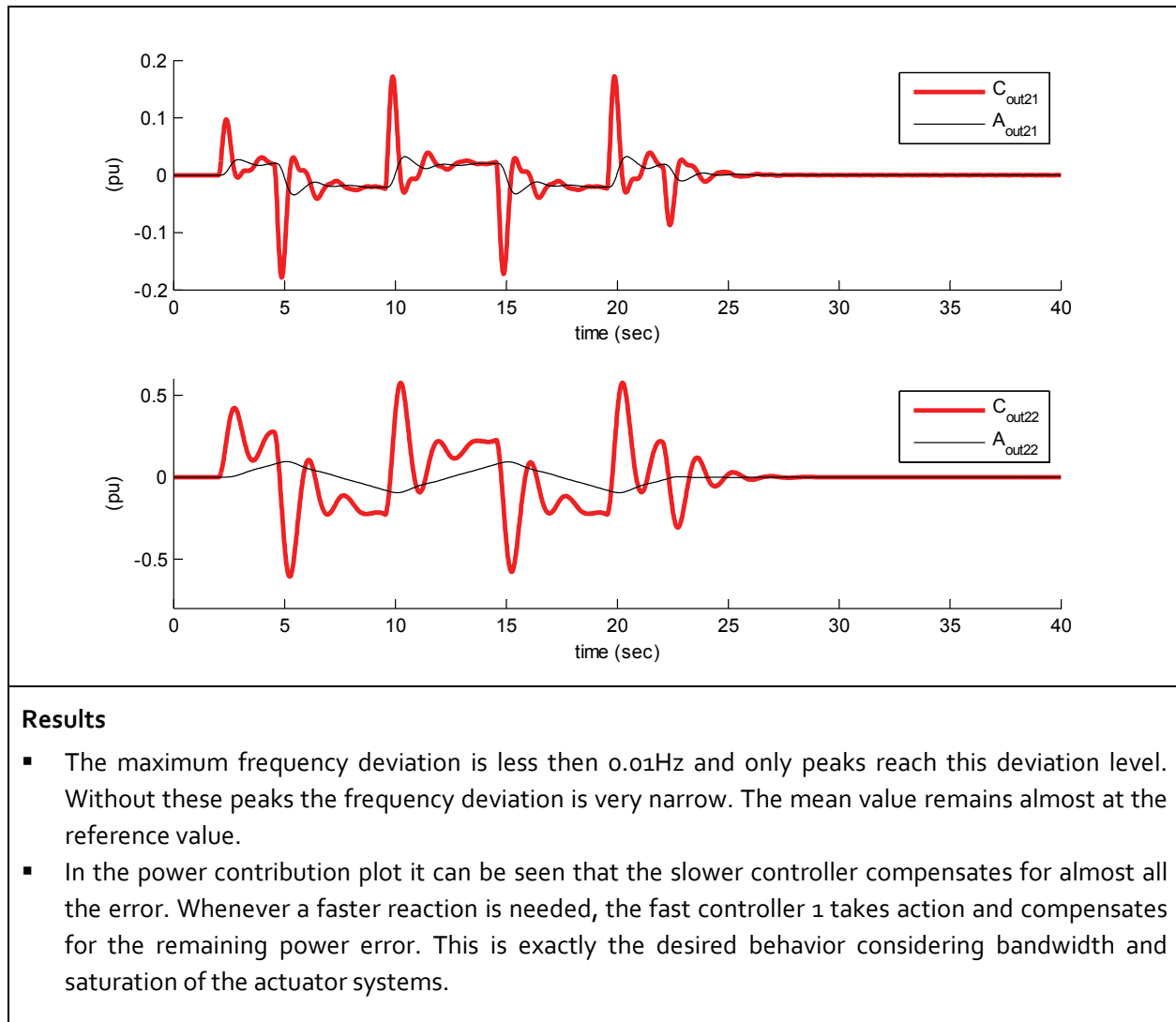


Table 4-8: Simulation Results – Controllers designed sequentially

### Findings

- The performance of this sequential design is very satisfying.
- Sharing between the controllers can be controlled by adjusting the controller parameter  $\omega_n$  of the second and slower controller.
- Finding a controller of reasonable order for the 2<sup>nd</sup> slower branch was difficult. By reduction, a controller of order 14 could be found in the end.

### Setting Hard Power Output Limits

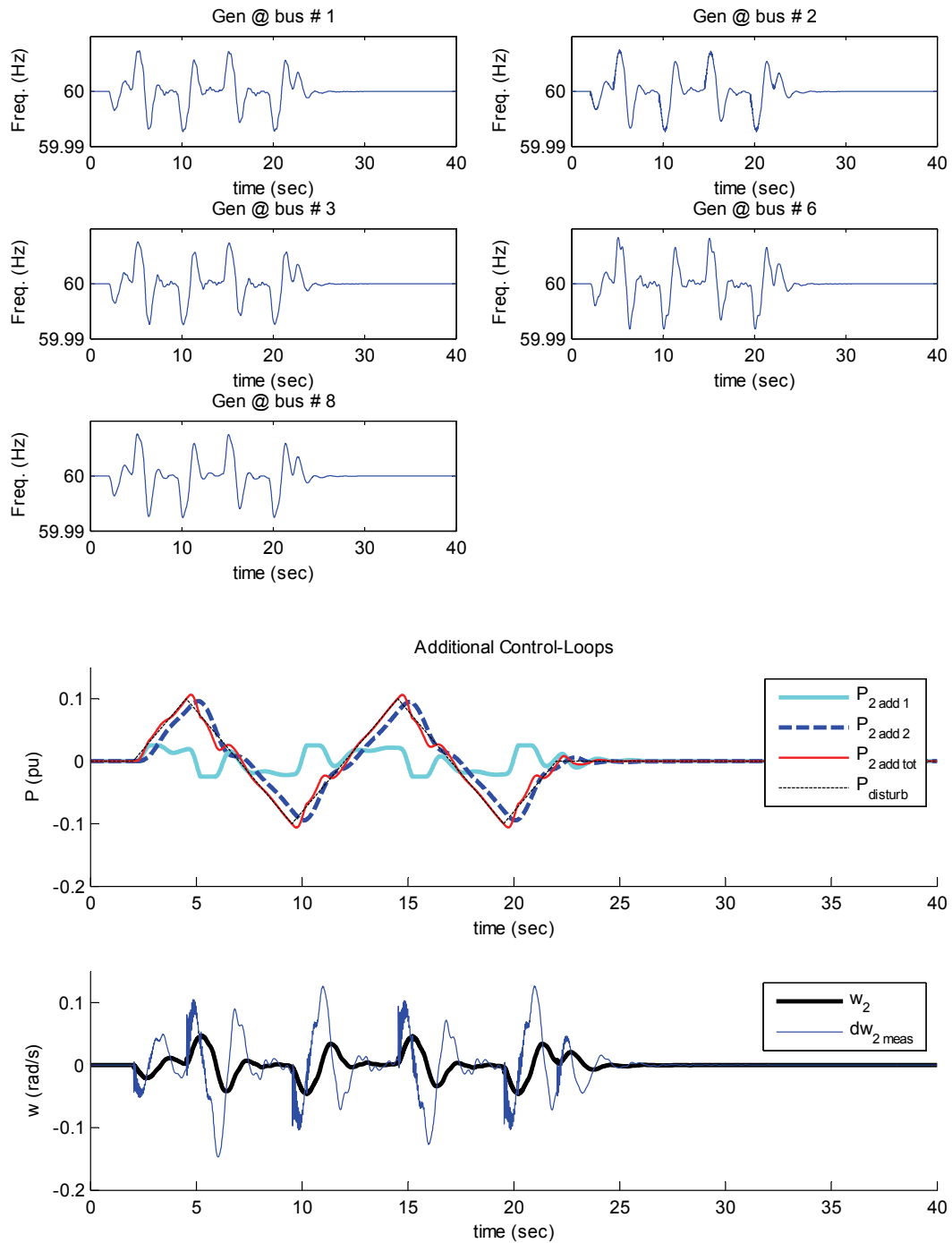
For further observations, hard power limits are now applied. As seen before in the results from the sequential controller design, the power output from the fast controller can roughly be determined to a defined, average power level with some initial peaks. By using a hard power output we limit these peaks. The saturation function takes action as soon as power output hits the saturation level. Applying this saturation to the sequential calculation results in a modest reduction of control performance.

Simulations show, however, that the saturation limit must only be reached for a short time in order to obtain an acceptable result. In particular, problems arise if the hard output power limit of the faster controller is set below the average output level; in this case the time domain simulations shows no convergence suggesting an unstable system response.

#### Simulation Results – Controllers designed sequentially with saturation

##### Simulation

- Based on standard system configuration (Chapter 3.1.3)
- Additional power path at bus 2
  - Measurement:  $\tau = 0.1\text{s}$
  - Power branch 1:
    - Actuator 1:  $\tau_1 = \tau_2 = 0.5\text{s}$
    - Limit 1: 0.03pu
    - Controller 1:  $\omega_{n1} = 5$
  - Power branch 2:
    - Actuator 2:  $\tau_1 = \tau_2 = 2\text{s}$
    - Limit 2: not active
    - Controller 2:  $\omega_{n2} = 2$
- Excitation scenario 2: 0.2pu p-p triangle-wave disturbance at generator bus 2





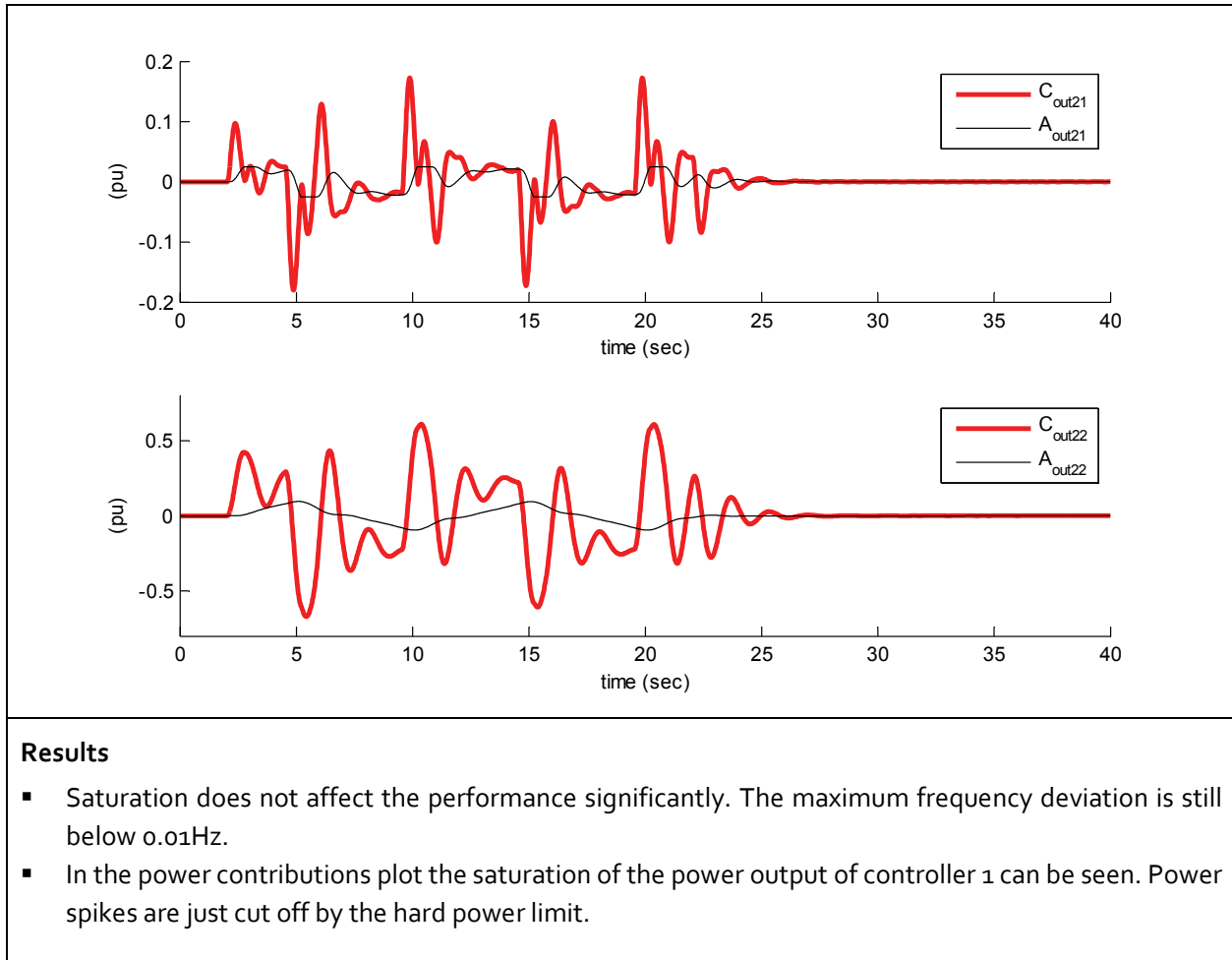


Table 4-9: Simulation Results – Controllers designed sequentially with saturation

### Findings

- Setting a hard saturation limit is sometimes problematic. If the limit is set too low, simulations showed no convergence. A reason for that might be that the controllers are designed in order to fully compensate a linear model of the system, without saturation, and are instead acting on a system with very different input-output behavior, due to the saturation. In physical terms, the power available to stabilize the system is limited. As a result the closed-loop gets unstable (program shows no convergence) if there's only limited resp. not enough power available.
- Keeping an actuator output at its saturation level means that the feedback loop is interrupted. The controller increases its output to go even more into saturation. If the controller output reaches too high values, convergence of the simulation is likely to fail.

### 4.3.3 Controllers Designed on MIMO-based Method

The 3<sup>rd</sup> and last approach is now to apply a MIMO-based control design. Unlike to the two previous cases, both controllers should now be designed simultaneously allowing a coupled characteristic. The general procedure for a MIMO Youla Parameterization is described at the beginning of the chapter. For the case here, the general procedure has to be modified to meet the special structure of the system.

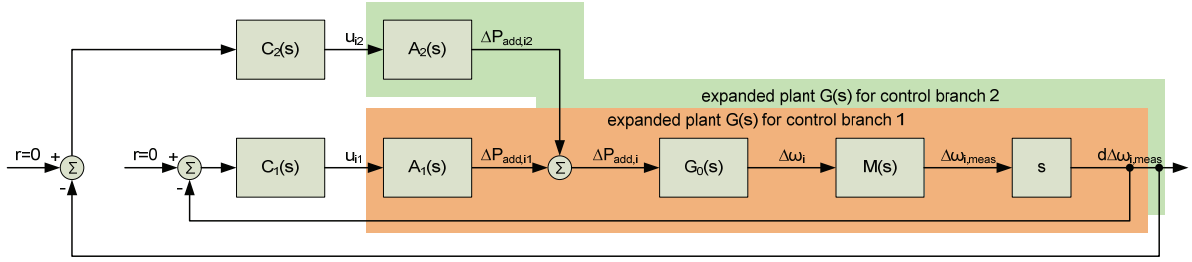


Figure 4-17: System structure for controllers designed on MIMO-based method

What is special in the system depicted above is that the number of inputs and outputs are not the same. There are two input signals, the two control signals from the two controllers, but only one output signal, the derivative of the frequency. Therefore the plant matrix  $\mathbf{G}$  is not a square matrix, but instead a  $2 \times 1$  vector matrix.

$$\mathbf{G} = \begin{bmatrix} y(s) / u_1(s) \\ y(s) / u_2(s) \end{bmatrix} = \begin{bmatrix} G_1(s) \\ G_2(s) \end{bmatrix} \quad (4.24)$$

If we split the two input-to-output TFs into actuator TFs  $A_i(s)$  and the rest of the system TF  $G_m(s)$ , the matrix  $\mathbf{G}$  can be written with numerators and denominators. This notation will then be helpful in the following steps.

$$\mathbf{G} = \begin{bmatrix} A_1(s) \cdot G_m(s) \\ A_2(s) \cdot G_m(s) \end{bmatrix} = \begin{bmatrix} \frac{n_{A1}(s)}{d_{A1}(s)} \cdot \frac{n_{Gm}(s)}{d_{Gm}(s)} \\ \frac{n_{A2}(s)}{d_{A2}(s)} \cdot \frac{n_{Gm}(s)}{d_{Gm}(s)} \end{bmatrix} \quad (4.25)$$

**Design Procedure**

1. Because we have only one output signal, we select a single closed-loop transfer function  $H(s)$  which provides an optimal closed-loop performance for both branches.

$$\mathbf{H} = \mathbf{T}_{cl} = (\mathbf{I} + \mathbf{T}_{ol})^{-1} \cdot \mathbf{T}_{ol} = (\mathbf{I} + \mathbf{C} \cdot \mathbf{G})^{-1} \cdot \mathbf{C} \cdot \mathbf{G} \quad (4.26)$$

2. In a next step the open-loop transfer function matrix  $\mathbf{Q}$  is introduced and the feedback system is represented by a simple open-loop structure as shown in Figure 4-18.

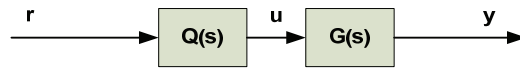


Figure 4-18: Open-loop equivalent system

$$\mathbf{T}_{eq} = \mathbf{Q} \cdot \mathbf{G} \quad (4.27)$$

The transfer function matrix  $\mathbf{T}_{eq}$  can then be replaced by the optimal closed-loop transfer function matrix  $\mathbf{H}$  selected in step 1. Because our plant TF matrix  $\mathbf{G}$  is not as in the general case a square matrix, an inverse cannot be taken directly. As a consequence, the matrix  $\mathbf{Q}$  cannot be calculated straightforward as in the general procedure.

In order to find  $\mathbf{Q}$ , we first have to find a pseudo inverse  $\mathbf{G}^\dagger$  with the following property:

$$\mathbf{G} \cdot \mathbf{G}^\dagger = \mathbf{I} \quad (4.28)$$

Suppose  $\mathbf{G}$  can be written with a common denominator  $d(s)$  for both transfer functions, then we can come up with the following equation:

$$\begin{bmatrix} \frac{n_1(s)}{d(s)} & \frac{n_2(s)}{d(s)} \end{bmatrix} \cdot d(s) \cdot \begin{bmatrix} G_1^\dagger(s) \\ G_2^\dagger(s) \end{bmatrix} \quad (4.29)$$

Where:

$$n_1(s) \cdot G_1^\dagger(s) + n_2(s) \cdot G_2^\dagger(s) \stackrel{!}{=} 1 \quad (4.30)$$

Consequently, one simple solution to this constraint is:

$$\begin{cases} G_1^\dagger(s) = 0.5 \cdot \frac{1}{n_1(s)} \\ G_2^\dagger(s) = 0.5 \cdot \frac{1}{n_2(s)} \end{cases} \quad (4.31)$$

With this result for a pseudo inverse, we can now calculate  $\mathbf{Q}$ . By using  $d(s) \cdot \mathbf{G}^\dagger$  instead of  $\mathbf{G}^{-1}$  we can find a matrix  $\mathbf{Q}$  that represents the open-loop equivalent of the feedback loops.

$$\mathbf{Q} = H(s) \cdot d(s) \cdot \mathbf{G}^\dagger = H(s) \cdot \begin{bmatrix} 0.5 \cdot \frac{d(s)}{n_1(s)} \\ 0.5 \cdot \frac{d(s)}{n_2(s)} \end{bmatrix} \quad (4.32)$$

As stated before, the use of these equations requires a plant TF matrix  $\mathbf{G}$  that has a common denominator for all transfer functions. If we have a look back to point 1, we see that our matrix  $\mathbf{G}$  has not the same denominator in both TFs. Therefore the TFs have to be expanded in order to make the denominators the same. The TF  $G_m(s)$  is the same in both TFs and so we do not have to consider it in the expansion.

$$\mathbf{G} = \begin{bmatrix} \frac{n_{A1}(s)}{d_{A1}(s)} \cdot G_m(s) \\ \frac{n_{A2}(s)}{d_{A2}(s)} \cdot G_m(s) \end{bmatrix} = \begin{bmatrix} \frac{n_{A1}(s)}{d_{A1}(s)} \cdot G_m(s) \cdot \frac{d_{A2}(s)}{d_{A2}(s)} \\ \frac{n_{A2}(s)}{d_{A2}(s)} \cdot G_m(s) \cdot \frac{d_{A1}(s)}{d_{A1}(s)} \end{bmatrix} = \begin{bmatrix} \frac{n_{A1}(s) \cdot d_{A2}(s)}{d_{A1}(s) \cdot d_{A2}(s)} \cdot G_m(s) \\ \frac{n_{A2}(s) \cdot d_{A1}(s)}{d_{A1}(s) \cdot d_{A2}(s)} \cdot G_m(s) \end{bmatrix} \quad (4.33)$$

3. The controller matrix  $\mathbf{C}$  is then computed with the standard equation given from the general case.

$$\mathbf{C} = (\mathbf{I} - \mathbf{Q} \cdot \mathbf{G})^{-1} \cdot \mathbf{Q} = \left( \mathbf{I} - \begin{bmatrix} Q_1(s) \\ Q_2(s) \end{bmatrix} \cdot \begin{bmatrix} G_1(s) & G_2(s) \end{bmatrix} \right)^{-1} \cdot \begin{bmatrix} Q_1(s) \\ Q_2(s) \end{bmatrix} \quad (4.34)$$

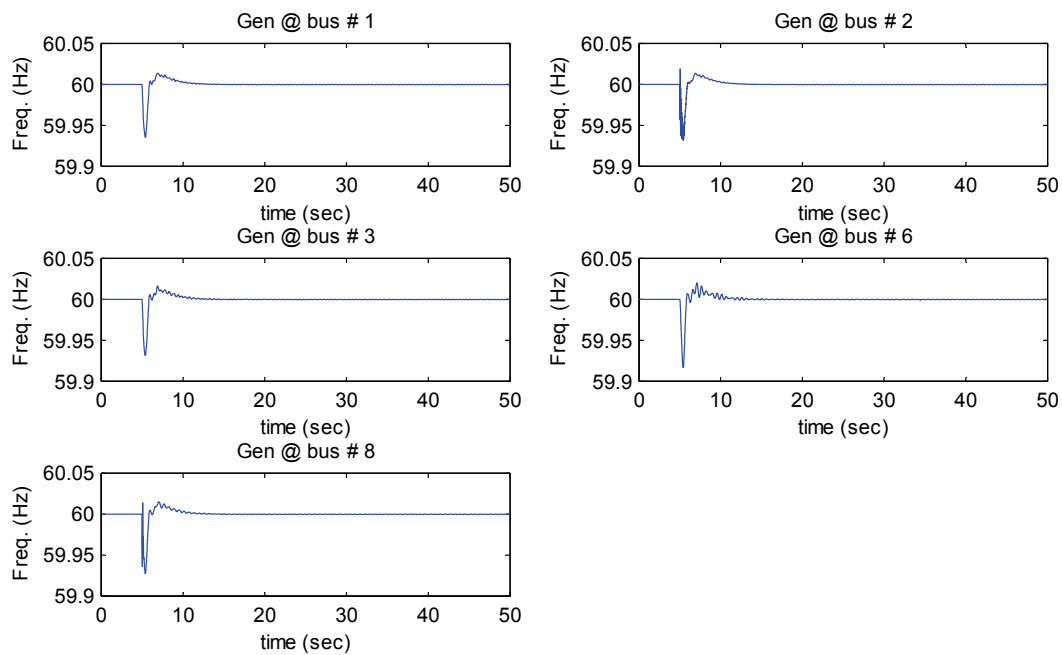
## Results

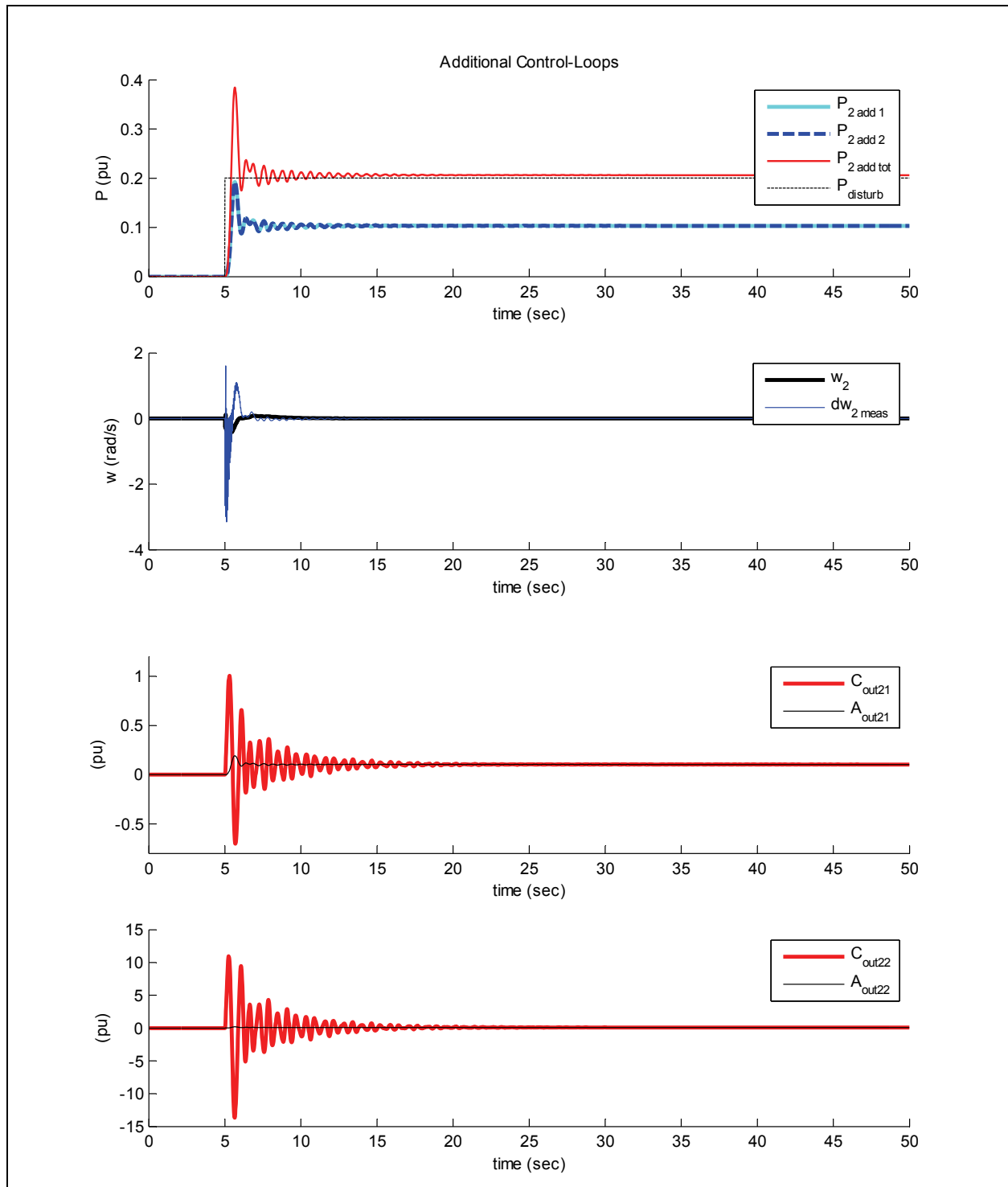
The MIMO-based design approach has been simulated for the standard problem. In general the obtained results do not show an improvement compared to the methods presented earlier.

### Simulation Results – Controllers designed on MIMO-based method

#### Simulation 1

- Based on standard system configuration (Chapter 3.1.3)
- Additional power path at bus 2
  - Measurement:  $\tau = 0.1\text{s}$
  - Power branch 1:
    - Actuator 1:  $\tau_1 = \tau_2 = 0.5\text{s}$
  - Power branch 2:
    - Actuator 2:  $\tau_1 = \tau_2 = 2\text{s}$
  - Controller:  $\omega_n = 4$
- Excitation scenario 1: 0.2pu step disturbance at load bus 4



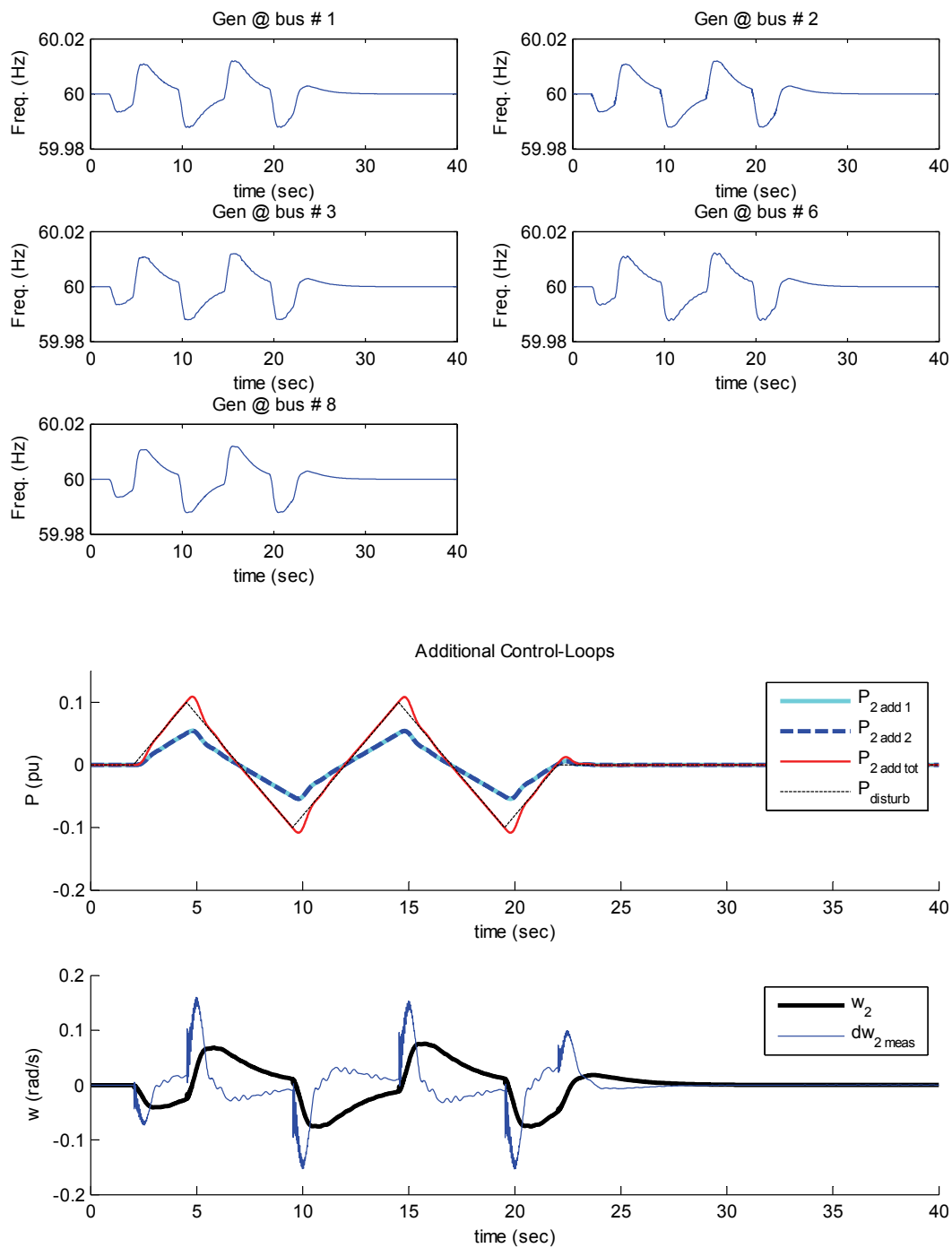


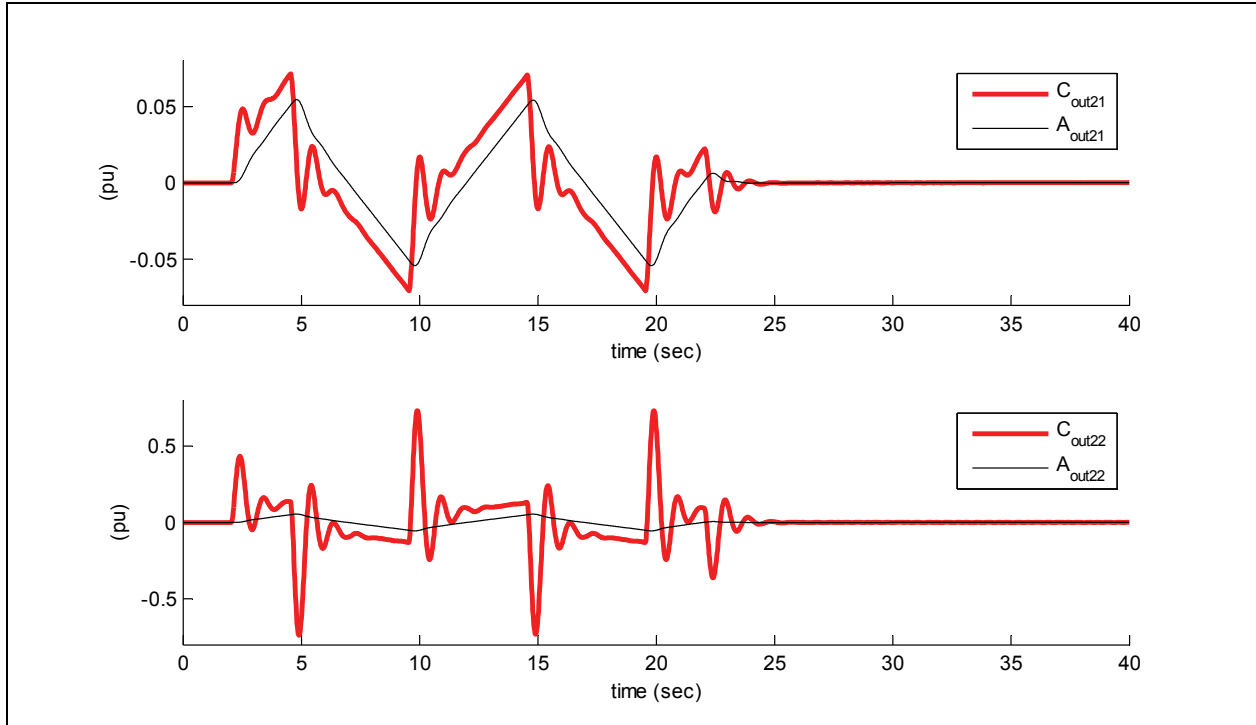
### Results

- Frequency deviations look similar to the individually designed controller case.
- The power contributions of both controllers are exactly the same.
- Considering the magnitude of the controller output signals, it can be seen that the controllers still compensate for slower actuator systems.

**Simulation 2**

- Based on standard system configuration (Chapter 3.1.3)
- Same additional configuration as in simulation 1
- Excitation scenario 2: 0.2pu p-p triangle-wave disturbance at generator bus 2





### Results

- The maximum frequency deviation is about 0.015Hz and worse than with the other design methods.
- Control tasks sharing between the two controllers is exactly 1 to 1. Both controllers have the same contribution.
- Controllers compensate for actuators as can be seen from scale of the controller output plots.

Table 4-10: Simulation Results – Controllers designed on MIMO-based method

### Findings

- The factors in equation (4.31) can adjust the power contribution of the two control paths very accurately. In the first configuration with a factor of 0.5 for both, the two additional branches have the same contribution. If for example factors of 0.3 and 0.7 are chosen, then one control branch compensates for 30% of the total deviation and the other compensates for the other 70%. So the ratio of these factors can be used to set a dispatch between the two branches.
- The characteristics and speeds of the actuator systems are not visible in the power contributions of the individual branches. The controller design again compensates for these delays by adjusting the controller output signal. Because only one  $\omega_n$  is used, both power contributions have nearly the same characteristics.
- Hard saturation limits can be implemented in a broader range than in the case of sequential designed controllers.



### Modified Design Procedure

In the procedure before, the design was based on one single optimal closed-loop transfer function, with one parameter  $\omega_n$ . In the parallel and sequential design methods, different parameters  $\omega_n$  for the two additional power paths were used. To allow two diverse parameters, the design procedure used before can be modified slightly.

1. Instead of choosing only one optimal closed-loop transfer function, we select for both control paths a separate TF and define a matrix of optimal transfer functions  $\mathbf{H}$ , with the TFs placed on its main diagonal.

$$\mathbf{H} = \begin{bmatrix} H_1(s) & 0 \\ 0 & H_2(s) \end{bmatrix} = \mathbf{T}_{cl} \quad (4.35)$$

2. In step 2, the same procedure can be followed as in the procedure before. Instead of  $H(s)$  in equation (4.32), we then have the diagonal matrix  $\mathbf{H}$  at its place.

$$\mathbf{Q} = \mathbf{H} \cdot d(s) \cdot G^\dagger = \begin{bmatrix} H_1(s) & 0 \\ 0 & H_2(s) \end{bmatrix} \cdot \begin{bmatrix} 0.5 \cdot \frac{d(s)}{n_1(s)} \\ 0.5 \cdot \frac{d(s)}{n_2(s)} \end{bmatrix} \quad (4.36)$$

The resulting matrix  $\mathbf{Q}$  is then a 2x1-matrix like before.

3. In step 3 no changes are made.

Simulations showed no improvement in performance as well as no significant benefits. Results are given in Appendix A.3.

#### 4.4 Conclusion on Single Bus Controller Design

Given the simulation results from all three controller design methods, an adequate comparison can now be conducted. As main indicator for performance the frequency deviations to a triangle-wave disturbance are evaluated.

In terms of performance it is safe to say that the sequential design method shows the best performance, with a maximum frequency deviation of less than 0.01Hz for the evaluated case. Except for some peaks, the frequency deviation stays within a very narrow band at the reference frequency (i.e. 60Hz). The saturation issue, however, is solved best by the MIMO-based design approach that allows exactly adjusting the partition of the power contribution. The MIMO-based design shows on the other hand not a favorable performance in quality of frequency regulation; in fact it was rather disappointing with respect to the expectations of our “natural” hypothesis entering this work.

Considering the fact that the sequential design method also includes a satisfying approach for treating the saturation issue, and shows a remarkable performance, it is obvious that the sequential control design is judged to be the most promising and is chosen for our further work.

The following table gives an overview of the results from simulations of the three parallel path design methods.

	Independently designed	Sequentially designed	MIMO-based designed
<b>Performance</b>	good	Very good	normal
<b>Saturation problematic</b>	Contribution of control branches can be adjusted by $\omega_n$ , but does not show the desired behavior.	Contribution of control branches can be well adjusted by the control parameters $\omega_n$	Contributions of control branches can be set accurately
<b>Quality of frequency signal</b>	Smooth	Smooth	Very smooth
<b>Order of controller 1</b>	12	12 (fast)	16
<b>Order of controller 2</b>	12	14 (slow)	16

Table 4-11: Controller design methods comparison

## 5 Control Design on Multiple Buses

The preceding chapter concluded that the optimal control design approach based on achieving a desirable closed-loop transfer function using Youla-Parameterization works very well for centralized control strategies on a single bus. In a next step we want to consider now supportive control action from multiple control buses and want to improve overall robust stability and performance.

As a first natural extension of the work of the previous chapter, the sequential-design methodology was applied to control loops at multiple buses. However, the ensuing studies of this approach showed clearly that the interaction of two or more of these controllers tended to destabilize the overall system, and reduce the overall performance (relative to control acting at a single bus). In considering this outcome in light of the history of frequency control in electric power grids, this result is perhaps unsurprising. The phenomenon of “hunting” oscillations is well documented for historic cases in which integral controllers to regulate frequency were installed at multiple buses. In the early developments of power system control, this problem was overcome by assigning responsibility for integral frequency control to a single, “master” generator, and allowing other generators to contribute to frequency control only with loops that incorporated “droop” (i.e., controller transfer characteristics that, taken along, did not regulate to zero steady-state error). This history provided the intuition that guides the heuristic design approach to be pursued in this chapter. One will note that the controllers that resulted from the target transfer functions and Youla-based design method pursued in the previous chapter all included at least one “pure” integrator (i.e., they were at least Type 1). It is clear that simultaneously implement such control at multiple buses would be likely to show the same general problems as multiple integral controllers. Hence, a promising design approach may also follow the analogy of the historic “master” integral controller. Our design heuristic here will use the Youla Parameterization and target transfer function design only at one “master” bus in the system. Additional control loops, active at other buses, will employ simpler control designs that do not attempt to drive the local frequency to zero steady-state error. As in the evolution of AGC, one could foresee improvements to this approach, in which the “master” control is computed at one location, but the control actuation is distributed to multiple buses. Such AGC-like improvements are here left to future work.

In brief, the approach to be pursued in this chapter will introduce additional controllers on multiple buses with no integral components; instead, these additional supplementary controls will take the form of the well-known and simple PD controller. This design approach provides modest control action, yet

supports grid stability in a manner that may be likened to Power System Stabilizer (PSS) action in the excitation loop of synchronous generators.

## 5.1 Concept of Master Controller

As a direct conclusion of the findings described above the concept of a Master controller and additional Slave controllers is now introduced. The Master controller is designed with the sequential design method of Chapter 4 and absorbs the main part of the control action. It embodies in a way the reference for further control performance. The Slave controllers (i.e. the PD controllers) are taking the part of being supportive controllers. They are based on a simple design and are so flexible and multiple applicable.

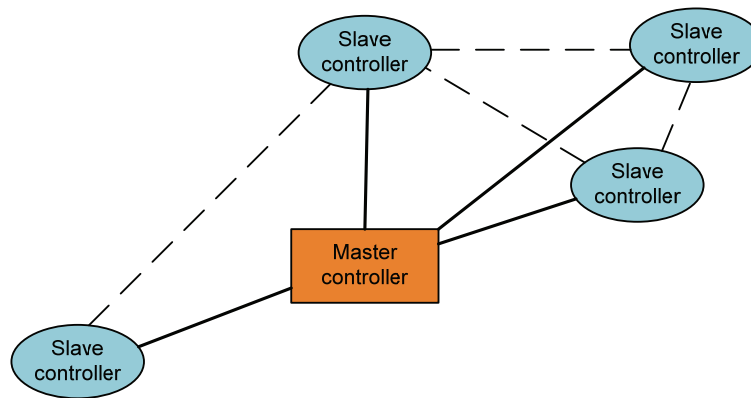


Figure 5-1: Concept of Master and Slave controllers

### 5.1.1 Locating the Master Controller

The bus location of the Master controller is a crucial consideration and needs to be aligned with the system design and characteristics. The bus that is used for the installation of the Master controller needs to be located centrally and, if possible, installed at a bus that is initially already critical concerning its stability (e.g. wind power bus with very slow inertia).

In our simulations we used buses 6 and 2 as locations for the Master controller. Both buses are quite centrally located, but bus 2 is a wind power bus with a very small inertia and bus 6 is a synchronous generator bus. Due to the fact that bus 2 is a “critical-stable” bus (i.e. very small inertia and a fluctuating power characteristic), the overall system performance was better with the Master controller installed at bus 2 than at bus 6.

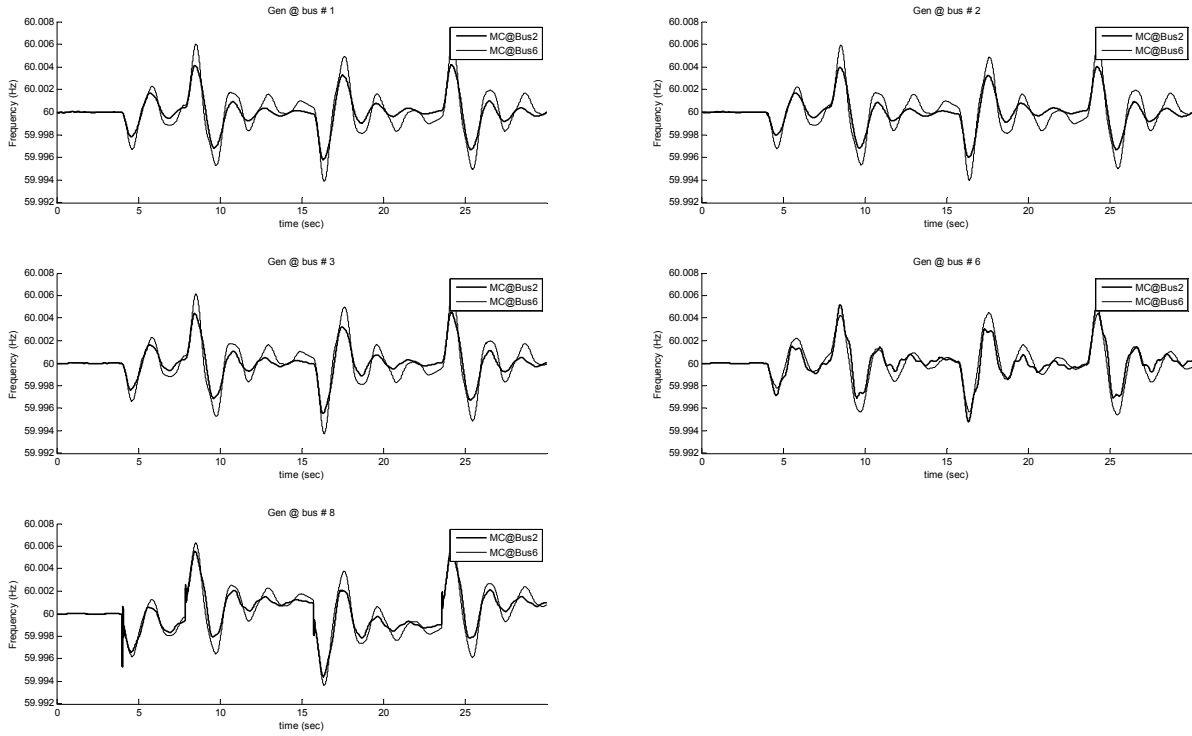


Figure 5-2: Influence of Master controller location

The simulation in Figure 5-2 shows this difference, assuming that the Master controller is the only control device and that the disturbance (i.e. triangle-wave) appears only on bus 8.

## 5.2 Distributed PD Controllers

A PD controller consists of a proportional and a derivative component and its behavior is described with the following transfer function

$$C_{PD}(s) = k_p + k_d \cdot s = k_p \cdot \left( 1 + \frac{k_d}{k_p} \cdot s \right) \quad (5.1)$$

The implementation in our test bed system appeared to be straight forward in general and is described in detail in Chapter 6.

### 5.2.1 Design of PD controllers

There was no formal, analytic design strategy developed for determining the two parameters  $k_p$  and  $k_d$ . The classical approach of choosing  $k_p$ , the proportional gain, in order to get a decent performance of the overall system assuming  $k_d = 0$ , and in a second step to adjust  $k_d$  according to minimize the

overshoot of the response, appeared to be a useful initial guess. However, the simulation results showed a better overall performance with other parameter values in particular using a larger  $k_p$ -value, i.e. increasing the proportional gain.

These significant differences in parameter values and the issue of not being able to obtain optimal parameter values from theory can be explained with the fact that the system response with the crucial influence of the Master controller, which is located on a different bus, could not be determined in closed form.

Consequently the values were adapted according to the simulation results. The magnitude of the values were one design criterion, the ratio of them (i.e.  $k_p/k_D$ ), however, appeared to be more important. The  $k_p$ -value was rather associated with the overall performance of the PD controller and the  $k_D$ -value could rather determine the time frame of control action.

There was an upper as well as a lower limit for both the magnitudes and the ratio. As described in more detail with the following simulations results, a trade-off has to be done up to what extent the PD control needs to get active and in what time frame. Choosing a too big magnitude or ratio of the PD values resulted in an unstable overall performance.

### 5.2.2 PD Controller as Slave Controller

The block diagram in Figure 5-3 shows the new control path of the system. Considering this control structure, an optimal ratio of the control parameters for the PD controller, acting as Slave controller, is determined to be in the order of 20, i.e. choosing  $k_p = 120$  and  $k_D = 6$ . As opposed to the Master controller design, the PD control is designed reacting on the frequency deviation (not its derivative) of the specific bus.

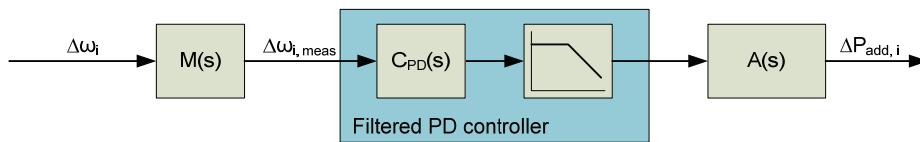


Figure 5-3: Additional power path with PD controller

The simulations show that PD controllers can generally bring an additional benefit to a centralized control design strategy (i.e. the concept of the Master controller), in particular if the PD controllers are implemented locally, on the bus where the disturbance appears. In order to make sure that the PD controller acts enough fast (i.e. faster than the centralized controller), the time constants from the PD control

unit as well as from the actuator have to be chosen very small, meaning in the order of milliseconds. Considering an external storage device with very high bandwidth such as a battery, this is judged to be a realistic approach.

In addition, the PD-controlled power contribution needs to fade out very quickly in order to avoid large interactions with the Master controller. Simulations show that the open-loop transfer function of the filtered PD controller with its actuator needs to have a big overshoot in its step response and a very quick fade out in the area of hundredths of a second to its steady-state value.

The Bode plot and step response of the PD control open-loop with a first-order filter as actuator ( $\tau = 0.003$ ), assuming a  $k_p$ -value of 120 resp. a  $k_D$ -value of 6, is shown in Figure 5-4.

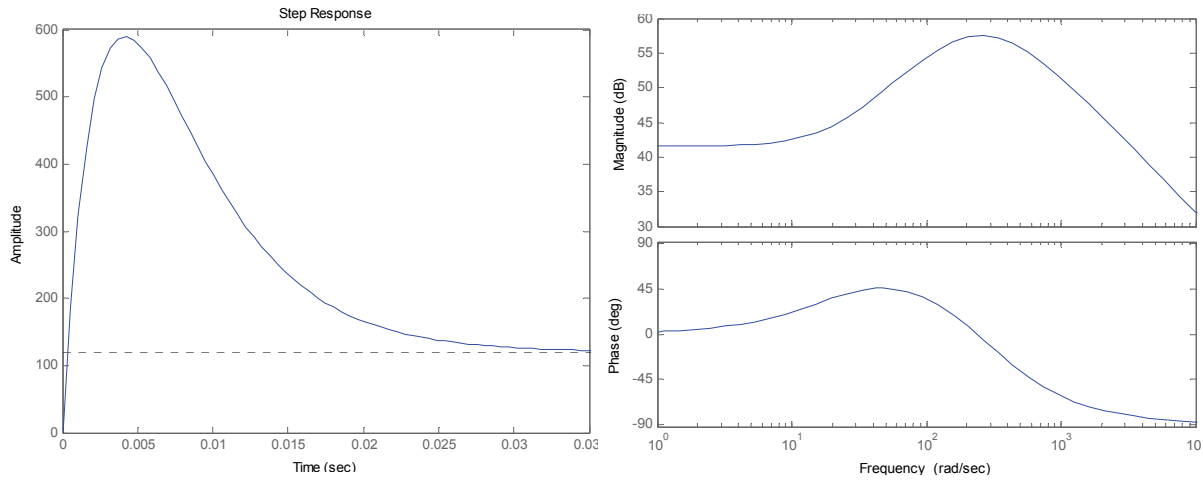


**Figure 5-4: Step response resp. Bode plot of PD control open-loop**

An important issue that should be pointed out is the magnitude of interaction of the PD controller. In general the PD controller is only supposed to support frequency control within the first second of the event of a disturbance because from that on the Master controller takes the control action and its design is already well-optimized, as seen in Chapter 4. So a trade-off exists between having a frequency regulation performance and overall system stability. A high  $k_p$ -value for instance improves the performance within the first seconds but on a long-term the high interaction with the Master controller and the system leads to instability, shown in Figure 5-5. Interestingly it affects bus 6 most distinctively where no control is installed.

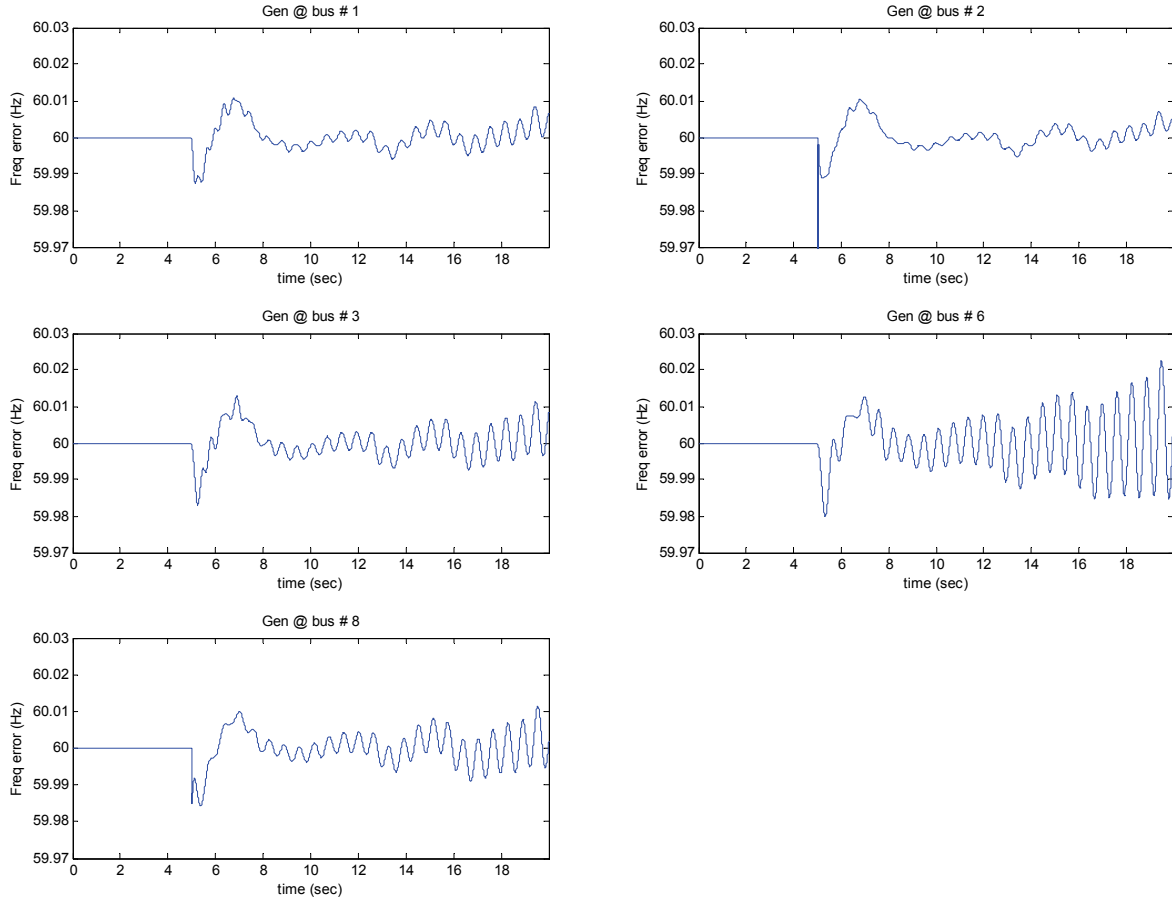


Figure 5-5: PD control - instability case

A detailed eigenvalue analysis conducted in Chapter 5.5 confirmed this instability. Considering the motion of the eigenvalues of the overall system with respect to varying the single parameter  $k_p$ , it can be clearly seen that increasing from a lower  $k_p$ -value the eigenvalues move to the right half plane and create an unstable mode.

### 5.2.3 Behavior on Step-Change Scenario

As mentioned before, an optimal ratio of the PD-values (i.e.  $k_p/k_D$ ) is about 20 assuming a  $k_p$ -value of 120 resp. a  $k_D$ -value of 6. For these simulations the standard system configuration from Chapter 3.1.3 is chosen with a different excitation.

Here, we want to observe the behavior of locally installed PD controllers on step change characteristics. We assume two different standard triangle-waves (emulating the fluctuating behavior of wind) as power inputs at buses 2 and 8. Additionally we introduce a step change on both wind buses with different magnitudes prior to the triangle-waves. Figure 5-6 shows the input characteristics of the system.



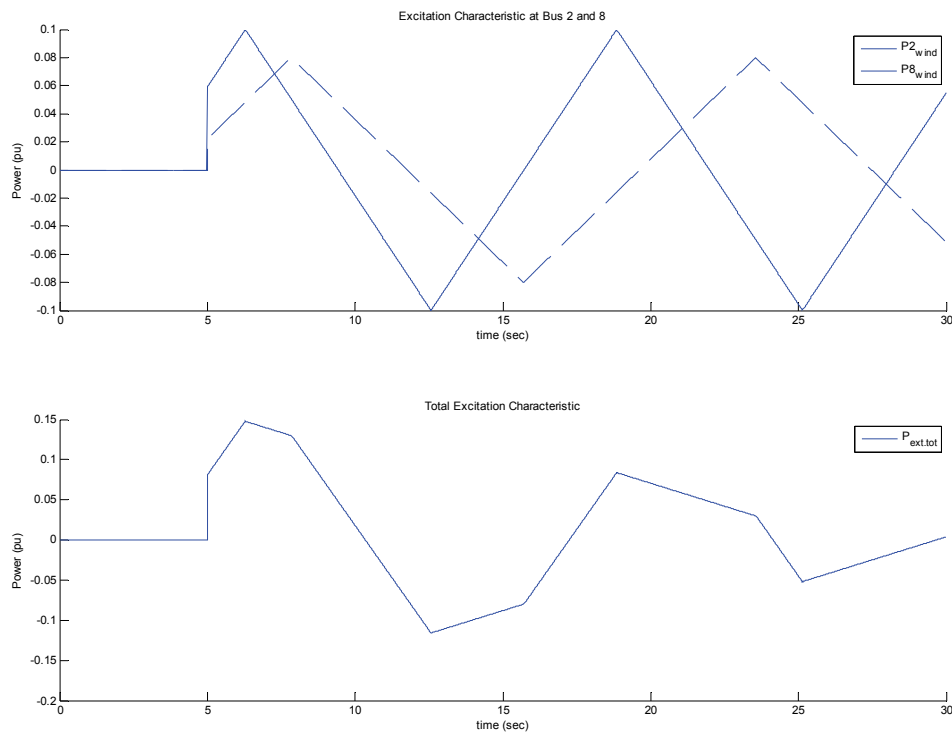


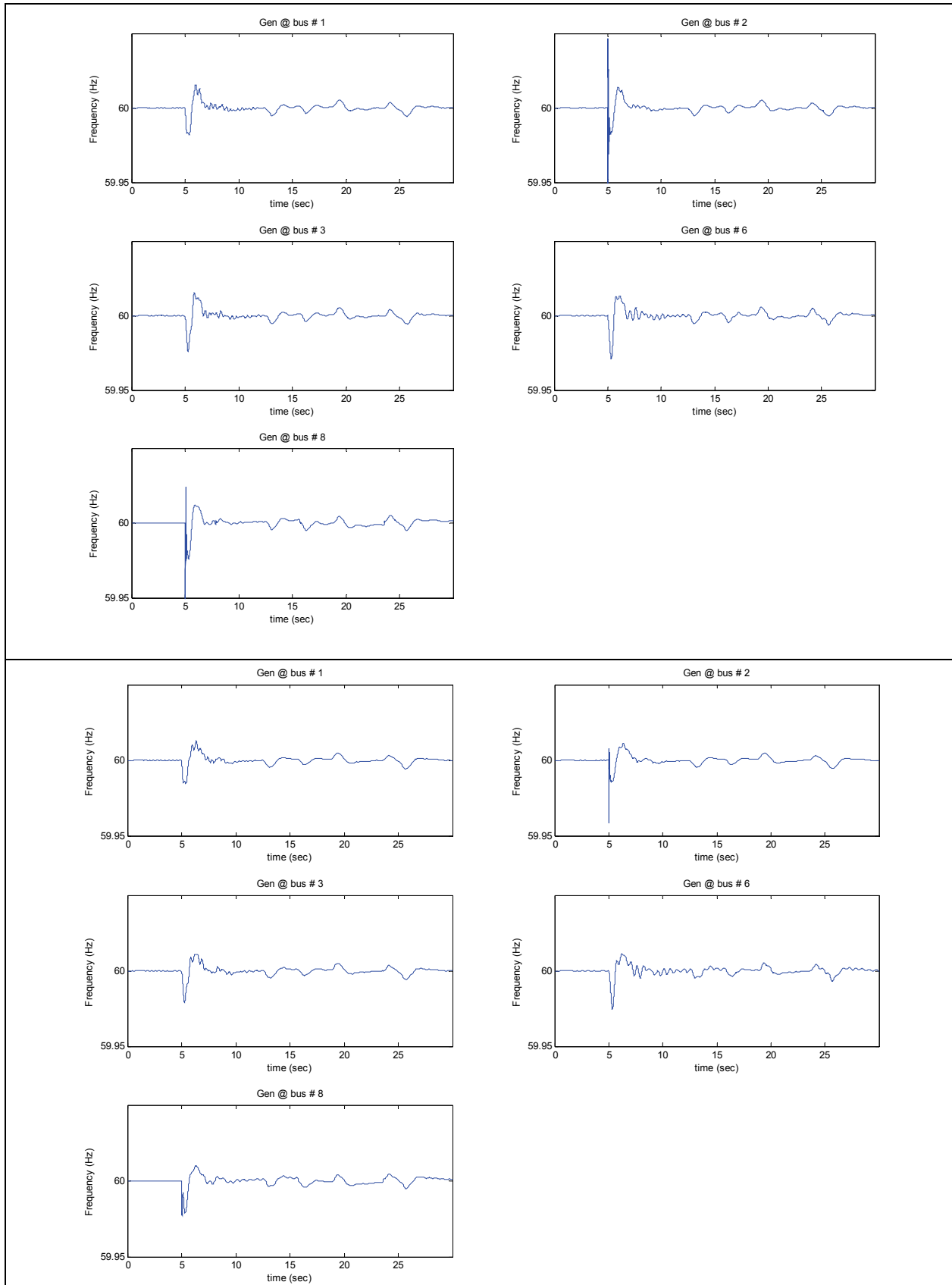
Figure 5-6: Excitation characteristic for step-change scenario

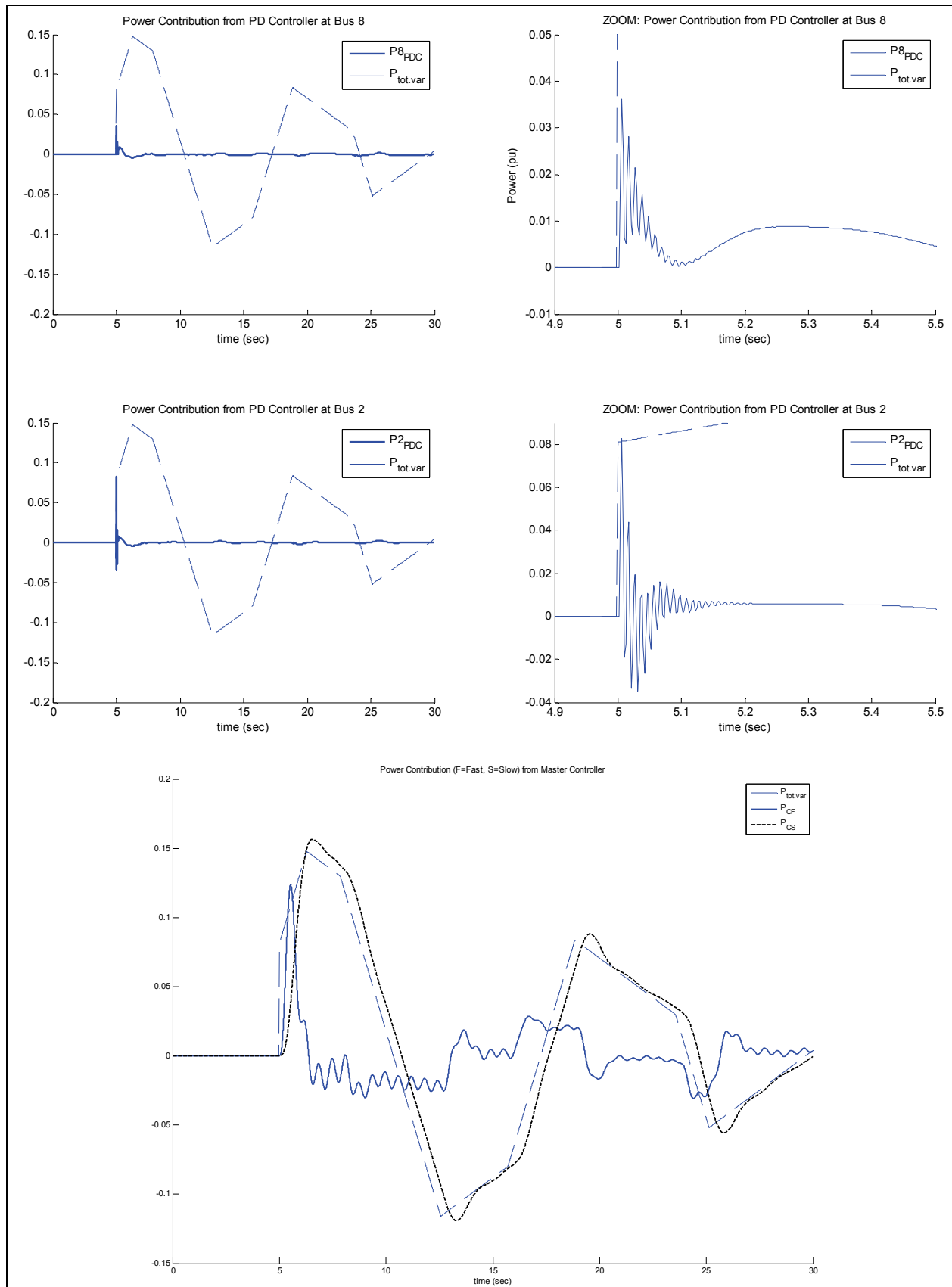
The following Table 5-1 shows the simulation results. The system is controlled by the Master controller implemented at bus 2 and two PD controllers installed at bus 2 and 8, i.e. at those buses where the excitation takes place. In general the performance, in terms of frequency deviation, only shows a significant improvement within the first few seconds at buses 2 and 8. One can see that the initial severe oscillations in magnitude can be damped out fairly well with additional, locally installed PD controllers.

#### Simulation Results – PD controller with step-change scenario

##### Simulation

- Based on standard system configuration (Chapter 3.1.3)
- Master controller at bus 2 (configuration of Chapter 4.3.2)
- PD controller at buses 2 and 8
  - $k_p = 120$ ,  $k_d = 6$
  - PD filter:  $\tau = 0.005$  s
  - Actuator:  $\tau = 0.003$  s
- Excitation: Step-change scenario described above





**Results**

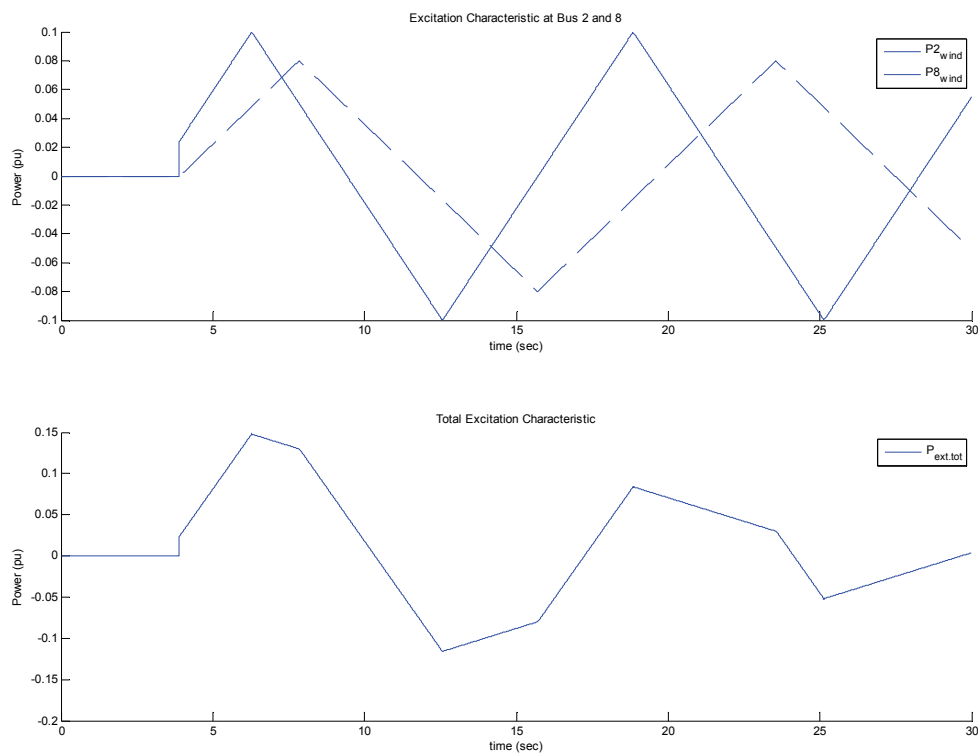
- The maximum frequency deviation can be significantly limited by the PD controllers.
- Power contribution of PD controllers appears in first milliseconds.
- Master controller keeps expected behavior.

**Table 5-1: Simulation Results – PD controller with step-change scenario**

As expected, the power controlled from the PD controllers make a significant contribution in the first tenths of a second, as can be well seen in the zoomed-in power contribution plots, and then fades out very quickly. The Master controller in contrast contributes constantly by supporting the abrupt power changes with its high bandwidth controller and by compensating the broad power mismatch with its low bandwidth controller.

**5.2.4 Behavior on Ramp-Change Scenario**

In a next step we want to investigate the system behavior on a ramp change. We consider another excitation case where the system is excited again by two triangle-waves on buses 2 and 8, but now the triangle-wave on bus 8 doesn't have a step behavior in prior and the magnitude of the step at bus 2 is reduced. Figure 5-7 shows the ramp-change scenario for this simulation. The PD controllers are again placed at buses 2 and 8. The Master controller is at bus 2.

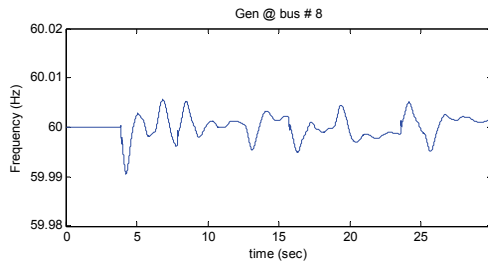
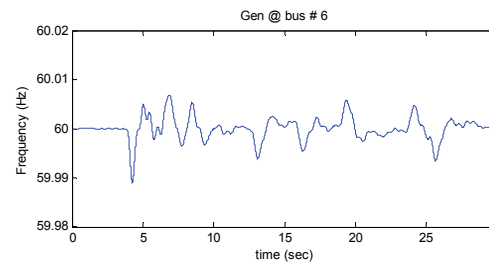
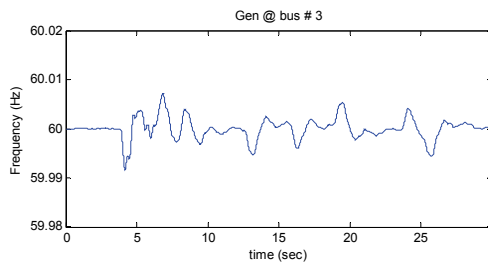
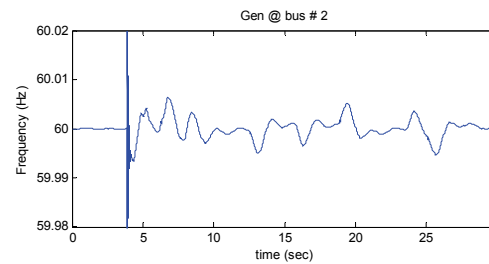
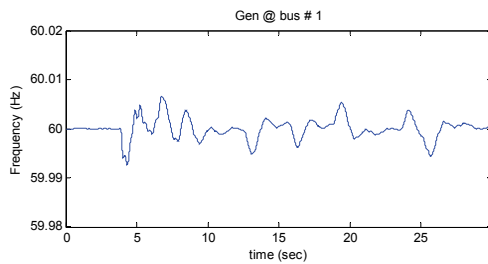
**Figure 5-7: Excitation characteristic for ramp-change scenario**

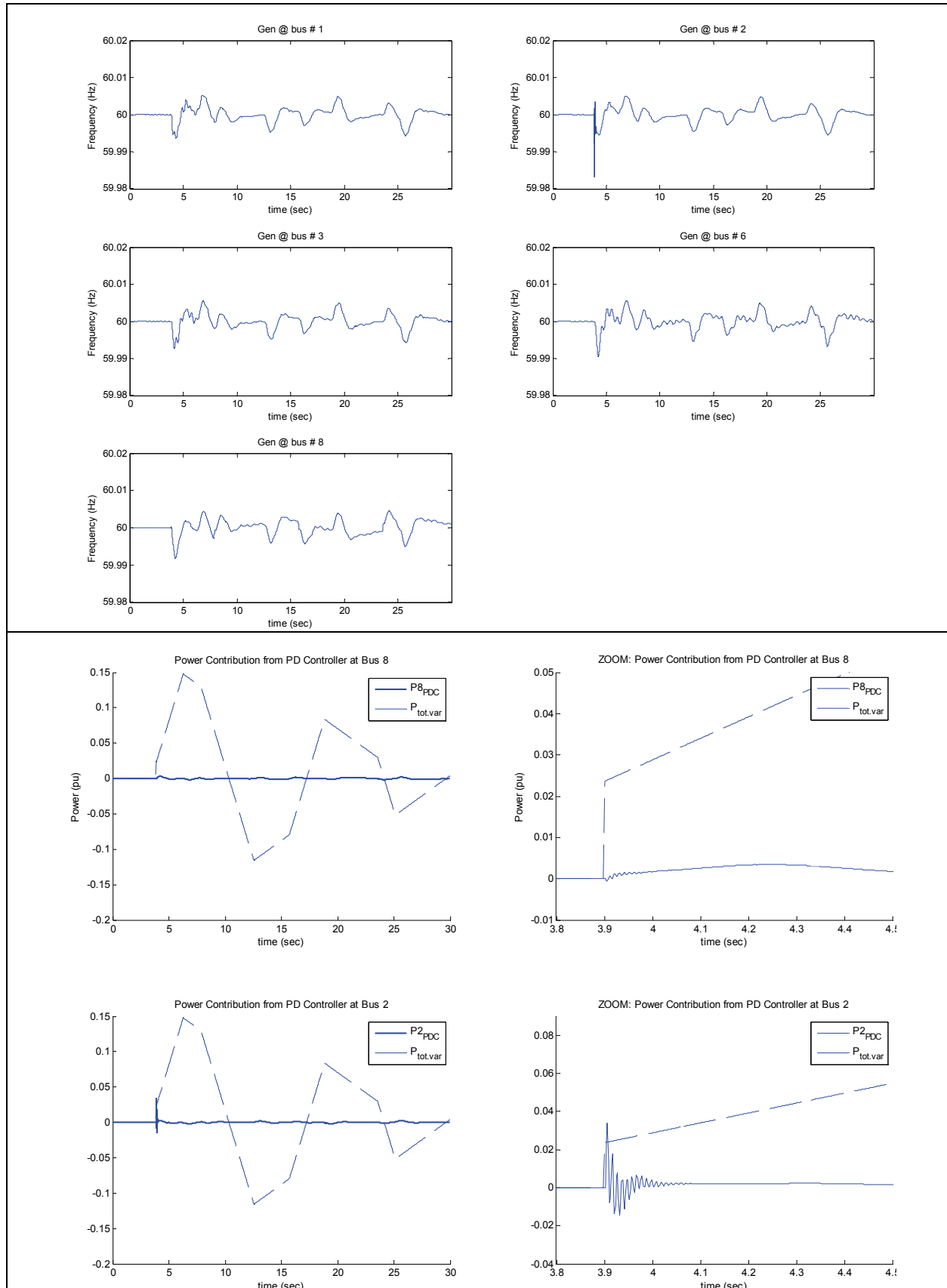
Besides considering the real good performance from the Master controller (consider the resolution of y-axis), as a result to the less severe excitation, there are again differences between the simulations with no PD controllers and with PD controllers installed. (see Table 5-2)

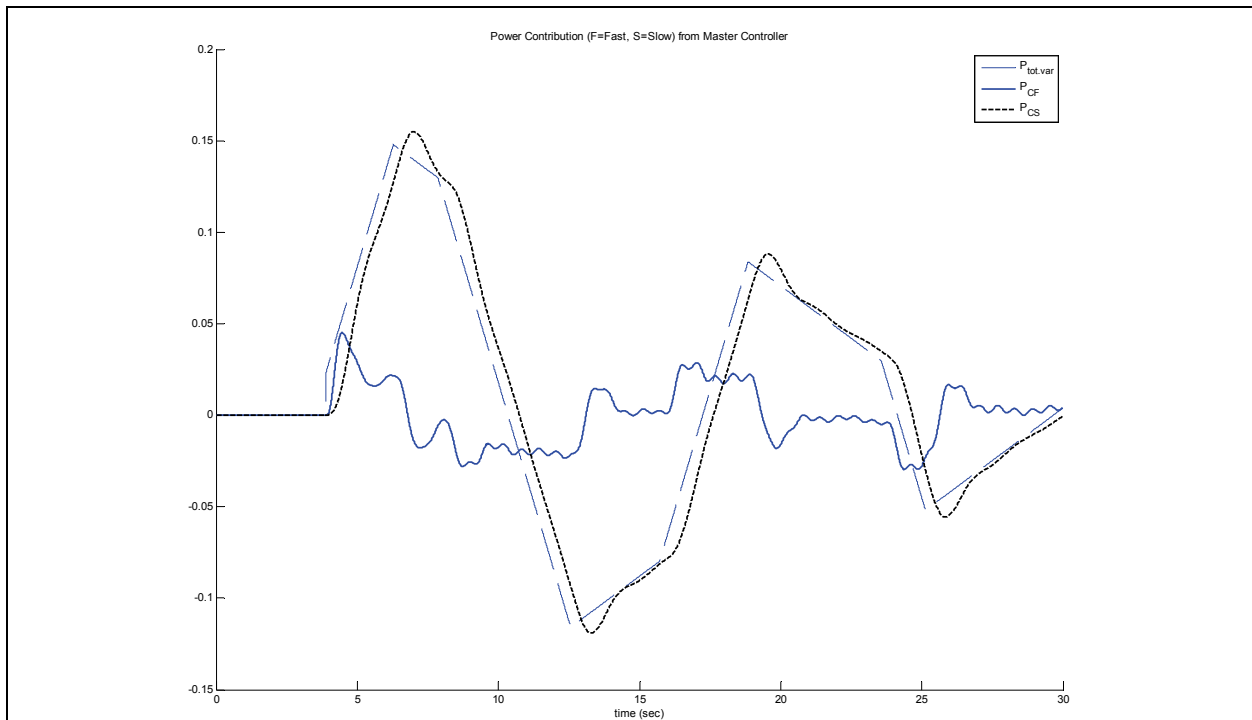
### Simulation Results – PD controller with ramp-change scenario

#### Simulation

- Based on standard system configuration (Chapter 3.1.3)
- Master controller at bus 2 (configuration of Chapter 4.3.2)
- PD controller at buses 2 and 8
  - $k_p = 120$ ,  $k_d = 6$
  - PD filter:  $\tau = 0.005$  s
  - Actuator:  $\tau = 0.003$  s
- Excitation: Ramp-change scenario described above







### Results

- The maximum frequency deviation can be still improved by the PD controllers but only marginal.
- Power contribution of PD controller is only small.
- Master controller performance is still very satisfactory.

**Table 5-2: Simulation Results – PD controller with ramp-change scenario**

In general, one can consider only a small benefit with a PD controller installed for a ramp excitation if we have a look at the performance of bus 8. The overall performance can only be improved a little but can be seen on all buses. Further on we observe on bus 8 that the PD controller is compensating local oscillations that are coming from the abrupt changes from the excitation

However, one can detect a drawback of the PD controller mentioned already in the beginning of the chapter with the instability analysis. Considering bus 6, one can see slight higher local oscillations that are coming from the interaction between Master controller and PD controller and possibly also influenced from the considerable inertia of the synchronous generator. A broader discussion of the overall benefits and drawbacks of distributed PD controllers is conducted in Chapter 7.

### 5.2.5 Battery Model as Actuator for PD Controller

Using the Battery Model described in 5.3.2 in place of the first-order filter that is used for the previous simulations, shows no significant difference in behavior. The benefits of the PD control can be also clearly shown with a battery acting as actuator. The nature of our design technique is such that order of the Master controller increases, based on the fact that the battery model is of higher order (order of 2 for battery, versus the first order actuator modeled earlier). The battery shows very high bandwidth and can so be ideally implemented into a PD control design. Simulations of the battery model as PD control actuator are conducted in 5.3.2 as well.



### 5.3 Actuator Models

Physical systems of power sources for the additional control are modeled as different actuator systems. So far, the actuator system was modeled as a simple 1<sup>st</sup> or 2<sup>nd</sup> order filter. The actuator  $A(s)$  is represented in block-diagram form as shown below and the two time constants of the 2<sup>nd</sup> order filter define the bandwidth of the actuator system.

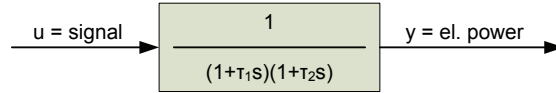


Figure 5-8: Second order filter actuator system

The frequency characteristics of a 2<sup>nd</sup> order filter show a low pass behavior. The crossover frequency  $\omega_c$  or the time constants  $\tau_i$  define the actuator systems bandwidth. Different actuator characteristics can be modeled by selecting slower or faster time constants.

In order to make simulations more accurate, more precise models should be considered. Systems that might be of interest for the wind power application are reviewed here.

#### 5.3.1 WTG Pitch-Control

The WTG pitch-control for example represents an actuator system with limited bandwidth, fairly wide range of power variation, and without an inherent energy limitation. In studies thus far the actuator system was modeled with a 1<sup>st</sup> or 2<sup>nd</sup> order filter and low time constants  $\tau_i$  of some seconds. This selection of model structure is supported by other work in the literature. In a paper from I. Hiskens [37] for example, the pitch-control actuator system was found to be modeled as a 1<sup>st</sup> order filter with a time constant  $\tau_p$ .

$$A(s) = \frac{1}{\tau_p \cdot s + 1} \quad (5.2)$$

It turned out to be difficult to find accurate values for time constants of the pitch-control. Discussion in the literature confirms that wind turbine manufacturers treat such data as highly proprietary, seeking to conceal precise information from competitors. Therefore manufacturer validated values for the time constants can be difficult to find, and a researcher is left to make rough estimates of these values based on engineering first principles. The selected time constants of 2-3 sec seem though to be reasonable if one considers the relative high inertia of a WTG rotor blade.

### 5.3.2 High Power Li-Ion Battery

For an actuator system with a higher bandwidth, one can think of batteries. Batteries are usually characterized by very fast reaction times, but with a narrow limit in energy.

In literature we found a paper about high power Li-Ion batteries [38] from the National Renewable Energy Laboratory, written in collaboration with SAFT America, a well-known battery manufacturer. In this paper, a 2-capacitance linearized model of a 12 Ah high power Li-Ion cell is presented according to the circuit diagram and state-space representation below. While such a linearized model is likely not accurate over the entire charge/discharge range of the battery, it is suitable for small signal modeling about an operating point, as is appropriate to control applications.

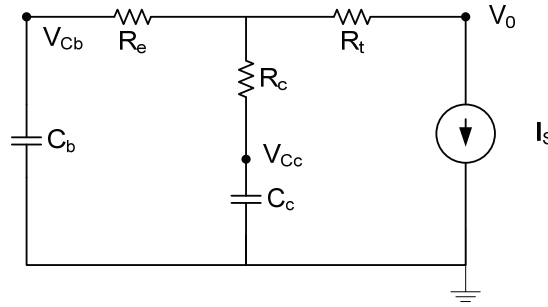


Figure 5-9: Original SAFT battery diagram

$$\begin{bmatrix} \dot{V}_{Cb} \\ \dot{V}_{Cc} \end{bmatrix} = \begin{bmatrix} -1/C_b \cdot (R_e + R_c) & 1/C_b \cdot (R_e + R_c) \\ 1/C_c \cdot (R_e + R_c) & -1/C_c \cdot (R_e + R_c) \end{bmatrix} \cdot \begin{bmatrix} V_{Cb} \\ V_{Cc} \end{bmatrix} + \begin{bmatrix} -R_c/C_b \cdot (R_e + R_c) \\ -1/C_c + R_c/C_b \cdot (R_e + R_c) \end{bmatrix} \cdot [I_s] \quad (5.3)$$

$$[V_0] = \begin{bmatrix} R_c/(R_e + R_c) & R_e/(R_e + R_c) \end{bmatrix} \cdot \begin{bmatrix} V_{Cb} \\ V_{Cc} \end{bmatrix} + \begin{bmatrix} -R_t - R_c \cdot R_e/(R_e + R_c) \end{bmatrix} \cdot [I_s]$$

This model is referred and will be referred as the “SAFT Capacitance Battery Model”. In order to allow the use of this battery model for our task of additional control, the model had to be slightly modified. The state-space representation of the battery model has current  $I_s$  as input  $u$  and battery voltage  $V_0$  as output  $y$ . A typical actuator used for the additional provision of power to a bus has to have electrical power as output regulated by a control signal input.

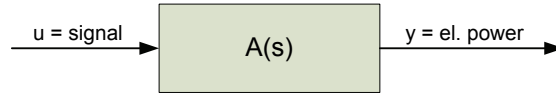


Figure 5-10: Input-output convention of actuator model

One has to approximately represent the action of an electronic circuit that would be present to regulate the electrical power output by a command signal. Our approach to representing power electronic regulation of power output in a simple circuit model is to include a controllable voltage source at the output of the battery (Figure 5-11).

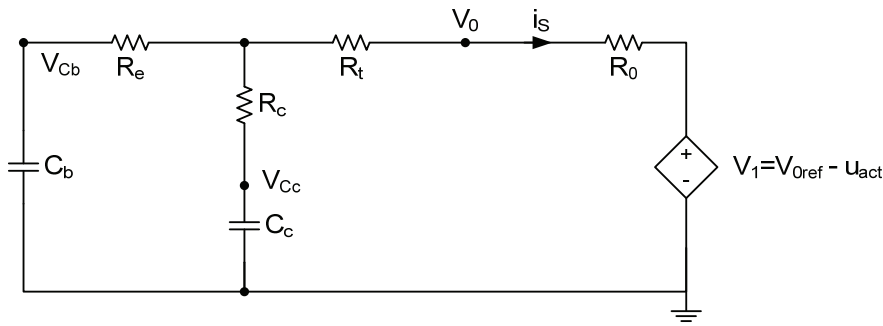


Figure 5-11: Applied SAFT battery diagram

If the input signal  $u_{act}$  is zero,  $V_1$  reduces to  $V_1 = V_{0,ref}$  and no current  $i_s$  is flowing because of  $V_0 \simeq V_1$ . If  $u = V_{0,ref}$ ,  $V_1$  is zero and a maximum current is flowing. The magnitude of the current can be limited by a serial output resistor  $R_0$ . This representation of battery power regulation is a simplification, and in practice more complex power electronics will be used to control the battery power output.

The output  $y$  of the adapted model is chosen to be the current  $i_s$  instead of the real power  $P = V_0 \cdot i_s$ , because the voltage  $V_0$  is assumed to be nearly constant. With a nominal voltage of the SAFT battery cells of 3.6V ( $V_{0,ref} = 3.6V$ ), the input signal  $u_{act}$  and the output signal  $y_{act} = i_s$ , a state-space representation can be formulated. The exact state-space equations are shown in Appendix A.4.1. The block diagram of the actuator model is depicted below.

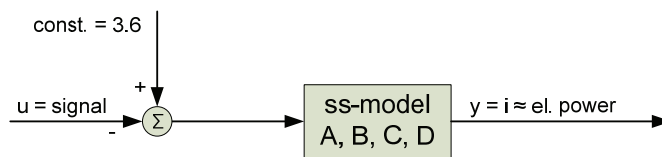


Figure 5-12: Block diagram of SAFT battery model

In order to validate the manual state-space calculations, the battery system was also constructed in MATLAB Simulink using the Power System toolbox. From that model the state-space description was obtained using the built-in *linmod* function.

In our additional control path, the controller output signal is used as input signal of the actuator. This signal has to be subtracted from the constant 3.6 and the resulting signal represents the adjustable voltage  $V_1$ . Because of the selection of the adjustable voltage source, the controller output signal should be limited to a band of  $[-1.8 \dots 3.6]$ . Table 5-3 below, shows the battery model behavior for the selected controller output signal range.

Controller output signal	Adjustable voltage source	Output current	Status of battery system
$u = 3.6$	$V_1 = 0\text{V}$	$i_s > 0$	power is taken from battery, discharge
$u = 0$	$V_1 = 3.6\text{V}$	$i_s = 0$	no charge or discharge
$u = -1.8$	$V_1 = 5.4\text{V}$	$i_s < 0$	power is fed into battery, charging

Table 5-3: Operating points of battery model

Parameters of the SAFT capacitance battery model are summarized in the table below. The resistor  $R_0$  is chosen to limit the magnitude of the output current  $i_s$  to a physically reasonable value.

Parameter	Value	Parameter	Value
$C_b$	82kF	$R_t$	1.2m $\Omega$
$C_c$	4.074kF	$R_0$	10m $\Omega$
$R_e$	1.1m $\Omega$	$V_{0,ref}$	3.6V
$R_c$	0.4m $\Omega$		

Table 5-4: Parameters of SAFT capacitance battery model

By calculating the transfer function  $A(s)$  from the state-space model and plotting the transfer functions Bode plot, the SAFT capacitance model can be compared to the 2<sup>nd</sup> order actuator model.

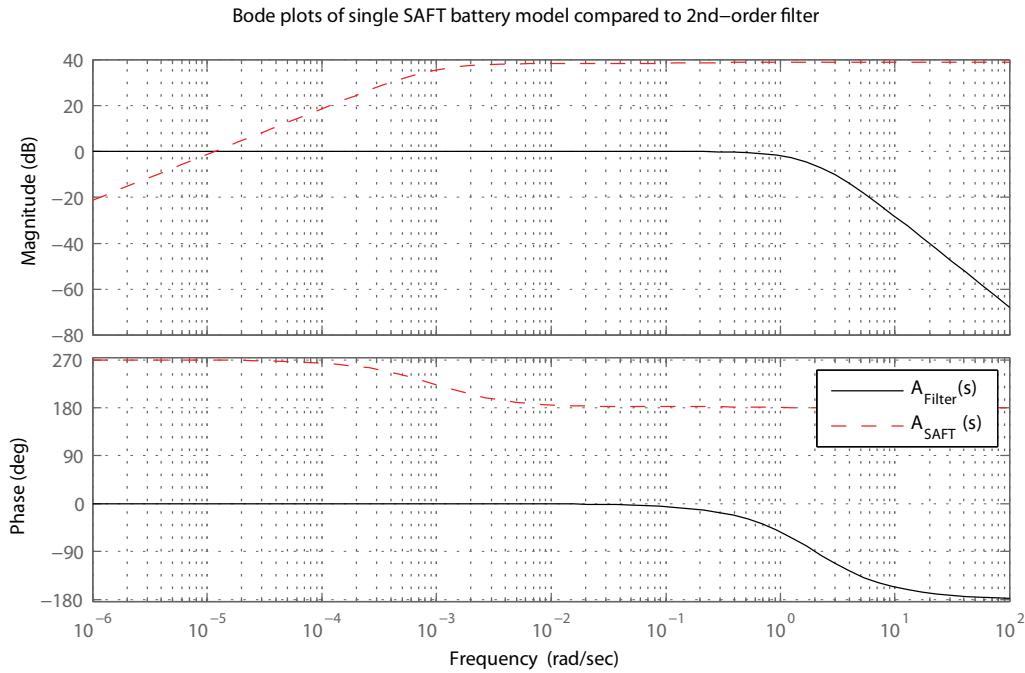


Figure 5-13: Bode plot comparison of single SAFT capacitance battery model and 2nd-order filter

The input  $u$  of the SAFT Capacitance model TF is chosen to be the voltage  $V_1$  of the model and not the input  $u$ . This does not affect the magnitude. Only the phase is shifted by  $180^\circ$ .

From the Bode plot it can be seen that the battery model has a high-pass characteristic with a pass band gain of 40dB. The high pass characteristic in a power-based transfer characteristic simply confirms the inherent energy limitation of the battery: It can not provide a steady-state power output all the way down to DC, because it becomes discharged. The 2<sup>nd</sup> order filter model with time constants of  $\tau = 0.5s$  in comparison has a low-pass characteristic. If the pass band gain of the battery is neglected, in a certain range  $[10^{-3} \dots 10^0]$ , both systems have the same unity gain. The Bode plot shows already that the battery system can provide very fast response in power output, but cannot maintain this power output down to DC. The 2<sup>nd</sup> order filter characteristic limits the speed of response. These behaviors will be seen in simulations to follow.

Because of the high-pass characteristic of the battery model, the transfer function is not strictly proper ( $\deg(n(s)) < \deg(d(s))$ ). The resulting TF is only proper; with a degree of 2 for both, numerator and denominator. This has to be considered for the control path design. As opposed to the strictly proper 1<sup>st</sup> and 2<sup>nd</sup> order filters used as actuators, in order to apply the battery model an additional filter has to be added to the open-loop control path to result again in a stable system.

### Connection of Batteries in Series and/or Parallel

Thus far we have examined the single battery model from literature and adapted it to our actuator system requirements. But the actual power and energy output of such a battery is very limited. In practical applications, large numbers of individual batteries would have to be connected in series or parallel to increase the power output and energy storage of the actuator system to appropriate values.

The SAFT capacitance model represents a 12Ah Li-Ion cell. The power required for additional control should be at least 0.5MW or 0.005pu (100MVA base for our simulation). With a single battery system the maximum power output can be calculated straight forward.

$u = 3.6$	$V_1 = 0V$	$i_s \approx \frac{3.6V}{1e-2\Omega} \approx 360A$	$P = 3.6V \cdot i_s \approx 1300W$
-----------	------------	--	------------------------------------

Table 5-5: Maximum power of single battery cell

The approximately calculated 1300W are far too low and therefore a serial and parallel combination of batteries has to be considered. Our interest is especially focused on the change in characteristics, if batteries are setup in series, parallel or a combination of these.

By connecting batteries in series mainly the voltage is increased, allowing a higher output power of the connected batteries. The Bode diagram below shows how the frequency characteristics change, from a single battery to two batteries in series to 10 batteries in series.

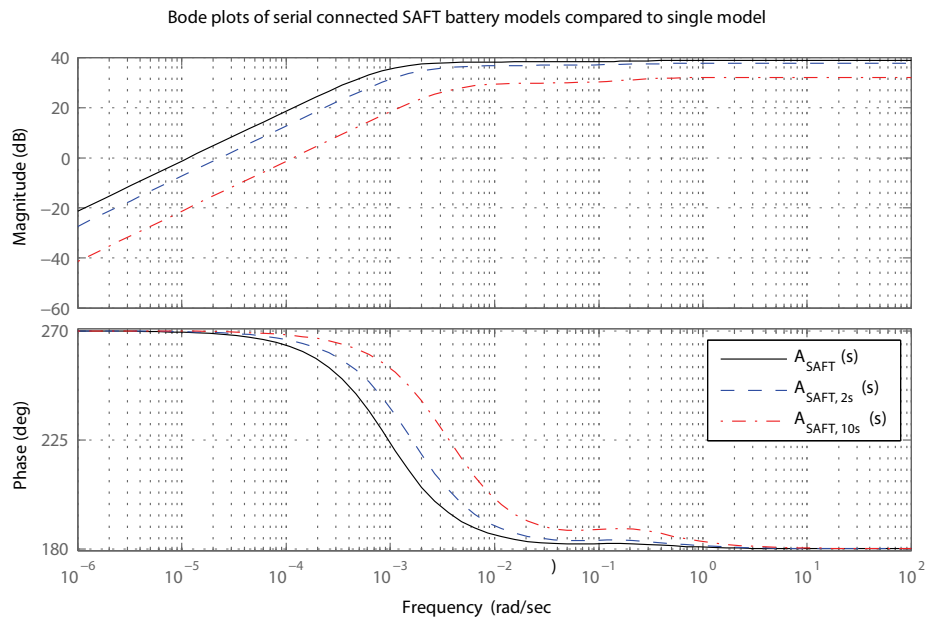


Figure 5-14: Batteries connected in series

From the Bode plots in Figure 5-14, one can see that by connecting more battery cells in series, the magnitude and phase are shifted towards a higher crossover frequency.

If a parallel connection of batteries is considered, the power output of the system can be increased. The connection of two batteries in parallel, for example, results in a doubled output current. This can be seen in the Bode diagram as well: The magnitude gain is increasing with two parallel connected batteries.

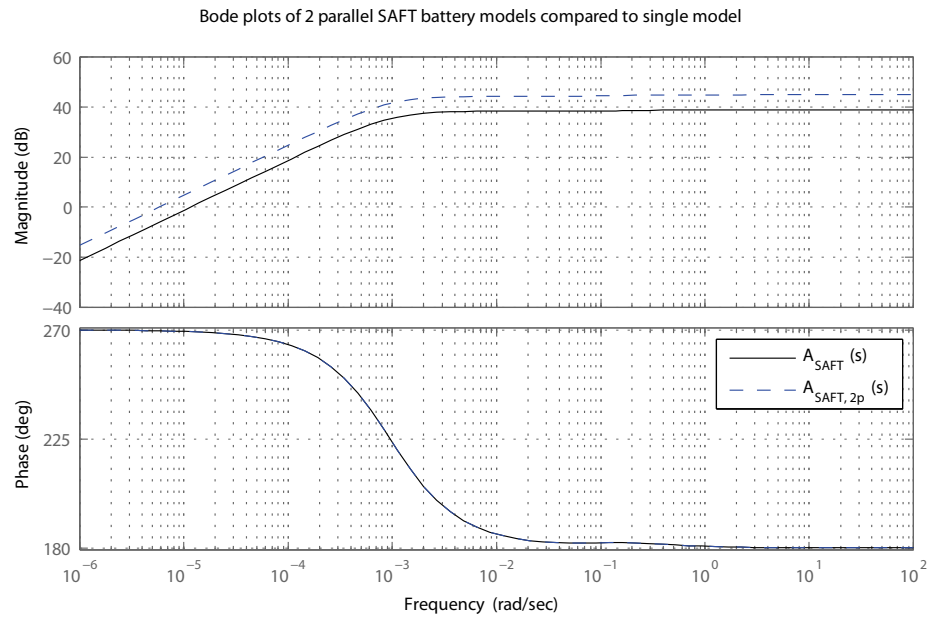


Figure 5-15: Batteries connected in parallel

If batteries are connected in series as well as in parallel, the following Bode plot results.

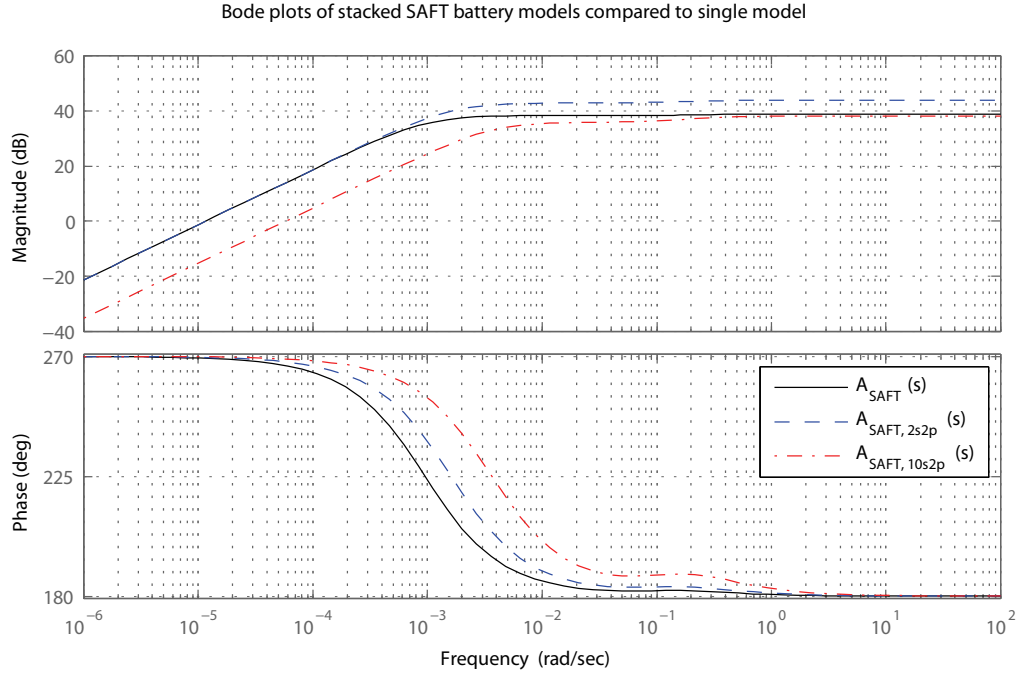


Figure 5-16: Batteries stacked in series and parallel

As a result from this analysis it can be seen that the characteristics change if batteries are stacked, but the change does not significantly alter the qualitative characteristics, and the fast response of the actuator system is not affected.

### Simulation Results with SAFT Capacitance Battery Model

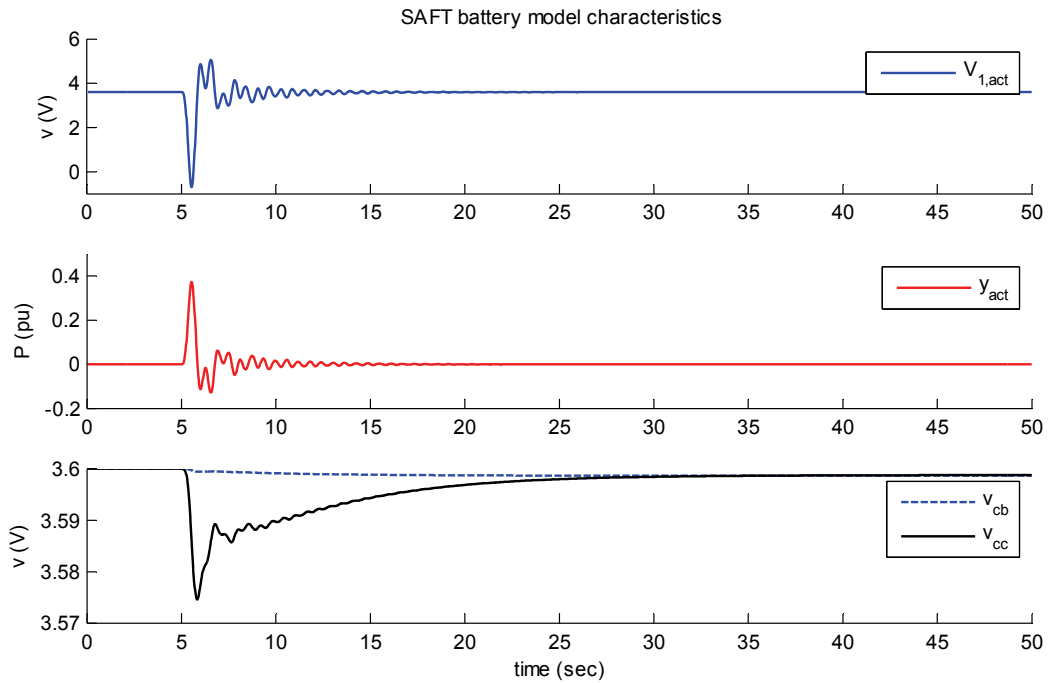
In the simulation, the faster 2<sup>nd</sup> order actuator system was replaced by the SAFT Capacitance battery model actuator. Serial and parallel stacking of cells is not yet considered in simulations, because as shown above, they do not significantly affect the characteristics of the actuator system. Instead the single SAFT capacitance battery model was used and the output was scaled to match the power requirements of the simulation scenario. Simulations showed that the battery model has such a fast performance, that the input signal almost exactly matches the output of the actuator. This means that the controller output signal is very close to the resulting power fed back to the system.



### Simulation Results – SAFT battery model

#### Simulation 1

- Based on standard system configuration (Chapter 3.1.3)
- Additional power path at bus 2
  - Measurement:  $\tau = 0.1\text{s}$
  - Power branch 1:
    - Actuator 1: SAFT battery model
    - Controller 1:  $\omega_{n1} = 5$
  - Power branch 2:
    - Actuator 2:  $\tau_1 = \tau_2 = 2\text{s}$
    - Controller 2:  $\omega_{n2} = 2$
- Excitation scenario 2: 0.2pu step disturbance at load bus 4

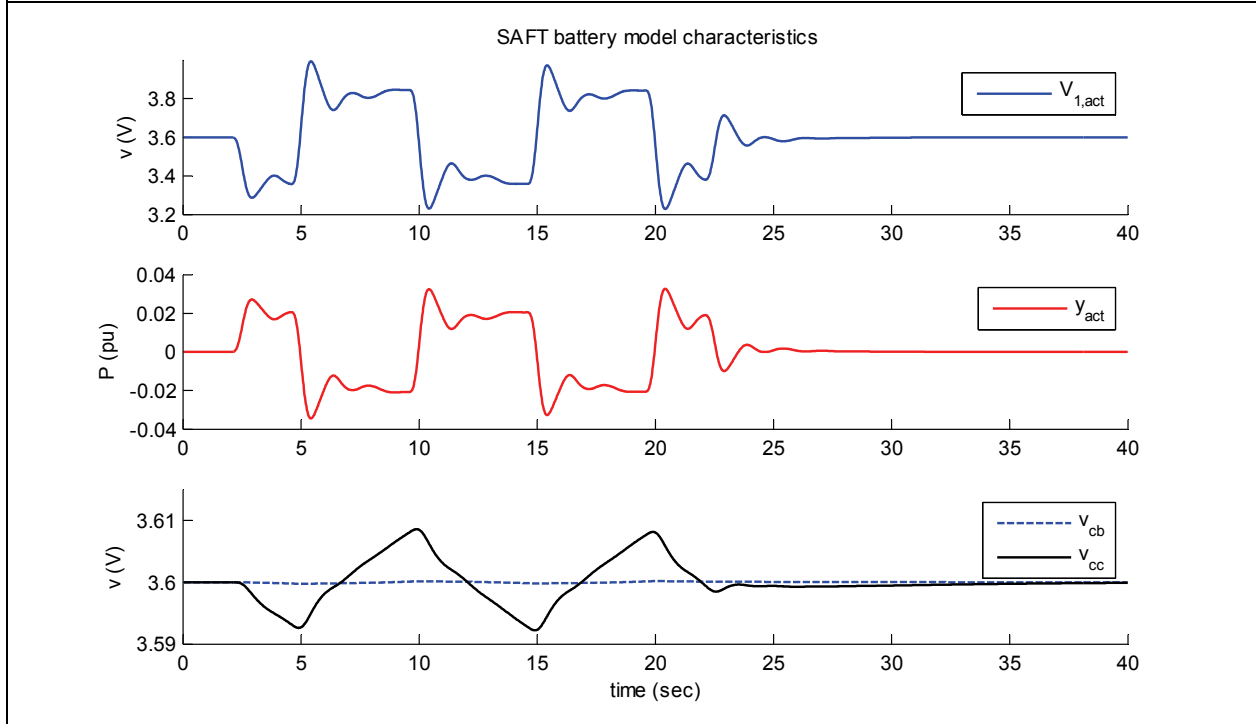


### Results

- In the first subplot of the diagram above, the actuator input voltage  $V_1 = 3.6\text{V} - y_C$  is shown.
- The second plot shows the actuator output power fed back into the power system at the point of common coupling. Comparing these two signals, it can be seen that the actuator output follows exactly the actuator input. In other words the SAFT battery model has a broad bandwidth that allows a very accurate control.
- The faster controller uses the broad bandwidth of the actuator to initially compensate the 0.2 pu until the slower controller starts reacting.
- In the lower part the voltages of the two capacitors of the battery model are plotted. The actual charging and discharging of the battery can be seen from this plot. As the voltage falls below 3.6V, the battery is discharged and a positive power output is observed ( $y_{\text{act}}$ ), meaning that power is fed into the network. If negative power has to be fed into the network, the battery is charged again.
- What can be seen from the voltage magnitude plots is that the battery is discharged constantly after the initial dynamics. This is due to the fact that the output power is not going back exactly to a zero value.

### Simulation 2

- Based on standard system configuration (Chapter 3.1.3)
- Same additional configuration as in simulation 1
- Excitation scenario 2: 0.2pu p-p triangle-wave disturbance at generator bus 2



**Results**

- In this simulation scenario the same fast characteristics of the battery can be seen. The output signal  $y_{act}$  follows the input  $v_{1,act}$  nearly 1 to 1.
- Observing the voltages  $v_{cb}$  and  $v_{cc}$ , one sees that the battery is charged and discharged according to the required power output. If the output power is positive  $t=2\dots5s$ ,  $v_{cc}$  decreases meaning the battery is discharged. For  $t=5\dots10s$ , negative power is fed into the network and the battery is charged again.

Table 5-6: Simulation Results – SAFT battery model

**Findings**

- It was mentioned before that the controller output signal should be limited to a certain range to be consistent with the adjustable voltage source definition. The simulation results are still within the proposed saturation limit of  $[-1.8 \dots 3.6]$ .
- The second limit is the energy content of the battery; in the adapted SAFT model, this effect is captured by the capacitances (though with limitations associated with a small signal model, using “linear” capacitances). The capacitor voltages represent the stored energy in the battery. As can be seen from the simulations above, the energy limits are not exceeding when using the battery for stabilizing control here. The maximum observed voltage drop is  $0.02V$ . The energy limits might become more significant if the battery were used to compensate for larger, long-term variability in power from alternative energy sources. However, that is not the nature of the control application here.
- If the battery model is replaced by a simpler 1<sup>st</sup> or 2<sup>nd</sup> order filter, simulations with time constants of  $\tau = 0.01s$  show performance very similar to simulations using the full SAFT capacitance model.

**Conclusion to SAFT Capacitance Battery Model**

The proposed model has a very broad bandwidth. Therefore the actuator system has almost no influence to the control path. The actuator can be replaced with a standard 1<sup>st</sup> or 2<sup>nd</sup> order filter with very fast time constants and the results correspond very well. This result motivates the use of 2<sup>nd</sup> order filters to represent actuator systems in power system studies.

### 5.3.3 Reduction Oxidation (Redox) Flow Batteries

Another interesting technology that seems to gain more and more attention is the technology of Redox flow batteries. Energy is stored as electrolytes that are pumped into a cell stack, where reduction and oxidation occurs, what builds up a current. Because the reaction is reversible, charging and discharging of the battery is possible. The technology is rather new, but there are some companies that already offer such battery systems. Companies also promote wind-power in particular as one promising area of application. For wind-power, such battery systems could be used to increase energy reliability of the fluctuating nature of wind power production. In a case study from Prudent Energy [39] an energy storage system with stored energy of 1100kW and a power rating of 200kW is shown. Reaction times of the battery system were mentioned to be within 5ms. While this would represent a very interesting area for further investigation, work here was hampered by the fact that more specific data was not given and detailed models of such battery systems were not found in literature. As in the case of wind manufacturers, companies tend to view battery data as highly proprietary. However, unlike blade pitch performance, where simple first principle analysis can provide reasonable estimates of parameters, new battery technologies do not lend themselves such simple engineering judgment.

However, even within these constraints of limited data, it is worthwhile to note that a reaction time of 5ms claimed for the Redox battery system seems to be very fast, comparable to our model for the Li-Ion battery.

## 5.4 Control at Load Bus

So far we have not considered load buses in this project. In the beginning it is mentioned that the management of load buses gains more and more attention. One special application that came up in the past few years is the concept of Plug-in Hybrid Electric Vehicles (PHEV), introduced in Chapter 2.

In the chapter before we already dealt with Li-Ion battery cells. The original purpose of these SAFT Li-Ion batteries is the use in hybrid-electrical vehicles. If one considers a whole parking garage of PHEV cars, this can be represented as a battery stack, as considered above but typically located at a load bus.

Up to now, we have dealt only with generator buses. But with the concept of PHEV it would be interesting to see if a load bus could also be used for our distributed PD control concept. One difficulty that could arise is the fact that load buses are often located in a certain distance from the next generator bus. If a fault occurs at the generator bus for example, it is questionable if the PD controller at the load bus is capable of contributing to grid stability. Because the impedances between the load bus and the bus where the fault occurs could be significantly, the control action could be limited. The presentation here will seek to address this question.

### 5.4.1 Load Bus Modeling

The modeling of a load bus has to be considered first. Without any changes in our simulation program, no local frequency is measured at load buses. But for the PD control a frequency has to be available and measurable at the selected bus. As noted in an earlier section, the approach taken was to perturb the load bus to a generator bus of very small inertia and damping. The equations that were used are then the same as used for a generator bus.

$$\begin{aligned} 0 &\approx M_i \cdot \Delta \dot{\omega}_i = (\Delta P_{mi} - \Delta P_{ei}) - D_i \cdot \Delta \omega_i \\ \Delta \dot{\delta}_i &= \Delta \omega_i \end{aligned} \tag{5.4}$$

With the selection of a very low inertia constant at that bus, the dynamics are then nearly eliminated and approach a simple power balance equation at that bus. The inertia constant  $H$  was set to a value of 0.001 sec which is by 2 orders lower than the inertia constant of the wind turbine buses.  $M_i$  is then accordingly:

$$M_i = \frac{2 \cdot H_i}{\omega_0} \tag{5.5}$$

For simulations, bus 14 was considered as load bus. Bus 14 in our test system is located “far” from the next bus, where the disturbances were applied.

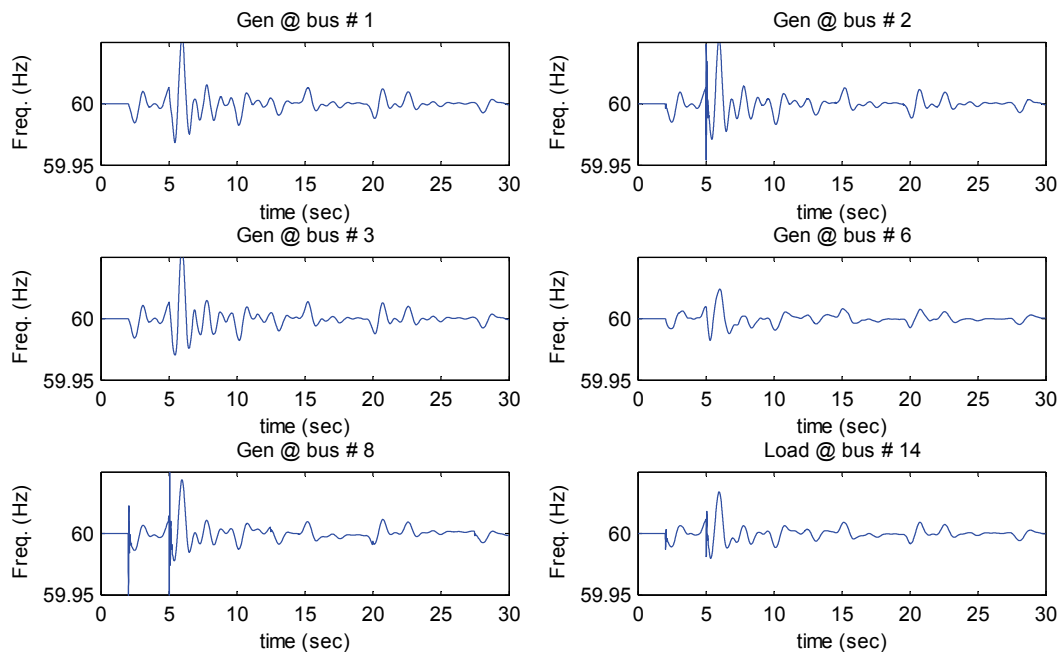
### 5.4.2 Results

In the following table simulation results of the PD controller at the load bus are presented.

#### Simulation Results – Load bus with PD control

##### Simulation 1

- Based on standard system configuration (Chapter 3.1.3)
- Master controller at bus 6
  - Power branch 1:
    - Actuator 1:  $\tau_1 = \tau_2 = 0.5\text{s}$
    - Controller 1:  $\omega_{n1} = 5$
  - Power branch 2:
    - Actuator 2:  $\tau_1 = \tau_2 = 2\text{s}$
    - Controller 2:  $\omega_{n2} = 2$
- Excitation:
  - 0.2pu p-p triangle-wave disturbance at buses 2 and 8
  - Step disturbances of 0.05p.u. at buses 2 and 8

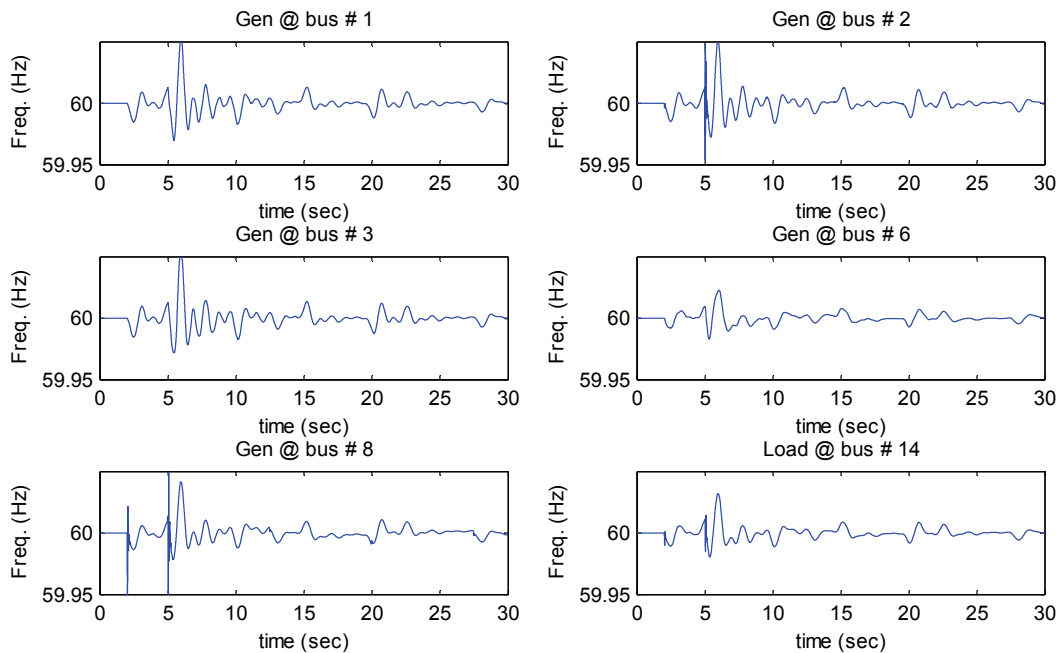


### Results

- The frequency plots above show the reference scenario with only the Master controller installed. The smallest frequency deviations are observed at bus 6, where the Master controller takes action. Higher frequency oscillations can be seen immediately after step disturbances at generator buses 2 and 8.

### Simulation 2

- Based on standard system configuration (Chapter 3.1.3)
- Based on additional configuration as in simulation 1 (Master controller at bus 6)
- Slave PD controller at load bus 14
  - Measurement of frequency:  $\tau_M = 0.001\text{s}$
  - Actuator: SAFT battery model
  - PD controller optimized
- Excitation: (same as in simulation 1)
  - 0.2p.u. p-p triangle-wave disturbance at buses 2 and 8
  - Step disturbances of 0.05p.u. at buses 2 and 8



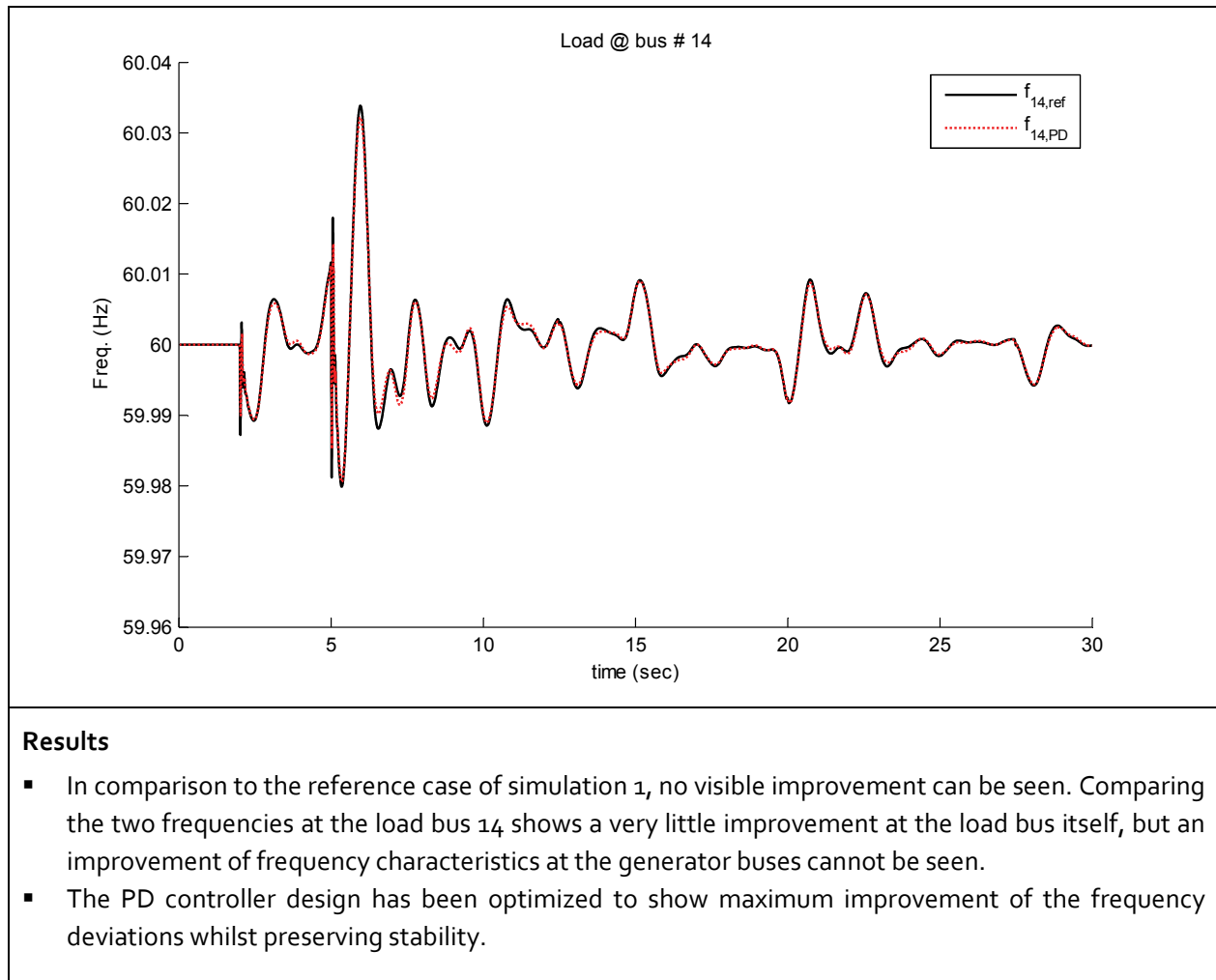


Table 5-7: Simulation Results – Load bus with PD control

Simulation results for this test case suggest that PD control at a load bus does not contribute appreciably to overall system performance. Only disturbances at the load bus itself were reduced slightly. The line impedances seem to have a significant influence on the location selection of controllers. As simulations showed, significant impedances between the location of the disturbance and the location of the control action reduced the ability of the controller to react fast enough to reduce the effect of disturbances at other buses. Therefore the control at load buses should be designed to reduce disturbances at that load bus itself, and suggests that focus should remain on generator buses for system-wide effectiveness in the distributed PD control.

In fact this load bus scenario just emphasizes our findings from before: A PD controller for our system configuration brings significant benefits only when installed locally.



## 5.5 Eigenvalue Analysis

In order to better understand the dynamics and stability of a power system, eigenvalue behavior of the linearized system can be examined and be used to assess stability margins and dynamic characteristics of the system. The evaluation of eigenvalues (EV) from the system state matrix is a well known method in power system analysis. [21]

The eigenproperties of the system matrix  $\mathbf{A}$  are defined with the following equation.

$$\mathbf{A} \cdot \mathbf{\Phi} = \mathbf{\Phi} \cdot \mathbf{\Lambda} \quad (5.6)$$

This equation consist of a vector of eigenvectors

$$\mathbf{\Phi} = [\mathbf{\Phi}_1 \quad \mathbf{\Phi}_2 \quad \dots \quad \mathbf{\Phi}_n] \quad (5.7)$$

and a diagonal matrix, with the eigenvalues.

$$\mathbf{\Lambda} = \begin{bmatrix} \lambda_1 & 0 & 0 & 0 \\ 0 & \lambda_2 & 0 & 0 \\ 0 & 0 & \ddots & 0 \\ 0 & 0 & 0 & \lambda_n \end{bmatrix} \quad (5.8)$$

The eigenvalues from the solution of equation (5.6) should show the same characteristics as the transient simulation of small magnitude disturbances to the system. To ensure consistency between the linearized state space model and the transient simulation, the work here extracted the state-space matrix from the same MATLAB code that implemented trapezoidal rule numerical integration in the transient simulation. The exact steps to extract the expanded system matrix  $\mathbf{A}$  from the numerical integration code are described in detail in the Appendix B.1.1.

Once calculated the system state matrix, MATLAB offers a function that allows direct computation of the eigenproperties from a matrix.

$$[\mathbf{\Phi} \quad \mathbf{\Lambda}] = \text{eig}(\mathbf{A}) \quad (5.9)$$

As pointed out in the appendix, the system matrix  $\mathbf{A}$ , calculated from the Jacobian matrix, consists not only of differential equations but of algebraic equations as well. The eigen-problem (5.6) can be modified slightly to reduce the eigenproperty calculation to the differential equations and its associated

modes. By adding a diagonal weighting matrix  $\mathbf{W}$  to the right side of equation (5.6), the eigenproperties are reduced to the desired dynamic modes of the system.

$$\mathbf{A} \cdot \Phi = \mathbf{W} \cdot \Phi \cdot \Lambda \quad (5.10)$$

$$\mathbf{W} = \begin{bmatrix} \mathbf{I}_G & \mathbf{0} & \mathbf{0} \\ \mathbf{0} & \mathbf{0} & \mathbf{0} \\ \mathbf{0} & \mathbf{0} & \mathbf{I}_S \end{bmatrix} \quad (5.11)$$

The identity matrices  $\mathbf{I}_G$  and  $\mathbf{I}_S$  of the weighting matrix stand for the generator states respectively the supplemental states of the added control structure. This problem is already implemented in a MATLAB function as well and can be accessed with the following command.

$$[\Phi \quad \Lambda] = \text{eig}(\mathbf{A}, \mathbf{W}) \quad (5.12)$$

Unwanted eigenvalues from the load bus algebraic variables result in values at infinity and can simply be ignored for the purposes here.

### 5.5.1 Eigenvalues of Basic System

First, the eigenvalues of the power system without any additional control implemented are calculated and their characteristics are studied.

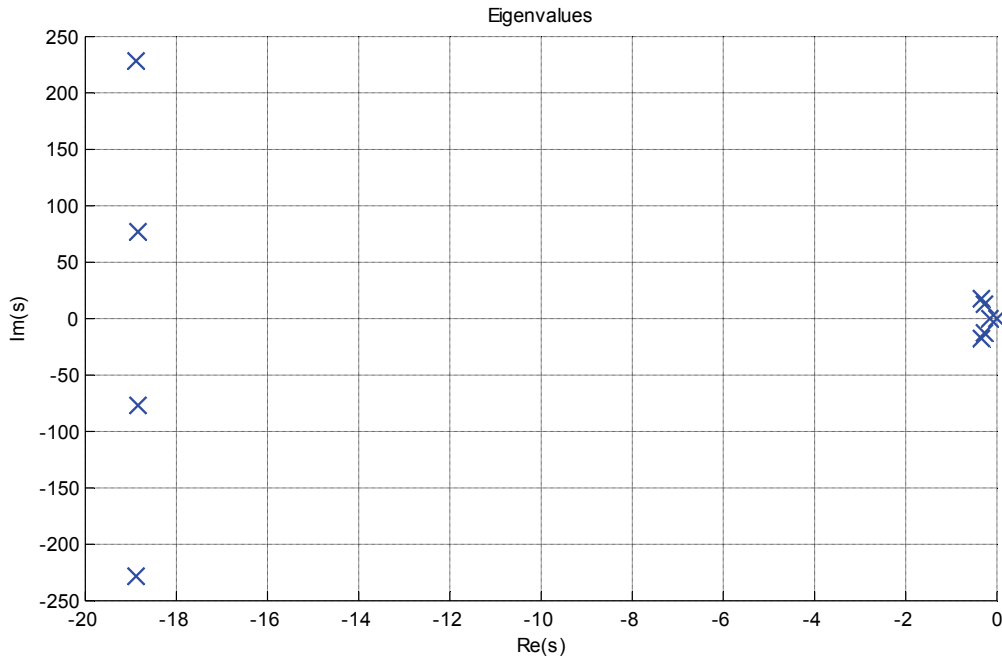


Figure 5-17: Eigenvalues of basic system

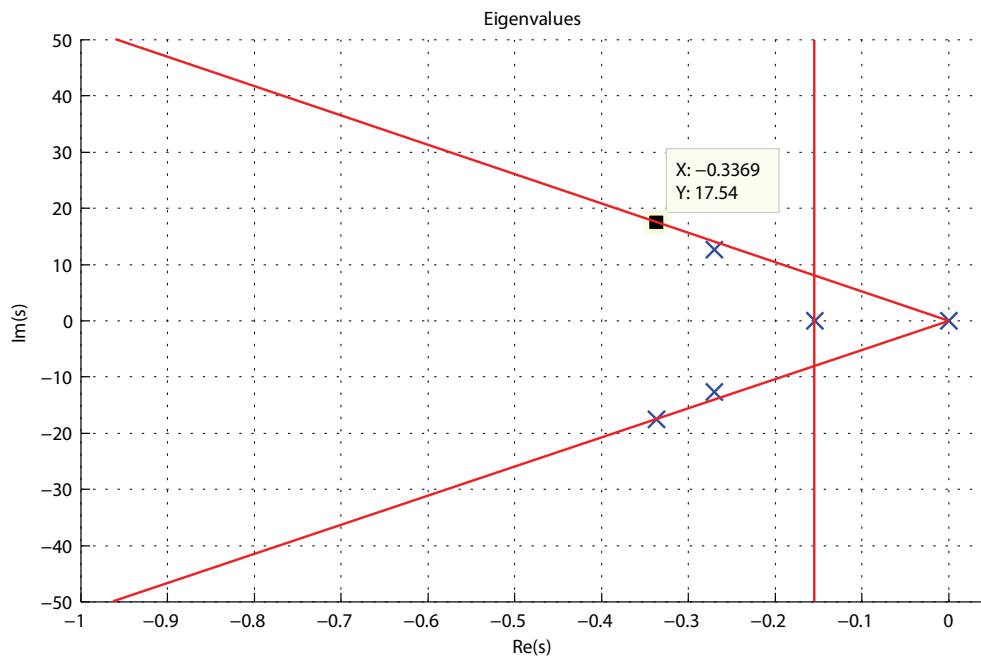


Figure 5-18: Eigenvalues of basic system (zoomed in)

From Figure 5-18, the characteristics of the basic system can be seen. The basic system has a single eigenvalue in the origin. This EV arises from the power systems fundamental behavior, and should not be interpreted as a physically meaningful instability.

An interpretation of the other eigenvalues can be made with classical control theory. As known, characteristics of poles or EVs can be described on an s-plane sketch according to [32] and the figure below.

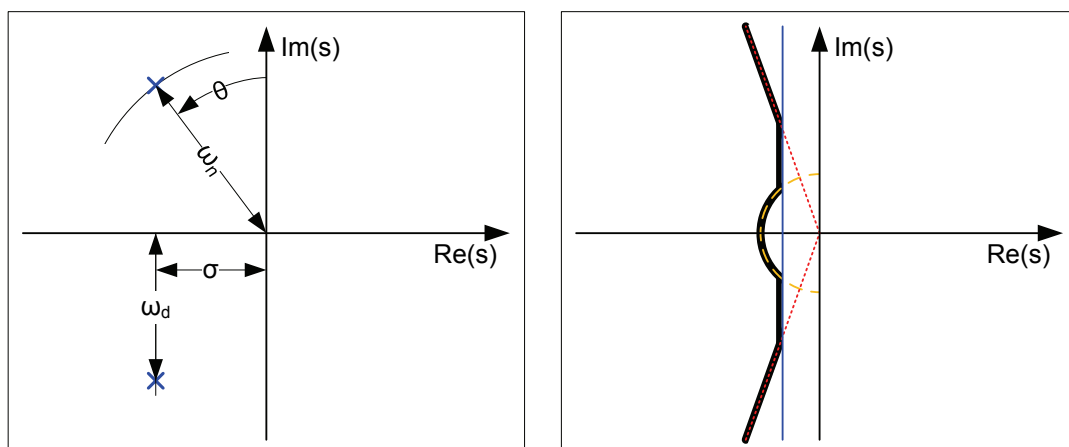


Figure 5-19: Standard eigenvalue properties and the system's characteristic region in the s-plane

Signals corresponding to EVs with only real part, located on the real axis, are characterized by the exponential impulse response of a single pole below.

$$h(t) = e^{-\sigma t} \quad (5.13)$$

The EV closest to the imaginary axis, has the slowest exponential decay and therefore defines the systems settling time. The time constant  $\tau = 1/\sigma$  can be used as characterization of the exponential decay.

Complex conjugate eigenvalues of the form

$$\lambda_i = -\sigma \pm j\omega_d \quad (5.14)$$

define the systems undamped natural frequency  $\omega_n$  and the damping ratio  $\zeta$ .

$$\begin{aligned} \sigma &= \zeta \cdot \omega_n \\ \theta &= \sin^{-1} \zeta \end{aligned} \quad (5.15)$$

The complex conjugate pair of eigenvalues with the smallest angle  $\theta$  defines the systems damping. All eigenvalues define then a region according to the figure above that characterizes desirable system behavior.

Going back to the basic system described before, the nearest EV to the imaginary axis has a real part of -0.1541. With equation (5.13) this results in a system time constant of  $\tau = 6.5$  s.

The complex conjugate eigenvalue pair with the smallest angle  $\theta$  is located at  $-0.3369 \pm j17.54$ . The values  $\omega_n$  and  $\zeta$  of the system are then:

$$\begin{aligned} \omega_n &= 17.54 \text{ rad/s} \\ \zeta &= 14.77 \text{ e-} 3 \end{aligned}$$

### 5.5.2 Eigenvalues of System with Master Controller and distributed PD Controllers

In the development of the distributed PD controllers, it was seen that with a too high proportional gain of the controllers, the system became unstable. The eigenvalue analysis can be useful in this case in particular. By varying parameters of the designed PD controller, eigenvalue movements can be observed and useful insights into the stability and performance characteristic can be gained.

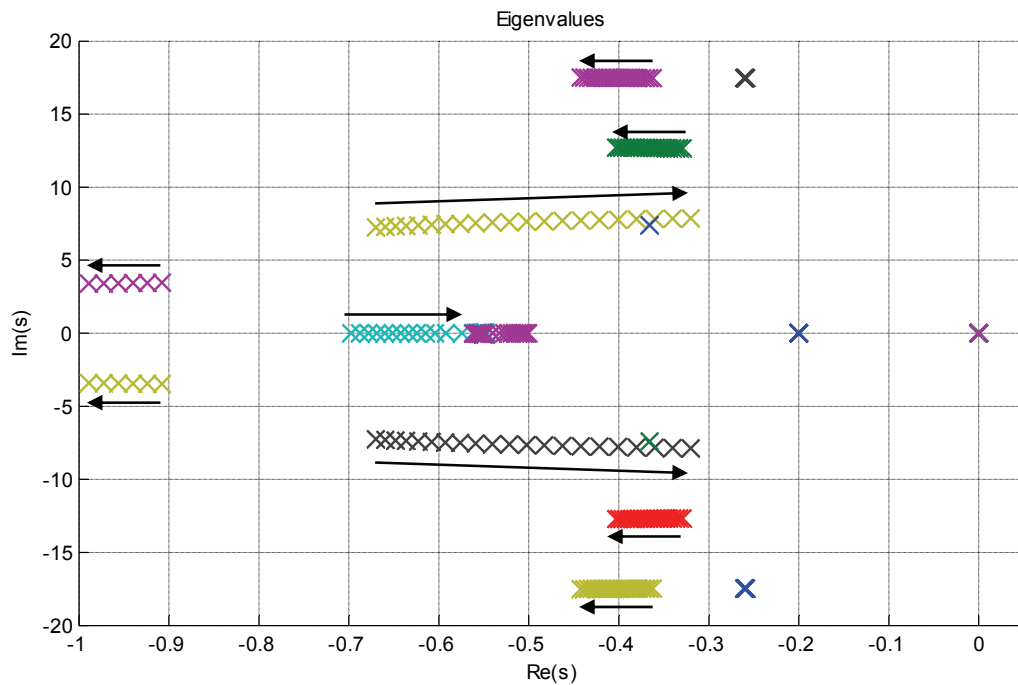
This analysis is done for the distributed PD controller design.

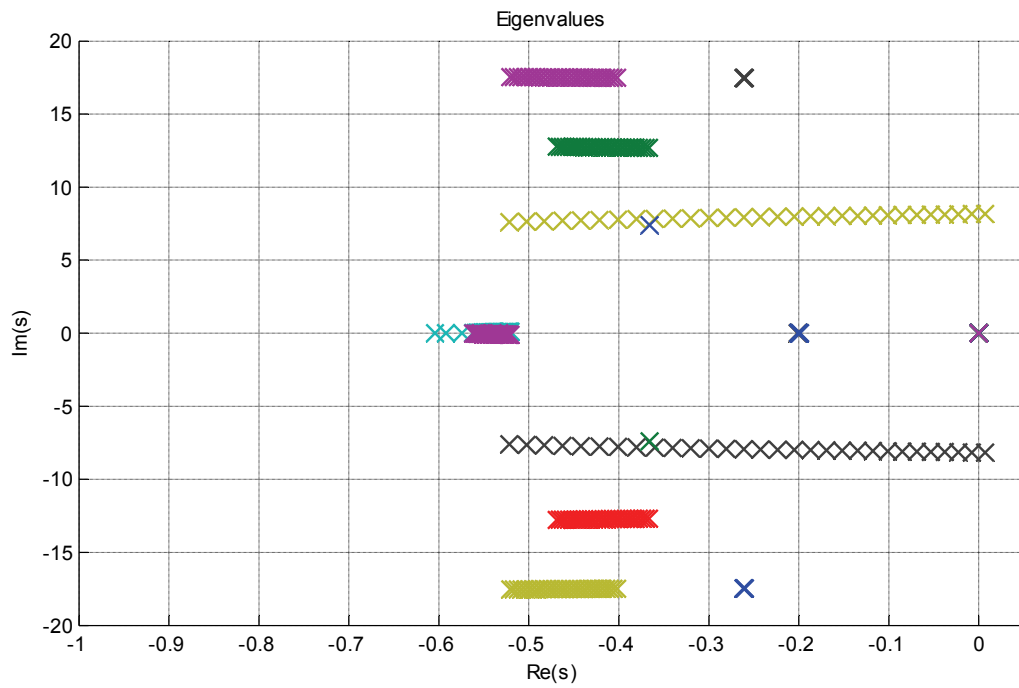
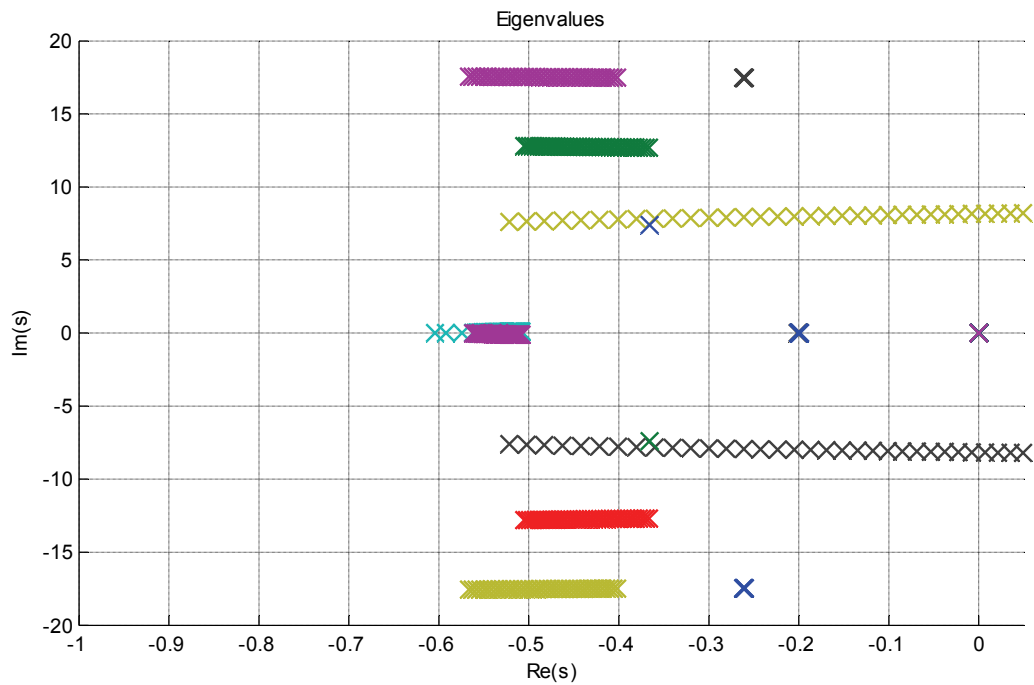
### Simulation Results – PD parameter variations

#### Simulation 1

- Based on standard system configuration (Chapter 3.1.3)
- Master controller at bus 6
  - Power branch 1:
    - Actuator 1:  $\tau_1 = \tau_2 = 0.5\text{ s}$
    - Controller 1:  $\omega_{n1} = 5$
  - Power branch 2:
    - Actuator 2:  $\tau_1 = \tau_2 = 2\text{ s}$
    - Controller 2:  $\omega_{n2} = 2$
- Slave PD controller at bus 2
  - Actuator:  $\tau_1 = \tau_2 = 0.01\text{ s}$
  - PD controller with varying parameter  $k_p$
  - $k_D = 0.001$
- Slave PD controller at bus 8
  - Actuator:  $\tau_1 = \tau_2 = 0.01\text{ s}$
  - Optimized,  $k_p = 0.02$ ,  $k_D = 0.001$
- EV calculation for varying parameter  $k_{p,21}$

**Plot 1:**  $k_{p,21} = 0.00 \dots 0.02$ , with a step of 0.001



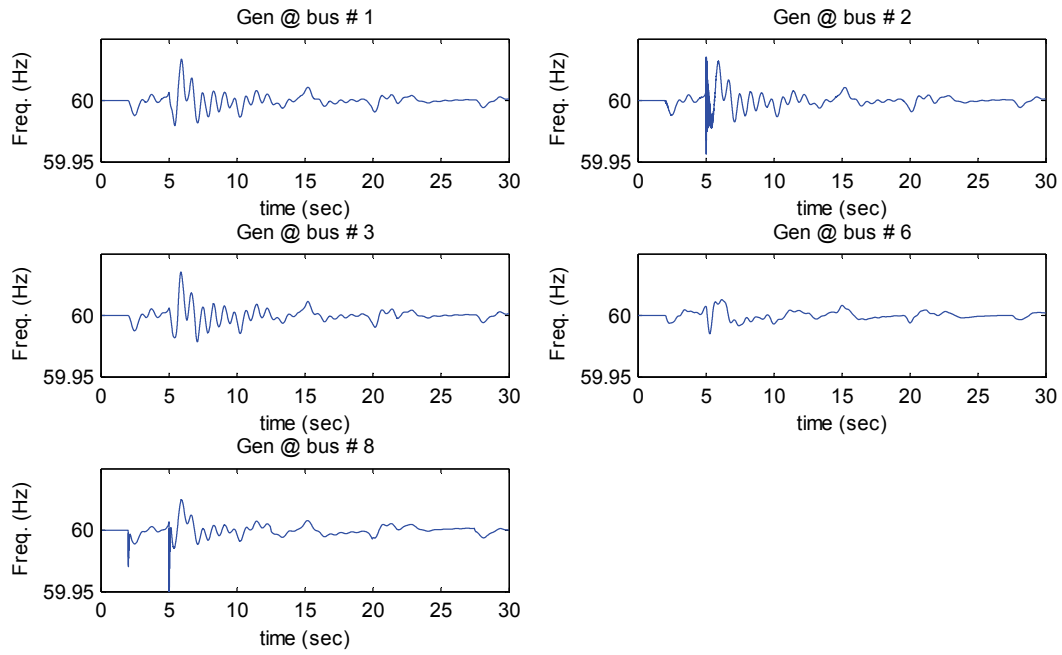
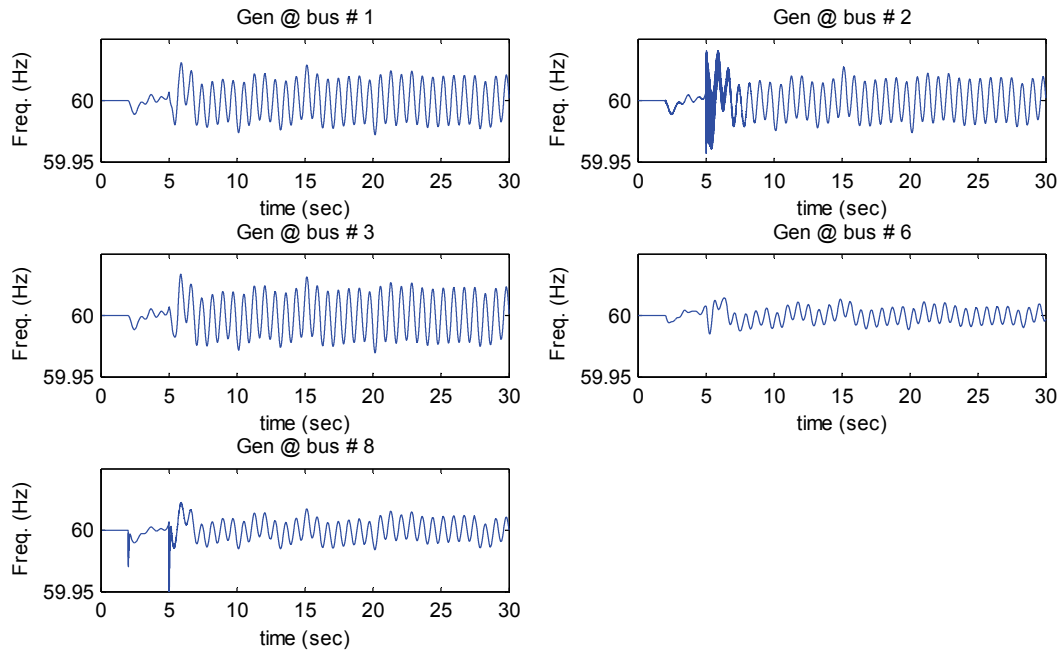
**Plot 2:**  $k_{p,21} = 0.01 \dots 0.039$ , with a step of 0.001**Plot 3:**  $k_{p,21} = 0.01 \dots 0.05$ , with a step of 0.001

**Results**

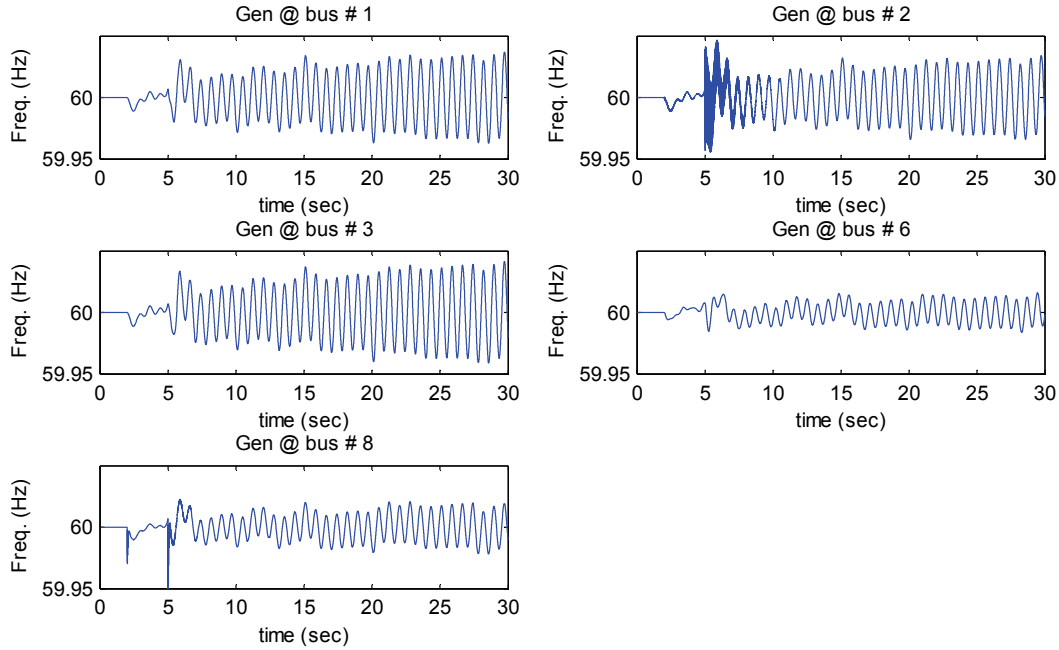
- As can be seen from the plots 1 to 3, eigenvalues are moving with the change of parameter  $k_{p,21}$  of the PD controller at bus 2. The direction of the movement is not uniform. Some EVs are moving towards a higher real part and the imaginary axis and other EVs are moving away from the imaginary axis.
- What can be seen is that a conjugate complex pair of eigenvalues is, with increasing  $k_{p,21}$ , moving to the imaginary axis and at a value of  $k_{p,21} = 0.039$  it crosses the axis. The system becomes then unstable and remains unstable with an even higher  $k_{p,21}$ . This finding confirms the results from the transient simulation of the same case (Simulation 2 below).

**Simulation 2**

- Based on standard system configuration (Chapter 3.1.3)
- Same additional configuration as in simulation 1
- Transient simulation for specific values of  $k_{p,21}$
- Excitation scenario 1: 0.2pu step disturbance at load bus 4

**Plot 1:**  $k_{P,21} = 0.02$ **Plot 2:**  $k_{P,21} = 0.037$ 



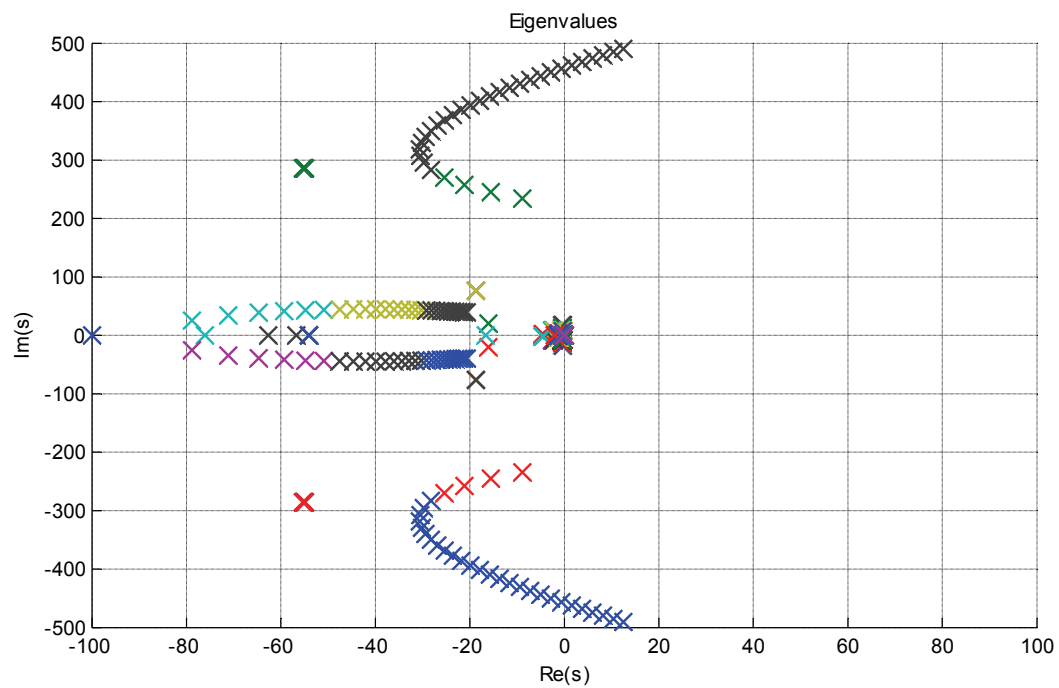
**Plot 3:**  $k_{P,21} = 0.039$ **Results**

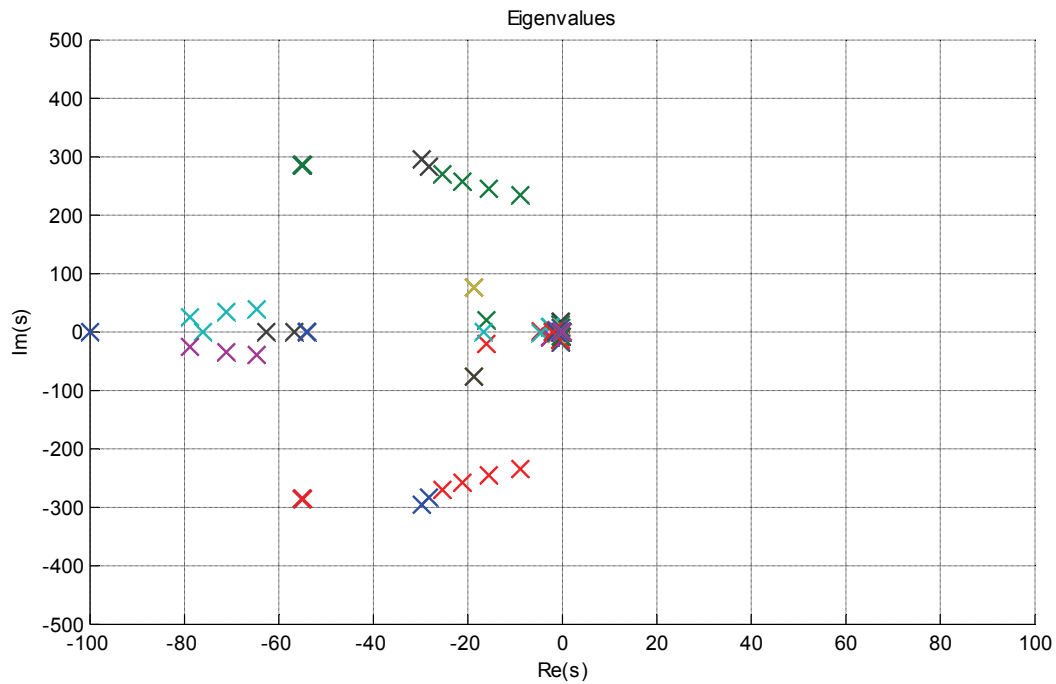
- The plots 1 to 3 are consistent with the results from the eigenvalue analysis. At a value of  $k_{P,21} = 0.037$ , the transient simulation shows a critically stable system. If the proportional gain is increased to  $k_{P,21} = 0.039$ , the simulation shows an unstable system.
- From the EV analysis in simulation 1, the critical situation was found to be at a value of  $k_{P,21} = 0.037$ . Knowing the eigenvalues at this point, the undamped natural frequency  $\omega_n$  of the complex pole pair crossing the imaginary axis can be calculated. With  $\omega_n = 8.2 \text{ rad/s}$  the frequency of the oscillations is then  $f_n = 1.3 \text{ Hz}$  and its period is  $T = 0.76 \text{ s}$ . This is exactly the frequency of oscillation in the transient simulation plots and therefore the eigenvalue analysis and transient simulation match to each other.

**Simulation 3**

- Based on standard system configuration (Chapter 3.1.3)
- Based on same additional configuration as in simulation 1
- Slave PD controller at bus 2
  - Actuator:  $\tau_1 = \tau_2 = 0.01\text{s}$
  - PD controller with varying parameter  $k_D$
  - $k_p = 0.02$
- EV calculation for varying parameter  $k_{D,21}$

**Plot 1:**  $k_{D,21} = 0.0 \dots 0.003$ , with a step of 0.0001



**Plot 2:**  $k_{D,21} = 0.0 \dots 0.0005$ , with a step of 0.0001**Results**

- With varying derivative gain, the behavior is different than observed in simulations 1 and 2 for the proportional gain. A pair of complex poles first moves away from the imaginary axis towards a higher negative real part. A further increasing of the parameter results in a movement back to the imaginary axis and ultimately in a crossing of the axis and movement into the RHP. This is where the system becomes unstable.
- The interesting thing at this simulation is that there is an optimum choice for the differential gain. According to the eigenvalue analysis, a gain of  $k_{D,21} = 0.0005$  seems to be most promising. Transient simulations for different values of  $k_{D,21}$  do not completely agree with this result. Simulations do not show significant differences between a  $k_D$  of 0.001 and one of 0.0005.

**Table 5-8: Simulation Results – PD parameter variations**

The PD controller parameters  $k_p$  and  $k_D$ , are referred to the loop gain of the additional power path. Because two different programs were used, their absolute value differs from results in other parts of this thesis. The parameters used in this section are scaled to the battery model. However, the ratio of the two controller parameters obviously does not change.

### 5.5.3 Conclusion of Eigenvalue Analysis

The eigenvalue Analysis is among the last analyses performed as part of this project. The analysis shows very interesting results and with the help of the eigenvalues of the system a better understanding of the transient simulations is obtained. The analysis serves as good tool for optimizing controller designs and evaluating the robustness of such designs.

With this analysis the PD controller design from Chapter 5.2 could be verified and optimized. From movements of eigenvalues by varying parameters of the PD controllers, it could be verified that there is an improvement in terms of stability with added distributed PD controllers. But one could also see that the PD control parameters have certain limits and can destabilize the system, if the parameters are set too high.

The eigenvalue analysis is a commonly used tool for power system studies. To base results not only on the transient simulations, but also on the eigenvalue analysis proved a very useful step in this project. The verification of simulation results through the eigenvalue analysis was important, and exploitation of eigenanalysis tools is highly recommended for any future extensions of this work.

## 6 Test Bed System

The test bed system used for this work is based on the IEEE 14-Bus Test System described in Chapter 3. MATLAB is used as software tool. For simulations of the IEEE test system, we start with an existing MATLAB program provided by our supervisor, Prof. DeMarco. The program was originally written to simulate the impact of non-standard generator control in a power system. Without the added control, the program provides a transient stability simulation of the 14 bus system.

### 6.1 Fundamentals

The MATLAB program performs a nonlinear simulation of system's swing dynamics. Differential equations from the swing dynamics and algebraic equations from the power flow equations form a nonlinear problem. The algebraic equations can be seen as constraints for the differential equations and the resulting set of differential equations with constraints can be numerically integrated using implicit trapezoidal solution method.

The set of equations can be described as:

$$\begin{cases} \dot{\mathbf{x}}_f = \mathbf{f}(\mathbf{x}_f, \mathbf{x}_g, t) \\ \mathbf{0} = \mathbf{g}(\mathbf{x}_f, \mathbf{x}_g, t) \end{cases} \quad (6.1)$$

The vectors  $\mathbf{x}_f$  and  $\mathbf{x}_g$  represent the state-vectors of the differential  $\mathbf{x}_f$  and algebraic equations  $\mathbf{x}_g$  from the equation system (6.1).

#### 6.1.1 Newton Raphson Algorithm

The Newton Raphson method is a well established iteration method to solve a set of nonlinear equations that can be written in the form of

$$\mathbf{f}(\mathbf{x}) = \mathbf{0} \quad (6.2)$$

where  $\mathbf{x}$  is a vector of  $n$  unknowns

$$\mathbf{x} = [x_1 \quad x_2 \quad \cdots \quad x_n]^T \quad (6.3)$$

and  $\mathbf{f}$  a vector of  $n$  functions of  $\mathbf{x}$ .

$$\mathbf{f}(\mathbf{x}) = [f_1(\mathbf{x}) \quad f_2(\mathbf{x}) \quad \cdots \quad f_n(\mathbf{x})]^T \quad (6.4)$$

For solvability  $\mathbf{f}(\mathbf{x})$  is linearized in a next step using the Taylor expansion

$$\mathbf{f}(\mathbf{x} + \Delta\mathbf{x}) \approx \mathbf{f}(\mathbf{x}) + \mathbf{J}(\mathbf{x}) \cdot \Delta\mathbf{x} \quad (6.5)$$

where  $\mathbf{J}(\mathbf{x})$  is the Jacobian Matrix, defined as

$$\mathbf{J}(\mathbf{x}) = \frac{\partial \mathbf{f}}{\partial \mathbf{x}} = \begin{bmatrix} \frac{\partial f_1}{\partial x_1} & \cdots & \frac{\partial f_1}{\partial x_n} \\ \vdots & \ddots & \vdots \\ \frac{\partial f_n}{\partial x_1} & \cdots & \frac{\partial f_n}{\partial x_n} \end{bmatrix} \quad (6.6)$$

The correction vector  $\Delta\mathbf{x}$  is the solution of the linearized problem

$$\mathbf{f}(\mathbf{x}) + \mathbf{J}(\mathbf{x}) \cdot \Delta\mathbf{x} = \mathbf{0} \quad (6.7)$$

The algorithm can thus be summarized as follows:

1. The iteration variable is set to zero ( $\nu = 0$ ) and an appropriate starting vector  $\mathbf{x}^0$  is chosen.
2.  $\mathbf{f}(\mathbf{x}^0)$  is computed
3. Loop and test for convergence:

If  $\|\mathbf{f}(\mathbf{x}^\nu)\| \leq \varepsilon$ , then  $\mathbf{x}^\nu$  is the solution

Otherwise continue with loop.

- a. The Jacobian matrix  $\mathbf{J}(\mathbf{x}^\nu)$  is computed
- b. Solution is updated

$$\begin{aligned} \Delta\mathbf{x}^\nu &= -\mathbf{J}^{-1}(\mathbf{x}^\nu) \cdot \mathbf{f}(\mathbf{x}^\nu) \\ \mathbf{x}^{\nu+1} &= \mathbf{x}^\nu + \Delta\mathbf{x}^\nu \end{aligned} \quad (6.8)$$

- c. Iteration variable is updated:  $\nu = \nu + 1$
- d.  $\mathbf{f}(\mathbf{x}^\nu)$  is computed

### 6.1.2 Numerical Integration using Trapezoidal Rule and Newton Raphson Algorithm

The program uses an implicit integration method to solve the set of first-order differential equations. The most common method used in power systems is the trapezoidal rule, as implemented in the MATLAB code employed here.

$$\frac{dx}{dt} = f(x, t) \quad (6.9)$$

A first order differential equation (6.9) can be written in integral form as:

$$x(t_1) = x(t_0) + \int_{t_0}^{t_1} f(x, \tau) \cdot d\tau \quad (6.10)$$

The use of the trapezoidal rule given in the equations below and recognizing that  $x_{n+1}$  appears on both sides, leads to an implicit equation that has to be solved.

$$x(t_1) = x(t_0) + \frac{\Delta t}{2} [f(x(t_0), t_0) + f(x(t_1), t_1)] \quad (6.11)$$

$$x(t_{n+1}) = x(t_n) + \frac{\Delta t}{2} [f(x(t_n), t_n) + f(x(t_{n+1}), t_{n+1})] \quad (6.12)$$

Considering a specific time  $t_{n+1}$  in the simulation, the use of implicit numerical integration allows us to solve the problem with standard techniques. The initial problem set has to be rewritten according to the trapezoidal rule, for convenience, all unknown terms are isolated on one side of the equation. This results in a well known equation system that allows the use of the standard Newton Raphson algorithm for solving the problem at that specific time.

$$\mathbf{0} = \mathbf{F}(\mathbf{x}_f(t_{n+1}), \mathbf{x}_f(t_n), \mathbf{x}_g(t_{n+1}), t_{n+1}) \quad (6.13)$$

Remember that  $\mathbf{x}_f$  and  $\mathbf{x}_g$  in equation (6.13) represent state variables of differential equations and algebraic equations respectively. The trapezoidal rule is only applied to the differential equations  $\mathbf{f}(\cdot)$ .

$$\begin{cases} \mathbf{0} = \mathbf{x}_f(t_n) - \mathbf{x}_f(t_{n+1}) + \frac{\Delta t}{2} [\mathbf{f}(\mathbf{x}_f(t_n), \mathbf{x}_g(t_n), t_n) + \mathbf{f}(\mathbf{x}_f(t_{n+1}), \mathbf{x}_g(t_{n+1}), t_{n+1})] \\ \mathbf{0} = \mathbf{g}(\mathbf{x}_f(t_{n+1}), \mathbf{x}_g(t_{n+1}), t_{n+1}) \end{cases} \quad (6.14)$$

The procedure used in the program follows the algorithm from the section before. If one remembers that the Newton Raphson algorithm is used to solve for  $\mathbf{x}$  at time  $t_{n+1}$  the procedure can be written in

that form. To allow a shorter notation, the two vectors  $\mathbf{x}_f$  and  $\mathbf{x}_g$  are combined to the vector  $\mathbf{x}$  and equation (6.13) is simplified to:

$$\mathbf{0} = \mathbf{F}(\mathbf{x}(t_{n+1}), \mathbf{x}(t_n), t_{n+1}) \quad (6.15)$$

1. The iteration step variable is set to zero ( $\nu=0$ ) and an appropriate starting value  $\mathbf{x}(t_{n+1})^0$  is chosen.

For time  $t_0$  this is done by solving the equilibrium power flow problem.

For all other times  $t_{n+1}$  the starting value is simply the values calculated for the time  $t_n$  before.

2.  $\mathbf{F}(\mathbf{x}(t_{n+1})^0, \mathbf{x}(t_n), t_{n+1})$  is computed

3. Loop and test for convergence:

If  $\|\mathbf{F}(\mathbf{x}(t_{n+1})^\nu, \mathbf{x}(t_n), t_{n+1})\| \leq \varepsilon$ , then  $\mathbf{x}(t_{n+1})^\nu$  is the solution

Otherwise continue with loop.

- a. The Jacobian matrix  $\mathbf{J}(\mathbf{x}(t_{n+1})^\nu)$  is computed
- b. Solution is updated

$$\begin{aligned} \Delta \mathbf{x}(t_{n+1})^\nu &= -\mathbf{J}^{-1}(\mathbf{x}(t_{n+1})^\nu) \cdot \mathbf{F}(\mathbf{x}(t_{n+1})^\nu, \mathbf{x}(t_n), t_{n+1}) \\ \mathbf{x}(t_{n+1})^{\nu+1} &= \mathbf{x}(t_{n+1})^\nu + \Delta \mathbf{x}(t_{n+1})^\nu \end{aligned} \quad (6.16)$$

- c. Iteration variable is updated:  $\nu = \nu + 1$
- d.  $\mathbf{F}(\mathbf{x}(t_{n+1})^\nu, \mathbf{x}(t_n), t_{n+1})$  is computed

*The principle of the Newton Raphson algorithm is the linearization of equations around an operating point. Solutions of the algorithm are valid only in the vicinity of this operating point. If too large disturbances are simulated, results might be wrong, because they are too far from the operating point. In our case with the trapezoidal rule time simulation, we choose a new operating point for every timestep. Therefore, if the time interval is chosen to be small, the results from the simulations should be accurate for our disturbance simulations.*



### 6.1.3 Computation of Jacobian Matrix

The use of the Newton Raphson algorithm from above requires the computation of the Jacobian matrix.

The Jacobian matrix is defined as follows:

$$\mathbf{J}(\mathbf{x}^v) = \frac{\partial \mathbf{F}}{\partial \mathbf{x}^v} \quad (6.17)$$

Applying the calculation on our system configuration turned out to be more difficult. In order to calculate  $\mathbf{x}(t_{n+1})$ , the solution at time  $t_{n+1}$ , the calculation of the Jacobian matrix is according to:

$$\mathbf{J}(\mathbf{x}(t_{n+1})^v) = \frac{\partial \mathbf{F}(\mathbf{x}(t_{n+1})^v, \mathbf{x}(t_n), t_{n+1})}{\partial \mathbf{x}(t_{n+1})^v} \quad (6.18)$$

It might be of interest to see that in taking the derivative of the first equation of (6.14), the differential equations, terms reduce to a simpler form.

$$\frac{\partial \mathbf{F}_f}{\partial \mathbf{x}(t_{n+1})^v} = -\mathbf{I} + \frac{\Delta t}{2} \cdot \frac{\partial}{\partial \mathbf{x}(t_{n+1})^v} \left[ \mathbf{f}(\mathbf{x}_f(t_{n+1})^v, \mathbf{x}_g(t_{n+1})^v, t_{n+1}) \right] \quad (6.19)$$

## 6.2 Applied State Vector and Associated Functions

In the section before, a general mathematical description is given of the state vector  $\mathbf{x}$  and the corresponding functions  $\mathbf{F}(\mathbf{x})$ . In the introduction of Chapter 6 it is also described that differential equations from generator dynamics and algebraic equations from power flow equations form the system of functions  $\mathbf{F}(\mathbf{x})$ . The differential equations from generators are according to (6.20) and describe the swing dynamics at that particular generator bus.

$$\begin{aligned} \Delta \dot{\omega}_i &= \frac{\Delta P_{mi} - \Delta P_{ei}}{M_i} - \frac{D_i}{M_i} \cdot \Delta \omega_i \\ \Delta \dot{\delta}_i &= \Delta \omega_i \end{aligned} \quad (6.20)$$

An adequate choice of the state vector what is used in this work consists of 28 states and is defined as follows:

$$\mathbf{x} = [\mathbf{x}_f^T \quad \mathbf{x}_g^T]^T = [\omega_{Gi} \quad \cdots \quad \theta_{Gi} \quad \cdots \quad \theta_{Lk} \quad \cdots \quad V_{Lk} \quad \cdots]^T \quad (6.21)$$

The states  $\mathbf{x}_f$  from the generator dynamic equations are the frequency deviations  $\omega_{Gi}$  and the phase angles  $\theta_{Gi}$  at the generator buses  $i$ . The states  $\mathbf{x}_g$  from the power flow equations are the phase angles

$\theta_{Lk}$  and the voltage magnitudes  $V_{Lk}$  at the load buses  $k$  according to the topology in Figure 3-1. In the IEEE 14 bus topology there are 5 generator buses and 9 load buses. This results in 10 generator bus states and 18 load bus states. The state vector  $\mathbf{x}$  of the test system has therefore 28 states.

The functions vector  $\mathbf{F}(\mathbf{x})$  consists likewise of 28 functions. The first 10 functions are the generators differential equations  $\mathbf{f}_G(\cdot)$  described in (6.20). These are the functions that are integrated using trapezoidal rule as described in the section before. The other 18 functions are algebraic equations that are based on the active respectively the reactive power mismatch at the load buses  $\mathbf{f}_L(\cdot)$ .

$$\mathbf{F}(\mathbf{x}) = \begin{bmatrix} \mathbf{f}(\mathbf{x}_f, \mathbf{x}_g) & \mathbf{g}(\mathbf{x}_f, \mathbf{x}_g) \end{bmatrix}^T = \begin{bmatrix} \mathbf{f}_G(\mathbf{x}_G, \mathbf{x}_L) & \mathbf{f}_L(\mathbf{x}_G, \mathbf{x}_L) \end{bmatrix}^T \quad (6.22)$$

### 6.3 Simulation Program in MATLAB

In this section the functions of the MATLAB program are explained in detail. Because the program was originally designed for another simulation case, some code adaption's had to be made first.

#### 6.3.1 Code Adaptation's

In order to meet the needs of our simulation scenarios, some functions of the program had to be modified.

##### *Infinite Bus*

Bus number 1 is treated as infinite bus in the original program. Due to this choice, possible power mismatches arising from disturbances in the network (increase or decrease of power) were immediately compensated by the infinite bus. Therefore no steady-state frequency deviations can be seen in the simulations. But these frequency deviations are central for this research and consequently this part of the simulation tool required modification. Without any frequency control, a power mismatch should result in a steady-state frequency deviation and adding frequency control should then bring the frequency back to its nominal value.

The simulation program is modified to simulate a closed system, without the unwanted compensation of the infinite bus. Bus 1 is considered as normal generator bus with its own frequency  $\Delta\omega_1$  and so our program is expanded by a fifth generator bus.

### Reference Frequency

The original program showed frequency deviations arising from each bus itself. In an interconnected power system, the frequency is usually referred to one frequency in the grid. The generator at bus 1 is chosen to provide the reference frequency of the system. Equations (6.20) can be slightly modified to show a frequency deviation referred to  $\omega_1$ .

$$\Delta\dot{\omega}_i = \frac{\Delta P_{mi} - \Delta P_{ei}}{M_i} - \frac{D_i}{M_i} \cdot (\Delta\omega_i - \Delta\omega_1)$$

$$\Delta\dot{\delta}_i = \Delta\omega_i - \Delta\omega_1 \quad (6.23)$$

### 6.3.2 General Structure

The program is structured in four main parts. In the start file, the configuration of the simulation can be set. Among others, bus configurations and fault types are selected.

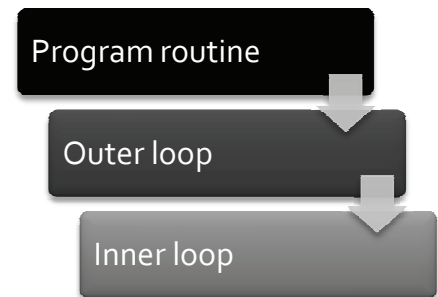
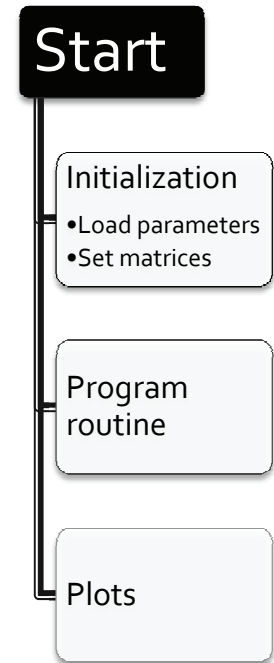
The next step of the program is the initialization. In this part, the system parameters are loaded and matrices are generated according to the selected configuration. After this step the program is ready for the actual simulation.

The program routine is implemented according to the trapezoidal rule Newton Raphson algorithm described in Section 6.1. Two loops characterize the program routine.

In an outer loop the simulation time is increased by the simulation time step  $\Delta t$  for every cycle. The Jacobian matrix  $\mathbf{J}(\mathbf{x})$  and the actual algebraic equations  $\mathbf{F}(\mathbf{x})$ , a set of trapezoidal rule integrated differential equations and algebraic equations, were computed for the time  $t_{n+1}$ .

The inner loop represents then the iteration process of the Newton Raphson algorithm for the specific time  $t_{n+1}$  of the transient simulation. The state vector  $\mathbf{x}_{t_{n+1}}$  is iteratively calculated until it meets the defined convergence criterion.

If the convergence criterion is met, the inner loop is terminated and the simulation time is increased by the time step  $\Delta t$  in the



outer loop. The inner loop Newton Raphson algorithm is then started from new for the time  $t_{n+1} = t_n + \Delta t$ . Once the simulation end time is reached the outer loop is terminated and the simulation is finished. If the convergence criterion in the inner loop is failed once, the simulation is terminated.

### 6.3.3 System Matrices

Basically there are two important subfunctions in the program that calculate on the one hand the Jacobian matrix  $\mathbf{J}(\mathbf{x})$  and on the other hand the function vector  $\mathbf{F}(\mathbf{x})$ , also called mismatch vector.

The function *trzjac.m* calculates the Jacobian matrix according to the description in Section 6.1. The important thing about the calculated matrix  $\mathbf{J}(\mathbf{x})$  is that the matrix also consists of algebraic equations from power flow mismatches at load buses and therefore it is a mixed matrix with trapezoidal rule solved differential equations and real algebraic equations.

$$\mathbf{J}(\mathbf{x}) = \begin{bmatrix} -\mathbf{I} + \frac{\Delta t}{2} \cdot \frac{\partial}{\partial \mathbf{x}} \mathbf{f}(\dots) \\ \frac{\partial}{\partial \mathbf{x}} \mathbf{g}(\dots) \end{bmatrix} \quad (6.24)$$

The other function *trzmiss.m* calculates the mismatch of the function vector. The calculation is according to the trapezoidal rule description in Section 6.1.

$$\mathbf{F}(\mathbf{x}) = \begin{bmatrix} \mathbf{x}_f(t_n) - \mathbf{x}_f(t_{n+1})^\nu + \frac{\Delta t}{2} \cdot (\mathbf{f}(\dots, t_{n+1}) + \mathbf{f}(\dots, t_n)) \\ \mathbf{g}(\dots, t_{n+1}) \end{bmatrix} \quad (6.25)$$

### 6.3.4 Expanded Matrices from Additional Control

Additional control mechanisms developed and presented in this work need to be implemented into the simulation program. The additional control paths can be represented in a state-space description and therefore they can be represented as a system of first order differential equations.

$$\begin{aligned} \dot{\mathbf{z}} &= \mathbf{A}_S \cdot \mathbf{z} + \mathbf{B}_S \cdot \mathbf{u} \\ \mathbf{y} &= \mathbf{C}_S \cdot \mathbf{z} + \mathbf{D}_S \cdot \mathbf{u} \end{aligned} \quad (6.26)$$

Adding the differential equations of this system to the simulation, results in an expansion of the system's states vector  $\mathbf{x}$ , the system's Jacobian matrix  $\mathbf{J}(\mathbf{x})$  and the mismatch function vector  $\mathbf{F}(\mathbf{x})$ . The new states from the additional control are described by a vector  $\mathbf{z}$ . The matrix  $\mathbf{A}_S$  is the state matrix of the added controls, the matrix  $\mathbf{B}_S$  represents the input matrix to the new state equations and

the matrix  $\mathbf{C}_s$  represents the output of the added equations to the basic system. The matrix  $\mathbf{D}_s$  is in our case zero and therefore not further considered. The input vector  $\mathbf{u}$  of the state-space system consists of all states and the expanded state vector  $\mathbf{x}_e$  is defined as:

$$\mathbf{x}_e = \begin{bmatrix} \mathbf{x}^T & \mathbf{z}^T \end{bmatrix}^T \quad (6.27)$$

With the three supplemental matrices  $\mathbf{A}_s$ ,  $\mathbf{B}_s$  and  $\mathbf{C}_s$ , the Jacobian matrix can be extended as follows:

$$\mathbf{J}(\mathbf{x}, \mathbf{z}) = \begin{bmatrix} \mathbf{J}(\mathbf{x}) & \frac{\Delta t}{2} \cdot \mathbf{C}_s \\ \frac{\Delta t}{2} \cdot \mathbf{B}_s & \frac{\Delta t}{2} \cdot \mathbf{A}_s - \mathbf{I} \end{bmatrix} \quad (6.28)$$

The Jacobian of the basic system is not modified through the additional control. The terms  $\frac{\Delta t}{2}$  and  $-\mathbf{I}$  arise from the trapezoidal rule implementation for differential equations (Section 6.1).

The mismatch function vector  $\mathbf{F}(\mathbf{x})$  is expanded as well.

$$\mathbf{F}(\mathbf{x}, \mathbf{z}) = \begin{bmatrix} \mathbf{F}(\mathbf{x}) + \frac{\Delta t}{2} \cdot \mathbf{C}_s \cdot (\mathbf{z}(t_{n+1})^\nu + \mathbf{z}(t_n)) \\ \mathbf{z}(t_n) - \mathbf{z}(t_{n+1})^\nu + \frac{\Delta t}{2} \cdot (\mathbf{B}_s \cdot (\mathbf{x}(t_{n+1})^\nu + \mathbf{x}(t_n)) + \mathbf{A}_s \cdot (\mathbf{z}(t_{n+1})^\nu + \mathbf{z}(t_n))) \end{bmatrix} \quad (6.29)$$

These three expansions allow the simulation of the new system.



## 7 Discussion and Results

In this chapter results of the thesis are summarized and brought together to allow an overall discussion of the performed work. A closer look is taken on the most promising results from single and multiple bus control design of the previous chapters in order to expose overall benefits as well as drawbacks.

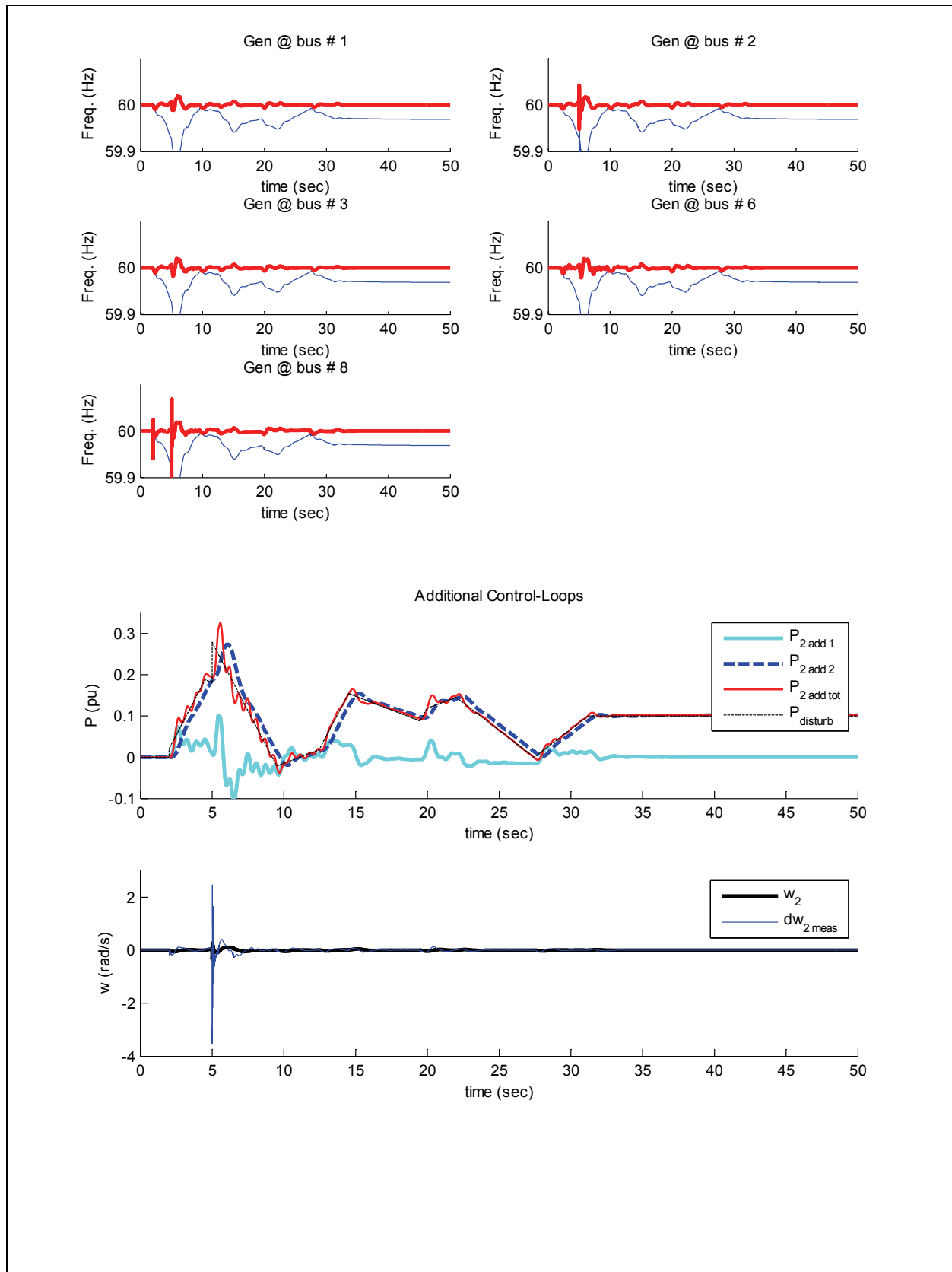
### 7.1 Simulation of Master Controller

Simulation results from the sequential designed controller case are given in the table below for a more realistic disturbance scenario. The results are a combination of step and triangle-wave simulations succeeding Section 4.3.

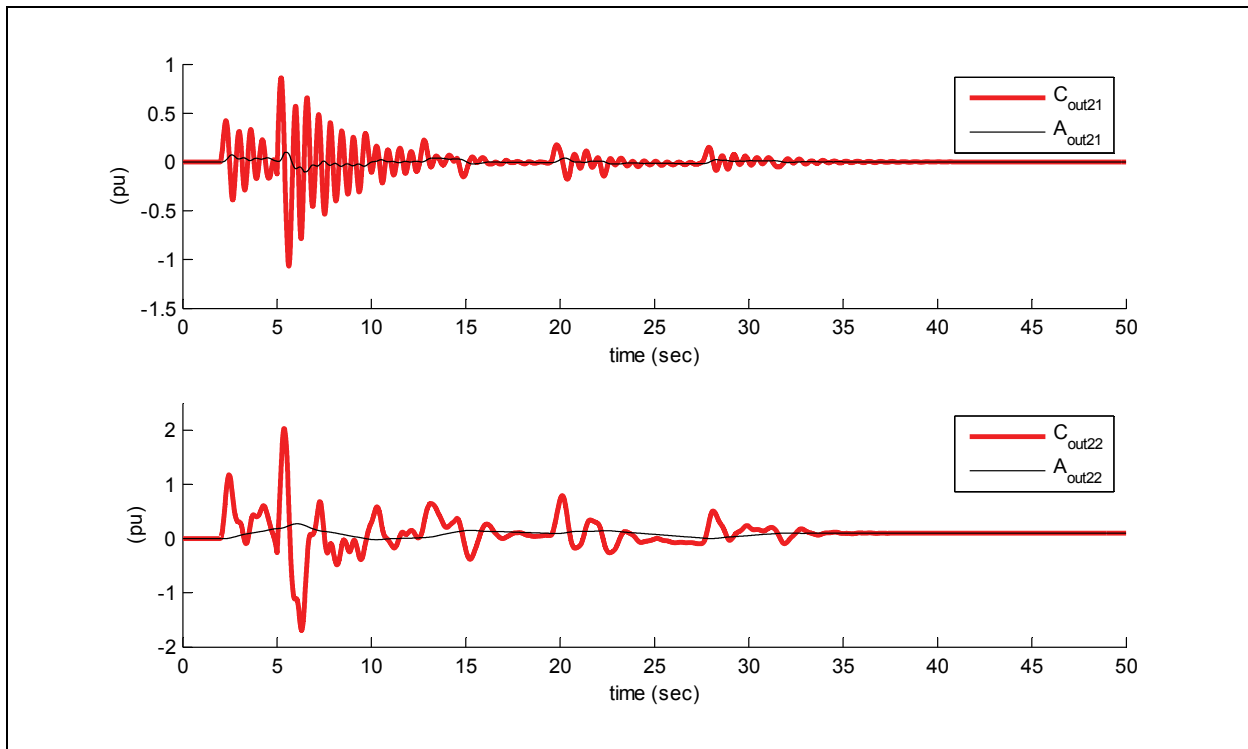
#### Simulation Results – Master controller (designed sequentially)

##### Simulation

- Based on standard system configuration (Chapter 3.1.3)
- Additional power path at bus 2
  - Measurement:  $\tau = 0.1\text{s}$
  - Power branch 1:
    - Actuator 1:  $\tau_1 = \tau_2 = 0.5\text{s}$
    - Controller 1:  $\omega_{n1} = 5$
    - Limit 1: 0.1pu
  - Power branch 2:
    - Actuator 2:  $\tau_1 = \tau_2 = 2\text{s}$
    - Controller 2:  $\omega_{n2} = 2$
- Excitation:
  - 0.05pu step disturbance at buses 2 and 8 at  $t=5\text{s}$
  - 0.2pu p-p triangle-wave disturbances at buses 2 and 8 (phase shifted to each other and with little initial step at bus 8)







### Results

- The designed Master controller shows a much better performance in terms of frequency deviation compared to a PI filter controlled simulation serving as reference scenario.
- From the frequency plots one can see that the maximum frequency deviation for ramp disturbances is below 0.1pu. But as soon as a step disturbance occurs, the frequency deviations increase. Step disturbances also result in high frequent spikes as can be seen at  $t=5s$  and  $t=2s$  at buses 2 and 8.
- From the power-contributions plot it can be seen that the faster controller compensates for the severe disturbances while the slower second controller compensates for the broad deviations. The different speed of reaction of the two control branches can be seen from the fact that only controller 1 reacts on fast changing disturbances. In general controller 1 tries to react whenever controller 2 is not able to provide the exact power.
- The controller output plots show that the controllers compensate for slower actuator systems.

Table 7-1: Simulation Results – Master controller (designed sequentially)

## 7.2 Discussion of Master Controller

Following to the results of Chapter 4, where mimicking inertia, advanced frequency control and control design was the focus, this section presents and summarizes final results. As a reference scenario, a PI filtered case is taken.

A system with more than one additional power source has several advantages compared to an additional control loop with just one power source. Advantages are:

- Redundancy: Control can come from different systems
- Different Characteristics of the power/energy sources can be summed up to a good overall characteristic with a broad bandwidth.
- Faster reaction, if saturation can be handled and fastest system does not remain in saturation.

As a result the considered additional control system consists of more than 1 additional power branch.

Three different design methods have been studied in Chapter 4. The method with the best performance and with the best possibility to handle the saturation problematic is found to be the sequential designed controller method. Results of this method and general points that have been faced throughout the simulations are listed hereafter.

- Performance:  
The performance of the control design method was measured through the frequency deviations observed in the system after a triangle-wave disturbance. The sequential design method showed a very low maximum frequency deviation and therefore a very good performance compared to the other design methods. Having a closer look at the signal, one can see that only some peaks have deviations of amplitude as in the other cases. The rest of the signal, the mean value, is in a very narrow bandwidth around the reference frequency. In comparison to PI control filter, the improvement in maximum frequency deviations is up to a factor 5.
- Actuator Characteristics:  
So far, in all our simulations, the actuator systems are modeled as 2<sup>nd</sup> order filters. Simulations showed that characteristics of these actuators are compensated through the controllers. The controller increases the output signal to compensate for a slower actuator characteristic. The question is if this behavior is allowed in practice. A possible way to answer this question is to look at more detailed actuator models and to check with these models if the controller still compensates for the ac-

tuator characteristics. It is somehow intuitive that actuator systems also have a limit on their input signal and therefore the controller output signal reaches a saturation level, too.

What could be considered in addition is that actuators have a fixed rate of power increase or decrease. This would mean that the controller could not compensate for the actuator characteristics, because an increased controller output would result in the same rate of increase as a lower. But again, such a limit would be a nonlinearity in the system and could not be represented by a transfer function.

In the case of sequential designed controllers different reaction times of control branches can be set satisfactorily by selecting different controller parameters  $\omega_n$ . Then the output power signals of the actuators show different reaction times and the physical characteristics of the actuator are represented more adequately.

- Saturation Issue:

With the design of the faster control system first and then developing the slower controller on top of the 1<sup>st</sup> controller, the contribution levels of the two control branches can be set. Adding hard output power limits to the actuator outputs has shown some difficulties in simulations. For a convergence of the simulation the output could not be limited to a too low value. A limit, where the simulation still converged was found to be at the mean value of the added power. If the limit is set too low, the controller, with its integral behavior, increases the controller output signal more and more in order to compensate for the missing power and finally the simulation does not converge anymore.

Another aspect is that our controller is designed to completely compensate for an error signal; that could be problematic, if too severe disturbances had to be compensated and the additional power could not be provided at the control bus.

Overall, a sequential controller design at a single bus, the so called Master controller, showed that a very good performance can be achieved in terms of inertia-like and frequency control. If the results of the higher-order controller design method are compared to the case with a standard PI controller, the improvements in performance, as speed of reaction or maximum frequency deviations are significant. In numbers, the maximal frequency deviations are reduced by a factor 5. Further on the modern control design allowed to access the question of saturation and bandwidth of controller actuators, so that the controllers are designed to meet these saturation limits in a satisfactory way.

### 7.3 Master Controller with Additional PD Controllers

The good performance of the Master controller was extensively described in chapters 4 and 5. Based on the Master controller design, that has shown best performance if installed on Bus 2, multiple additional distributed PD controllers showed still an improvement in overall performance and stability.

In this chapter we want to take a closer look and want to point out the advantages as well as the disadvantages of distributed PD controllers in presence of the Master controller.

#### 7.3.1 Simulation Scenario

As introduced in Chapter 5.2.2, in order to mimic a rather realistic as well as extreme scenario, a situation is developed where on both buses 2 and 8, the system is excited by two triangle-waves with different gradients as power input signals. Further on, an initial step change prior to the triangle-wave input characteristic on Bus 2 was introduced in order to emulate a more severe disturbance.

#### System Configuration

- Based on standard system configuration (Chapter 3.1.3)
- Master controller at bus 2 (configuration of Chapter 4.3.2)
- PD controller at buses 2 and 8
  - $k_p = 120$ ,  $k_D = 6$
  - PD filter:  $\tau = 0.005\text{ s}$
  - Actuator:  $\tau = 0.003\text{ s}$
- Excitation: ramp-change scenario

Table 7-2: System Configuration

This excitation case refers exactly to the ramp-change scenario described in Chapter 5.2.4.

#### 7.3.2 Results and Discussion

Based on the simulation scenario described above, we want to show and discuss the performance of the Master controller with additional distributed PD controllers in detail.

- It can be seen that the overall performance applying this ramp scenario can be improved by looking at the different peak-values and comparing the performance of the Master controller with and without PD control in Figure 7-1.

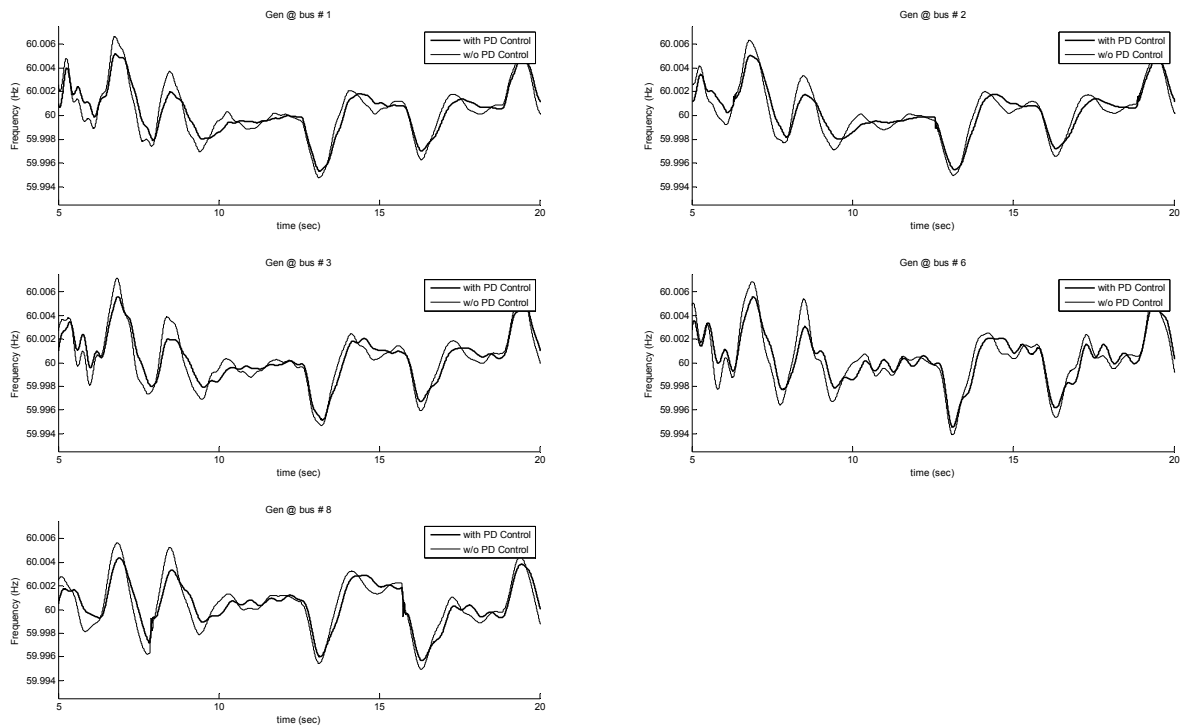


Figure 7-1: Overall benefit of PD controllers

- Further on a PD controller reduces resp. smoothes local oscillations originating from the abrupt changes of the triangle-wave. This can be seen by looking at bus 8 where a PD controller is locally installed. Figure 7-2 shows this benefit.

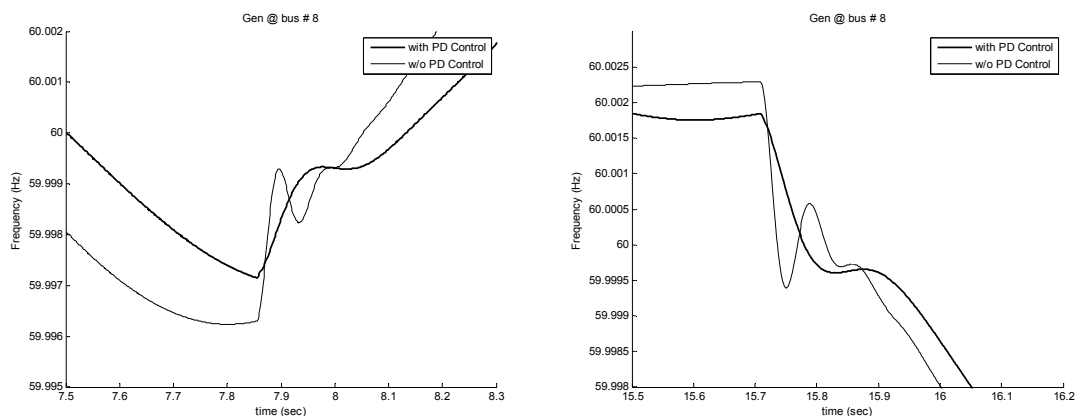


Figure 7-2: PD control damps local oscillations

- The performance can be significantly improved by applying a step change (here: on bus 2) as depicted in Figure 7-3. Keeping in mind that the Master controller is optimized in terms of a ramp change that may not be surprising. However, the applied step changes are chosen to be rather realistic and so it can be shown that PD controllers can improve the robustness of the control design.

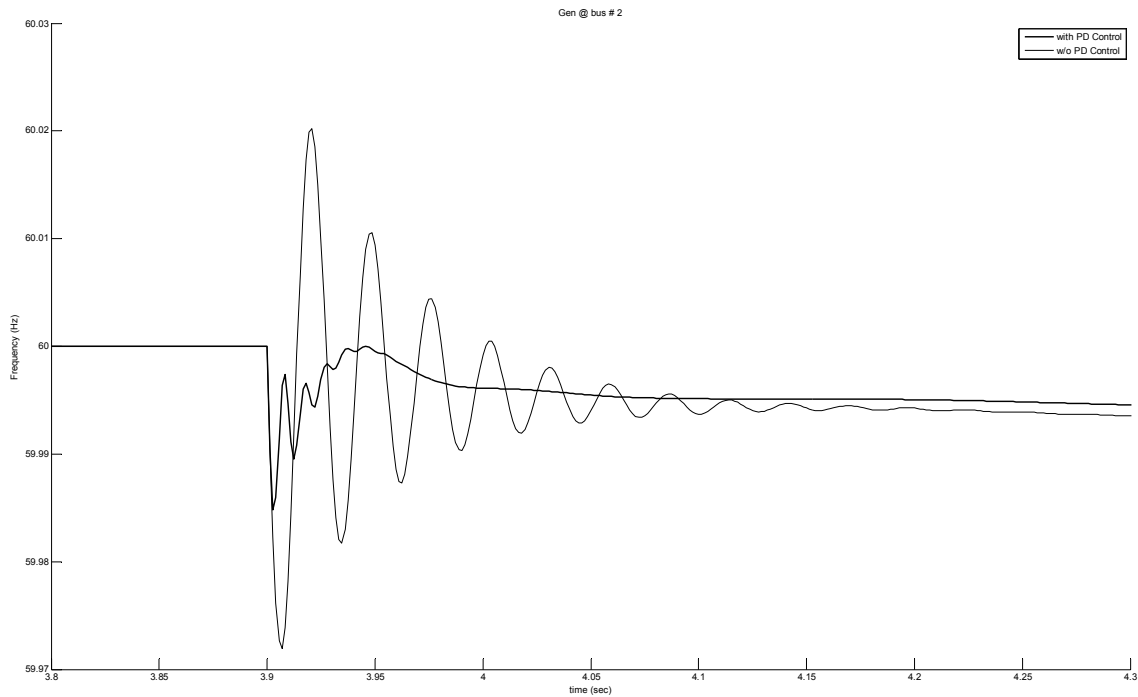


Figure 7-3: PD control shows improved behavior on a step change

*More extreme step changes are not analyzed in this work assuming that such disturbances are treated in practice by additional "emergency" control loops and are consequently not topic of this work.*

- The performance is limited due to the degree of interaction, adjusted by the PD-values in particular the proportional gain. One can observe higher oscillations on bus 6, for instance, as shown in Figure 7-4. These stronger oscillations are likely to come from the interaction of the controllers as well as from the inertia of the synchronous generator. Due to the fact that there is no local control on bus 6, the extent of these oscillations has to be kept in mind. Increasing the PD-gain would result in instability as described in Chapter 5.

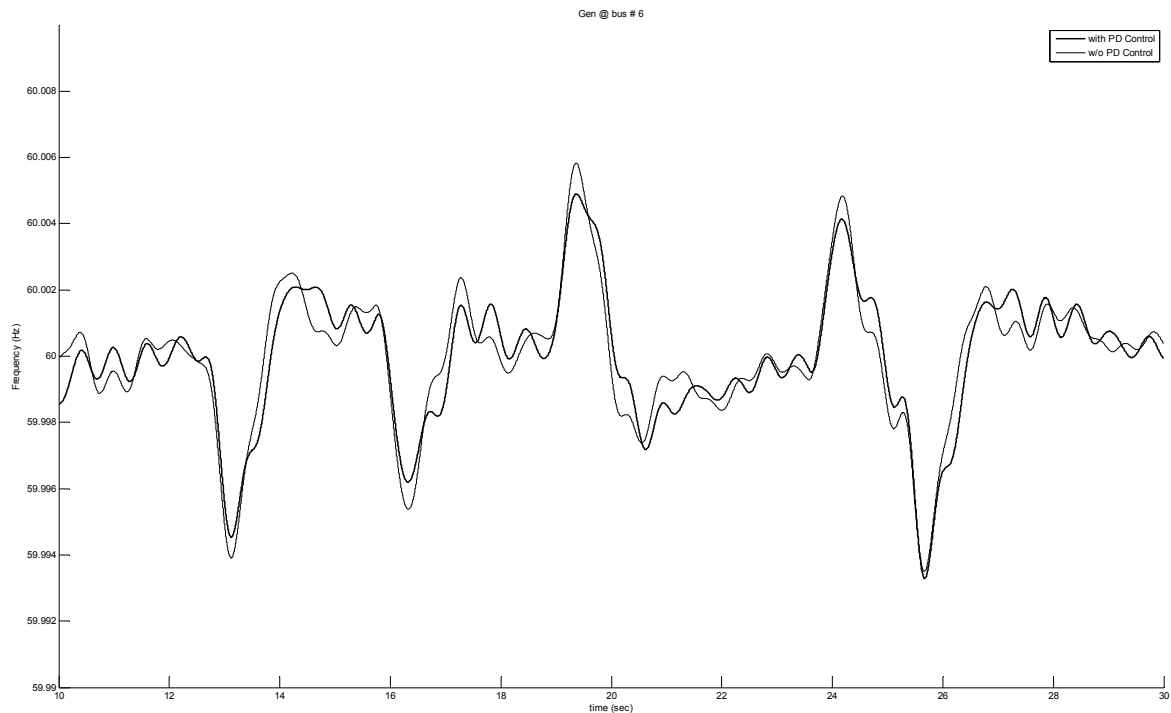


Figure 7-4: Higher oscillations at buses with no control

- Overall stability can be improved as shown by the eigenvalue analysis in Chapter 5.5. A trade-off exists between performance and stability.
- PD controllers are applicable on multiple buses and do not show undesirable destabilizing behavior if adjusted with adequate PD-values. Implementing PD control on a load bus is possible but does not show any control contribution unless the disturbance appears on the same bus.
- Grid impedance has a considerable influence to the control behavior by limiting control reaction times. The location of the Master controller is therefore a crucial consideration (Chapter 5) and also the fact that PD controllers show particular control support if installed locally is explained hereby.

In general, the benefits of additional distributed PD controllers can be clearly shown. However, one has to keep in mind that using other test bed systems resp. network layouts might lead to certain readjustments and may change findings and conclusions of this Master-Slave concept.





## 8 Conclusions and Outlook

### 8.1 Conclusions

The aim of this project is to show that inverter-connected renewable energy sources have the ability to contribute to frequency control and stability enhancement in power systems. To simulate effects of controlled RES, a test system is evaluated and judged to meet the requirements of our work. All results and findings, presented in this thesis, are based on this test system.

First the focus is set on a single generator bus. With modern control theory an additional control path is developed that shows promising results. Additional power is provided for the control tasks by internal and/or external power sources. Different actuator characteristics such as bandwidth and saturation limits are successfully considered in the control design. Compared to standard control filters, the new control design shows an improvement by a factor of up to 5.

The concept of Master and Slave controllers is introduced later on to further improve the performance. Designing the Master controller with the developed sequential design method and using PD controllers as Slave controllers appears to be a very promising design approach. By implementing additional Slave controllers on multiple buses, supporting the control action of the single and centralized Master controller, shows significant improvements in our simulations. Especially in the case of more severe disturbances, imitated by step changes, the frequency deviation can be significantly limited by the control support of the distributed PD controllers.

Locating the Master controller turns out to be an important consideration. The overall system control performance varies as a function of the bus location of the Master controller. Another aspect is to consider saturation limits in the control design. The Master controller is designed to fully compensate frequency errors, so if a too severe disturbance takes place, the amount of required additional power will simply become too large. This problem could be addressed by splitting up the physical control action to different generation buses but keeping the computation on the Master bus. This concept is comparable to the AGC concept used in today's power systems, but requires fast communication between generator buses.

With the described control sharing, the Master-Slave control concept seems very applicable to modern power systems considering the increasing penetration of inverter connected RES in the future. Ade-

quate frequency control and stability enhancement is possible by our concept of additional control path (also enables mimicking of inertia) for inverter-connected RES.

Concluding, we believe the project shows a promising outcome that can be used for further studies and can help solving the issues that arise with integrating renewable energy sources into the grid. And last but not least we hope this work can satisfy one of our initial motivations, namely making a contribution to a more efficient and sustainable use of energy in the future.

## 8.2 Outlook

At the end of the project we want to give suggestions how this project can be continued and what aspects may need to be investigated further on.

Results elaborated in this thesis are all based on the same test system and simulation program. To affirm results, simulations for larger and differently configured test systems should be performed. The used program MATLAB is definitely a widely spread software in research and industry, but especially for industrial applications there are other software tools that should be considered too. A well known program used intensively in industry is PSS/E<sup>TM</sup> that allows for instance dynamic simulations of very large power systems. It should be a next step to implement and affirm the functionality of our developed control concepts in PSS/E<sup>TM</sup>.

Frequency control requires additional power for the control actions either coming from internal or external sources. Adding external power storage systems may involve huge investment costs and from an economical point of view costs are one of the crucial factors whether installing a system or not. Using internal sources means changing the power-set point of generation systems what results in lower profits. Economic aspects are not considered in this thesis and they are one of the points that need to be addressed further on, particularly if it comes to a real implementation of these control concepts.

If further simulations affirm the obtained results, we believe that in prospective power systems control concepts applying this approach for inverter-connected RES, in particular wind power, should be considered. The share of renewable energy sources will increase rapidly in the upcoming years and the need of new concepts to control frequency and enhance stability of power systems is evident.

## Appendix

### A. Further Aspects

#### A.1. Standard Control Modeling

In order to understand the functionality of the MATLAB simulation program, standard classical frequency control has been modeled and implemented on synchronous generators in the system.

##### A.1.1. Primary Frequency Control

Primary frequency control has been described in Chapter 2. In the simulation, primary frequency control is performed by the three synchronous generators in the system. Each of these generators has a specified droop constant and a defined activation level, where droop control is activated. Between the droop control output and the physical power output change filtering occurs. This filtering represents the dynamics of the turbine system. These turbine systems are implemented and modeled by the following transfer function characteristics.

$$G_T(s) = F_{HP} + (F_{IP} + F_{LP}) \cdot \frac{1}{s \cdot \tau_{RH} + 1} \quad (9.1)$$

This transfer function represents a simplified TF of a tandem compound, single reheat steam turbine [25]. The block diagram of the implemented primary frequency control at generator buses 3 or 6 is shown below.

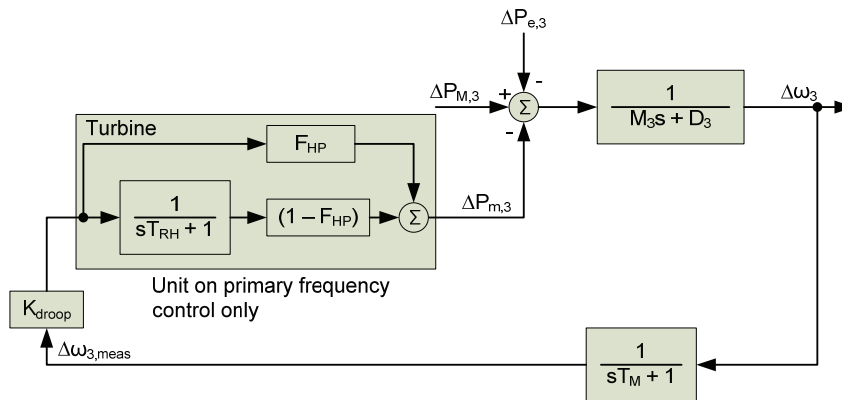


Figure A-1: Implemented primary freq. control at generator bus 3

### A.1.2. Secondary Frequency Control

In order to bring the system frequency back to the equilibrium value (e.g. 60Hz in the U.S. system) an additional controller has to be implemented in the system. Usually an integral controller is implemented through AGC, or secondary frequency control, with only selected generators participating. In our test system, generator 1 is selected for secondary frequency control. In addition to the defined droop control at generator 1, an integral controller is added.

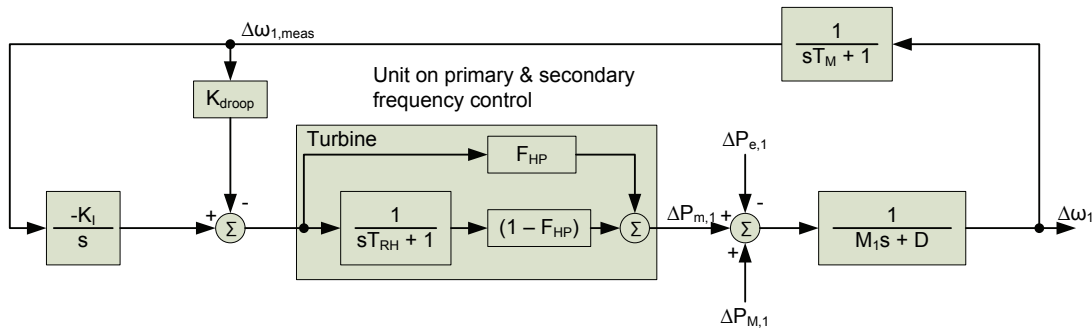


Figure A-2: Implemented primary and secondary freq. control at generator bus 1

### A.1.3. Results

The implementation of primary and secondary frequency control showed the expected behavior of the simulated power system. If only primary frequency control was activated, a steady-state frequency deviation was observed. With the addition of the secondary frequency controller at generator bus 1, the frequency could be brought back to its reference value of 60Hz. These results showed that the simulation tool is working as expected and therefore provides a suitable base case to which control loops may be added in our attempt to improve frequency regulation and system stability.

## A.2. Order of Controller

It was mentioned in Chapter 4 that the order of controller could be reduced, if the controller calculation is slightly changed and the actuator TF is not considered to the expanded system TF  $G(s)$ . Additionally to these findings, a calculation comparison between the two methods is shown here:

New calculation	Old calculation
$G(s) = G_0(s) \cdot M(s) \cdot s = G_M(s)$ $Q(s) = G(s)^{-1} \cdot H(s)$ $C(s) = \frac{Q(s)}{A_1(s) \cdot (1 - Q(s) \cdot G(s))}$	$G(s) = A_1(s) \cdot G_0(s) \cdot M(s) \cdot s = A_1(s) \cdot G_M(s)$ $Q(s) = G(s)^{-1} \cdot H(s)$ $C(s) = \frac{Q(s)}{1 - Q(s) \cdot G(s)}$
$= \frac{G_M(s)^{-1} \cdot H(s)}{A_1(s) \cdot (1 - \cancel{G_M(s)^{-1}} \cdot H(s) \cdot \cancel{G_M(s)})}$ $= \frac{H(s)}{A_1(s) \cdot G_M(s) \cdot (1 - H(s))}$	$= \frac{(A_1(s) \cdot G_M(s))^{-1} \cdot H(s)}{1 - (\cancel{A_1(s) \cdot G_M(s)})^{-1} \cdot H(s) \cdot (\cancel{A_1(s) \cdot G_M(s)})}$ $= \frac{H(s)}{A_1(s) \cdot G_M(s) \cdot (1 - H(s))}$

Table A-1: Comparison between controller calculations

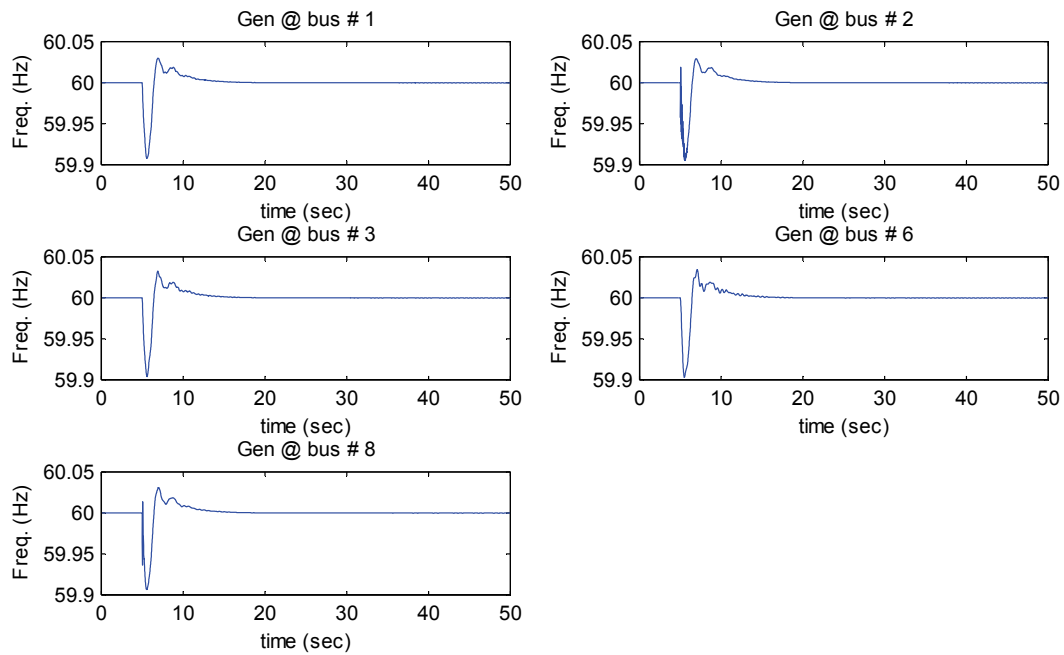
### A.3. Results of Modified MIMO Design Procedure

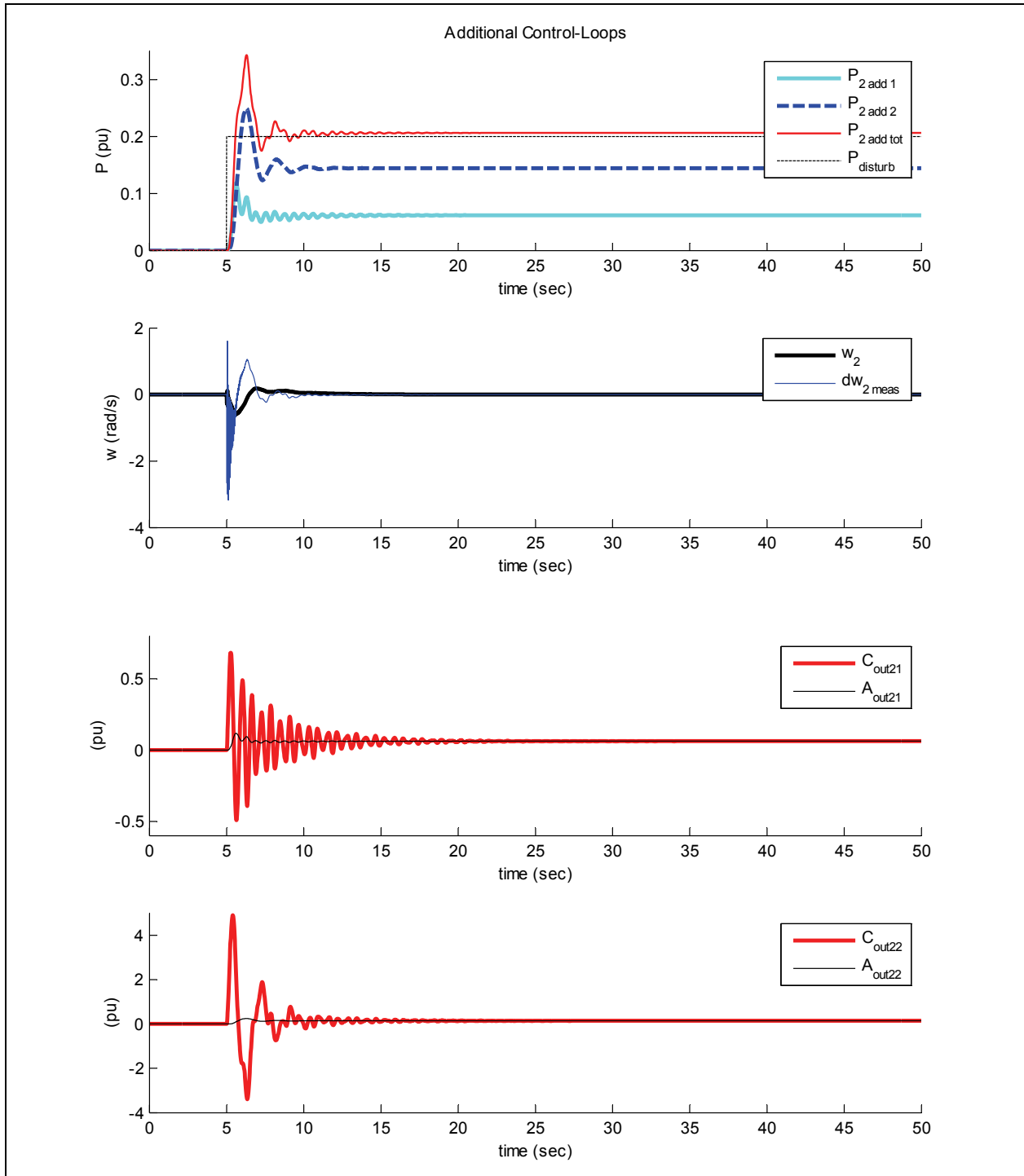
Results of the modified MIMO design, not shown in Chapter 4, are shown hereafter.

#### Simulation Results – Controllers designed on modified MIMO-based method

##### Simulation 1

- Based on standard system configuration (Chapter 3.1.3)
- Additional power path at bus 2
  - Measurement:  $\tau = 0.1\text{s}$
  - Power branch 1:
    - Actuator 1:  $\tau_1 = \tau_2 = 0.5\text{s}$
    - Controller 1:  $\omega_{n1} = 4.5$
  - Power branch 2:
    - Actuator 2:  $\tau_1 = \tau_2 = 2\text{s}$
    - Controller 2:  $\omega_{n2} = 2$
  - MIMO factors: 0.3/0.7
- Excitation scenario 1: 0.2pu step disturbance at load bus 4



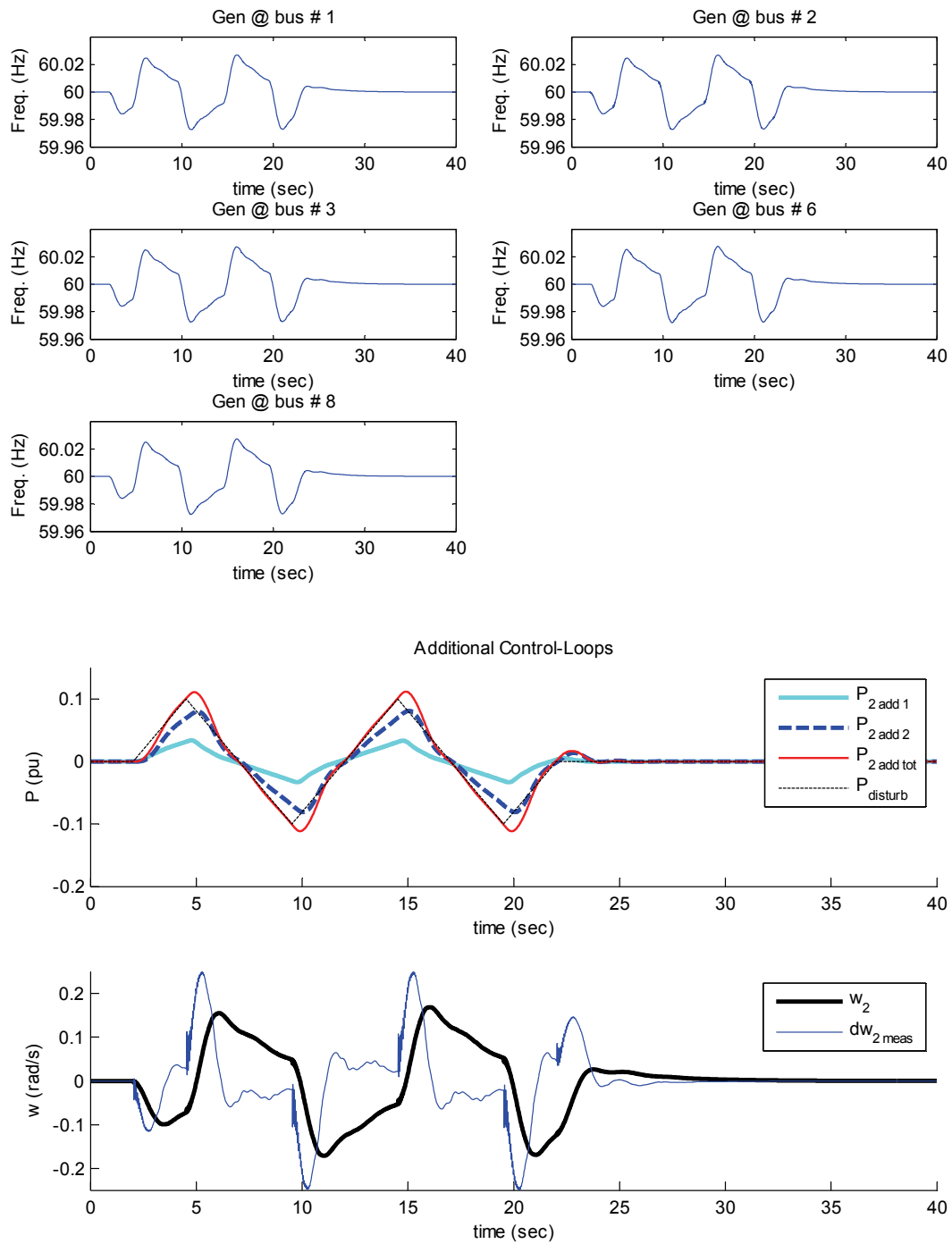


### Results

- The simulated frequency deviations are higher than in the other MIMO case.
- The different reaction speeds of the two actuator systems can now be seen in the power contribution plot.
- As seen from the power contributions, the sharing of control action can be accurately adjusted by the selection of the MIMO-factors (30% to 70%).

**Simulation 2**

- Based on standard system configuration (Chapter 3.1.3)
- Same additional configuration as in simulation 1
- Excitation scenario 2: 0.2pu p-p triangle-wave disturbance at generator bus 2





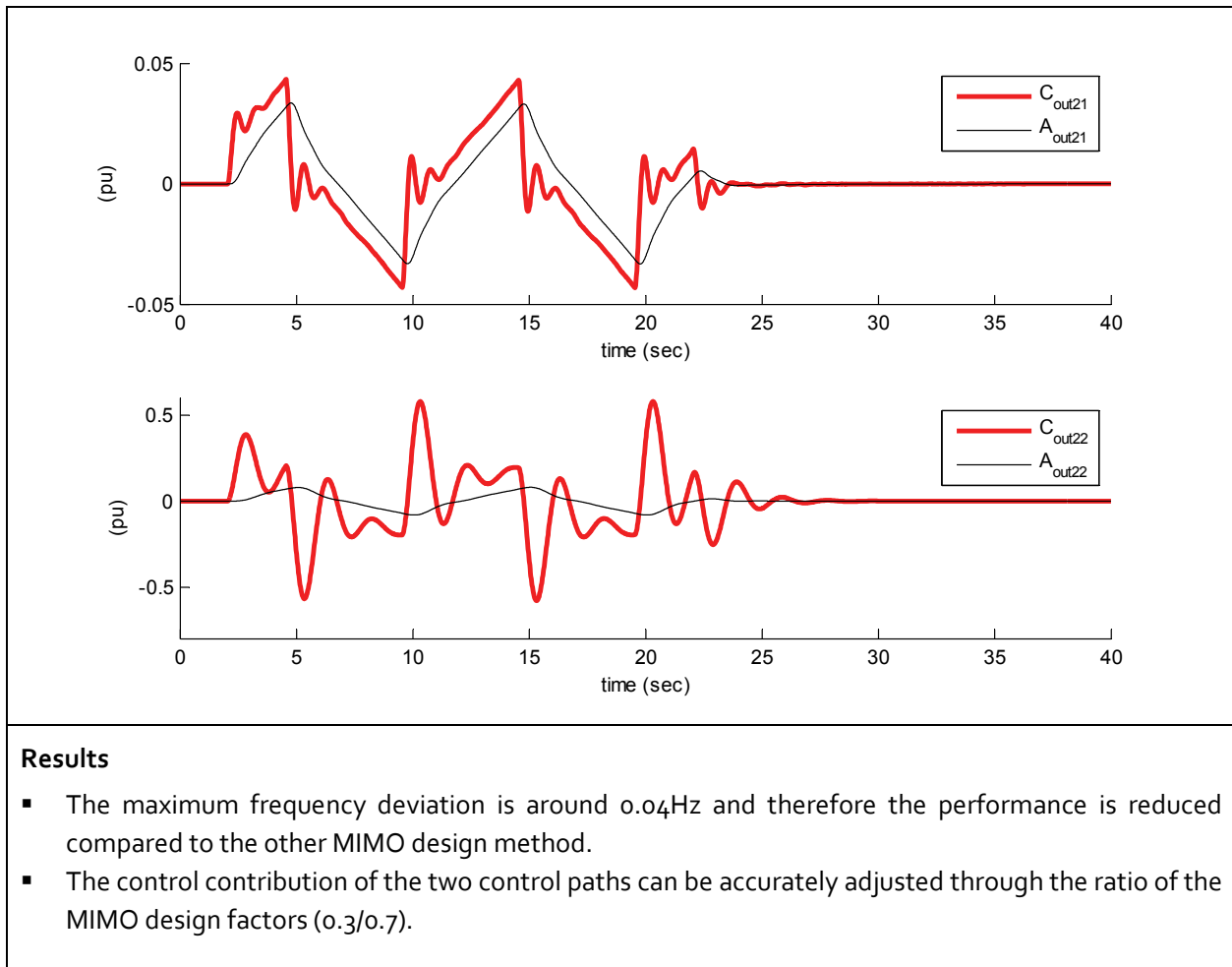


Table A-2: Simulation Results – Controllers designed on modified MIMO-based method

## A.4. SAFT Capacitance Battery Model

### A.4.1. State-Space Representation of Battery Model

The following equation describes the state-space model of the single SAFT battery model.

$$\begin{bmatrix} \dot{V}_{Cb} \\ \dot{V}_{Cc} \end{bmatrix} = \begin{bmatrix} -\frac{(R_e + R)}{C_b \cdot (R_e \cdot R_c + R \cdot (R_e + R_c))} & \frac{R}{C_b \cdot (R_e \cdot R_c + R \cdot (R_e + R_c))} \\ \frac{R}{C_c \cdot (R_e \cdot R_c + R \cdot (R_e + R_c))} & -\frac{(R_e + R)}{C_c \cdot (R_e \cdot R_c + R \cdot (R_e + R_c))} \end{bmatrix} \begin{bmatrix} V_{Cb} \\ V_{Cc} \end{bmatrix} + \begin{bmatrix} \frac{R_e}{C_b \cdot (R_e \cdot R_c + R \cdot (R_e + R_c))} \\ \frac{R_e}{C_c \cdot (R_e \cdot R_c + R \cdot (R_e + R_c))} \end{bmatrix} \cdot [V_{0,ref} - u_{act}]$$

$$[i_0] = \begin{bmatrix} \frac{R_e}{R_e \cdot R_c + R \cdot (R_e + R_c)} & \frac{R_e}{R_e \cdot R_c + R \cdot (R_e + R_c)} \end{bmatrix} \begin{bmatrix} V_{Cb} \\ V_{Cc} \end{bmatrix} + \left[ -\frac{(R_e + R)}{R_e \cdot R_c + R \cdot (R_e + R_c)} \right] \cdot [V_{0,ref} - u_{act}]$$

### A.4.2. 2 Batteries in Series

The addition of two batteries in series is according to the figure hereafter.

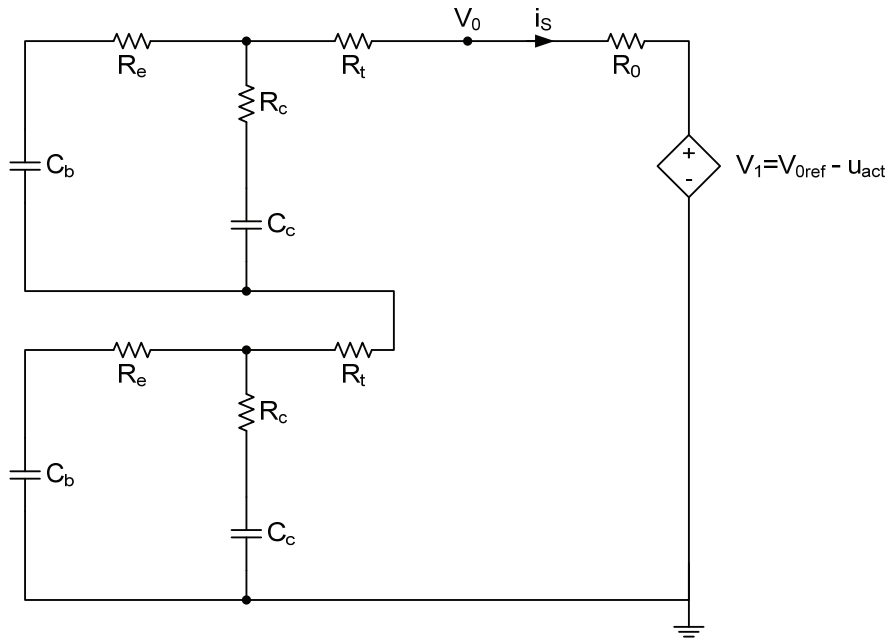


Figure A-3: Diagram of 2 SAFT batteries in series

### A.4.3. 2 Batteries in Parallel

The diagram of two batteries in parallel is according to the figure below:

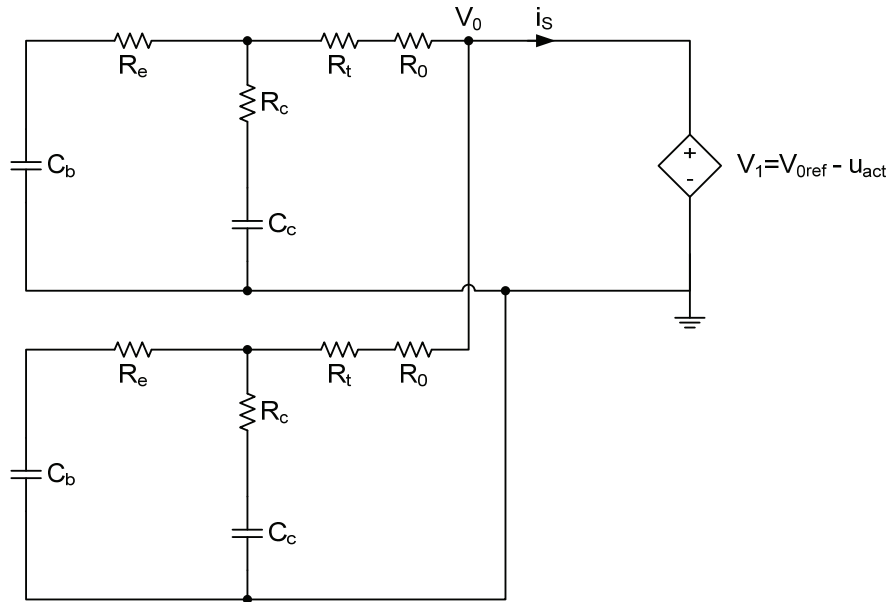


Figure A-4: Diagram of 2 SAFT batteries in parallel

### A.4.4. Stacked Batteries in Series and Parallel

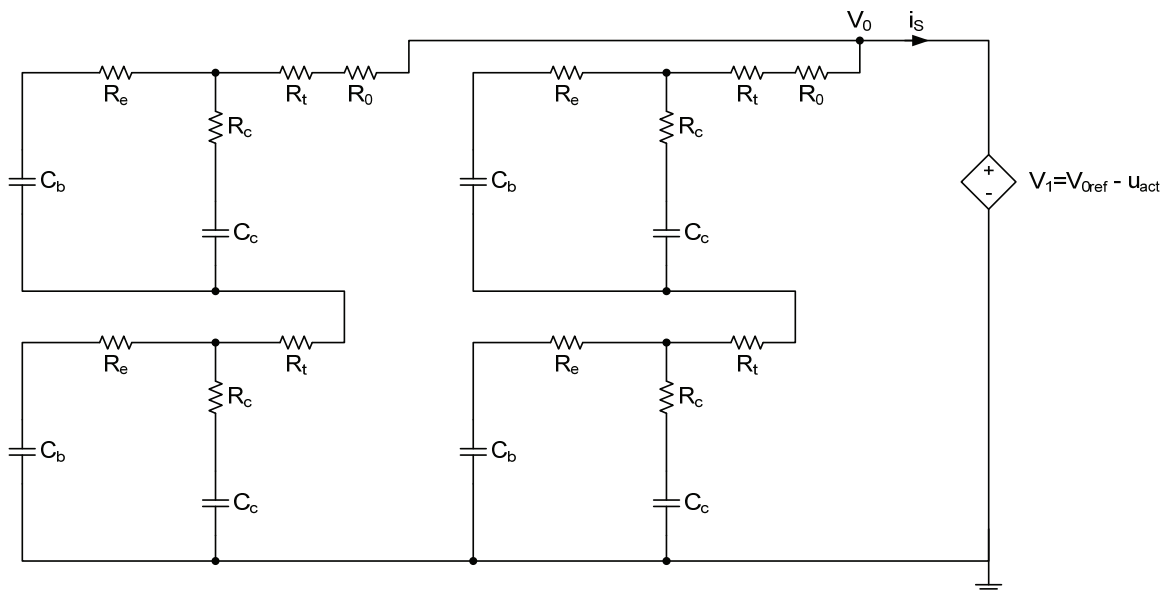


Figure A-5: Diagram of battery stack

## B. Analysis Methods and Calculations

### B.1. Eigenvalues

#### B.1.1. Expanded System State Matrix

To calculate eigenvalues and eigenvectors of the system, the system state matrix  $\mathbf{A}$  has to be known. In the iteration routine of our MATLAB programs, a system Jacobian matrix is calculated. Based on this Jacobian Matrix, the system performs then the transient simulations. Because the Jacobian Matrix is already known, the system state matrix  $\mathbf{A}$  can be gained directly from this Jacobian matrix.

In the program routine, the Jacobian matrix was built using the trapezoidal rule. The matrix contains differential and algebraic equations.

$$\mathbf{J}(\mathbf{x}_f, \mathbf{x}_g) = \begin{bmatrix} \frac{\Delta t}{2} \cdot \frac{\partial \mathbf{f}}{\partial \mathbf{x}_f} - \mathbf{I} & \frac{\Delta t}{2} \cdot \frac{\partial \mathbf{f}}{\partial \mathbf{x}_g} \\ \frac{\partial \mathbf{g}}{\partial \mathbf{x}_f} & \frac{\partial \mathbf{g}}{\partial \mathbf{x}_g} \end{bmatrix} \quad (9.2)$$

As explained earlier, the differential equations are solved using the trapezoidal rule. To gain the system matrix  $\mathbf{A}$ , the trapezoidal rule has to be undone. This can be done by simply adding an identity matrix to the differential equation terms and multiplying the differential equation part by  $2/\Delta t$ .

The resulting matrix represents then the basic power system state matrix without the additional control. The additional control can be added by expanding the state matrix  $\mathbf{A}_0$  with the matrices from the additional control.

$$\mathbf{A} = \begin{bmatrix} \mathbf{A}_0 & \mathbf{C}_s \\ \mathbf{B}_s & \mathbf{A}_s \end{bmatrix} \quad (9.3)$$

With this state matrix, the eigenvalues and eigenvectors can be calculated. The only thing that should be kept in mind, is that the matrix still contains algebraic equations.

### B.1.2. Eigenvalue Analysis for Parameter Sensitivity

As the number of parameters in our simulation system grows, it would be nice to have a quantitative number of how large the impact of each of these parameters on the overall system is. Our system can be linearized and be represented with a state matrix  $\mathbf{A}$  representing the full nonlinear model.

$$\Delta \dot{\mathbf{x}} = \mathbf{A}(\boldsymbol{\gamma}) \cdot \Delta \mathbf{x} \quad (9.4)$$

This state matrix is then dependent on many different parameters  $\gamma_i$ . Possible parameters are for example inertia constants of generators, constants from additional control paths or parameters from other sources. If only a few parameters are given, one can, by trial and error, easily find out which parameters have the strongest impact on the system. But with an increasing number this evaluation needs a large effort. Therefore a methodology is used to quantify the impact of system parameters in an automated way.

With an eigenvalue-analysis the influence of a large number of parameters can be assessed. In a first step eigenvectors  $\mathbf{V}_i$  and eigenvalues  $\lambda_i$  of the system state matrix  $\mathbf{A}(\boldsymbol{\gamma})$  have to be calculated.

$$[\mathbf{V} \quad \boldsymbol{\Lambda}] = \text{eig}(\mathbf{A}) \quad (9.5)$$

With:

$$\mathbf{V} = [\mathbf{v}_1 \quad \mathbf{v}_2 \quad \dots \quad \mathbf{v}_n]$$

$$\boldsymbol{\Lambda} = \begin{bmatrix} \lambda_1 & 0 & & 0 \\ 0 & \lambda_1 & & 0 \\ & & \ddots & \\ 0 & 0 & & \lambda_n \end{bmatrix} \quad (9.6)$$

The provided eigenvalues are distinct and the matrix of eigenvectors  $\mathbf{V}$  is invertible. Therefore we can take the inverse of the eigenvector matrix  $\mathbf{V}$  and call this inverse  $\mathbf{W}$ .

$$\mathbf{W} = \mathbf{V}^{-1} \quad (9.7)$$

With the  $i^{\text{th}}$  row of that inverse  $\mathbf{w}_i^T$  we can then come up with an equation describing the influence of parameter  $\gamma_j$  on the eigenvalue  $\lambda_i$ .

$$\frac{\partial \lambda_i}{\partial \gamma_j} = \mathbf{w}_i^T \cdot \frac{\partial \mathbf{A}}{\partial \gamma_j} \cdot \mathbf{v}_i \quad (9.8)$$

Writing this equation for all parameters  $\gamma_j$  we come up with an equation in matrix form.

$$\frac{\partial \lambda_i}{\partial \gamma} = \begin{bmatrix} \frac{\partial \lambda_i}{\partial \gamma_1} & \frac{\partial \lambda_i}{\partial \gamma_2} & \dots & \frac{\partial \lambda_i}{\partial \gamma_m} \end{bmatrix} = \mathbf{w}_i^T \cdot \frac{\partial \mathbf{A}}{\partial \gamma} \cdot \mathbf{v}_i \quad (9.9)$$

This equation implies, that for every  $\lambda_i$  a matrix exists. For all  $\lambda_i$ 's we then have a 3-dimensional array, or an array of matrices.

Implementations of the eigenvalue analysis have shown parameter dependences as expected from trial and error experimentation.

## B.2. State Matrix $A_0$ and System TF $G_0$

For the control design developed in this thesis, always a system  $G_0$ , representing the power system, is used. The question may arise, how the system transfer function is built.

Equation (4.15) in Chapter 4.2 describes the standard procedure of how to calculate a transfer function from a state-space representation ( $A_0, B_0, C_0$ ). The matrix  $A_0$  is gained directly from the transient simulation program. Because in the simulation program the Jacobian matrix contains all states (including states from algebraic power flow equations), the matrix is reduced to the desired generator states of the basic system. The reduced matrix is then referred as  $A_0$ .

For an additional control path, the input to the basic system and the output from the system have to be chosen. This is done by selecting appropriate vectors  $B_0$  and  $C_0$ . As example, an additional power path at bus 2 can be considered and the according input and output matrices are then of the form:

$$\begin{aligned} B_0 &= [0 \quad 1 \quad 0 \quad \dots \quad 0]^T \\ C_0 &= [0 \quad 1 \quad 0 \quad \dots \quad 0] \end{aligned} \quad (9.10)$$

And with equation (4.15) one gets then the system transfer function at the considered bus:

$$G_0(s) = C_0^T \cdot (s \cdot I - A_0)^{-1} \cdot B_0 \quad (9.11)$$

## C. MATLAB Program – Lucas Friedrich

### C.1. General Program Description

The MATLAB program starts with the *main.m* file, where the basic system parameters are defined, and where the system further on calls the main-routine (*routine.m*) resp. the control design files (e.g. *getOptCtr.m*). Only initial parts of the simulation code for simulating a basic scenario is shown here.

### C.2. Detailed .m-Files

#### main.m

```
% Main-File for Simulation

%% working history

clc;
clear all;
close all;

%% load data and modify data from original data:

j=sqrt(-1);
setdata;          % reads standard power flow data, constructs network description
                  % in the bus admittance matrix, and the node-to-branch incidence
                  % matrix.

%set power change
snet(8) = -.6;
snet(1) = -.1603 +j*0;          % set power to get system in balance
sneteq = snet;

%inertias
H1=8;          % at genbus 1 (MG)
H2=0.1;        % at genbus 2
H3=8;          % at genbus 3
H4=8;          % at genbus 6
H5=0.1;        % at genbus 8

D=.02*ones(length(genlist)+1,1); % generator rotational damping
M=(1/(pi*60))*[H1;H2;H3;H4;H5];  % generator inertias

%% Executive Control

% Bus Control on Bus Number:
NrBusC=2;
% 1 = refers to omega at bus 1 (MG)
% 2 = refers to omega at bus 2
% 3 = refers to omega at bus 3
% 4 = refers to omega at bus 6
% 5 = refers to omega at bus 8

control1=1;
control2=1;
saturation_on=0;
pd_control=1;

% parameters Master Controller
wn1=5;          % fast control branch
wn2=2;          % slow control branch
```

```

% parameters PD control
kp=120;
kd=6;

limit_fast=0.021;           % set power limits if needed
% limit_fast=0.005;
% limit_slow=0.01;

%definition axis for plotting
magn_diff=0.05;             % for frequency deviatons
p_diff=0.15;                % for power deviations

fault_type = 1;             % select the type of fault

fstart = 3.9;               % fault occurs at (sec)
fend = 59.5;                % fault is cleared at (sec)
t_end = 30;                 % simulation time (sec)

delttime=.0166666/12;       % 1 time step = 1 cycle at 60 Hz, high resolution sometimes necessary,
                             % depends on magnitude of time constants!
nsteps=round(t_end/delttime);

%% Fault Type

% fault type 1: triangle wave input
if (fault_type == 1)
    snet_save = snet;
end

% fault type 2: line loss of most critical: line 10!
% requirements: system needs to stay stable
if (fault_type == 2)
    ysave=yb;
    line_num=10;
    evenindex=line_num*2;
    oddindex=evenindex-1;
    aa(:,oddindex)=zeros(nbus,1);
    aa(:,evenindex)=zeros(nbus,1);
    yfault=aa*bb*aa';
    %yb=yfault;
end

% fault type 3:
% loss of generation in bus 6 (SynchMach Bus)
if (fault_type == 3)
    delta_P = 0.2;          % amount of lost generation power @ bus 8
    snet_fault = snet;      % define new snet vector during fault
    snet_fault(6) = snet_fault(6)+delta_P;
    snet_save = snet;       % store snet before fault
end

% fault type 4:
% loss of generation in bus 8 (Wind Bus)
if (fault_type == 4)
    delta_P = 0.2;          % amount of load increase @ bus 4
    snet_fault = snet;      % define new snet vector during fault
    snet_fault(8) = snet_fault(8)+delta_P;
    snet_save = snet;       % store snet before fault
end

%% get optimal controller and run routine

getOptCtr;
buildPDContr;
%buildPDContrBat;
routine;

%% display results

```



```

loss=0;
whatplot = zeros(15,1);
whatplot(1) = 0; % frequencies (ref. 60Hz)
whatplot(2) = 0; % plot in- and output of controller 1
whatplot(3) = 0; % plot in- and output of controller 2
whatplot(11)= 0; % power contribution of controller 1 and 2
whatplot(13)= 0; % power contribution with zoom
whatplot(12)= 0; % system's excitation
whatplot(4) = 0; % voltages and angles at buses
whatplot(5) = 0; % power at buses, and bus 2
whatplot(9) = 0; % electrical power at generator buses, each one plot
whatplot(10)= 0; % fed-into-power at generator buses, each one plot
whatplot(6) = 0; % average system frequency
whatplot(7) = 0; % power balance at bus 1
whatplot(8) = 0; % external power from fuel cell, flywheel, etc...
plots;

```

### routine.m

```

% Main-Routine

%% start of program

del=angle(vbus); % extract phase angles from complex vector vbus
xeq=[zeros(5,1);del([1;genlist])]; % construct "natural" 10-dimensional state vector: geerator
freq deviations and % generator phase angles. Note that freq deviation at equi-
librium is forced to zero.

%% routine starts here

ybsave=yb;
vbus = pfsolve(yb,vbus,snet,slacklist,genlist,loadlist);
veq=vbus;
pfout(vbus);

ngen=length(genlist);
nload=length(loadlist);
nnew=length(genlist)+length(slacklist); %plus MasterGenerator at slack bus

%% control filter design

ord_Diff=1;
ord_IN1=2; % specify order of additional control design
ord_C1=ordC1; % specify order of additional control design
ord_IN2=2;
ord_C2=ordC2;
ord_PD1=PDord;
ord_PD2=PDord;
ord_PD3=PDord;

ord=ord_Diff+ord_IN1+ord_IN2+ord_C1+ord_C2+ord_PD1+ord_PD2+ord_PD3; % specify
order of additional control design
ord_x=length(xeq);
ord_diff=ord_x-ord;

if ord_diff<0
    ord_diff=0;
end

Ac=zeros(ord);
Bc=zeros(ord,ord_x);
Cc=zeros(ord_x,ord);
%Dc=zeros(ord,1);

% specify postitions

```

```

indIN1 =1; %virtual inertia delay
indIN1e=indIN1+ord_IN1-1;

indDf=3;

indC1=4;
indC1e=indC1+ord_C1-1;

indIN2=indC1e+1;
indIN2e=indIN2+ord_IN2-1;

indC2=indIN2e+1;
indC2e=indC2+ord_C2-1;

indPD1=indC2e+1;
indPD1e=indPD1+ord_PD1-1;

indPD2=indPD1e+1;
indPD2e=indPD2+ord_PD2-1;

indPD3=indPD2e+1;
indPD3e=indPD3+ord_PD3-1;

%% inertial-like control
% specify in-output relation for B and C Matrices!

if (control1 == 1)

    Ac(indIN1:indIN1e,indIN1:indIN1e)=Ain1;
    Ac(indIN1,indC1:indC1e)=-Ccc; % input of External-Storage-Characteristics-Delay is
negative output of controller with its states as signal
    Ac(indIN1,indDf)=-Dcc*Cdf; % state of Differentiator as signal

    Bc(indIN1,NrBusC)=-Dcc*Ddf; % omega 2 as signal

    Ac(indC1:indC1e,indC1:indC1e)=Acc; % controller state correlation
    Ac(indC1,indDf)=Cdf; % diff state as signal
    Bc(indC1,NrBusC)=Ddf; % omega 2 as signal

    Cc(NrBusC,indIN1:indIN1e)=Cin1; % output of External-Storage-Characteristics-Delay
is power contribution to system!

    Ac(indDf,indDf)=Adf; % diff state correlation
    Bc(indDf,NrBusC)=Bdf; % omega 2 as input for Differentiator

end

if (control2 == 1)

    Ac(indIN2:indIN2e,indIN2:indIN2e)=Ain2;
    Ac(indIN2,indC2:indC2e)=-Ccc2; % input of INertia Delay is negative output of
controller with its states as signal
    Ac(indIN2,indDf)=-Dcc2*Cdf; % state of Differentiator as singal

    Bc(indIN2,NrBusC)=-Dcc2*Ddf; % omega 2 as signal

    Ac(indC2:indC2e,indC2:indC2e)=Acc2; % controller state correlation
    Ac(indC2,indDf)=Cdf; % diff state as signal
    Bc(indC2,NrBusC)=Ddf; % omega 2 as signal

    Cc(NrBusC,indIN2:indIN2e)=Cin2; % output of inertia delay is power contribu-
tion to system!
end

if (pd_control == 1)

    % at Bus 8
    Ac(indPD1:indPD1e,indPD1:indPD1e)=Apd1;
    Bc(indPD1:indPD1e,5)=-Bpd1; % omega as input signal
    Cc(5,indPD1:indPD1e)=Cpd1;

```

```

    % at Bus2
    Ac(indPD2:indPD2e,indPD2:indPD2e)=Apd1;
    Bc(indPD2:indPD2e,2)=-Bpd1;          % omega as input signal
    Cc(2,indPD2:indPD2e)=Cpd1;

%      %at Bus6
%      Ac(indPD3:indPD3e,indPD3:indPD3e)=Apd1;
%      Bc(indPD3:indPD3e,4)=-Bpd1;      % omega as input signal
%      Cc(4,indPD3:indPD3e)=Cpd1;
end

%% define HI
HI = (delttime/2)*[diag(-(D)./(M))-[0;-(D(2:5))./(M(2:5))] zeros(5,4)] diag(-ones(nnew,1)./M); [0
zeros(1,4); -ones(4,1) eye(nngen) 0*eye(nnew)];

%% initialize Variables
omega=0*ones(nngen+nslack,1);
z=zeros(ord,1);          % this vector saves the values of the additional control
states                   % states
vsave=zeros(length(vbus),nsteps); % this vector saves the values bus voltage phasors at
each time step.
omegasave=zeros(nngen+nslack,nsteps); % this vector saves the values generator frequency devia-
tions at each time step.
timesave=zeros(1,nsteps); % this is an array of the time values at each time step
for plotting
zsave=zeros(ord,nsteps); % this vector saves the values of the additional control
states
snetsave=zeros(length(snet),nsteps); % this vector saves the complex loads at each loadbus
ssave = zeros(length(snet),nsteps); % this vector saves the complex powers at each bus

%% Loops...

vbusold=vbus;
del=angle(vbus);
xs=[omega;del([1;genlist]])]-xeq;
xold=xs;
omegaold=omega;
delold=angle(vbusold);

% index2=ngen+1;
index2=ngen+nslack+1; % position 6
% index3=2*ngen;
index3=2*(ngen+nslack); % position 10
index4=index3+1; % position 11
index5=index3+length(loadlist); % position 19
index6=index5+1; % position 20
index7=index5+length(loadlist); % position 28
index8=index7+1; % position 29
index9=index7+ord; % position last state

outer_loop_cnt=0;
loop_continue=1;

%
% The "outer loop" below steps sequentially forward in time
%
while (outer_loop_cnt<nsteps && loop_continue)
    outer_loop_cnt=outer_loop_cnt+1;

    if (fault_type == 1)
        %s_add=0.1*cos((outer_loop_cnt*delttime)/2);
        s_add1=0.1*sawtooth((outer_loop_cnt*delttime)/2,0.5);
        s_add1_save(:,outer_loop_cnt) = s_add1;
        s_add2=0.08*sawtooth((outer_loop_cnt*delttime)/2.5,0.5);
        s_add2_save(:,outer_loop_cnt) = s_add2;
        snet = snet_save;
        if ((outer_loop_cnt+.5)*delttime > fstart && (outer_loop_cnt+.5)*delttime < fend)
            snet(2) = snet(2) + s_add1;

```

```

        snet(8) = snet(8) + s_add2;
    end
end

if (( fstart) <= (outer_loop_cnt+.5)*delttime) && ...
    (( outer_loop_cnt - .5)*delttime < fstart)

    if (fault_type == 2)
        yb=yfault;
    end

    if (fault_type == 3 || fault_type == 4)
        snet = snet_fault;
    end

    disp('Fault initiated at time:')
    disp(outer_loop_cnt*delttime)

end

if ((fend) <= (outer_loop_cnt+.5)*delttime) && ...
    (( outer_loop_cnt - .5)*delttime < fend)
    if (fault_type == 3 || fault_type == 4)
        snet = snet_save;
    end
    if (fault_type == 2)
        yb=ysave;
    end
    disp('Fault cleared at time: ')
    disp(outer_loop_cnt*delttime)
end

if (saturation_on == 1 && abs(Cc(2,2)*M(2)*z(2))>limit_fast) % check saturation
    z(2)=zsav(2,outer_loop_cnt-1);
end

vbusold=vbus; % save previous time step value for bus voltages
omegaold=omega; % save previous time step value for generator frequency deviations
zold = z;

vsav(:,outer_loop_cnt)=vbus; % save values for plotting
omegasav(:,outer_loop_cnt)=omega; % save values for plotting
zsav(:,outer_loop_cnt)=z; % save values for plotting
snetsave(:,outer_loop_cnt) = snet; % save values for plotting

del=angle(vbus); % extract phase angles from complex bus voltages
xs=[omega,del([slacklist;genlist])]; % construct dynamic state vector for generators
xsold=xs; % save previous time step value of dynamic state

ibus = yb*vbus;
stemp = diag(vbus)*conj(ibus); % calculate complex power at buses
ssav(:,outer_loop_cnt) = stemp;

timesav(1,outer_loop_cnt)=outer_loop_cnt*delttime; % update vector of sample time values

%% core functions

trapjac=trzjac(yb,vbus,genlist,loadlist,HI,delttime);
nt=length(trapjac)-ord_x;
trapjac=[trapjac, (delttime/2)*[Cc; zeros(nt,ord)];...
    (delttime/2)*Bc zeros(ord,nt) (delttime/2)*Ac-eye(ord)];

jacmiss=trzmiss(yb,omega,omegaold,vbus,vbusold,snet,HI,genlist,loadlist,delttime,veq);
jacmiss=[jacmiss+ (delttime/2)*[(Cc*[z+zold]);zeros(nt,1)];...
    zold - z + (delttime/2)*(Ac*(z+zold)+Bc*(xs+xsold))];

inner_loop_cnt=0;

% The "inner loop" below controls the Newton-Raphson iteration, which solves for the new values
% of the
% system variables at each forward time step.

```

```

while(norm(jacmiss)>.000005 && loop_continue)

    inner_loop_cnt=inner_loop_cnt+1;
    del=angle(vbus);
    vmag=abs(vbus);
    trapjac=sparse(trapjac);
    dx=-trapjac\jacmiss;    % solve change in unknowns for on Newton-Raphson iterate, solve:
trapjac*dx = -jacmiss

    % "translate" N-R unknowns back to physical variables
    omega=omega+dx(1:(ngen+1),1);
    del([1;genlist])=del([1;genlist])+dx(index2:index3,1);    % positions 6 to 10
    del(loadlist)=del(loadlist)+dx(index4:index5,1);    % positions 11 to 19
    vmag(loadlist)=vmag(loadlist)+dx(index6:index7,1);    % positions 20 to 28
    z=z+dx(index8:index9);    % positions 29 to last
    %zsavein2(inner_loop_cnt,outer_loop_cnt)=z(2);

    vbus=vmag.*exp(j*del);    % reconstruct update complex bus voltages

    trapjac=trzjac(yb,vbus,genlist,loadlist,HI,delttime);
    nt=length(trapjac)-ord_x;
    trapjac=[trapjac, (delttime/2)*[Cc; zeros(nt,ord)];...
            (delttime/2)*Bc zeros(ord,nt) (delttime/2)*Ac-eye(ord)];

    jacmiss=trzmiss(yb,omega,omegald,vbus,vbusold,snet,HI,genlist,loadlist,delttime,veq);
    jacmiss=[jacmiss+ (delttime/2)*[(Cc*[z+zold]);zeros(nt,1)];...
            zold - z + (delttime/2)*(Ac*(z+zold)+Bc*(xs+xsold))];

    error = norm(jacmiss); % prepare for check for N-R convergence
    if (inner_loop_cnt>12) % don't allow more than 12 N-R iterates
        type bconv.msg
        loop_continue=0;    % this will force termination of inner loop "while"
    end
end
end

```

Table C-1: Details on .m-files

## D. MATLAB Program – Matthias Gautschi

### D.1. General Program Description

The developed MATLAB program has been used throughout the whole project. Many different approaches had to be simulated and therefore different program extensions have been made. All obtained results shown in this thesis, cannot be accessed from a single program, but there are different program versions that allow the simulation of all results in this thesis. For chapters 3 and 4, configuration files have been written that allow an easy reproduction of the different simulations.

The transient simulations can be started from the m-file *start.m*. In this file the simulation configuration can be selected or directly set. In the files *setconfig.m* and *setparam.m*, other settings can be made.

The additional control tasks, simulated in this thesis are implemented in the *setmatrix\_num.m* files. For every considered generator bus there is a specific file, where the matrices of that bus are generated.

For the eigenvalue analysis, the start file is *routine\_eigv.m*. The configurations are made in the *start2.m* file and the other files mentioned above.

I want to mention here, that the MATLAB program was intended to be used for research and therefore many settings have to be done manually and a user interface that allows an easy use is not implemented. The program was just a tool to simulate all the different aspects of this project.

### D.2. Detailed .m-Files

The files *start.m* and *setconfig.m* for simulations of chapters 3 and 4 are given below.

#### start.m

```

%%%%%%%%%%%%%%%%%%%%%%%%%%%%%%%%%%%%%%%%%%%%%%%%%%%%%%%%%%%%%%%%%%%%%%%%
% IEEE 14bus network for frequency studies of interconnected power system %
% Main File - Start of program                                           %
%%%%%%%%%%%%%%%%%%%%%%%%%%%%%%%%%%%%%%%%%%%%%%%%%%%%%%%%%%%%%%%%%%%%%%%%

%% initialize
clc;
clear all;
% close all;

%% select configuration
config = 0; % select configuration
% set config to:
% 0: manual configuration in file setconfig.m
% 1: simulation for section 3.1.3, reference scenario
% 2: simulation for section 3.2.1
% 3: simulation for section 3.3.1
% 4: simulation for section 3.4      PI
% 5: simulation for section 4.2.5
% 6: simulation for section 4.3.1    IND

```

```

% 7:  simulation for section 4.3.2      Seq
% 8:  simulation for section 4.3.2b    Seq + Limit
% 9:  simulation for section 4.3.3      MIMO
% 10: simulation for section 4.3.3      MIMO2
% 11: simulation for section 4.2.3      Controller output
% 12: simulation for section 7.1        master controller
% 13: simulation for section 5.3.2      SAFT model
% 14: simulation for section 7.1        same as 12 but PI

sim = 1;          % select simulation scenario
% set sim to:
% 0:  no scenario, manual disturbance selection
% 1:  std. scenario 1: 0.2pu step @ bus 4
% 2:  std. scenario 2: 0.2pu p-p triangle-wave @ bus 2
setconfig;

```

### setconfig.m (only first part...)

```

% setconfig.m

%% initialize
par.kP21 = 0.02;
par.kD21 = 0.001;
j=sqrt(-1);

%% standard configuration:

% timestep:
delttime=.0166666; % 1 time step = 1 cycle at 60 Hz
% deltime=.0166666/12;

% type 4: 0.2pu added load @ bus 4
% type 6: 0.2pu_pp triangle gen. variation @ bus 2
% type 7: same as 6, but with white-noise
% type 8: step at bus 2 and triangle-wave at buses 2 and 8
% type 9: lucas std.
if sim == 0
    fault_type = 6; % manual selection
elseif sim == 1
    fault_type = 4; % std. simulation case 1
elseif sim == 2
    fault_type = 6; % std. simulation case 2
else
    fault_type = 8; % manual selection
end
fstart = 5; % when does fault occur (sec)
fend = 100; % when is fault cleared (sec)
% fend = 0.5 + 10*delttime;
t_end = 50; % simulation time (sec)
if sim == 1
    t_end = 50;
elseif sim == 2
    t_end = 40;
end

% plots:
% set to 0 if plot is not desired
% set to 1 if plot is desired
whatplot = zeros(20,1);
whatplot(1) = 1; % frequencies (ref. 60Hz)
whatplot(2) = 0; % frequencies (ref. 0)
whatplot(3) = 0; % system frequencies together

```

```

whatplot(4) = 0;    % voltages and angles at buses
whatplot(5) = 1;    % power at buses
whatplot(6) = 0;    % filtered w3 and w2
whatplot(7) = 1;    % power balance at bus 1
whatplot(8) = 0;    % droop power
whatplot(9) = 0;    % eigenvalues
whatplot(10) = 0;   % power balance at buses
whatplot(11) = 1;   % controller @ bus 2
whatplot(12) = 1;   % controller @ bus 6
whatplot(13) = 1;   % controller @ bus 8
whatplot(14) = 1;   % controller @ bus 14

%% sets program values

master_on = 1;      % activate master control
slave_on = 1;       % activate slave control

out1_t = 0;

out2_a1 = 1*slave_on;
out2_a2 = 0;
out2_a3 = 0;
eval_contr2 = [0; 0];

out3_t = 0;

out6_t = 0;
out6_a1 = 1*master_on;
out6_a2 = 1*master_on;
out6_a3 = 0;
eval_contr6 = [0; 0];
% eval_contr6 = [1; 0];
% eval_contr6 = [0; 1];

out8_a1 = 1*slave_on;
out8_a2 = 0;
out8_a3 = 0;
eval_contr8 = [0; 0];

% set to:
% 0:    unity control
% 1:    P control
% 2:    PI control
% 3:    ind. calculation (Q ext.)
% 4:    ind. calculation
% 5:    seq. calculation (Q ext.)
% 6:    seq. calculation
% 7:    MIMO calculation
% 8:    MIMO calculation (2 H(s))
% 9:    serial, cut-off of TF
%10:    PD control

C2_calc = 10;      % choose controller calc. method @ bus 2
C6_calc = 5;       % choose controller calc. method @ bus 6
C8_calc = 10;      % choose controller calc. method @ bus 8

% choose system:
% 0:    classical generator bus
% 1:    master control
% 2:    wind bus slave control
% 3:    slave PHEV
b2.system = 2;
b6.system = 1;
b8.system = 2;

% set model to:
% 0:    no actuator model
% 1:    2nd order filter model

```



```

% 2:      -
% 3:      single SAFT model
% 4:      single SAFT model with pre-filter
% 5:      single SAFT model with pre- and post-filter
% 6:      2nd order filter with pre- and post-filter
% 7:      2 parallel battery SAFT model with pre- and post-filter
% 8:      different feed through filter for testing

b2.a1.model = 1;
b2.a2.model = 1;
b2.a3.model = 1;

b6.a1.model = 1;
b6.a2.model = 1;
b6.a3.model = 1;

b8.a1.model = 1;
b8.a2.model = 1;
b8.a3.model = 1;

calc_sym = 0; % set to 1 for eigv analysis for parameter sens. (not complete)

if config == 0
    %% manual configuration
    % ...

elseif (config == 1)
    %% configuration for section 3.1.3 - reference scenario
    param = 1;
    setparam; % loads parameters of added control
    setdata; % loads standard grid configuration

    % additional control configuration
    out1_t = 0;

    out2_a1 = 0;
    out2_a2 = 0;
    out2_a3 = 0;
    eval_contr2 = [0; 0];

    out3_t = 0;

    out6_t = 0;
    out6_a1 = 0;
    out6_a2 = 0;
    out6_a3 = 0;
    eval_contr6 = [0; 0];

    out8_a1 = 0;
    out8_a2 = 0;
    out8_a3 = 0;
    eval_contr8 = [0; 0];

    % controller calculation method:
    C2_calc = 0; %
    C6_calc = 0;
    C8_calc = 0;

    % bus system:
    b2.system = 1; % master controller
    b6.system = 0;
    b8.system = 0;

    % actuator model:
    b2.a1.model = 1;
    b2.a2.model = 1;
    b2.a3.model = 1;

```

```
b6.a1.model = 1;
b6.a2.model = 1;
b6.a3.model = 1;

b8.a1.model = 1;
b8.a2.model = 1;
b8.a3.model = 1;

% plots:
whatplot = zeros(20,1);
whatplot(1) = 1; % bus frequencies (ref. 60Hz)
if sim == 1
    y_u = 60.1; % upper limit for freq. plots
    y_l = 58; % lower limit for freq. plots
elseif sim == 2
    y_u = 60.4;
    y_l = 59.6;
else
    y_u = 60.1;
    y_l = 58;
end

elseif (config == 2)
    % ...
end

%% run programs
setvalues; % set values and matrices

% calceigv; % perform EV analysis for parameter sens.
gotrans; % start transient simulation

%% display results
plots;
```

Table D-1: Details on .m-files

## Bibliography

- [1] International Energy Agency (IEA). (2008). *World Energy Outlook 2008*. Paris, France. OECD/IEA.
- [2] World Wind Energy Association (WWEA). (2009). *World Wind Energy Report 2008*. Bonn, Germany. Retrieved from: <http://www.wwindea.org>
- [3] Ackermann, T. (2007). *Wind Power in Power Systems*. Stockholm, Sweden. Royal Institute of Technology, Stockholm. Wiley.
- [4] Morren, J.; Pierik, J.; de Haan, S. W.H. (2005). *Inertial Response of Variable Speed Wind Turbines*. Delft, The Netherlands. Electric Power Systems Research.
- [5] Mullane, A.; O'Malley, M. (2005). *The Inertial Response of Induction-Machine-Based Wind Turbines*. Dublin, Ireland. IEEE Transactions on Power Systems.
- [6] Mullane, A.; Bryans, G.; O'Malley, M. (2005). *Kinetic Energy and Frequency Response Comparisons for Renewable Generation Systems*. Dublin, Ireland. International Conference on Future Power Systems.
- [7] Lalor, G.; Mullane, A.; O'Malley, M. (2005). *Frequency Control and Wind Turbine Technologies*. Dublin, Ireland. IEEE Transactions on Power Systems.
- [8] Lei, Y.; Mullane, A.; Lightbody, G.; Yacamini, R. (2006). *Modeling of the Wind Turbine with a Doubly Fed Induction Generator for Grid Integration Studies*. Cork, Ireland. IEEE Transactions on Energy Conversion.
- [9] Mullane, A.; O'Malley, M. (2006). *Modifying the Inertial Response of Power-Converter Based Wind Turbine Generators*. Dublin, Ireland. The 3rd IET International Conference on Power Electronics, Machines and Drives.
- [10] Morren, J.; de Haan, S. W.; Ferreira, J. (2005). *Contribution of DG Units to Primary Frequency Control*. Delft, The Netherlands. 2005 International Conference on Future Power Systems.
- [11] Morren, J.; de Haan, S. W.; Kling, W. L.; Ferreira, J. A. (2006). *Wind Turbines Emulating Inertia and Supporting Primary Frequency Control*. Delft, The Netherlands. IEEE Transactions on Power Systems.
- [12] Morren, J.; de Haan, S. W.; Ferreira, J. (2006). *Primary Power/Frequency Control with Wind Turbines and Fuel Cells*. Delft, The Netherlands. 2006 IEEE Power Engineering Society General Meeting.
- [13] Erlich, E.; Brakelmann, H. (2007). *Integration of Wind Power into the German High Voltage Transmission Grid*. Duisburg, Germany.

- [14] Lalor, G.; Ritchie, J.; Rourke, S.; Flynn, D.; O'Malley, M. J. (2004). *Dynamic Frequency Control with Increasing Wind Generation*. Dublin, Ireland. IEEE Power Engineering Society General Meeting, 2004.
- [15] Wright, A. D. (2004). *Modern Control Design for Flexible Wind Turbines*. Golden, CO, USA. NREL - National Renewable Energy Laboratory.
- [16] Nasiri, A. (2008). *Integrating Energy Storage with Renewable Energy Systems*. Milwaukee, WI, USA. 34th Annual Conference of IEEE Industrial Electronics, 2008. IECON 2008.
- [17] Zabalawi, S. A.; Mandic, G.; Nasiri, A. (2008). *Utilizing Energy Storage with PV for Residential and Commercial Use*. Milwaukee, WI, USA. 34th Annual Conference of IEEE Industrial Electronics, 2008. IECON 2008.
- [18] Senjyu, T.; Kikunaga, Y.; Yona, A.; Sekine, H.; Saber, A.Y.; Funabashi, T. (2008). *Coordinate Control of Wind Turbine and Battery in Wind Power Generation System*. Okinawa, Japan. 2008 IEEE Power and Energy Society General Meeting - Conversion and Delivery of Electrical Energy in the 21st Century.
- [19] Nasiri, A.; Rimmalapudi, V. S.; Emadi, A.; Chmielewski, D. J.; Al-Hallaj, S. (2004). *Active Control of a Hybrid Fuel Cell-Battery System*. Chicago, IL, USA. 4th International Power Electronics and Motion Control Conference, 2004. IPEMC 2004.
- [20] Abedini, A.; Nasiri, A. (2008). *Applications of Super Capacitors for PMSG Wind Turbine Power Smoothing*. Milwaukee, WI, USA. 34th Annual Conference of IEEE Industrial Electronics, 2008. IECON 2008.
- [21] Kundur, P. (1994). *Power System Stability and Control*. New York, USA. McGraw-Hill.
- [22] Andersson, G. (2007). *Modelling and Analysis of Electric Power Systems*. Zurich, CH. EEH – Power Systems Laboratory, ETH Zurich.
- [23] Bergen, A. R.; Vittal, V. (2000). *Power Systems Analysis*. New Jersey, USA. Prentice Hall.
- [24] Alvarado, F.L.; Meng, J.; DeMarco, C.L.; Mota, W.S. (2001) *Stability Analysis of Interconnected Power Systems Coupled with Market Dynamics*. Madison, WI, USA. IEEE Transactions on Power Systems.
- [25] Andersson, G. (2008). *Dynamics and Control of Electric Power Systems*. Zurich, CH. EEH – Power Systems Laboratory, ETH Zurich.
- [26] Wei Li; Joos, G.; Abbey, C. (2006). *Attenuation of Wind Power Fluctuations in Wind Turbine Generators using a DC Bus Capacitor Based Filtering Control Scheme*. Montreal, Canada. Conference Record of the 2006 IEEE Industry Applications Conference, 2006. 41st IAS Annual Meeting.

- [27] Abedini, A.; Mandic, G.; Nasiri, A. (2008). *Wind Power Smoothing using Rotor Inertia aimed at reducing Grid Susceptibility*. Milwaukee, WI, USA. IEEE 34th Annual Conference of Industrial Electronics, 2008. IECON 2008.
- [28] Daimler Inc. (2009). *Electric Drive. The Age of Electric Mobility Begins*. Retrieved from: <http://www.daimler.com>
- [29] Saberi, A.; Lin, Z.; Teel, A. R. (1996). *Control of Linear Systems with Saturating Actuators*. Pullman, WA, USA. IEEE Transactions on Automatic Control. Vol. 41. No. 3.
- [30] Zongli, L.; Mantri, R.; Saberi, A. (1995). *Semi-Global Output Regulation for Linear Systems Subject to Input Saturation – A Low-and-High Gain Design*. Pullman, WA, USA. Proceeding of the American Control Conference 1995.
- [31] Saberi, A.; Stoorvogel, A.A.; Sannuti, P. (1999). *Control of Linear Systems with Regulation and Input Constraints*, Springer.
- [32] Franklin, G. F.; Powell, J. D.; Emami-Naeini, A. (2006). *Feedback Control of Dynamic Systems*. New Jersey, USA. Pearson Prentice Hall.
- [33] Maciejowski, J. (1989). *Multivariable Feedback Design*. Cornwall, GB. Addison-Wesley Publishing Company Inc.
- [34] Dorf, R.C.; Bishop, R.H. (2001). *Modern Control System*. New Jersey, USA. 9<sup>th</sup> edition. Prentice-Hall Inc.
- [35] The MathWorks, Inc. (2000). *The Optimal ITAE Transfer Functions*. Retrieved from: <http://www.mathworks.com/matlabcentral/>
- [36] The MathWorks, Inc. (2008). *MATLAB User's Guide*. MATLAB Version R2008A.
- [37] Hiskens, I.A. (2006). *Generic Type-3 Wind Turbine-Generator Model for Grid Studies*. WECC Wind Generator Modeling Group.
- [38] Johnson, V. H.; Pesaran, A. A.; Sack, T. (2001). *Temperature-Dependent Battery Models for High-Power Lithium-Ion Batteries*. NREL - National Renewable Energy Laboratory. Golden, CO, USA.
- [39] Prudent Energy Inc. (2009). *Remote Area Power Systems: King Island*. Retrieved from Prudent Energy: <http://www.pdenenergy.com>